IMPLEMENTATION OF MACHINE LEARNING IN PROTON THERAPY QUALITY ASSURANCE

A THESIS SUBMITTED TO

D.Y. PATIL EDUCATION SOCIETY (DEEMED TO BE UNIVERSITY), KOLHAPUR.

FOR THE DEGREE OF

DOCTOR OF PHILOSOPHY

IN

PHYSICS

UNDER THE FACULTY OF

INTERDISCIPLINARY STUDIES

BY

Mr. RANJITH C. P., M.Sc.

UNDER THE SUPERVISION OF

Dr. K. MAYAKANNAN. M.Sc., Ph.D.

ASSISTANT PROFESSOR

CENTRE FOR INTERDISCIPLINARY RESEARCH,
D. Y. PATIL EDUCATION SOCIETY
(DEEMED TO BE UNIVERSITY),
KOLHAPUR- 416 006, MAHARASHTRA, INDIA.

2025

D.Y. PATIL EDUCATION SOCIETY (DEEMED TO BE UNIVERSITY), KOLHAPUR

CENTRE FOR INTERDISCIPLINARY RESEARCH

CERTIFICATE

This is to certify that, **"Implementation of Machine Learning in Proton Therapy Quality Assurance"** the present thesis which is being submitted herewith for the award of **Doctor of Philosophy (Ph.D.)** in **Physics** under the faculty of the Center for Interdisciplinary Research (CIR) of the D. Y. Patil Education Society (Deemed to be University), Kolhapur, is the result of original research work completed by **Mr. Ranjith C P** under my supervision and guidance and the best of my knowledge and belief, the work embodied in this thesis has not formed earlier the basis for the award of any degree or similar title of this or any other University or examining body

Research Guide

Place: Kolhapur

Date: 16/04/2025

K. Hayakannan 16/04/2025

Dr. K. Mayakannan.

Assistant Professor

D. Y. Patil Education Society,
(Deemed to be University),
Kolhapur, Maharashtra, India.

DECLARATION

I hereby declare that the work contained in this thesis, entitled, **"Implementation of Machine Learning in Proton Therapy Quality Assurance"** which has not been previously submitted to meet requirements for an award at this or any other higher education institute in India or any other country. To the best of my knowledge and belief, the thesis contains no material previously published or written by another person except where due reference is made further, I declare that I have not violated any of the provisions under the copyright and piracy/cyber/IPR act amended from time to time

Research student

Place: Kolhapur

Date: 16/04/2025

RANJITH C. P.

D. Y. Patil Education Society,
(Deemed to be University),
Kolhapur, Maharashtra, India.

D. Y. Patil Educational Society

Certificate of Plagiarism Check for Thesis

Author Name	Mr. Ranjith C P
Course of Study	Ph.D.
Name of Guide	Dr. K. Mayakannan
Department	Department of Medical Physics, Centre for Interdisciplinary Research
Acceptable Maximum Limit	10
Submitted By	shivajikashte.cir@dypgroup.edu.in
Paper Title	Implementation of Machine Learning in Proton Therapy Quality Assurance.
Similarity	4%
Paper ID	3459686
Total Pages	121
Submission Date	2025-04-03 13:26:13

Signature of Student

Signature of Guide

University Coordinator

Head of the Department

* This report has been generated by DrillBit Anti-Plagiarism Software

ACKNOWLEDGEMENT

I want to express my deepest gratitude and profound respect to my esteemed guide, Dr Mayakannan Krishnan, Assistant Professor at the Centre for Interdisciplinary Research, D. Y. Patil Education Society (Deemed to be University), Kolhapur. His insightful guidance, unwavering support, and constant encouragement have been indispensable throughout my Ph.D. journey. This work would not have been possible without his mentorship and inspiration.

Dr Mayakannan Krishnan has been much more than a guide to me; his support and care have been akin to that of a family member I am sincerely grateful to him for selecting me as his student during such a pivotal stage of my academic career His constructive advice, extensive discussions, and genuine dedication to my research have provided a strong foundation for my PhD work I deeply appreciate his understanding, patience, and personal attention, which made this journey both fulfilling and rewarding His flexibility, calm demeanour, and motivating encouragement fostered an excellent working relationship and inspired me to persevere and complete my work Dr. Mayakannan Krishnan's unwavering faith in my abilities and balanced approach to life and academia have been a source of strength, enabling me to achieve my goals.

I would also like to express my heartfelt gratitude to Dean and Research Director Prof Lohkande, Vice-Chancellor Prof R K Sharma, IQAC Coordinator Dr Shimpa Sharma, and Registrar Dr. V. V. Bhosale for their invaluable inspiration and unwavering support throughout my academic journey. Their encouragement has been a source of motivation and has significantly contributed to the successful completion of my Ph.D.

I would like to sincerely thank Dr. Siddhartha Laskar, Deputy Director (Academic) and In-charge of the Proton Therapy Centre, ACTREC, Mumbai, for his instrumental support and administrative guidance. His permission and encouragement have been pivotal in facilitating my research, and I deeply appreciate his role in enabling me to carry out my work effectively.

I also wish to express my gratitude to Dr. Vedang Murthy, the Head of the Department of Radiation Oncology, ACTREC, at the time I received permission to pursue my Ph.D. and Dr. Rajesh Kinhikar, Head of the Medical Physics Department, TMH, Mumbai Their

invaluable support in facilitating the initial administrative processes and securing permission for my PhD was crucial to the commencement of my research I am deeply thankful for their guidance and encouragement during this formative phase of my academic journey.

A special and heartfelt thanks to my colleague, Dr. Vysakh Raveendran, Medical Physicist at ACTREC, who has been working alongside me for the past nine years. His constant support and encouragement have been truly invaluable throughout my PhD journey. His expertise has been critical in guiding me through every step, from admission and synopsis preparation to publication. His meticulous proofreading, detailed corrections, and thoughtful suggestions for all my research publications have been indispensable. His unwavering support has had a profound impact on my work, and I am deeply grateful for his contribution.

I am deeply thankful to Mr Nithin Narayanan, Technical Lead at IBA, and Engineers Mr Jithin P, and Mr Mahesh for their invaluable assistance in obtaining the log file data from the IBA machine, which formed the core data of my thesis. Their guidance in understanding the contents of the log file and how to interpret it was instrumental in enabling me to work with the data effectively.

I would also like to express my heartfelt thanks to all my colleagues in the Department of Radiation Oncology, ACTREC, for their constant support and camaraderie throughout my research journey Special thanks to Lalit N C, A C Prabhu, Kantharam D, Prakash S, Rohidas P, Umesh G, Lilawati, Subhajit Panda, and Manimala K Their collaboration and encouragement have significantly enriched my experience, and I am truly grateful for their friendship and assistance.

I extend my sincere thanks to my colleagues, Ratheesh K. E, Pooja R Patil, Dilip Patil, Vikas, and Ajinkya from the Ph.D. Scholars, Centre for Interdisciplinary Research, D. Y. Patil Education Society (Deemed to be University), Kolhapur for their support and camaraderie throughout my Ph.D. journey have been invaluable.

I am also thankful to Dr. Krushnath Shirke, Mr. Nirmal, Mrs. Namrata, Mr. Ramdas, Mr. Omkar, and Mrs. Sarita from Centre for Interdisciplinary Research (CIR) at D. Y. Patil

Education Society (Deemed to be University), Kolhapur for their cooperation and support in various ways throughout my Ph.D. journey.

I would like to express my deepest gratitude to my family, whose unwavering love and support have been my strength throughout this challenging journey To my wonderful wife, Ramya Mohan, and my dear son, Harshil, your patience, understanding, and encouragement have meant the world to me Ramya, your constant belief in me, even during the toughest times, has been a source of inspiration You have been my rock, offering emotional support and helping me stay grounded when things seem overwhelming Your sacrifices and dedication to our family have allowed me to focus on my work, and for that, I am forever grateful Harshil, your innocent joy and love have been a reminder of what truly matters. Your presence has brought light into my life during the most trying moments, and I cherish every moment with you I am deeply thankful to both of you for standing by me and making this journey not only possible but meaningful.

I would like to dedicate my heartfelt gratitude to my late father, Chandran C P Though he is no longer with us, I know that if he were alive today, he would have been the happiest and proudest father His unwavering support, love, and belief in me shaped the person I am today His values and teachings continue to guide me, and I carry his memory with me every step of this journey I miss him deeply, but I know he would have shared in the joy and pride of this accomplishment I am also deeply grateful to my mother, Usha Kumari, whose love and sacrifices have been a constant source of strength.

Finally, I would like to thank God for His divine blessings, guidance, and strength that have helped me navigate this journey. Without His grace, none of this would have been possible.

Table of Contents	Page No
Abstract	1
Chapter 1: Introduction	5
1.1 Radiotherapy	6
1.2 Particle therapy	8
1.2.1 Proton therapy	8
1.2.2 Carbon ion therapy	9
1.2.3 Helium and other heavy ion therapy	9
1.3 Pencil Beam Scanning Proton Therapy System	10
1.3.1 Beam Production System (BPS)	11
1.3.2 Energy Selection and Beam Transport System (ESBTS)	13
1.3.3 Beam Delivery System (BDS)	14
1.4 Quality Assurance of Pencil Beam Scanning Proton Therapy	16
1.4.1 Mechanical QA	16
1.4.2 Dosimetric QA	17
1.4.3 Range or Energy	17
1.4.5 Patient-Specific QA	20
1.5 Log file analysis	20
1.6 Machine Learning models	21
1.6.1 Supervised Learning	22
1.6.2 Unsupervised Learning	22
1.6.3 Reinforcement Learning	23
1.7 Research Problem	23
1.8 Objective of the study	25
1.9 References	27
Chapter 2: Literature Survey	30
2.1 History of Proton Therapy	31
2.2 Proton Therapy in Clinical Practice	33
2.3 The Role of Log Files in Radiotherapy Quality Assurance	35
2.4 Machine Learning-Driven Quality Assurance in Modern Radiotherapy	38

2.5 References	40
Chapter 3: Measurement and Evaluation of Spot Dosimetric Parameters Using a Scintillator Detector and Comparison with Irradiation Log File Data	46
3.1 Introduction	47
3.2 Materials and Methods	48
3.2.1 Five-spot Pattern	48
3.2.2 Lynx 2D Detector	50
3.2.3 Spot Measurement	51
3.2.4 Nozzle and Beam Monitoring	53
3.2.5 Log File Generation	55
3.2.6 Tuning Pulse	56
3.2.7 Data Extraction from Log File	57
3.3 Results	58
3.3.1 Five-Spot Measurement	58
3.3.2 Log File Data Analysis	62
3.4 Discussion	66
3.5 Conclusions	68
3.6 References	69
Chapter 4: Development and Validation of Machine Learning Models for Predicting Spot Dosimetric Parameters	71
4.1 Introduction	72
4.2 Materials and Methods	74
4.2.1 Artificial Neural Network (ANN)	74
4.2.2 ANN Model Architecture	74
4.2.2.1 Multi-Layer Perceptron (MLP) Model	74
4.2.2.2 Input Layer Parameters	76
4.2.2.3 Output Layer	77
4.2.2.4 Hidden Layers	77
4.2.2.5 Rectified Linear Unit – Activation Function	78
4.2.2.6 Optimiser	79
4.2.2.7 Loss Function	81

4.2.3 Model Training	81
4.2.4 Model Validation	83
4.2.4.1 Quantitative Analysis	84
4.2.4.1.1 Mean Squared Error (MSE)	84
4.2.4.1.2 Root Mean Squared Error (RMSE)	85
4.2.4.1.3 Mean Absolute Percentage Error (MAPE)	85
4.2.4.1.4 R-Squared (R^2) – Coefficient of Determination	86
4.2.4.2 K-Fold Cross-Validation	86
4.2.4.3 Quartile-Quartile (Q-Q) Plot	88
4.2.4.4 Histogram of Residuals	90
4.3 Results	90
4.3.1 Correlation Analysis Between Input and Output Variable	90
4.3.2 Model Hyper parameter Tuning	92
4.3.3 Model Performance Evaluation	93
4.4 Discussion	99
4.5 Conclusions	101
4.6 References	102
Chapter 5: Development of an In-House Tool for Patient-Specific Quality Assurance Analysis Using Machine Learning Models and Log File Data.	104
5.1 Introduction	105
5.2 Materials and Methods	106
5.2.1 IBA Proteus plus multi-room system	107
5.2.2 Log File Data Extraction	107
5.2.2.1 beam csv	108
5.2.2.2 beam configure csv	108
5.2.2.3 beam settings csv	108
5.2.2.4 event csv	108
5.2.2.5 map record tuning csv	108

5.2.2.6 map specific csv	109
5.2.2.7 map record csv	109
5.2.3 Conversion of Spot Position in IC23 to the Isocentre Plane	110
5.2.4 Range Calculation	112
5.2.5 Spot Size Calculation	113
5.3 Results	113
5.3.1 Nozzle WET Calculation	113
5.3.2 Automated Script Workflow	114
5.3.3 Report Generation	115
5.4 Discussion	117
5.5 Conclusions	118
5.6 References	118
Chapter 6: Application of the In-House Automated Tool for Patient-Specific and Machine Quality Assurance in Proton Beam Therapy Using Log Files and Machine Learning Models.	120
6.1 Introduction	121
6.2 Materials and Methods	123
6.2.1 Data Collection	124
6.2.2 Data Processing	125
6.3 Results	125
6.3.1 Machine QA Data	125
6.3.2 PSQA Beam Data Analysis	129
6.3.2.1 Spot Position	129
6.3.2.2 Spot Size and Symmetry	130
6.3.2.3 Monitor Unit Accuracy	133
6.4 Discussion	134
6.5 Conclusions	138
6.6 References	138
Chapter 7: Summary and Recommendations	141
Chapter 8: Recommendations	147

List of Tables

Table No	Table Name	Page No
Table 3.1	Tabulated the baseline spot size values used for this study Tabulated the baseline spot size value of each range and the MU per spot of each spot	50
Table 3.2	Comparison of AAPM-TG224 Recommended Tolerances for Spot Parameters and IBA-Proteus Plus Log File Tolerances for Triggering Beam Interruption	56
Table 3.3	The statistics of all Lynx2D scintillator measured spot parameters	59
Table 3.4	Comparison of Lynx2D-measured X and Y spot sizes with the manufacturer-specified baseline values, including the differences in X and Y spot sizes, along with the mean, standard deviation, and root mean square error (RMSE)	60
Table 3.5	The difference in spot size along X and Y directions between the Lynx2D measured and log file recorded data The maximum difference, RMSE, mean and standard deviation of the difference are given for different gantry angles	65
Table 4.1	The person correlation coefficients between the input variables and label values of the x spot size, y spot size, major axis spot size and minor axis spot size prediction ANN models	91
Table 4.2	The Pearson correlation coefficients between the input variables and label values of the x and y relative positional error prediction ANN models	91
Table 4.3	The summary of different hyper parameter combinations used for the six ML model tuning and the obtained RMSE and R-square are tabulated	93
Table 4.4	The evaluation matrices of all the Six ML Models The values of MSE, MAPE, RMSE, R- square and maximum error of each ML model	94
Table 4.5	Root Mean Square Error (RMSE) and R-Square Values of the K-Fold Cross-Validation (k=5) of Six Machine Learning Models	96
Table 5.1	The tabulation of different distance values for the calculation of spot position conversion from the IC23 plane to the isocentre GTR- represents each gantry	111
Table 5.2	The coefficients of equation 5 1 for different gantries GTR- Gantry	112
Table 5.3	Provided the calculated nozzle WET values for different energies for all three gantries	114
Table 5.4	Sample data table illustrating the total number of spots, layers, and MU This table represents the format generated by the in-house script when processing the irradiated log file data of a beam * all values are sample values only	116
Table 5.5	Sample format of the table displaying spot information for each layer This table represents the structure generated by the in-house script when processing the log file data for a patient's treatment beam * all values are sample values only	116
Table 5.6	Sample table displaying the results of spot parameter analysis, including the percentage of spots in the beam with spot size differences of less than 10%, spot symmetry of less than 10%, spot position errors within	116

	1 mm, and MU per spot variation of less than 2% * All values are sample values only	
Table 6.1	Summary statistics of beam parameters analyzed in this study The number of layers, Energy range, spot size range, spot position in X and Y directions, and MU per spot	124
Table 6.2	Comparison of spot parameters using the 5-spot pattern for machine QA: measured, predicted, and log file-recorded spot sizes (X and Y axes) along with measured versus log file-recorded spot positions Mean and standard deviation values across 12 gantry angles are presented	126

List of Figures

Figure No	Figure Name	Page No
Figure 1.1	Evolution of Radiotherapy Treatment Planning from 1935 to 2010, Demonstrating Dose Distributions for Prostate Cancer Using Various External Radiation Therapy Modalities from 200 kV X-ray to Carbon Ions	7
Figure 1.2	The depth dose distribution of different charge particles used for particle therapy Pion 50MeV, Carbon ion 300MeV/u, Proton 175MeV, Helium 170MeV/u	10
Figure 1.3	The IBA Proteus Plus treatment gantry installed at National Hadron Therapy Centre, ACTREC, Tata Memorial Centre, Mumbai	11
Figure 1.4	The Cyclotron C230 installed at National Hadron Therapy Centre, ACTREC, Tata Memorial Centre, Mumbai	12
Figure 1.5	The Degrader wheel with different density materials to degrade energy from 226 2MeV to 70 18MeV	13
Figure 1.6	The energy selection system of the IBA Proteus Plus machine	14
Figure 1.7	Rotary feedthrough	14
Figure 1.8	The Schematic Diagram of the rotating gantry. The bending magnets and rotating system are depicted in the figure	15
Figure 1.9	The representation of the spot size of a Pencil Beam Scanning (PBS) Proton therapy beam (a) Schematic representation of a typical spot in PBS, (b) 1D Gaussian distribution of the spot	19
Figure 3.1	The Schematic diagram of the 5-spot pattern Representing spot in each Cartesian coordinate	49
Figure 3.2	Lynx 2D Detector and graphical representation of the spot measurement process	51
Figure 3.3	The Lynx2D attached to the gantry head using the Lynx holder The levelling plumb is attached to level the detector	52
Figure 3.4	PBS spot shows an elliptical shape (a) represents the elliptical shape of the spot, (b) Representation of spot size (1sigma) measurement	53
Figure 3.5	The IBA Proteus plus dedicated PBS nozzle schematic representation	54
Figure 3.6	(a) IC23 assembly in the nozzle (b) IC23 chamber schematic representation	55
Figure 3.7	The measures of spot size (X and Y direction) plotted against the range	61
Figure 3.8	The measured spot size along X and Y direction versus range plotted for different gantry angles (a) X spot size versus range for different gantry angles (b) Y spot size versus range for different gantry angles	61
Figure: 3.9	Range versus X scanning magnet current recorded in the log file data	62
Figure 3.10	Range versus X scanning magnet current recorded in the log file data	63
Figure 3.11	Range versus log file recorded X spot size with error bar	63
Figure 3.12	Range versus log file recorded X spot size with error bar	64
Figure 3.13	Plots of measured spot parameters versus log file recorded spot parameters (a) Measured X-spot size versus log file recorded X-spot size (b) Measured Y spot size versus log file recorded Y spot size	65

	(c) Measured relative X positional error versus log file recorded relative X-positional error (d) Measured relative Y positional error versus log file recorded relative Y positional error	
Figure 4.1	Schematic diagram of an MLP neural network model with one input layer, two hidden layers and one output layer	75
Figure 4.2	The visualisation of ReLU activation function	79
Figure 4.3	The ANN model architecture of the spot size prediction models The x-spot size, y-spot size, major axis spot size and minor axis spot size prediction models are shown in the figure All four models share the same input variables, hidden layers and hyper parameters *IC- Ionisation chamber	82
Figure 4.4	The ANN model architecture of the relative positional error prediction models The x-spot relative positional error and y-spot relative positional error prediction models are shown in the figure All the two models share the same input variables, hidden layers and hyper parameters * IC- Ionisation chamber	83
Figure 4.5	Graphical representation of how the K fold cross-validation works in a model validation (Picture courtesy Sevinç E et al [21])	87
Figure 4.6	Q-Q Plots Demonstrating Distribution Characteristics: (a) Normal Distribution, (b) Heavy Tails, (c) Left-Skewed Data, (d) Right-Skewed Data, and (e) Data with Outliers (Pleil JD et al [22])	88
Figure 4.7	Model accuracy metrics plot for the X spot size prediction model, showing a reduction in MAPE (%) as epochs increase Train- training data, Val- validation set	92
Figure 4.8	Plots of measured and ML model predicted spot parameters (a) The measured and predicted X spot size (b) The measured and predicted Y spot size (c) The measured versus predicted relative positional error in the X direction (d) The measured versus predicted relative positional error in the Y direction (e)The measured versus predicted Major axis spot sizes (f) The measured versus predicted Minor axis spot sizes	95
Figure 4.9	Histogram of residuals (Difference between measured and predicted) of the ML models (a) Histogram of residuals of the X spot size prediction model (d) Histogram of residuals of the Y spot size prediction model (c) Histogram of residuals of the X relative positional error prediction model (d) Histogram of the Y relative positional error prediction model (e) Histogram of residuals of the Major axis spot size prediction model (f) Histogram of Minor axis spot size prediction model	97
Figure 4.10	Figure 4 10: Quartile- Quartile (Q-Q) plot of the model residuals (a) Q-Q plot of residuals of the X spot size prediction model (b) Q-Q plot of residuals of the Y spot size prediction model (c) Q-Q plot of residuals of the X relative positional error prediction model (d) Q-Q plot of residuals of the Y relative positional error prediction model (e) Q-Q plot of the residual of the Major axis spot size prediction model (f) Q-Q plot of residuals of the Minor axis spot size prediction model	98
Figure 5.1	The Schematic representation of the layout of the Proton therapy system installed at ACTREC Proton Therapy Centre, Navi Mumbai, India GTR- Gantry	107

Figure 5.2	Equivalent triangle method. This method converts the spot positions from the isocentre plane to the IC23 plane	111
Figure 5.3	The Illustration of the steps involved in the log file analysis using the In-house automated tool	115
Figure 6.1	The plot of measured spot sizes versus ML model predicted (Blue) and Log file (Red) recorded X spot size	128
Figure 6.2	The plot of measured spot sizes versus ML model predicted (Blue) and Log file recorded (Red) Y spot size	128
Figure 6.3	Box plots show the X positional error in different gantry angle intervals	129
Figure 6.4	box plots showing Y positional error in different gantry angle intervals	130
Figure 6.5	The box plot of the percentage of spots in each gantry angle interval has an X spot size variation of less than 10% from the baseline values	131
Figure 6.6	The box plot shows the percentage of spots in each gantry angle interval with a Y spot size variation of less than 10% from the baseline values	131
Figure 6.7	Histogram of the number of spots in each energy interval, with each bar divided into the percentage of spots with spot size variation less than 10% and those with spot size variation greater than 10% of baseline spot size	132
Figure 6.8	The box plot shows the percentage of spots in each gantry angle interval with a Monitor Unit(MU) difference of less than 2%	133
Figure 6.9	Scatter plot Showing the difference of Monitor Unit (MU) between planned and delivered beams	134

Abbreviations

AAPM	American Association of Physicists in Medicine
ACTREC	Advanced Centre for Treatment, Research and Education in Cancer
ADAM	Adaptive Moment Estimation
AI	Artificial Intelligence
ANN	Artificial Neural Networks
ARIMA	Autoregressive Integrated Moving Average
BDS	Beam Delivery System
BPS	Beam Production System
CCD	Charge Coupled Device
CNN	Convolutional Neural Networks
CSI	Cranio Spinal Irradiation
CSV	Comma Separated Value
CT	Computed Tomography
DD	Dose Difference
DNA	Deoxyribonucleic Acid
DTA	Distance-to-Agreement
ESBTS	Energy Selection and Beam Transport System
GAN	Generative Adversarial Network
GPR	Gaussian Process Regression
HCL	Harvard Cyclotron Laboratory
HIMAC	Heavy Ion Medical Accelerator in Chiba
HIT	Heidelberg Ion Beam Therapy Centre
IC	Ionisation Chamber
ID	Integrated Depth Dose
IDE	Integrated Development Environment
IGRT	Image-Guided Radiation Therapy
IMPT	Intensity Modulated Proton Therapy
IMRT	Intensity-Modulated Radiation Therapy
KV	Kilo-Voltage
LC	Local Control Rate
LET	Linear Energy Transfer
LBNL	Lawrence Berkeley National Laboratory
LLUMC	Loma Linda University Medical Center
LC	Local Control Rate
LET	Linear Energy Transfer
LLUMC	Loma Linda University Medical Center
LBNL	Lawrence Berkeley National Laboratory
MLIC	Multi-Layer Ionization Chamber
ML	Machine Learning
MLP	Multi-Layer Perceptron
MSE	Mean Squared Error
MRI	Magnetic Resonance Imaging
MU	Monitor Unit
OAR	Organs-At-Risk
OIS	Oncology Information System
OS	Overall Survival
PBS	Pencil Beam Scanning
PET	Positron Emission Tomography
PSI	Paul Scherrer Institute
PSQA	Patient-Specific Quality Assurance
QA	Quality Assurance
RBE	Radio Biological Effect
ReLU	Rectified Linear Unit
RF	Radio Frequency
RMSE	Root Mean Square Error
SAD	Source-to-Axis Distance
SBRT	Stereotactic Body Radiation Therapy
SD	Standard Deviation
SNN	Shallow Neural Network
SOBP	Spread-Out Bragg Peak
STP	Standard Temperature and Pressure
TG	Task Group
TOPAS	Tool for Particle Simulation
TPS	Treatment Planning System
WET	Water-Equivalent Thickness

Abstract

Quality Assurance (QA) is critical in ensuring precision, safety, and effectiveness in proton radiotherapy, directly influencing patient outcomes. However, conventional QA methods are labour-intensive and time-consuming, challenging efficiency and workflow optimisation. Machine Learning (ML) models provide a transformative solution by automating complex QA processes, streamlining workflows, and enhancing operational efficiency without compromising care. This study investigates the application of ML models for automating QA in pencil beam scanning (PBS) proton therapy systems, underscoring the need for automated tools to optimise QA.

The study was conducted using data from the IBA Proteus Plus Proton Therapy System. The accuracy of PBS delivery relies on critical spot dosimetric parameters such as spot size, spot position, spot symmetry, energy or range, and machine output calibration. Routine QA involves measuring these parameters using dedicated dosimeters. A log file records data during beam delivery, including spot position, charge, spot size, scanning magnet currents, beam current, gantry angle, and ionisation chamber readings. Even though log files monitor spot parameters in real time and trigger beam interruptions if deviations exceed predefined tolerances, discrepancies between log file data and dedicated dosimeter-measured values can limit their direct use for QA.

In the initial part of this study, the correlation between log file-recorded and scintillator-measured spot parameters is examined to understand the limitation and highlight the importance of log file analysis. Spot measurements were conducted using a Lynx2D scintillator detector by irradiating a 5-spot pattern across the energies ranging from 70.18 MeV to 226.2 MeV at 12 gantry angles. A total of 9,000 spots were measured which recorded key parameters (spot size, position, and symmetry) along X-Y axes and major-minor axes. These measurements were compared with the corresponding baseline values and also with log file recorded data to evaluate accuracy. The comparison between Lynx 2D-measured spot parameters and their corresponding baseline values set during initial beamline commissioning showed excellent agreement. Maximum variations in X-axis spot size were 6.5 % at a range of 25.5 g/cm² (gantry angle 270°), while Y-axis variations were 7.31 % at 30.5 g/cm² (gantry angle 30°). Standard Deviations (SD) were below 2.6 % (X-axis) and 3 % (Y-axis), and root mean square errors (RMSEs) were 2.5 % (X-axis) and 2.9

% (Y-axis). Relative positional errors were well within 1 mm, and all variations met the AAPM TG-224 tolerance limits of 10 % for spot size and 1 mm for position, indicating machine stability and measurement reliability.

In contrast, comparisons between log file-recorded and Lynx2D-measured parameters revealed significant discrepancies. Maximum differences in X-spot size (23.90 %) were observed for the range 19.5 g/cm² (gantry angle 90°), and Y-spot size differences (21.04 %) observed for the range 4.1 g/cm² (gantry angle 240°). Both exceeded the TG-224 tolerance of 10 %. Mean differences were 7.64 % (X-axis, SD: 5.62%) and 6.7 % (Y-axis, SD: 4.75 %), with maximum RMSEs of 9.5 % (X-axis) and 8.21 % (Y-axis). Positional errors are marginal to the 1mm tolerance, with maximum errors of 0.910 mm (X-axis) and 1.610 mm (Y-axis). Hence the direct use of log file data for machine QA is limited due to significant discrepancies observed between Lynx2D-measured spot parameters and log file-recorded spot parameters.

ML models, such as Artificial Neural Networks (ANNs), can effectively address the poor correlation between log file recorded data and measured data. These models leverage their ability to handle non-linear relationships and uncertainties, enabling more accurate predictions of spot dosimetric parameters. By bridging the gap between log file data and measured values, ML models enhance the reliability of machine QA and patient-specific QA (PSQA). In the second part of this study, six ANN models using a Multi-Layer Perceptron (MLP) architecture to predict spot size and relative positional error were developed. The Input parameters for model development were log file recorded data and the output parameters were the Lynx2D-measured values. Each model featured one input layer, three hidden layers, and one output layer, with Rectified Linear Unit (ReLU) activation functions and the Adam optimiser. The dataset was split into 70 % training, 15 % validation, and 15% testing subsets. Hyper parameter tuning yielded an optimal configuration: 100 epochs, three hidden layers, 30 neurons per layer, a batch size of 30, and a learning rate of 0.001. The Mean Squared Error (MSE) was used as the loss function. The models were developed using ML libraries TensorFlow and Keras in Python, with validation through metrics such as RMSE, R-squared, scatter plots, and Q-Q plots. Cross-validation (k=5) confirmed robust generalisation, with RMSE values below 0.150 mm and R-squared above 0. 960. The ML models demonstrated high prediction accuracy. For spot size prediction, MSE values were below 0.0028 mm, RMSE was 0.050 mm, and R-squared

was 0.991. Relative positional error models achieved MSE of 0.001 mm, RMSE of 0.035 mm, and R-squared of 0.996. Cross-validation and normality tests validated their reliability and generalisability. The models effectively bridged the gap between the log file data and measured values, enabling their use for QA.

The final part of the study discusses the development and implementation of an in-house script-based tool to integrate log file data extraction and ML models for predicting spot parameters for machine QA and patient-specific QA. The patient treatment beam contains usually thousands of spots. The measurement and analysis of each spot's accuracy is practically impossible and time-consuming. The in-house script automates the analysis of all the spot dosimetric parameters from irradiation log files using ML models. The comparison of the Treatment Planning System (TPS) specified spot parameters with the delivered spot parameters using the automated tool for quick analysis and reporting. It processes the log and specification files to extract spot position and MU values, generating input data for the ML models to predict spot sizes. The script then produces comprehensive reporting of all the spot parameters including the total number of layers, spots per layer, MU values, and the percentage of spots with variations in size, position, symmetry, and MU. It highlights the percentage of spots with less than 10% size variation, 1 mm position variation, below 10 % symmetry, and less than 2 % MU variation. The tool was evaluated using routine QA data and post-irradiation log files from PSQA beams. Routine QA involved 5-spot pattern measurements across 30 energy levels (70.18–226.2 MeV) at 12 gantry angles. Data from 1080 five-spot patterns across three gantries over three months were analysed. For PSQA, log file data from 935 PSQA beams (approximately 3 million spots) were evaluated.

The results of the use of the in-house tool for machine QA data revealed notable discrepancies between measured and log file-recorded spot sizes, with mean differences ranging from 0.7 % to 4.0 % and standard deviations between 6.3 % and 8.6 % across gantry angles. Predicted spot sizes showed closer alignment, with mean differences ranging from 0.5 % to 1.25 % and standard deviations between 0.9 % and 1.6 %. Predicted spot symmetry deviated by less than 1 % from the measured values, and MU differences were within 1 % of the specified values.

Analysis of 935 PSQA beams revealed promising results. Over 99.5 % of spot positions were within 1 mm accuracy. Mean positional errors were -0.021 mm (SD: 0.181

mm) along the X-axis and -0.002 mm (SD: 0.132 mm) along the Y-axis. ML models maintained strong performance in predicting spot sizes, with over 95 % of spots showing variations within 10 % of baseline values. RMSEs for spot size differences were 0.15 mm (X-axis) and 0.16 mm (Y-axis). Spot symmetry was within 10 %, and MU accuracy showed that 95 % of spots had variations below 2 %.

This study highlights the effectiveness of integrating ML models with log file data to enhance the QA process in PBS proton therapy. By combining ML-based predictive models with an in-house tool, this approach provides an efficient and reliable alternative to traditional QA methods. The automation of log file analysis, prediction of spot parameters, and evaluation of dosimetric accuracy for both routine and PSQA significantly improves workflow efficiency, reduces the time required for QA, and minimizes the reliance on dedicated dosimeters. The strong correlation between ML predictions and dosimeter measurements, within established tolerance limits, further underscores the potential of this integrated tool to optimize dosimetric precision, enhance patient safety, and streamline the QA process, ultimately reducing the need for extensive manpower and improving overall operational efficiency in proton therapy.

Chapter 1

Introduction

Chapter 1- Introduction

1.1. Radiotherapy

Radiotherapy is an advanced cancer treatment modality that employs high-energy radiation to destroy or damage cancer cells [1]. This treatment approach originated in the early 20th century after Wilhelm Conrad Roentgen discovered X-rays in 1895 and the subsequent realization of their potential in cancer treatment. Radiotherapy works by directing radiation at cancer cells, damaging their deoxyribonucleic acid (DNA) and hindering their ability to replicate [2]. Healthy cells can typically recover from this damage, whereas cancer cells struggle to repair themselves, ultimately leading to death. Radiotherapy can be employed on its own or in combination with other treatments, such as surgery, chemotherapy, and immunotherapy, to enhance its effectiveness. Over time, technological and technical advancements have significantly enhanced radiotherapy's precision, effectiveness, and safety. A review by Chandra R. A. et al. [3] examined the advancements in radiotherapy techniques and imaging technologies in the current era. The introduction of techniques like Three-Dimensional Conformal Radiation Therapy (3D-CRT) and Intensity-Modulated Radiation Therapy (IMRT) has enabled more precise targeting of tumours, reducing unnecessary radiation exposure to surrounding healthy tissues [4]. Advanced imaging techniques, such as Computed Tomography (CT), Magnetic Resonance Imaging (MRI), and Positron Emission Tomography (PET) scans, are employed to locate the tumour and guide radiation delivery accurately [5]. Radiotherapy is a continually evolving field driven by ongoing research and technological advancements to improve therapeutic effectiveness and minimize side effects. This progress highlights the essential role of radiotherapy in the multidisciplinary treatment of cancer, providing hope and better outcomes for patients globally.

Radiotherapy employs a range of advanced techniques and modalities to enhance cancer treatment, including both conventional photon therapy and advanced particle therapy. For many years, conventional photon therapy, primarily X-rays and γ-rays, has been the cornerstone of radiotherapy. It uses linear accelerators to produce high-energy photons that penetrate tissues, targeting the tumour and affecting nearby healthy tissues. Techniques such as 3D-CRT and IMRT have enhanced the accuracy of photon therapy by shaping the radiation dose to match the tumour and adjusting the beam intensity accordingly. However, due to the inherent properties of photons, some radiation inevitably

passes through the tumour and continues to deposit energy in the surrounding healthy tissues, which can cause side effects [6]. Despite this limitation, photon therapy remains highly effective for treating various types of cancer and is widely accessible. In contrast, advanced particle therapy, such as proton and carbon ion therapy, provides superior dose distribution because of the unique characteristics of charged particles [7]. These particles have the distinct advantage of the Bragg peak, where the highest energy deposition occurs just before the particles stop, enabling a highly localized delivery of radiation with minimal exit dose. Proton therapy is especially beneficial for treating tumours located near critical structures or in paediatric patients, as it minimizes the risk of radiation-induced secondary cancers [8-10]. Carbon ion therapy, which has a higher linear energy transfer (LET), inflicts more complex and irreparable DNA damage on cancer cells [11]. The increased biological effectiveness of carbon ions allows for greater tumour control with potentially fewer treatment sessions. As a result, although conventional photon therapy is still widely used and effective for many types of cancer, particle therapy marks a significant advancement by offering greater precision and reduced toxicity. A study by Tinganelli W. et al. [12] found that the radiobiological features of carbon ion therapy are more effective in treating radio-resistant hypoxic tumours. This expands the therapeutic window and improves patient outcomes. Additionally, integrating advanced imaging techniques and real-time monitoring enhances the accuracy and safety of both photon and particle therapies, highlighting the ongoing evolution of radiotherapy in the quest for better cancer treatment. Figure 1.1 illustrates the differences in dose distributions across various radiotherapy modalities for a prostate cancer patient.

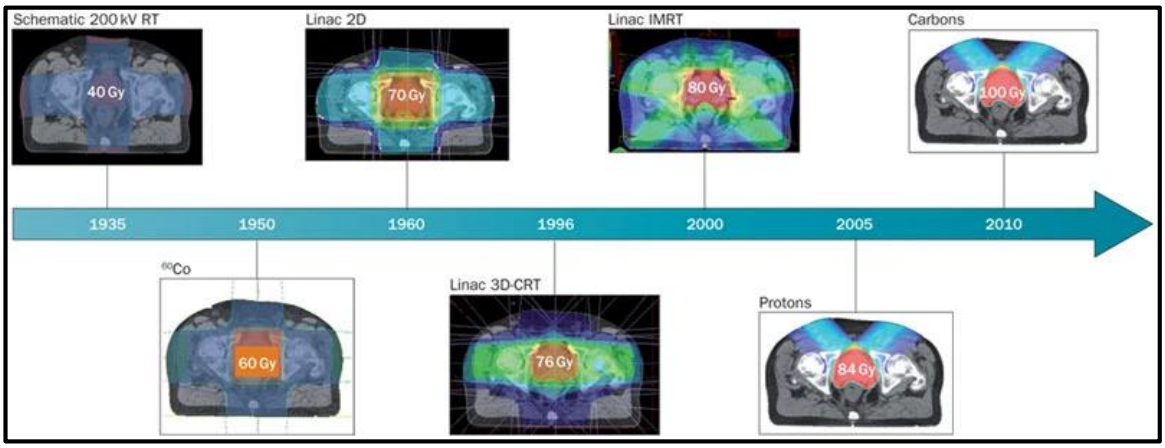

Figure 1.1: Evolution of Radiotherapy Treatment Planning from 1935 to 2010, Demonstrating Dose Distributions for Prostate Cancer Using Various External Radiation Therapy Modalities from 200 kV X-ray to Carbon Ions (Thariat, J et al 2013 [1]).

1.2 Particle therapy

The use of accelerated protons, carbons, or other heavy ions for cancer treatment is called particle therapy [13-14]. The protons and heavy ions interact with matter and deposit maximum energy in the Bragg peak position. The maximum dose deposition by the sharp Bragg peak ensures tumour dose coverage and better normal tissue sparing than conventional photon-based radiotherapy. The high Radio Biological Effect (RBE) and LET near the Bragg peak provide additional biological advantages to particle therapy. Currently, proton and carbon ion therapy are the advanced particle therapy systems used worldwide.

1.2.1 Proton therapy

The therapeutic use of protons was introduced by Wilson et al. In 1946 [15]. The physical properties, such as Bragg peak and zero exit dose, enhanced the application of proton therapy. Currently, there are more than 100 centres that use proton therapy for cancer treatment. Most proton therapy systems use cyclotron or synchrotron-based particle acceleration and dedicated energy selection and transport systems to ensure accurate dose delivery to the patient. Passive scattering and Pencil Beam Scanning (PBS) techniques are the most used proton therapy delivery techniques [16]. In the passive scattering system, the mono-energetic proton beam passes through scattering foils and a rotating range modulation wheel to create a uniform beam in the lateral direction, and the target conformity in the longitudinal direction is ensured by patient-specific range compensator and collimator used for lateral field conformity. The technique is widely used for treating many treatment sites [17]. However, passive scattering has disadvantages, such as needing patient-specific and beam-specific range compensators and collimators. This increases treatment time and lateral penumbra due to secondary particles from interactions with the range modulator and scattering materials.

The Paul Scherrer Institute (PSI) introduced the PBS technique of particle therapy [18]. The PBS technique uses different technology compared to passive scattering. In a cyclotron-based PBS system, the mono-energetic proton beam produced by the cyclotron passes through a dedicated degrader wheel with varying blocks of materials which produce different energy proton beams. A proton beam with an energy range of 70 MeV to 250 MeV is commonly used for clinical treatment [19]. The mono-energetic pencil beams pass through an energy selection system and many dipole and quadrupole magnets to ensure

proper beam size, energy and position. Finally, the pencil beams enter the gantry head called the nozzle. The nozzle has two scanning magnets, which defect each pencil beam to different X and Y directions to cover the tumour lateral shape and deliver different energy pencil beams to ensure longitudinal dose conformity to the tumour. Compared to a passive scattering system, the PBS system does not require dedicated range compensators and collimators. The Spread-Out Bragg Peak (SOBP) is created by overlapping multiple mono-energetic proton beams to cover the tumour volume and ensure minimal dose to surrounding normal tissues. The PBS technique is a very fast and conformal treatment compared to passive scattering systems.

1.2.2 Carbon ion therapy

The accelerated carbon ions interact with matter in a way that is almost similar to proton beams. However, the carbon ions have a sharper Bragg peak width and higher RBE and LET distribution than proton therapy. Carbon ions are used for radiotherapy because of their physical and biological properties. The invention of the Synchrotron by Vladimir Veksler [20] in 1944 boosted the use of particles for radiation therapy. The first carbon ion therapy was done by the Heavy Ion Medical Accelerator in Chiba (HIMAC) in 1994 [21]. Due to the high LET and RBE of carbon ions, the damage created by carbon ions clustered in DNA overwhelms the cellular repair system. The carbon ion therapy also uses passive scattering and active scanning systems for beam delivery. Carbon ion therapy is very efficient for dose escalation to radio-resistant tumours.

1.2.3. Helium and other heavy ion therapy

The helium ion shows intermediate physical and biological properties between proton and carbon ion therapy. The lateral penumbra and range straggling are less with helium ions than protons and high RBE and LET. The first Helium ion therapy started at Lawrence Berkeley National Laboratory (LBNL) in 1994 [22]. The Heidelberg Ion Beam Therapy Centre (HIT) have started raster scanning helium ion therapy [23]. The high cost of construction and operation of particle therapy is the limiting factor of particle therapy. Protons and carbon ions gain popularity in particle therapy in the early 90's. Between 1975 and 1992, the potential of various heavy ions, including helium, pions, neon, and argon, was investigated for radiotherapy in a laboratory setup at the LBNL [24]. Currently, only protons, carbon, and helium ions are used in clinical radiotherapy. In the future, advancements in technology and reductions in cost are expected to expand the use of other

heavy ions in particle therapy. Figure 1.2 represents the depth dose distribution of different particles used for particle beam therapy.

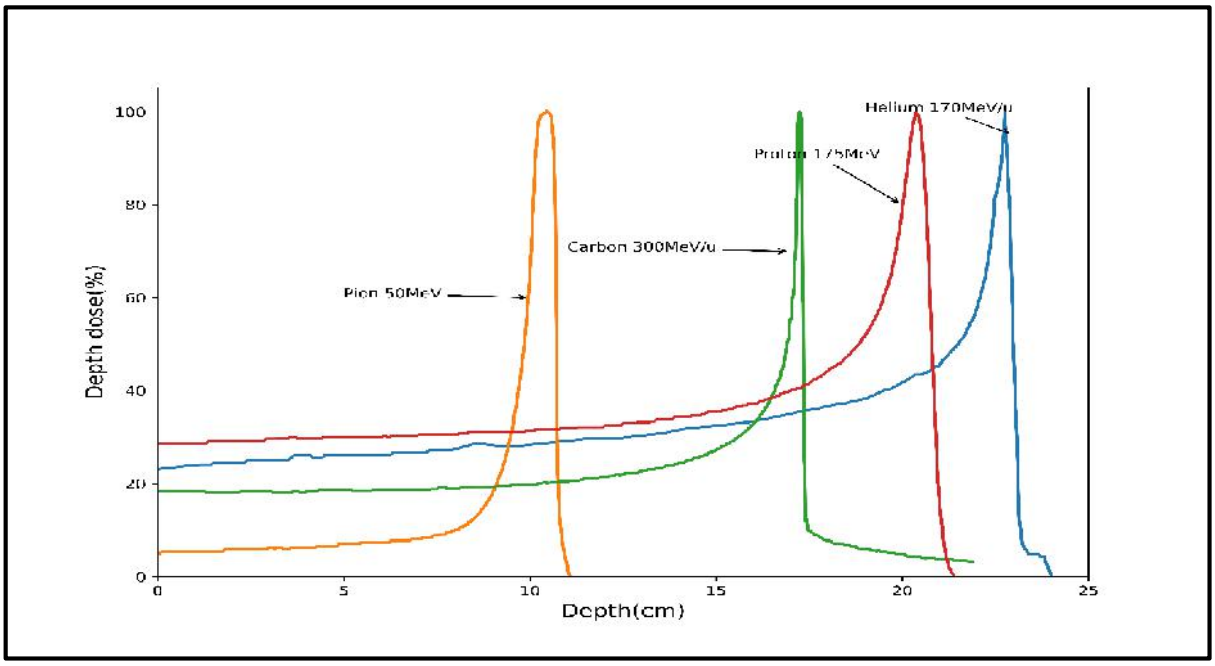

Figure 1.2: The depth dose distribution of different charge particles used for particle therapy. Pion 50MeV, Carbon ion 300MeV/u, Proton 175MeV, and Helium 170MeV/u.

1.3 Pencil Beam Scanning Proton Therapy System

The introduction of the PBS technique in proton therapy has significantly enhanced the utility of proton therapy through various technological advancements. PBS allows for highly precise and accurate dose delivery by scanning a narrow proton beam across the tumour in a controlled manner, reducing the treatment time and improving efficiency. PBS also offers superior accuracy in targeting tumours, especially those with complex shapes or located near critical structures, minimizing damage to surrounding healthy tissues. These benefits make PBS a superior and more efficient option in modern proton therapy, offering improved treatment outcomes and a better quality of life for patients.

The PBS proton therapy technique utilizes two types of particle accelerators for proton beam production: Cyclotrons and Synchrotrons. Most commercial systems employ cyclotron-based systems for beam production. However, centres that use multiple particles for therapy typically use synchrotrons for beam production. Figure 1.3 shows the IBA Proteus Plus machine treatment room. The dosimetric data measurement for this thesis was obtained from the IBA Proteus Plus proton therapy machine installed at ACTREC, Tata Memorial Centre, Mumbai. The Proteus Plus uses an isochronous cyclotron. The system

has multiple components, including the Beam Production System (BPS), Energy Selection and beam Transport System (ESBTS), and Beam Delivery System (BDS).

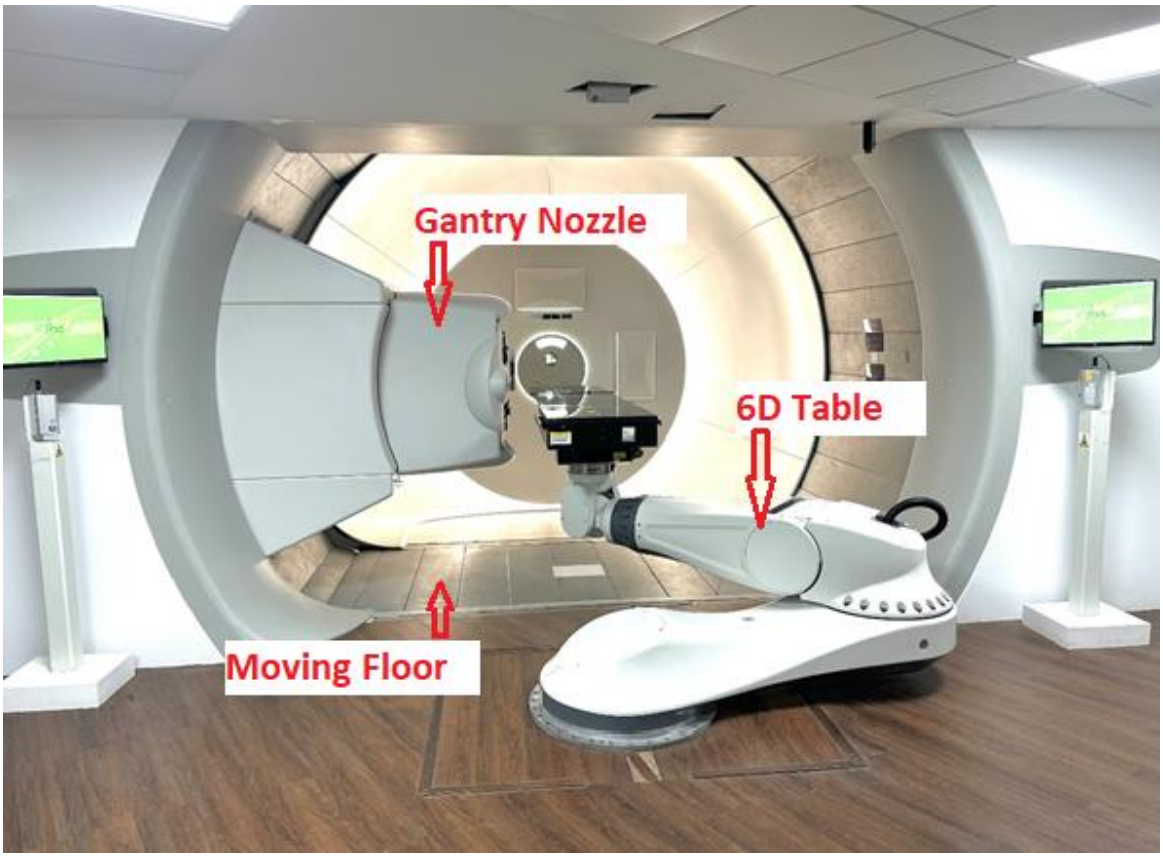

Figure 1.3: The IBA Proteus Plus treatment gantry installed at National Hadron Therapy Centre, ACTREC, Tata Memorial Centre, Mumbai.

1.3.1 Beam production system (BPS)

The BPS predominantly consists of the cyclotron and the beam extraction system. The 230 MeV isochronous cyclotron accelerates protons to high energies utilizing a combination of magnetic and electric fields (Figure 1.4). Protons, introduced from a hydrogen gas ion source into the cyclotron's central region, are constrained to move in circular orbits by a static magnetic field. An alternating electric field, produced by two D-shaped electrodes (Dees), accelerates the protons each time they traverse the gap between the Dees [25]. The isochronous design ensures that the magnetic field strength increases with radius, maintaining a constant cyclotron frequency for protons at all radii. This synchronization enables the protons to gain energy and spiral outward until they reach 230 MeV. Upon reaching this energy, the protons are extracted via a deflector, which diverts them from their circular trajectory into the energy selection and transport system. The

cyclotron can extract a maximum beam current of 300 nA and a minimum current of 1 nA. Key components include the ion source, Radio Frequency (RF) source, main coil, and deflector.

The RF system generates the alternating electric field necessary for proton acceleration. It includes RF cavities, or Dees, positioned within the cyclotron's vacuum chamber. The RF system produces an oscillating electric field between the Dees, with an oscillator generating a signal that matches the cyclotron's resonance frequency. This ensures that the electric field oscillates in synchrony with the protons' circular motion. RF amplifiers then boost this signal to the power required to create a sufficiently strong electric field to effectively accelerate the protons with each pass through the Dee gap.

Figure 1.4: The Cyclotron C230 installed at National Hadron Therapy Centre, ACTREC, Tata Memorial Centre, Mumbai.

The main coil produces the magnetic field that confines protons to their circular paths during acceleration. This is achieved with large electromagnets forming the main coil, which generates a uniform magnetic field perpendicular to the proton's plane of motion. Powered by a high-current supply, the main coil maintains the necessary magnetic field strength for proton guidance throughout the acceleration process. After acceleration,

the proton beam is deflected by a dedicated deflector, passes through quadrupole magnets, and proceeds to the energy selection system.

1.3.2 Energy Selection and Beam Transport System (ESBTS)

The ESBTS is responsible for converting the 230 MeV fixed-energy beam produced by the cyclotron into a variable energy beam, adjustable between 70.18 MeV and 226.2 MeV. Additionally, the energy selection devices in the ESBTS are designed to block unwanted beam particles from proceeding through the beam line. They also verify and regulate the absolute energy, energy spread, and emittance of the beam as it exits the energy selection section and enters the static beam line. This control is achieved using a combination of quadrupole and dipole magnets, along with an energy degrader, collimators, and slits.

The degrader wheel is a rapidly adjustable, servo-controlled rotating variable-thickness cylinder. The diagram of the degrader wheel is given in figure 1.5. The purpose of the degrader wheel is to degrade the energy of the beam produced from the cyclotron to the clinically required energies, which range from 70.18 MeV to 226.2 MeV. The rotation of the wheel is synchronized to pass the proton beam through the variable thickness portion of the wheel. The beam energy is changed in function of the variable thickness of the block of absorbing material. The total time needed to adjust the degrader's orientation to achieve different beam energies is less than one second. This adjustment is facilitated by a stepper motor that controls the degrader's rotation.

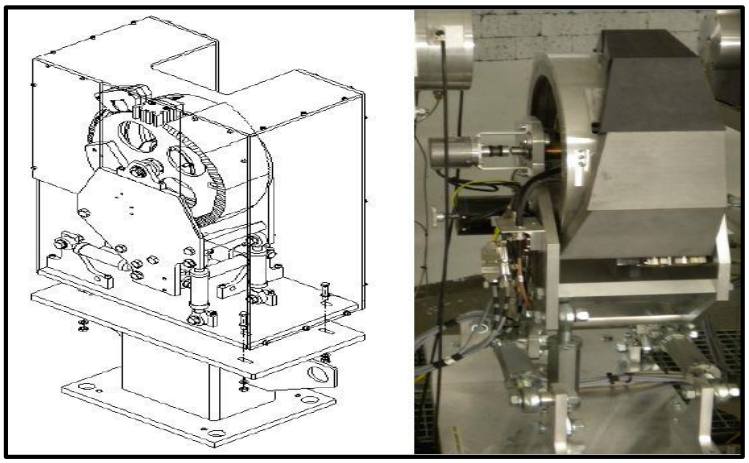

Figure 1.5: The Degrader wheel with different density materials to degrade energy from 226.2MeV to 70.18 MeV (Picture courtesy to IBA user Manual).

After adjusting the beam energy with the degrader wheel, the beam will exhibit divergence and angular spread. Dedicated slits and a collimator assembly are employed to eliminate beams that are too off-centred or have excessively large divergence angles. Following the collimator assembly, the beam passes through multiple quadrupole and bending magnets to reach the beam delivery system. The quadrupole magnets ensure the beam remains centred in the beam-transporting tube, while the bending magnets redirect the beam as needed. Finally, the beam enters the beam delivery system. The figure 6 shows the components in the energy transport system of the IBA Proteus Plus machine.

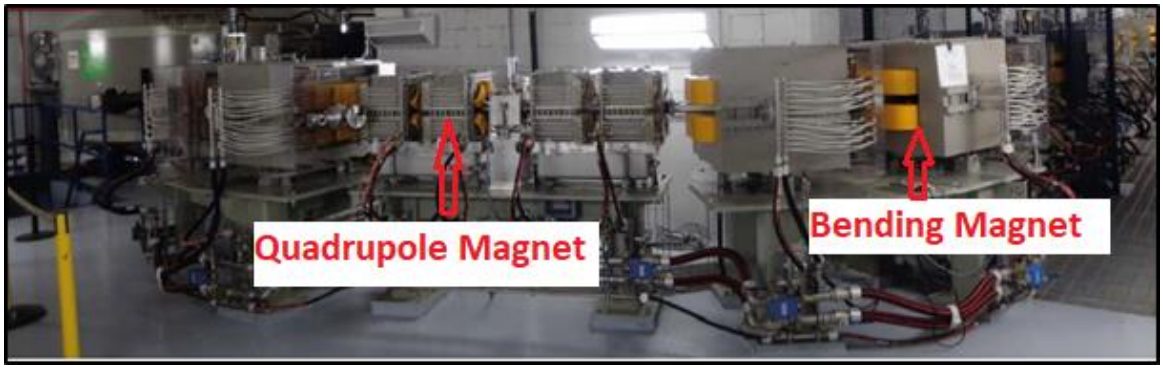

Figure1.6: The energy selection system of the IBA Proteus Plus machine.

1.3.3 Beam Delivery System (BDS)

The BDS consists of a rotating gantry and a nozzle. The beam transport line connects to the rotating gantry using a coupler known as a rotary feedthrough. Figure 1.7

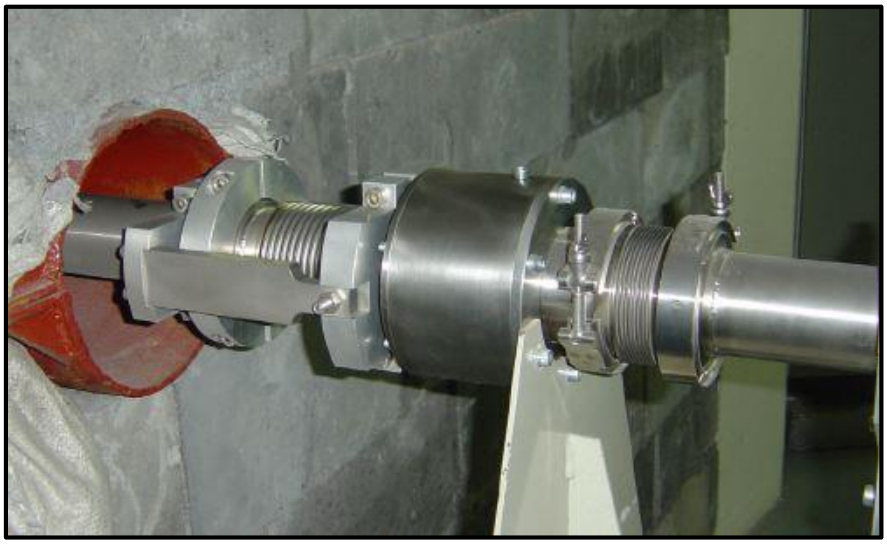

Figure 1.7: Rotary feedthrough.

shows the rotary feedthrough accessory. This rotary feedthrough provides a vacuum coupling that allows the static beamline to transition into a rotating beamline, which is essential for the gantry's rotation.

Once the beam enters the rotating gantry, it encounters multiple quadrupole magnets that focus the beam. A 135^0 large bending magnet then bends the beam, directing it towards the nozzle. The entire gantry assembly is capable of 360^0 rotations and is connected to a rotating assembly, allowing for precise beam direction and flexibility in treatment angles. Figure 1.8 represents the rotating gantry assembly.

The nozzle consists of an initial Ionization Chamber (IC1), followed by a quadrupole magnet. The IC1 monitors the spot position accuracy to ensure precise targeting. The quadrupole magnet focuses the beam along the central line. After the quadrupole magnet, there are two scanning magnets used to deflect the pencil beam in the X and Y directions as required for patient treatment. The deflected beam then passes through another set of ICs known as IC23. The IC23 monitors record the spot size and position of each beam spot. Finally, the beam is delivered to the patient, who is positioned using the patient positioning system to ensure accurate and effective treatment.

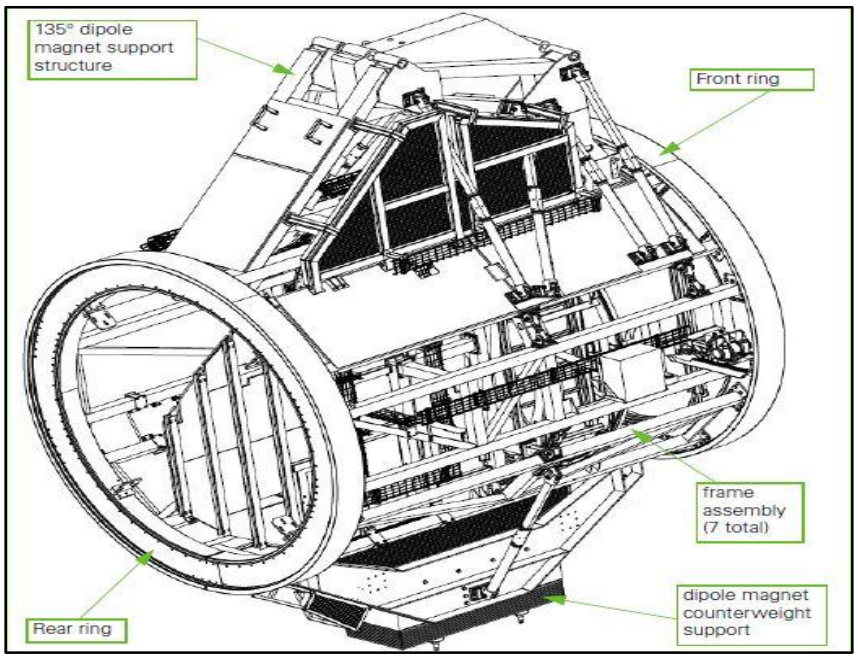

Figure 1.8: The Schematic Diagram of the rotating gantry. The bending magnets and rotating system are depicted in the figure (Picture courtesy to IBA user Manual).

1.4 Quality Assurance of Pencil Beam Scanning Proton Therapy

Quality assurance (QA) in PBS proton therapy is essential for ensuring accurate and safe treatment administration [26]. The QA process encompasses thorough evaluations and adjustments of the proton beam's energy, intensity, and spatial accuracy. This includes routine machine performance assessments, verification of patient-specific treatment plans, and dosimetric evaluations using sophisticated detectors and imaging technologies. Accurately controlling the proton beam's parameters is crucial for optimising tumour eradication while minimising harm to surrounding healthy tissues. Comprehensive QA procedures are vital for detecting and rectifying any discrepancies from the prescribed treatment plan, thereby ensuring optimal patient outcomes and upholding the high standards of proton therapy.

The American Association of Physicists in Medicine (AAPM) Task Group (TG) 224 report [27] recommends standardized QA procedures for PBS proton therapy systems. The report outlines QA protocols to be performed on a daily, weekly, monthly, and annual basis to ensure the optimal performance and safety of the proton therapy system. Specifically, the report highlights the importance of monitoring key dosimetric parameters for PBS systems. These include the energy of each proton beam, the spot size in both the X and Y directions, spot symmetry, spot position accuracy, and dose accuracy. Regular checks and calibrations of these parameters are essential to maintain the precision and effectiveness of PBS proton therapy, ensuring that the treatment is delivered accurately and consistently to achieve the best possible patient outcomes.

1.4.1 Mechanical QA

Mechanical QA in PBS proton therapy includes the performance evaluation of all mechanical parts, such as the patient positioning system, gantry, snout, imaging system, and laser system. Specifically, it involves assessing the gantry angle accuracy of the rotating gantry, the snout position accuracy, and the table translational and rotational movement accuracy. Additionally, the accuracy of the laser system and its coincidence with the machine isocentre must be evaluated to ensure proper patient positioning.

The mechanical accuracy of each component is crucial to ensuring accurate patient positioning before beam delivery. This precision is vital for delivering the proton beam to the exact location as planned, minimizing radiation exposure to surrounding healthy

tissues. Mechanical QA is integral to the daily, monthly, and annual QA protocols for PBS systems. Regular testing and verification of mechanical components help maintain the high standards required for effective and safe proton therapy treatments. By adhering to stringent mechanical QA procedures, PBS proton therapy systems can achieve the precise and conformal radiation doses necessary for optimal patient outcomes.

1.4.2 Dosimetric QA

The dosimetric QA in a PBS system includes the measurement of beam energy, spot size, spot position, and output. Any variation in the range of each spot in the PBS beam can lead to a shift in the Bragg peak position. If the actual range is less than the set value, the distal edge of the target will be under-dosed. Errors in the range can result in significant dose differences at the target's distal edge. Similarly, variations in spot size can cause inhomogeneous dose distributions, leading to underdoing or overdosing within the target volume. Regular and accurate dosimetric QA ensures that the proton therapy system delivers the correct dose distribution as planned, maintaining the effectiveness and safety of the treatment. By meticulously measuring and verifying these parameters, any deviations can be identified and corrected promptly.

1.4.3 Range or Energy

The energy of a proton beam refers to its initial kinetic energy, which determines how deeply the beam can penetrate tissue. As the energy of the protons increases, their penetration depth also increases. The relationship between the energy and the range of the proton beam is directly proportional, meaning that higher-energy protons achieve greater depths. The range is defined as the distal depth where 90% of the proton beam's energy is deposited. This relationship between range and energy can be quantitatively described by a specific equation (Equation 1.1).

$$Range(cm) = Exp(a * \ln(E)^3 + b * \ln(E)^2 + c * \ln(E) + d) \quad (1.1)$$

Where, E- Energy in MeV. a, b, c and d are the coefficients. a=-0.0133, b=0.15248, c=1.2193, and d=-5.5064.

The range of each energy pencil beam in proton therapy is typically measured using large-area parallel plate ionization chambers through two main methods. The first method

involves a single parallel plate chamber to measure dose at various depths and plot the integrated depth dose (IDD) curve, from which the R90 range the depth where 90% of the proton's energy is deposited is determined. The second method employs a Multi-Layer Ionization Chamber (MLIC), a specialized array detector with multiple stacked chambers that simultaneously measures dose at different depths. The data from the MLIC is combined to produce the IDD curve and determine the proton range.

1.4.4 Spot size

In pencil beam scanning proton therapy, determining the spot size of the beam is essential for accurately delivering radiation doses to tumours while minimizing damage to surrounding healthy tissues. The pencil beam typically exhibits a Gaussian distribution of intensity, where the intensity is highest at the centre and decreases symmetrically when moving away from it. Figure 1.9 plots the Gaussian distribution of the spot. In PBS, the spot size is defined by the width of one standard deviation (σ) or sigma of this Gaussian distribution, called sigma. The spot size is typically measured in air using dedicated scintillator detectors. Equation 1.2 shows the relationship between Full Width Half Maximum (FWHM) and sigma.

$$FWHM = 2.355\,\sigma \tag{1.2}$$

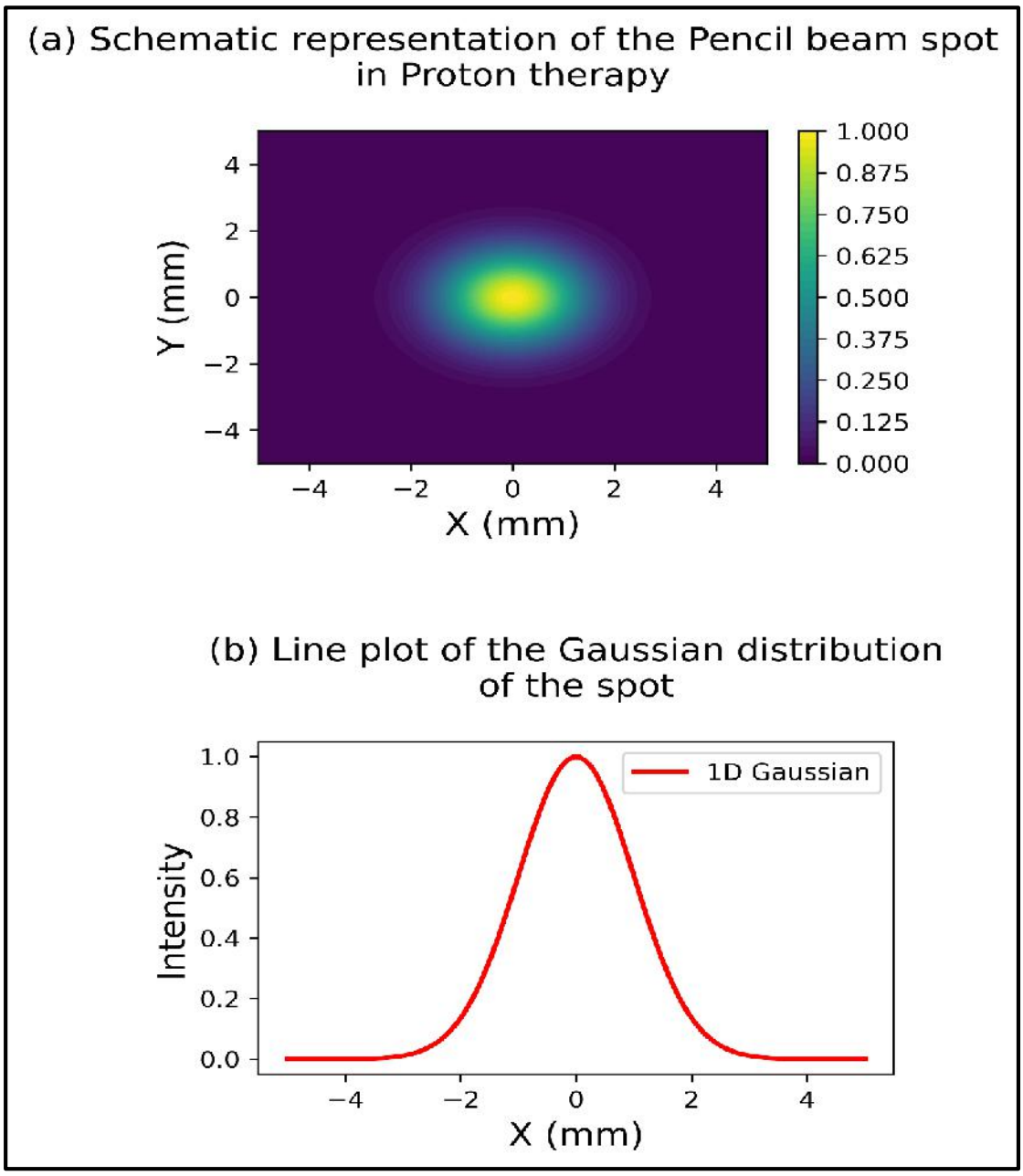

Figure 1.9: The representation of the spot size of a Pencil Beam Scanning (PBS) Proton therapy beam. (a) Schematic representation of a typical spot in PBS, (b) 1D Gaussian distribution of the spot.

The spot size is energy-dependent. For lower energy beams, the spot size is larger due to increased lateral scattering of protons in air. In contrast, for higher energy beams, the spot size is smaller because there is less lateral scattering. This energy dependence must be considered in treatment planning to ensure accurate dose delivery and effective tumour targeting.

1.4.5 Patient-Specific QA

The patient-specific QA (PSQA) is the procedure to ensure the dose delivery accuracy of each patient treatment plan before the start of actual treatment. The PSQA compare the dose distribution calculated in the Treatment Planning system (TPS) with the dose distribution measured using dedicated dose measurement devices. The conventional method of PSQA in a PBS system is to measure dose fluence using a dedicated ionisation array detector compare the fluence with the TPS dose fluence and perform gamma analysis [28]. Gamma analysis is a process of comparing two dose fluence matching. It utilizes two main criteria: Distance-to-Agreement (DTA), which assesses the spatial proximity of measured and planned dose points, and Dose Difference (DD), which evaluates the discrepancy in dose levels. The results are represented as a gamma index, where a passing rate indicates successful treatment delivery.

In the PBS system, the conventional method of PSQA involves measuring dose fluence using a dedicated ionization array detector. This method compares the 2D fluence measured for individual beams. A study by Zhu XR et al. [29] involving 249 prostate cancer patients treated with a spot-scanning proton therapy system found that the gamma index was greater than 96% for all patients when performing PSQA with a 2D detector array. Another method of PSQA is Monte-Carlo (MC) based independent dose calculation algorithms [30-31].

1.5 Log file analysis

Log files in radiotherapy are vital records that capture comprehensive data on various parameters and events during each beam irradiation session. These logs include details such as machine settings, beam characteristics, patient information, and system events. The use of log files in radiotherapy includes analysis of the accuracy of beam delivery, statistical data analysis and also used for retrospective data analysis and audit. They allow for the identification of trends or patterns that may indicate issues with treatment delivery or equipment performance. In the event of an incident or adverse outcome, log files can serve as an essential resource for investigating the root cause and implementing corrective actions.

Log files play a critical role in photon therapy by recording detailed information about the treatment delivery process. These files capture the positions of Multi-Leaf

Collimators (MLCs) at each control point, the monitor units (MU) delivered for each MLC segment, and the gantry and collimator angles, along with other beam-related parameters. Numerous studies have leveraged these log files in conjunction with MC simulations for routine QA and PSQA [32-33].

Similarly, in proton therapy, log files are equally essential as they document vital data regarding the beam's energy, position, and various delivery parameters. This information is crucial for ensuring the precision and accuracy of the treatment. The potential of log files as a tool for routine QA and PSQA in proton therapy is increasingly recognized.

In PBS proton therapy, log files capture data at intervals of every 200 microseconds, resulting in extensive records for each spot. Each spot's log file may contain multiple rows of data detailing parameters such as the position and size of the spot as measured by different transmission ICs, the current and voltage of scanning magnets, the charge collected in primary and secondary dose meters, the beam current, and the set range value. After each spot is delivered, these parameters are meticulously recorded. The spot position and MU data are particularly valuable, as they can be used to independently re-calculate the delivered dose using MC algorithms. The log file data is used for a detailed audit of the beam delivery. One limitation of log file data is the inherent uncertainty associated with the recorded information. This uncertainty can impact the accuracy of dosimetric evaluations and QA processes that rely on log files. Therefore, further studies are required to mitigate these uncertainties, allowing log file data to be used more effectively and confidently in accurate dosimetric assessments and QA in proton therapy.

1.6 Machine Learning models

Machine Learning (ML) is a subset of Artificial Intelligence (AI) that focuses on developing algorithms and statistical models that enable computers to learn from and make predictions based on data. According to Rahmani AM et al [34], ML is a field of study that allows computers to learn without being explicitly programmed. Instead of being explicitly programmed to perform a task, ML systems use patterns and insights derived from existing data to improve their performance over time. ML involves training a model on a dataset, allowing it to identify relationships and patterns. Once trained, the model can be applied to

new, unseen data to make predictions or decisions. There are several types of ML, including supervised learning, unsupervised learning, and reinforcement learning.

1.6.1 Supervised Learning

Supervised learning is an ML approach where models are trained on labelled data, pairing input with the correct output to make accurate predictions on new data [35]. This technique finds broad application across various fields, such as image classification, where models categorize images into predefined groups, or spam detection, where systems differentiate between spam and non-spam emails using labelled examples. In sentiment analysis, models learn to classify text sentiment, while predictive maintenance uses labelled sensor data to foresee equipment failures. Medical diagnosis models, trained on labelled patient data, aid in disease identification, and speech recognition systems convert spoken language into text. Fraud detection and house price prediction also benefit from supervised learning, using labelled data to flag suspicious activities and estimate property values. In radiotherapy, supervised learning enhances treatment accuracy, efficiency, and QA. Models are trained to segment tumours and Organs-At-Risk (OARs) in imaging scans using manually labelled data, optimise radiation distribution through dose prediction models, and automate treatment planning based on historical cases. Additionally, supervised learning is crucial in predicting patient outcomes and identifying potential errors in treatment delivery by analyzing log files, ensuring precise and effective radiation delivery. These applications streamline radiotherapy processes, leading to more accurate treatments and improved QA.

1.6.2 Unsupervised Learning

This method involves training models on data without labelled outcomes. The goal is to identify patterns or groupings within the data, such as clustering similar data points together [36]. Unsupervised learning is a powerful tool in radiotherapy, enabling the discovery of patterns and relationships in data without the need for labelled examples. It is particularly useful for clustering patient data based on characteristics like tumour type or treatment response, which can inform personalized treatment strategies. In QA, unsupervised learning helps detect anomalies in treatment delivery by identifying deviations from expected patterns, enhancing safety. Additionally, dimensionality reduction simplifies complex imaging data, making it easier to analyse and visualize. Unsupervised learning also aids in feature extraction from medical images, identifying

regions of interest that are crucial for treatment planning, ultimately contributing to more effective and individualized radiotherapy.

1.6.3 Reinforcement Learning

In this type of learning, an agent interacts with an environment and learns to make decisions by receiving rewards or penalties based on their actions. The agent aims to maximise its cumulative reward over time [37]. Reinforcement learning is increasingly valuable in radiotherapy for optimizing treatment strategies through trial and error. This approach involves training models to make decisions by receiving feedback in the form of rewards or penalties based on their actions. In radiotherapy, reinforcement learning can be used to enhance treatment planning by learning from simulations to determine the most effective radiation doses and delivery techniques. For instance, it can optimize dose distribution by continuously adjusting parameters to minimize damage to healthy tissues while maximizing tumour targeting. Additionally, reinforcement learning is applied to adapt treatment plans in real time based on patient responses and evolving clinical conditions. This method improves the precision and efficacy of radiotherapy by enabling dynamic adjustments and personalized treatment approaches.

1.7 Research Problem

Proton beam therapy represents a cutting-edge advancement in radiotherapy, utilizing the PBS technique that involves irradiating thousands of proton pencil beam spots to target tumours precisely. The PBS system involves a highly sophisticated process of beam production using a cyclotron, followed by precise beam selection and transport. This is achieved through intricate components, including multiple quadrupole magnets for focusing and bending magnets for beam steering. Additionally, the system incorporates complex beam-tuning mechanisms and dosimeters to ensure precise control over beam parameters. However, the intricate nature of the PBS technique necessitates systematic and rigorous QA methods. Conventional PBS-QA methods are fraught with challenges. They typically use dedicated dosimeters to measure critical parameters such as energy, spot size, position, symmetry, and MU accuracy. These conventional methods are time-consuming and labour-intensive, posing a significant burden on physicists and dosimetrists. The conventional methods' inherent complexity and the extensive effort needed highlight the

need for more efficient solutions to streamline the machine QA and PSQA processes in proton beam therapy.

In recent years, numerous studies have explored using log files in photon and proton radiotherapy systems. Siochi et al. [38] utilised log files from a photon therapy linear accelerator to automate the physics checks for plan delivery accuracy. Similarly, Rangaraj D et al. [39] investigated the effectiveness of Linac log file data for analysing data transfer and evaluating beam delivery accuracy across 914 patient cases. Many other studies [40-41] have also assessed the potential of irradiation log file data for machine performance evaluation. This approach significantly reduces the time required compared to traditional measurement methods. Another use of log file data in photon therapy is to verify the accuracy of MLC leaf positions and MU. Stell AM et al [42] and Chow V.U. et al. [43] studied the accuracy of log file-recorded MLC positions and MU compared with the values specified by the TPS. Their results are promising and contribute significantly to the automation of quality assurance for Linac. Apart from the application in routine QA, the log files are used PSQA in Linac. The MC algorithm computed the delivered dose using the log file recorded MLC positions and MU information. The results are comparable to the measurement-based PSQA [44,45]. The potential use of log files in Linac-based photon radiotherapy is well-established for routine and patient-specific QA.

The log file data is also used in the PBS proton therapy to compare the spot position and MU values with the TPS-specified values. A study by Li H et al [46] concludes that the log file recorded spot position and MU values are accurate and precise enough to use for routine QA. Later many studies used the log file recorded spot position and MU values for evaluating the PBS beam delivery accuracy using the MC algorithm to calculate the delivered dose and compare it with the planned dose for PSQA [47,48]. All the studies used only spot position and MU information from the log file for dose evaluation. The spot size and symmetry are also a critical parameter that can cause dose differences if the values deviate from the baseline values. Also, there are no studies to mitigate the uncertainties associated with log file data. A study by, Rana S et al [49] evaluated the dose difference with different percentage differences in spot size. The spot size variation of more than 10 % from the baseline causes a significant dose difference. The evaluation of all spot dosimetric parameters such as spot size, symmetry, position, and MU is important to ensure machine beam delivery accuracy as well as patient treatment accuracy.

The existing research on log file data in PBS proton therapy has primarily focused on spot position and MU information, leaving significant gaps in the analysis of other crucial spot parameters. Few studies have examined the accuracy of log file data or explored its correlation with values measured by dedicated detectors. Additionally, there is limited research addressing methods to mitigate uncertainties in log file data used for machine and PSQA. These gaps hinder the reliability and effectiveness of log file data in QA processes, which are essential for ensuring precision and safety in proton therapy.

To date, there has been limited development of a comprehensive method to analyse the dosimetric accuracy of each spot used in patient treatment, particularly for spot size, symmetry, MU, and position. This presents an exciting opportunity to establish a systematic approach for evaluating these critical parameters, ensuring enhanced precision and reliability in proton therapy

Contemporary research increasingly emphasises the potential of ML applications in radiotherapy QA. ML models offer a promising solution by automating QA tasks in proton therapy, including machine QA and PSQA, utilizing the vast amounts of data captured in log files. By doing so, ML can reduce the time and manpower required for QA processes while improving the accuracy of dosimetric predictions and addressing uncertainties. Despite this potential, the use of ML in this context remains underexplored, presenting a valuable opportunity to enhance treatment outcomes and streamline workflows in proton therapy.

1.8 Objective of the study

This study focuses on implementing ML to automate QA protocols in PBS proton therapy. The irradiation log file is a potential tool for developing various ML models to automate machine QA and PSQA workflow. The study begins with the measurement of spot dosimetric parameters and analysis of the corresponding log file data recorded in the IBA Proteus Plus PBS proton therapy system installed at Advanced Centre for Treatment Research and Education in Cancer(ACTREC), Tata Memorial Centre, Mumbai, India. during beam irradiation and studies the correlation between the log file data and the data measured using dedicated dosimeters. The scintillator detector measures proton spot dosimetric parameters. After studying the correlation between the log file and detector

measured data, the study develops ML models to predict PBS spot size in different axes such as X, Y, major, and minor axes and also predict the relative positional error of each spot. The ML models were validated using different statistical tools. The developed ML models can predict spot dosimetric parameters using the irradiation log file as an input parameter. The models can help to automate the routine QA of PBS spot measurement.

Another study objective is automating the PSQA workflow using ML models. The PBS machine is capable of delivering proton beams in different gantry angles. A single beam contains thousands of pencil beams with different energy and MU per spot. The complex beam delivery accuracy was confirmed using PSQA. In the conventional method of PSQA, the dose is measured at different depths for each beam, and the dose plane is compared with the dose plane exported from the TPS. In this study, the ML-based automated method was developed to alternate the PSQA. In the automated model, the ML models predict the spot size of all spots used in the patient treatment beam and the spot position, range, and MU information of each spot compared with TPS-specified values. The in-house Python script is used to extract data from patient-specific irradiation files, and the data is inputted into the ML models to predict spot parameters and evaluate the accuracy of each delivered spot. This method needs only the irradiated beam log file as input data to the model. No need for dedicated dosimeter measurement.

In summary, this study successfully demonstrates the potential of ML to automate QA processes in PBS proton therapy. By utilising irradiation log files and dedicated dosimetric measurements, the study develops and validates ML models capable of accurately predicting spot dosimetric parameters. These models offer a significant advancement in streamlining routine QA, reducing the need for time-consuming and resource-intensive manual measurements. Furthermore, the study's automated approach to PSQA presents a promising alternative to conventional methods, enabling efficient and accurate verification of complex beam deliveries without the need for additional dosimetric tools. These innovations pave the way for enhanced efficiency, reliability, and safety in proton therapy, ultimately contributing to improved patient outcomes.

1.9 References

1. Thariat J, Hannoun-Levi JM, Sun Myint A, Vuong T, Gérard JP. Past, present, and future of radiotherapy for the benefit of patients. Nature reviews Clinical oncology. 2013 Jan;10(1):52-60.
2. Brailsford JF. Roentgen's Discovery of X rays: Their Application to Medicine and Surgery. The British journal of radiology. 1946 Nov 1;19(227):453-61.
3. Chandra RA, Keane FK, Voncken FE, Thomas CR. Contemporary radiotherapy: present and future. The Lancet. 2021 Jul 10;398(10295):171-84.
4. Bakiu E, Telhaj E, Kozma E, Ruçi F, Malkaj P. Comparison of 3D CRT and IMRT tratment plans. Acta Informatica Medica. 2013;21(3):211.
5. Lecchi M, Fossati P, Elisei F, Orecchia R, Lucignani G. Current concepts on imaging in radiotherapy. European journal of nuclear medicine and molecular imaging. 2008 Apr;35:821-37.
6. Wang K, Tepper JE. Radiation therapy-associated toxicity: Etiology, management, and prevention. CA: a cancer journal for clinicians. 2021 Sep;71(5):437-54.
7. Durante M, Orecchia R, Loeffler JS. Charged-particle therapy in cancer: clinical uses and future perspectives. Nature Reviews Clinical Oncology. 2017 Aug;14(8):483-95.
8. Mohan R. A review of proton therapy–Current status and future directions. Precision radiation oncology. 2022 Jun;6(2):164-76.
9. Thomas H, Timmermann B. Paediatric proton therapy. The British journal of radiology. 2020 Mar 1;93(1107):20190601.
10. Olsen DR, Bruland ØS, Frykholm G, Norderhaug IN. Proton therapy–a systematic review of clinical effectiveness. Radiotherapy and oncology. 2007 May 1;83(2):123-32.
11. Wang X, Chen X, Li G, Han X, Gao T, Liu W, Tang X. Application of carbon ion and its sensitizing agent in cancer therapy: A systematic review. Frontiers in Oncology. 2021 Jul 5;11:708724.
12. Tinganelli W, Durante M. Carbon ion radiobiology. Cancers. 2020 Oct 17;12(10):3022.
13. Schaub L, Harrabi SB, Debus J. Particle therapy in the future of precision therapy. The British journal of radiology. 2020 Oct 1;93(1114):20200183.
14. Hwang EJ, Gorayski P, Le H, Hanna GG, Kenny L, Penniment M, Buck J, Thwaites D, Ahern V. Particle therapy tumour outcomes: an updated systematic review. Journal of medical imaging and radiation oncology. 2020 Oct;64(5):711-24.
15. Wilson RR. Radiological use of fast protons. Radiology. 1946 Nov;47(5):487-91.
16. Bussiere M, Daartz J, Verburg J, Depauw N, Kooy HM, Loeffler JS, Chapman PH, Shih HA. Proton radiosurgery: a clinical transition from passive scattering to pencil beam scanning. International Journal of Radiation Oncology* Biology* Physics. 2021 Nov 1;111(3):e544.
17. Kim C, Kim YJ, Lee N, Ahn SH, Kim KH, Kim H, Shin D, Lim YK, Jeong JH, Kim DY, Shin WG. Evaluation of the dosimetric effect of scattered protons in clinical practice in passive scattering proton therapy. Journal of Applied Clinical Medical Physics. 2021 Jun;22(6):104-18.
18. Schippers JM, Duppich J, Goitein G, Jermann M, Lomax A, Pedroni E, Reist H, Timmermann B, Verweij J. The use of protons in cancer therapy at PSI and related instrumentation. InJournal of Physics: Conference Series 2006 May 1 (Vol. 41, No. 1, p. 61). IOP Publishing.

19. Paganetti H, Bortfeld T. Proton therapy. InNew technologies in radiation oncology 2006 (pp. 345-363). Berlin, Heidelberg: Springer Berlin Heidelberg.
20. Veksler VI. New method for the acceleration of relativistic particles. InDoklady Akademii Nauk USSR 1944 (Vol. 43, No. 8, pp. 346-348).
21. Sato K, Yamada S, Ogawa H, Kawachi K, Araki N, Itano A, Kanazawa M, Kitagawa A, Kohno T, Kumada M, Murakami T. Performance of HIMAC. Nuclear Physics A. 1995 May 29;588(1):c229-34.
22. Castro JR, Quivey JM. Clinical experience and expectations with helium and heavy ion irradiation. International Journal of Radiation Oncology* Biology* Physics. 1977 Jan 1;3:127-31.
23. Galonska M, Scheloske S, Cee R, Höppner K, Winkelmann T, Peters A, Haberer T. Commissioning of the ion beam gantry at HIT. IPAC. 2011;11:2874.
24. Jäkel O, Kraft G, Karger CP. The history of ion beam therapy in Germany. Zeitschrift für medizinische Physik. 2022 Feb 1;32(1):6-22.
25. Kumada H. Accelerator Systems for Proton Radiotherapy. Proton Beam Radiotherapy: Physics and Biology. 2020:85-96..
26. Ding X, Younkin JE, Shen J, Bues M, Liu W. A critical review of the practices of proton daily quality assurance programs. Therapeutic Radiology and Oncology. 2021 Dec 30;5.
27. Arjomandy B, Taylor P, Ainsley C, Safai S, Sahoo N, Pankuch M, Farr JB, Yong Park S, Klein E, Flanz J, Yorke ED. AAPM task group 224: comprehensive proton therapy machine quality assurance. Medical physics. 2019 Aug;46(8):e678-705.
28. Hanley J, Dresser S, Simon W, Flynn R, Klein EE, Letourneau D, Liu C, Yin FF, Arjomandy B, Ma L, Aguirre F. AAPM Task Group 198 Report: An implementation guide for TG 142 quality assurance of medical accelerators. Medical physics. 2021 Oct;48(10):e830-85.
29. Zhu XR, Poenisch F, Song X, Johnson JL, Ciangaru G, Taylor MB, Lii M, Martin C, Arjomandy B, Lee AK, Choi S. Patient-specific quality assurance for prostate cancer patients receiving spot scanning proton therapy using single-field uniform dose. International Journal of Radiation Oncology* Biology* Physics. 2011 Oct 1;81(2):552-9.
30. Aitkenhead AH, Sitch P, Richardson JC, Winterhalter C, Patel I, Mackay RI. Automated Monte-Carlo re-calculation of proton therapy plans using Geant4/Gate: implementation and comparison to plan-specific quality assurance measurements. The British Journal of Radiology. 2020 Oct 1;93(1114):20200228.
31. Chen M, Yepes P, Hojo Y, Poenisch F, Li Y, Chen J, Xu C, He X, Gunn GB, Frank SJ, Sahoo N. Transitioning from measurement-based to combined patient-specific quality assurance for intensity-modulated proton therapy. The British journal of radiology. 2020 Mar 1;93(1107):20190669.
32. Kumar MD, Thirumavalavan N, Krishna DV, Babaiah M. QA of intensity-modulated beams using dynamic MLC log files. Journal of medical physics. 2006 Jan 1;31(1):36-41.
33. Park H, Paganetti H, Schuemann J, Jia X, Min CH. Monte Carlo methods for device simulations in radiation therapy. Physics in Medicine & Biology. 2021 Sep 14;66(18):18TR01.
34. Rahmani AM, Yousefpoor E, Yousefpoor MS, Mehmood Z, Haider A, Hosseinzadeh M, Ali Naqvi R. Machine learning (ML) in medicine: Review, applications, and challenges. Mathematics. 2021 Nov 21;9(22):2970.

35. Singh A, Thakur N, Sharma A. A review of supervised machine learning algorithms. In2016 3rd international conference on computing for sustainable global development (INDIACom) 2016 Mar 16 (pp. 1310-1315). Ieee.
36. Usama M, Qadir J, Raza A, Arif H, Yau KL, Elkhatib Y, Hussain A, Al-Fuqaha A. Unsupervised machine learning for networking: Techniques, applications and research challenges. IEEE access. 2019 May 14;7:65579-615.
37. François-Lavet V, Henderson P, Islam R, Bellemare MG, Pineau J. An introduction to deep reinforcement learning. Foundations and Trends® in Machine Learning. 2018 Dec 19;11(3-4):219-354.
38. Siochi RA, Pennington EC, Waldron TJ, Bayouth JE. Radiation therapy plan checks in a paperless clinic. Journal of Applied Clinical Medical Physics. 2009 Dec;10(1):43-62.
39. Rangaraj D, Zhu M, Yang D, Palaniswaamy G, Yaddanapudi S, Wooten OH, Brame S, Mutic S. Catching errors with patient-specific pretreatment machine log file analysis. Practical radiation oncology. 2013 Apr 1;3(2):80-90.
40. Tai YM, Heng VJ, Renaud MA, Serban M, Seuntjens J. Quality assurance for mixed electron–photon beam radiation therapy using treatment log files and MapCHECK. Medical Physics. 2023 Dec;50(12):7996-8008.
41. Olasolo-Alonso J, Vázquez-Galiñanes A, Pellejero-Pellejero S, Pérez-Azorín JF. Evaluation of MLC performance in VMAT and dynamic IMRT by log file analysis. Physica Medica. 2017 Jan 1;33:87-94.
42. Stell AM, Li JG, Zeidan OA, Dempsey JF. An extensive log-file analysis of step-and-shoot intensity modulated radiation therapy segment delivery errors. Medical physics. 2004 Jun;31(6):1593-602.
43. Chow VU, Kan MW, Chan AT. Patient-specific quality assurance using machine log files analysis for stereotactic body radiation therapy (SBRT). Journal of Applied Clinical Medical Physics. 2020 Nov;21(11):179-87.
44. Luo W, Li J, Price Jr RA, Chen L, Yang J, Fan J, Chen Z, McNeeley S, Xu X, Ma CM. Monte Carlo based IMRT dose verification using MLC log files and R/V outputs. Medical physics. 2006 Jul;33(7Part1):2557-64.
45. Teke T, Bergman AM, Kwa W, Gill B, Duzenli C, Popescu IA. Monte Carlo based, patient-specific RapidArc QA using Linac log files. Medical physics. 2010 Jan;37(1):116-23.
46. Li H, Sahoo N, Poenisch F, Suzuki K, Li Y, Li X, Zhang X, Lee AK, Gillin MT, Zhu XR. Use of treatment log files in spot scanning proton therapy as part of patient-specific quality assurance. Medical physics. 2013 Feb;40(2):021703.
47. Meier G, Besson R, Nanz A, Safai S, Lomax AJ. Independent dose calculations for commissioning, quality assurance and dose reconstruction of PBS proton therapy. Physics in Medicine & Biology. 2015 Mar 17;60(7):2819.
48. Belosi MF, Van der Meer R, de Acilu Laa PG, Bolsi A, Weber DC, Lomax AJ. Treatment log files as a tool to identify treatment plan sensitivity to inaccuracies in scanned proton beam delivery. Radiotherapy and oncology. 2017 Dec 1;125(3):514-9
49. Rana S, Rosenfeld AB. Impact of errors in spot size and spot position in robustly optimized pencil beam scanning proton-based stereotactic body radiation therapy (SBRT) lung plans. Journal of Applied Clinical Medical Physics. 2021 Jul;22(7):147-54.

Chapter 2

Literature Survey

Chapter 2- Literature Survey

2.1 History of Proton Therapy

The discovery of X-rays by Wilhelm Roentgen [1] and the discovery of radioactivity by Henri Becquerel [2], both in 1895, laid the groundwork for the application of radiation in cancer treatment. These ground-breaking discoveries paved the way for technological advancements, leading to the development of high-energy linear accelerators. By the mid-20th century, these accelerators were utilizing X-rays in the 4-15 MV range for external beam radiotherapy. In the 1990s, Dr. M. J. Zelefsky and his team at Memorial Sloan Kettering Cancer Center advanced the field by developing IMRT [3]. IMRT significantly improved the precision of radiotherapy by modulating the intensity of radiation beams, enabling the delivery of higher doses directly to tumour tissues while minimizing exposure to surrounding healthy tissues. This technique employs advanced computational algorithms and sophisticated beam-shaping technologies to enhance targeting accuracy. The subsequent introduction of Image-Guided Radiation Therapy (IGRT) further refined this approach by incorporating imaging techniques to improve the accuracy of radiation delivery, thereby reducing the risk of damage to normal tissues [4].

Despite these advancements, X-ray radiation inherently exhibits exponential attenuation, which means the beam continues to deliver a dose to tissues as it exits the body. While modern techniques have minimized this effect, exponential attenuation remains challenging in optimizing radiotherapy protocols to balance efficacy and normal tissue sparing. The advent of particle therapy, made possible by Ernest Lawrence's cyclotron development in 1929 [5], introduced a new era in radiotherapy. Particle therapy, including proton and heavy ion therapies, allows for the precise treatment of tumours with minimal radiation to surrounding healthy tissues. Unlike X-rays, particles such as protons can be engineered to release their maximum energy at a specific depth within the tissue, significantly reducing the dose delivered beyond the tumour and sparing adjacent normal tissues from unnecessary radiation exposure.

The early exploration of particle therapy began with John Lawrence and Robert Stone, who used neutron beams produced by a cyclotron for cancer treatment. Between 1938 and 1943, they treated around 250 patients, but significant toxicities such as bone necrosis and ulcers emerged, leading to the discontinuation of this approach [6,7]. The

concept of proton therapy for cancer treatment gained momentum after a study by Robert Wilson [8], highlighting the advantages of the proton beam's finite range and the Bragg peak phenomenon over conventional X-ray therapy. The first clinical treatment using a proton beam commenced at LBNL in 1954 [9], marking a significant milestone in the field. LBNL also pioneered research on heavy ion therapy, further expanding the scope of particle therapy.

In 1955, Sweden initiated proton therapy trials on rats and goats to study its biological effects [10,11]. The initial patient treatments used the plateau region of the proton beam rather than the Bragg peak, employing a crossfire technique. Subsequent advancements led to the development of range shifters and modulation wheels [12]. The Gustav Werner Institute in Sweden was the first to use a ridge filter for range modulation, creating Spread-Out Bragg Peak (SOBP) for treatment [13]. In 1959, the Harvard Cyclotron Laboratory (HCL) developed a cyclotron capable of producing protons with a maximum energy of 160 MeV, sufficient to penetrate up to 16 cm in water [14]. Preclinical studies began with this system, and in 1961 [15], Massachusetts General Hospital (MGH) collaborated with HCL to start clinical proton therapy trials, initially focusing on treating pituitary tumours using a single scattering technique. During the 1970s, double-scattering proton therapy was developed at HCL, enabling the treatment of larger targets [16]. However, the passive scattering system had limitations, such as needing patient-specific customized range shifters and collimators.

In 1961, Larsson et al. [17] explored using magnets to deflect the proton beam. Still, it wasn't until 1977 that Leemann and colleagues [18] developed a beam scanning technique for three-dimensional modulation of the pencil beam. This innovation led to various scanning techniques, such as spot-by-spot and continuous scanning. Throughout the 1980s, extensive studies on different scanning techniques were conducted at LBL, focusing on advancing passive scattering and pencil beam scanning to enhance the utility and efficiency of proton therapy. The first fully hospital-based proton therapy facility was established at Loma Linda University Medical Center (LLUMC) in 1990 [19], followed by installing the first commercial proton therapy system at MGH [20].

Since 2000, the global installation of commercial proton therapy systems has expanded significantly, with over 300,000 patients treated by 2024 [21]. The PBS system

has become the dominant method for proton beam delivery. It is known for its precision in dose distribution and ability to target tumours with minimal impact on surrounding healthy tissues. Recent advancements in proton therapy systems include the development of superconducting synchrocyclotrons and compact gantry designs, which have significantly reduced the size and cost of these systems [22]. Innovations like multi-room proton therapy centres and Flash therapy delivering ultra-high dose rates in milliseconds are being explored to enhance treatment efficiency and outcomes [23]. These cutting-edge developments aim to broaden the accessibility and clinical application of proton therapy, making it more affordable and available to a broader range of patients and healthcare facilities.

2.2 Proton Therapy in Clinical Practice

Proton beam therapy offers many clinical applications, particularly in treating paediatric tumours and radio-resistant cancers. Its effectiveness stems from unique advantages, such as the sharp dose fall-off after the Bragg peak, which allows for precise targeting of tumours while sparing surrounding healthy tissues. The biological benefits associated with high RBE and LET effects further enhance its therapeutic potential.

However, initial enthusiasm for proton therapy, driven by these promising characteristics, has been moderated by clinical outcomes, suggesting that early expectations may have been overly optimistic. Challenges such as the sensitivity of proton dose distributions to anatomical changes, assumptions about RBE, and the ongoing evolution of treatment planning and delivery technologies have underscored the complexities of fully realizing its potential. Despite the high costs and currently limited evidence of clear clinical superiority, ongoing research is uncovering protons' distinct biological and clinical effects, highlighting the need to deepen our understanding and apply these insights to maximize therapeutic outcomes.

The children are the most beneficial group of patients because of the lower normal tissue irradiation. A study by Jimenez RB et al. [24] concluded that proton therapy leads to better survival rates and improved tumour control in paediatric patients treated for Medulloblastoma. A similar study by Ladra MM et al. [25] evaluated the Overall Survival rate (OS) and Local Control rate (LC) of children with rhabdomyosarcoma. The 5-year results show that the OS and LC are similar and comparable to photon therapy studies, but

the acute and late toxicity rates are less with proton therapy. So, proton therapy may be a safer option for children. Cranio Spinal Irradiation (CSI) is the treatment that irradiates the brain and spine [26]. As the total irradiation area is high, the photon therapy leads to significant doses to many normal tissues such as the eye, kidneys, lungs, bowel, heart, etc. The proton therapy for CSI is considered the most beneficial use of protons. Many studies reported the benefit of proton therapy over photon therapy. Howell et al. [27] compared the dosimetric data of proton and photon treatment plans for 18 patients aged 2 to 18 who underwent CSI. The results indicated that all patients experienced better normal tissue sparing with proton therapy while maintaining consistent tumour dose coverage. Many studies compared the dosimetric benefit of proton therapy over photon for CSI cases, and all reported less dose to normal tissues than photon therapy [28-30].

Another group of tumours that benefit significantly from proton therapy includes skull base and Sinonasal tumours, which are often located near critical structures such as the spinal cord, brain, brainstem, and optic pathways. These tumours typically require high doses of radiation for effective treatment. However, in photon therapy, the ability to increase the dose is constrained by the maximum allowable dose for nearby normal tissues. In contrast, proton therapy allows for dose escalation due to the sharp dose fall-off characteristic of protons, enabling higher doses to be delivered to the tumour while minimizing exposure to surrounding healthy tissues [31,32]. Proton therapy has demonstrated potential for treating brain tumours, particularly by reducing the risk of adverse effects such as cognitive dysfunction. A study by Hauswald H et al. [33] on nineteen patients with low-grade glioma reported minimal toxicities with proton therapy. A key study by Shih et al. [34] presented findings from a prospective trial involving patients with grade II gliomas, evaluating cognitive function and quality of life after receiving proton therapy. The study revealed that cognitive function metrics either remained stable or showed improvement compared to baseline levels.

In head and neck tumours, the dose to the midline structures and contralateral structures, such as parotids, oral cavity, submandibular glands, and oral cavity, etc., are significantly reduced using proton therapy compared to photon therapy [35]. A study by Manzar et al. [36] reported that patients treated with proton therapy for oesophageal cancer experienced less use of feeding tubes, as well as reduced cough and dysphagia, compared to those who underwent IMRT. A similar result was reported by Hutcheson et al. [37], such

as a 20 % reduction in the use of feeding tubes in patients treated with protons compared to photons for head and neck treatment sites. The chordomas and chondrosarcomas are radio-resistant tumours and require high radiation doses. In such cases, the impact of the proton is high in sparing normal tissues. A study by McDonald et al. [38] reported the LC and OS of patients treated with protons for clival chordomas. A report from the PSI reported the 10-year disease-free survival of patients treated for chordomas and chondrosarcoma [39].

Proton therapy is challenging for treating moving tumours such as lung, pancreatic, and liver tumours. The heterogeneity in the tissue, along with movement during treatment, can cause large deviations from the prescribed dose. So, treating moving tumours requires more attention, and the treatment planning system should have a method to address such issues. [40-41]. The normal tissue toxicity rate is less in lung tumours treated with protons, as seen in all other treatment sites. A report by Nguyen QN et al. [42] found that only 1.4 % of proton therapy patients developed grade 3 pneumonitis. All previously discussed clinical studies have shown significant differences in early and late toxicities. Still, the OS and LC rates of proton therapy are almost similar or comparable to those of photon therapy.

In conclusion, proton therapy has emerged as a highly effective treatment modality, offering significant benefits in reducing both early and late treatment-related toxicities while maintaining comparable or even superior outcomes to conventional therapies. Its precise targeting capabilities, particularly in challenging tumour locations near critical structures, make it an invaluable tool in modern oncology, providing a promising option for improving patient quality of life and long-term survival.

2.3 The Role of Log Files in Radiotherapy Quality Assurance

In radiotherapy, log files are digital records that capture detailed information about the treatment delivery process, including machine settings, dose delivery, patient positioning, and errors or deviations. These files are vital for QA, ensuring that radiation therapy is delivered precisely and safely, and identifying potential issues during treatment. The application of log files for troubleshooting and QA originated with linear accelerators, which provide essential data on the position and speed of the MLC during each beam segment, the MU delivered at each control point, and the gantry and collimator angles. This information is used to analyze beam delivery accuracy, conduct audits, and perform

machine- and PSQA. Log files are equally valuable in proton therapy, particularly in PBS systems. They record critical data such as spot position, spot size, selected range, beam current, scanning magnets set points, MU, and the number of spots, which can be used for patient-specific and machine QA.

Modern radiotherapy systems include numerous electronic and automated components for data transfer and beam delivery, resulting in extensive log files that record many data points. Manually verifying each point—such as the positions of the MLC at each control point or the speed of MLC movement during delivery—can be challenging. As treatment complexity increases, the volume of parameters to be checked also rises, making manual verification time-consuming and prone to errors. Recently, computer-assisted tools have been introduced to automate this process, enhancing efficiency and accuracy. Using log files and in-house scripts, Siochi et al. [43] automated the physics checks of treatment plans and delivery data, significantly reducing manual errors. Another study by Rangaraj D et al. [44] utilised Varian radiotherapy Linac Dynalog files to analyse data from 914 patients, assessing the integrity of plan transfer and beam delivery. They identified 14 errors, all of which were linked to human intervention, such as data modification during plan transfer. The study concluded that log file-based data analysis is a robust and efficient method for detecting errors in the process. Stell AM et al. [45] studied log files from 91 step-and-shoot IMRT patient plans and found that segment MU errors depended on dose rate. They reported a maximum segment MU error of 1.8 MU at a dose rate of 600 MU/min and 0.5 MU at 100 MU/min. Chow V.U. et al. [46] utilised trajectory log files to evaluate the delivery accuracy of Stereotactic Body Radiation Therapy (SBRT) in a study involving 120 patients. Their analysis focused on dose indices, MLC positions, and gantry angles. The study reported a maximum MLC position deviation of 0.3 mm and a gantry angle difference of less than 0.2 degrees. Based on their findings, they recommended using log file-based analysis for SBRT to replace patient-specific QA.

The conventional technique for patient-specific QA in IMRT and VMAT plans involves measurement-based analysis. For instance, dose fluence is typically measured using ionisation array chambers and then compared with the TPS data. However, with the introduction of MC dose algorithms for independent dose calculation using log files, many centres have transitioned to MC-based patient-specific QA utilizing log files. A study by Luo W. et al. [47] used a MC dose calculation engine to reconstruct the dose distribution

for eight prostate patients treated with IMRT using log files. The results indicated a mean leaf position error of 0.2 mm, which led to a 1 % dose difference in the target. The accuracy of the MC calculation algorithm in Rapid Arc plans was evaluated by Teke T. et al. [48], demonstrating its high accuracy in these plans. In addition to dose calculation accuracy and dose delivery evaluation, log files have been used to analyse plans involving moving targets. By synchronizing log file data with respiratory tracking data, the MLC positions and MU for each breathing amplitude can be accurately determined, allowing for precise dose reconstruction using MC.

Given the complexity of PBS beam delivery, which involves thousands of spots and multiple energy layers, routine QA cannot comprehensively analyse all the data using detector measurements alone. Instead, routine QA focuses on assessing the accuracy of selected energy spot dosimetric parameters, with more extensive verification of energy spot data conducted during monthly and yearly QA. However, by analyzing log file data, a broader range of energy spot parameters can be evaluated, facilitating machine performance assessment and patient-specific QA using MC dose calculations. The PSI has been using log files as a tool for QA since 2009 [52]. Later, the MD Anderson Cancer Centre also studied [53] the utility of irradiation log files from the PBS system for evaluating beam delivery accuracy. They examined the correlation between the log file-recorded spot positions and each spot's MU. The positional accuracy of each spot was measured using film and compared with the values recorded in the log files, finding that all values were within 0.5 mm. Additionally, the MU accuracy was compared between the log file-recorded values and the planned MUs, revealing a precision of 0.1 %. After confirming the accuracy of the log file-recorded spot positions and MU, physicists began using log file data to reconstruct the dose with an independent MC dose engine. This method has emerged as a potential tool for patient-specific QA in PBS proton therapy by leveraging the recorded spot positions and MU information. In 2015 Meier G et al. [54] developed an independent dose calculation system for dose calculation using log file information. Belosi MF et al. [55] calculated the dose in the patient CT scan using information from log files to evaluate dose differences at the anatomical level. A similar study on line scanning proton therapy was conducted by Jeon C et al. [56]. Using log file data, they used the Tool for Particle Simulation (TOPAS) MC dose engine for dose calculation. Another study by Chung K et al. [57] investigated line scanning accuracy by comparing film measurements with log file data, finding that the results were within 1 mm. Meijers et al. [58] utilized PBS proton

therapy log file data and patient breathing patterns to reconstruct 4D dose distributions based on weekly 4D computed tomography scans.

In conclusion, the use of log files in proton therapy, particularly for PBS systems, has become a crucial tool for machine QA and patient-specific QA since its introduction in 2009. These log files have primarily been used to verify only the spot position and MU accuracy, facilitating MC-based dose calculations for independent dose verification. However, uncertainties and potential errors in log file data, as highlighted by Toscano S et al. [59], emphasize the need to fully understand these limitations before relying on this data for QA purposes. The importance of spot size and symmetry in dose delivery accuracy is significant; for instance, Rana S et al. [60] demonstrated that changes in spot size by 10 %, 15 %, and 20 % resulted in notable dose variations in the target. Consequently, accurately addressing spot size, symmetry, position, and MU is critical for comprehensive QA and PSQA.

Existing literature has focused predominantly on spot position and MU information from log files. There is a lack of studies critically analyzing the accuracy of spot parameters recorded in log files or investigating their correlation with values measured by dedicated detectors. Additionally, research on solutions to mitigate uncertainties in log file data used for machine QA and patient-specific QA is limited. Addressing these research gaps is essential for enhancing the reliability and effectiveness of log file data in QA processes, ultimately improving the precision and safety of proton therapy.

2.4 Machine Learning-Driven Quality Assurance in Modern Radiotherapy

The ML can transform various processes and workflows in radiation oncology, enhancing patient care quality and efficiency [61]. It can automate radiotherapy contouring, planning, QA and data analysis workflow. The other advantage of the ML model is that it can analyse complex data and accurately predict or extract meaningful patterns. The most developed ML model in radiotherapy is the auto-contouring system [62]. Nowadays, ML-based auto-contouring systems are commercially available, helping to reduce time, improve efficiency, and minimize errors in the contouring workflow of radiotherapy. Routine QA of Linac and proton therapy systems generates a large amount of data often used only once. ML models can leverage this big data to learn from past information and apply these insights to enhance future QA and analysis.

In radiotherapy, popular ML models include linear regression, lasso, ridge regression [63], and ensemble methods such as Random Forest and Gradient Boosting. Neural network models, like Convolutional Neural Networks (CNN) and Artificial Neural Networks (ANN) [64], are also widely used. The selection of a specific algorithm depends on the characteristics of the data. In Li et al. [65] study, 5-year daily QA data from a Linac was used to predict beam symmetry. The researchers developed an ANN-based model with one hidden layer of six neurons and two input parameters. The ANN model demonstrated superior prediction accuracy compared to the Autoregressive Integrated Moving Average (ARIMA) statistical model. A study by Valdes G et al [66] used Poisson regression and lasso regularisation to predict the IMRT QA passing rate using different plan matrices. This model helped predict the passing rate before the actual measurement-based QA. Interian Y et al. [67] extended the study using CNN models to predict the gamma passing rate using a fluence map as input to the model. A similar study by Lam D et al. [68] used 182 IMRT QA measurements obtained through portal dosimetry and plan metrics to predict gamma passing rates. The introduction of log files helped the physicists use the log file data and ML models to predict the MLC leaf positional and dose delivery errors. In 2016, Carlson JN et al. [69] were the first to use delivery log files and ML models to predict MLC positional errors. They developed a supervised ML model and evaluated the gamma passing rate using the predicted MLC leaf positions. This resulted in a higher gamma passing rate than the measurement-based gamma analysis. Osman A F et al. [70] introduced the application of a feed-forward ANN model to predict MLC positional errors. They utilised 400 log files and 14 features from the treatment plan to predict MLC leaf positions during beam delivery. The ANN model demonstrated good prediction accuracy, with a maximum Mean Squared Error (MSE) of 0.0001 mm. Another application of ML is in auto-planning algorithms that utilize deep learning networks [71-72]. These methods involve training deep-learning models on a database of previous plans to predict dose distribution for new plans. The primary deep learning algorithms employed for auto-planning are U-Net [73] and Generative Adversarial Networks (GANs).

The application of ML models in proton therapy started in passive scattering techniques for predicting output factor and MU of the beam using range, modulation and field size as input parameters [74]. The study used Gaussian process regression (GPR) and shallow neural network(SNN) deep learning models. Li et al. [75] employed both feed-forward and recurrent neural network models to predict the range and dose in proton

therapy by utilizing data from proton-induced positron emitters. There are only a few studies that have applied ML models to the passive scattering technique. However, with the advent of PBS techniques and the availability of irradiation log files, few studies have utilized ML models to predict spot dosimetric parameters based on these log files. Dominic Maes et al. [76] demonstrated the application of ML techniques to accurately predict delivered PBS spot positions and MU by integrating irradiation log file data into the training dataset. The study utilised TPS and log file data for model development but did not compare the measurement data with the log file data. Kouwenberg J et al. [77] employed an ML model, specifically a Gaussian naive Bayes classifier, to classify which patients require Intensity Modulated Proton Therapy(IMPT).

Using ML models with log file data in PBS proton therapy systems is a promising technique for automating the process, including machine QA and PSQA. This approach leverages the enormous data captured in log files to enhance the accuracy and efficiency of QA procedures, potentially leading to more reliable treatment outcomes and streamlined workflows. In proton therapy, the application of ML using log file data is very limited. ML models can be used to predict dosimetric parameters with high accuracy and to mitigate the uncertainties associated with log file data.

2.5 References

1. Roentgen WC. On a new kind of rays. CA: a cancer journal for clinicians. 1972 May 1;22(3):153-7.
2. Myers WG. Becquerel's Discovery of Radioactivity in 1896. Journal of Nuclear Medicine. 1976 Jul 1;17(7):579-82.
3. Zelefsky MJ, Fuks Z, Leibel SA. Intensity-modulated radiation therapy for prostate cancer. InSeminars in radiation oncology 2002 Jul 1 (Vol. 12, No. 3, pp. 229-237). WB Saunders.
4. Xing L, Thorndyke B, Schreibmann E, Yang Y, Li TF, Kim GY, Luxton G, Koong A. Overview of image-guided radiation therapy. Medical Dosimetry. 2006 Jun 1;31(2):91-112.
5. Lawrence EO. The evolution of the cyclotron. Nobel Lecture. 1951:23.
6. Lawrence JH, Lawrence EO. The biological action of neutron rays. Proc Natl Acad Sci USA 1936;22:124-33.
7. Stone RS, Larkin JC. The treatment of cancer with fast neutrons. Radiology 1942;39:608-20.
8. Wilson RR. Radiological use of fast protons. Radiology 1946;47:487-91
9. Lawrence JH. Proton irradiation of the pituitary. Cancer. 1957 Jul;10(4):795-8.
10. Falkmer S, Larsson B, Sténson S. Effects of single dose proton irradiation of normal skin and Vx2 carcinoma in rabbit ears: a comparative investigation with protons and roentgen rays. Acta radiologica. 1959 Sep(3):217-34.

11. Leksell L, Larsson B, Andersson B, Rexed B, Sourander P, Mair W. Lesions in the depth of the brain produced by a beam of high energy protons. Acta radiologica. 1960 Oct 1;54(4):251-64.
12. Kumada H. Beam delivery system for proton radiotherapy. Proton Beam Radiotherapy: Physics and Biology. 2020:97-112.
13. Koehler AM, Schneider RJ, Sisterson JM. Flattening of proton dose distributions for large-field radiotherapy. Medical Physics. 1977 Jul;4(4):297-301.
14. Kjellberg RN, Koehler AM, Preston WM, Sweet WH. Stereotaxic instrument for use with the Bragg peak of a proton beam. Stereotactic and Functional Neurosurgery. 1962;22(3-5):183-9.
15. Kjellberg RN, Sweet WH, Preston WM, Koehler AM. The Bragg peak of a proton beam in intracranial therapy of tumors. Transactions of the American Neurological Association (US). 1962 Jan 1;87.
16. Sisterson JM. Overview of proton beam applications in therapy. Nuclear Instruments and Methods in Physics Research Section B: Beam Interactions with Materials and Atoms. 1990 Jan 2;45(1-4):718-23.
17. Larsson B. Pre-therapeutic physical experiments with high energy protons. The British journal of radiology. 1961 Mar 1;34(399):143-51
18. Leemann C, Alonso J, Grunder H, Hoyer E, Kalnins G, Rondeau D, Staples J, Voelker F. A 3-Dimensional beam scanning system for particle radiation therapy. IEEE Transactions on Nuclear Science. 1977 Jun;24(3):1052-4.
19. Slater JM, Archambeau JO, Miller DW, Notarus MI, Preston W, Slater JD. The proton treatment center at Loma Linda University Medical Center: rationale for and description of its development. International Journal of Radiation Oncology* Biology* Physics. 1992 Jan 1;22(2):383-9.
20. Paganetti H. Proton therapy: history and rationale. Proton Therapy Physics. 2012:1-8.
21. Facilities in Operation. https://www.ptcog.ch/index.php/facilities-in-operation.
22. Collings EW, Lu L, Gupta N, Sumption MD. Accelerators, gantries, magnets and imaging systems for particle beam therapy: recent status and prospects for improvement. Frontiers in Oncology. 2022 Feb 15;11:737837.
23. Mazal A, Prezado Y, Ares C, de Marzi L, Patriarca A, Miralbell R, Favaudon V. FLASH and minibeams in radiation therapy: the effect of microstructures on time and space and their potential application to protontherapy. The British Journal of Radiology. 2020 Mar 1;93(1107):20190807.
24. Jimenez RB, Sethi R, Depauw N, Pulsifer MB, Adams J, McBride SM, Ebb D, Fullerton BC, Tarbell NJ, Yock TI, MacDonald SM. Proton radiation therapy for pediatric medulloblastoma and supratentorial primitive neuroectodermal tumors: outcomes for very young children treated with upfront chemotherapy. International Journal of Radiation Oncology* Biology* Physics. 2013 Sep 1;87(1):120-6.
25. Ladra MM, Szymonifka JD, Mahajan A, Friedmann AM, Yong Yeap B, Goebel CP, MacDonald SM, Grosshans DR, Rodriguez-Galindo C, Marcus KJ, Tarbell NJ. Preliminary results of a phase II trial of proton radiotherapy for pediatric rhabdomyosarcoma. Journal of Clinical Oncology. 2014 Nov 20;32(33):3762-70.
26. Halperin EC. Impact of radiation technique upon the outcome of treatment for medulloblastoma. Int J Radiat Oncol Biol Phys 1996;36:233-9.
27. Howell RM, Giebeler A, Koontz-Raisig W, Mahajan A, Etzel CJ, D'Amelio AM, et al. Comparison of therapeutic dosimetric data from passively scattered proton and photon craniospinal irradiations for medulloblastoma. Radiat Oncol 2012;7:116.

28. Brodin NP, Rosenschöld M, Aznar MC, Kiil-Berthelsen A, Vogelius IR, Nilsson P, et al. Radiobiological risk estimates of adverse events and secondary cancer for proton and photon radiation therapy of pediatric medulloblastoma. Acta Oncol 2011;50:806-16
29. Barney CL, Brown AP, Grosshans DR, McAleer MF, De Groot JF, Puduvalli V, et al. Technique, outcomes, and acute toxicities in adults treated with proton beam craniospinal irradiation. Neuro Oncol 2014;16:303-9.
30. Lee CT, Bilton SD, Famiglietti RM, Riley BA, Mahajan A, Chang EL, et al. Treatment planning with protons for pediatric retinoblastoma, medulloblastoma, and pelvic sarcoma: How do protons compare with other conformal techniques? Int J Radiat Oncol Biol Phys 2005;63:362-72.
31. Debus J, Hug EB, Liebsch NJ, et al. Brainstem tolerance to confor-mal radiotherapy of skull base tumors. Int J Radiat Oncol Biol Phys.1997;39:967-975.
32. Fagundes MA, Hug EB, Liebsch NJ, et al. Radiation therapy for chor-domas of the base of skull and cervical spine: patterns of failure andoutcome after relapse. Int J Radiat Oncol Biol Phys. 1995;33:579-584.
33. Hauswald H, Rieken S, Ecker S, Kessel KA, Herfarth K, Debus J, Combs SE. First experiences in treatment of low-grade glioma grade I and II with proton therapy. Radiation Oncology. 2012 Dec;7:1-7.
34. Shih HA, Sherman JC, Nachtigall LB, et al. Proton therapy for low-grade gliomas: results from a prospective trial. Cancer. 2015:29237.
35. Kandula S, Zhu X, Garden AS, Gillin M, Rosenthal DI, Ang KK, et al. Spot-scanning beam proton therapy vs intensity-modulated radiation therapy for ipsilateral head and neck malignancies: A treatment planning comparison. Med Dosim 2013;38:390-4.
36. Manzar GS, Lester SC, Routman DM, et al. Comparative analysis ofacute toxicities and patient reported outcomes between intensity-modulated proton therapy (impt) and volumetric modulated arctherapy (vmat) for the treatment of oropharyngeal cancer. Radio-ther Oncol. 2020;147:64-74.
37. Hutcheson K, Lewin JS, Garden AS, Rosenthal DI, Weber RS, William WN, et al. Early experience with IMPT for treating oropharyngeal tumors: Acute toxicities and swallowing-related outcomes. Int J Radiat Oncol Biol Phys 2013;87:S604
38. McDonald MW, Linton OR, Moore MG, Shah MV. Initial results of proton therapy for clival chordoma. Int J Radiat Oncol Biol Phys 2013;87:S277-8.
39. Rutz HP, Weber DC, Goitein G, Ares C, Bolsi A, Lomax AJ, et al. Postoperative spot-scanning proton radiation therapy for chordoma and chondrosarcoma in children and adolescents: Initial experience at Paul Scherrer Institute. Int J Radiat Oncol Biol Phys 2008;71:220-5
40. Van Dyk J, Smathers JB. The modern technology of radiation oncology: A compendium for medical physicists and radiation oncologists. Med Phys 2000;27:626-7.
41. Liu W, Liao Z, Schild SE, Liu Z, Li H, Li Y, et al. Impact of respiratory motion on worst-case scenario optimized intensity modulated proton therapy for lung cancers. Pract Radiat Oncol 2015;5:e77-86
42. Nguyen QN, Ly NB, Komaki R, Levy LB, Gomez DR, Chang JY, et al. Long-term outcomes after proton therapy, with concurrent chemotherapy, for stage II–III inoperable non-small cell lung cancer. Radiother Oncol 2015;115:367-72.
43. Siochi RA, Pennington EC, Waldron TJ, Bayouth JE. Radiation therapy plan checks in a paperless clinic. Journal of Applied Clinical Medical Physics. 2009 Dec;10(1):43-62.

44. Rangaraj D, Zhu M, Yang D, Palaniswaamy G, Yaddanapudi S, Wooten OH, Brame S, Mutic S. Catching errors with patient-specific pretreatment machine log file analysis. Practical radiation oncology. 2013 Apr 1;3(2):80-90.
45. Stell AM, Li JG, Zeidan OA, Dempsey JF. An extensive log-file analysis of step-and-shoot intensity modulated radiation therapy segment delivery errors. Medical physics. 2004 Jun;31(6):1593-602.
46. Chow VU, Kan MW, Chan AT. Patient-specific quality assurance using machine log files analysis for stereotactic body radiation therapy (SBRT). Journal of Applied Clinical Medical Physics. 2020 Nov;21(11):179-87.
47. Luo W, Li J, Price Jr RA, Chen L, Yang J, Fan J, Chen Z, McNeeley S, Xu X, Ma CM. Monte Carlo based IMRT dose verification using MLC log files and R/V outputs. Medical physics. 2006 Jul;33(7Part1):2557-64.
48. Teke T, Bergman AM, Kwa W, Gill B, Duzenli C, Popescu IA. Monte Carlo based, patient-specific RapidArc using Linac log files. Medical physics. 2010 Jan;37(1):116-23.
49. Shiha M, Cygler JE, MacRae R, Heath E. 4D Monte Carlo dose reconstructions using surface motion measurements. Physica Medica. 2023 Oct 1;114:103135.
50. Oliver M, Gladwish A, Staruch R, Craig J, Gaede S, Chen J, Wong E. Experimental measurements and Monte Carlo simulations for dosimetric evaluations of intrafraction motion for gated and ungated intensity modulated arc therapy deliveries. Physics in Medicine & Biology. 2008 Oct 21;53(22):6419.
51. Oliver M, Staruch R, Gladwish A, Craig J, Chen J, Wong E. Monte Carlo dose calculation of segmental IMRT delivery to a moving phantom using dynamic MLC and gating log files. Physics in Medicine & Biology. 2008 Apr 30;53(10):N187.
52. Lin S, Boehringer T, Coray A, Grossmann M, Pedroni E. More than 10 years experience of beam monitoring with the Gantry 1 spot scanning proton therapy facility at PSI. Medical physics. 2009 Nov;36(11):5331-40.
53. Li H, Sahoo N, Poenisch F, Suzuki K, Li Y, Li X, Zhang X, Lee AK, Gillin MT, Zhu XR. Use of treatment log files in spot scanning proton therapy as part of patient-specific quality assurance. Medical physics. 2013 Feb;40(2):021703.
54. Meier G, Besson R, Nanz A, Safai S, Lomax AJ. Independent dose calculations for commissioning, quality assurance and dose reconstruction of PBS proton therapy. Physics in Medicine & Biology. 2015 Mar 17;60(7):2819.
55. Belosi MF, Van der Meer R, de Acilu Laa PG, Bolsi A, Weber DC, Lomax AJ. Treatment log files as a tool to identify treatment plan sensitivity to inaccuracies in scanned proton beam delivery. Radiotherapy and oncology. 2017 Dec 1;125(3):514-9.
56. Jeon C, Lee J, Shin J, Cheon W, Ahn S, Jo K, Han Y. Monte Carlo simulation-based patient-specific using machine log files for line-scanning proton radiation therapy. Medical Physics. 2023 Nov;50(11):7139-53.
57. Chung K. A pilot study of the scanning beam quality assurance using machine log files in proton beam therapy. Progress in Medical Physics. 2017;28(3):129-33.
58. Meijers A, Jakobi A, Stützer K, Guterres Marmitt G, Both S, Langendijk JA, Richter C, Knopf A. Log file-based dose reconstruction and accumulation for 4D adaptive pencil beam scanned proton therapy in a clinical treatment planning system: implementation and proof-of-concept. Medical Physics. 2019 Mar;46(3):1140-9.
59. Toscano S, Souris K, Goma C, Barragán-Montero A, Puydupin S, Vander Stappen F, Janssens G, Matic A, Geets X, Sterpin E. Impact of machine log-files

uncertainties on the quality assurance of proton pencil beam scanning treatment delivery. Physics in Medicine & Biology. 2019 Apr 29;64(9):095021
60. Rana S, Rosenfeld AB. Impact of errors in spot size and spot position in robustly optimized pencil beam scanning proton-based stereotactic body radiation therapy (SBRT) lung plans. Journal of Applied Clinical Medical Physics. 2021 Jul;22(7):147-54.
61. Feng M, Valdes G, Dixit N, Solberg TD. Machine learning in radiation oncology: opportunities, requirements, and needs. Frontiers in oncology. 2018 Apr 17;8:110.
62. Robert C, Munoz A, Moreau D, Mazurier J, Sidorski G, Gasnier A, Beldjoudi G, Grégoire V, Deutsch E, Meyer P, Simon L. Clinical implementation of deep-learning based auto-contouring tools–Experience of three French radiotherapy centers. Cancer/Radiothérapie. 2021 Oct 1;25(6-7):607-16.
63. Owen AB. A robust hybrid of lasso and ridge regression. Contemporary Mathematics. 2007 Jan;443(7):59-72.
64. Katal A, Singh N. Artificial neural network: Models, applications, and challenges. Innovative Trends in Computational Intelligence. 2022:235-57.
65. Li Q, Chan MF. Predictive time-series modeling using artificial neural networks for Linac beam symmetry: an empirical study. Annals of the New York Academy of Sciences. 2017 Jan;1387(1):84-94.
66. Valdes G, Scheuermann R, Hung CY, Olszanski A, Bellerive M, Solberg TD. A mathematical framework for virtual IMRT using machine learning. Medical physics. 2016 Jul;43(7):4323-34.
67. Interian Y, Rideout V, Kearney VP, Gennatas E, Morin O, Cheung J, Solberg T, Valdes G. Deep nets vs expert designed features in medical physics: an IMRT case study. Medical physics. 2018 Jun;45(6):2672-80.
68. Lam D, Zhang X, Li H, Deshan Y, Schott B, Zhao T, Zhang W, Mutic S, Sun B. Predicting gamma passing rates for portal dosimetry-based IMRT using machine learning. Medical physics. 2019 Oct;46(10):4666-75.
69. Carlson JN, Park JM, Park SY, Park JI, Choi Y, Ye SJ. A machine learning approach to the accurate prediction of multi-leaf collimator positional errors. Physics in Medicine & Biology. 2016 Mar 7;61(6):2514.
70. Osman AF, Maalej NM, Jayesh K. Prediction of the individual multileaf collimator positional deviations during dynamic IMRT delivery priori with artificial neural network. Medical Physics. 2020 Apr;47(4):1421-30
71. Ge Y, Wu QJ. Knowledge-based planning for intensity-modulated radiation therapy: a review of data-driven approaches. Medical physics. 2019 Jun;46(6):2760-75.
72. Zhou J, Peng Z, Song Y, Chang Y, Pei X, Sheng L, Xu XG. A method of using deep learning to predict three-dimensional dose distributions for intensity-modulated radiotherapy of rectal cancer. Journal of applied clinical medical physics. 2020 May;21(5):26-37.
73. Ronneberger O, Fischer P, Brox T. U-net: Convolutional networks for biomedical image segmentation. InMedical image computing and computer-assisted intervention–MICCAI 2015: 18th international conference, Munich, Germany, October 5-9, 2015, proceedings, part III 18 2015 (pp. 234-241). Springer International Publishing.
74. Grewal HS, Chacko MS, Ahmad S, Jin H. Prediction of the output factor using machine and deep learning approach in uniform scanning proton therapy. Journal of applied clinical medical physics. 2020 Jul;21(7):128-34.

75. Li Z, Wang Y, Yu Y, Fan K, Xing L, Peng H. Machine learning approaches for range and dose verification in proton therapy using proton-induced positron emitters. Medical physics. 2019 Dec;46(12):5748-57.
76. Maes D, Bowen SR, Regmi R, Bloch C, Wong T, Rosenfeld A, Saini J. A machine learning-based framework for delivery error prediction in proton pencil beam scanning using irradiation log-files. Physica Medica. 2020 Oct 1;78:179-86.
77. Kouwenberg J, Penninkhof J, Habraken S, Zindler J, Hoogeman M, Heijmen B. Model based patient pre-selection for intensity-modulated proton therapy (IMPT) using automated treatment planning and machine learning. Radiotherapy and Oncology. 2021 May 1;158:224-9.

Chapter 3

Measurement and Evaluation of Spot Dosimetric Parameters Using a Scintillator Detector and Comparison with Irradiation Log File Data

Chapter 3

Title: Measurement and Evaluation of Spot Dosimetric Parameters Using a Scintillator Detector and Comparison with Irradiation Log File Data.

3.1 Introduction

The accuracy of PBS proton therapy is contingent upon the precise delivery of each spot by the energy, MU, position, and size specified by the TPS. Any deviation in these parameters during beam delivery can result in discrepancies between the dose calculated by the TPS and the actual dose delivered to the patient [**1**]. To ensure this accuracy, regular dosimetric assessments are performed to measure critical spot parameters, including spot size, position, symmetry, energy, and absolute dose. The AAPM TG224 [2] provides detailed guidelines for daily, weekly, monthly, and annual QA protocols in PBS proton therapy. A deviation in spot size greater than 10 % from the baseline value can lead to significant discrepancies in the dose delivered to the tumour region [3], while a spot position deviation exceeding 1 mm can also compromise dose accuracy [4]. Consequently, routine monitoring and analysis of spot parameters are critical for ensuring accurate dose delivery in PBS proton therapy. Given that spot size varies with energy, it is essential to measure these parameters across a range of energies and gantry angles to account for potential variations.

Conventional spot measurements are generally conducted using specialized scintillation detectors or film-based systems. In contrast, the proton therapy machine monitors the accuracy of spot delivery specifically position, size, and MU using ionisation chambers positioned within the treatment nozzle. These chambers continuously record and verify spot parameters during beam delivery, triggering an interruption of the beam if any parameter exceeds the manufacturer's specified tolerance limits. The recorded data is then stored in irradiation log files for further analysis.

Log files are digital records that capture various machine parameters during beam delivery, including machine settings, gantry position, table values, and any errors that occur. In PBS proton therapy, irradiation log files contain detailed dosimetric information for each spot. However, routine QA procedures typically focus on a limited number of spots at specific energy levels and gantry angles, which may not fully represent the accuracy of all spots delivered during patient treatments. Since treatments can involve thousands of spots across a wide range of energies, analyzing log file data allows for a more

comprehensive evaluation of spot accuracy [5,6]. A study by Siochi et al. [7] demonstrated that log file data can serve as a valuable tool for machine QA, especially when data extraction and analysis are automated using in-house scripts. However, research by Toscano et al. [8] indicated that PBS log files may be subject to uncertainties and potential errors. Consequently, it is essential to understand these uncertainties before applying log file data directly in clinical practice. To ensure accuracy, log file data must be validated against measurements from dedicated dosimetric tools, such as scintillation detectors, which remain the standard for measuring spot parameters.

This chapter highlights the importance of analysing log file data and examines the discrepancies between spot parameters recorded in log files and those measured by dedicated dosimeters. It describes the process of measuring spot parameters with a scintillation detector, extracting corresponding log file data, and performing a comparative analysis to assess the accuracy and clinical relevance of log file data for both machine and patient-specific QA.

3.2 Materials and Method

3.2.1 Five-spot Pattern

Spot measurements were performed on an IBA Proteus Plus PBS proton therapy system (Louvain-la-Neuve, Belgium) with three rotating gantries installed at the National Hadron Therapy Centre, ACTREC, Tata Memorial Centre, Mumbai. The Study was conducted after the ethical committee clearance from D. Y. Patil Education Society (Deemed to be University), Kolhapur (DYPMCK/11/2022/IEC) and approval from ACTREC for data collection. The system is capable of delivering a proton beam with energies from 226.2 MeV to 70.18 MeV, corresponding to water-equivalent ranges of 32.02 g/cm² and 4.1 g/cm², respectively. The spot size, defined as one standard deviation or sigma (σ) of the Gaussian distribution of the spot profile, varies with energy; the manufacturer specifies a spot size of 2.8 mm for 226.2 MeV and 6.5 mm for 70.18 MeV, measured in air at the isocentre plane.

This chapter evaluates the accuracy of spot dosimetric parameters of different energies including analysis of spot size and position along the X and Y-axis and the spot symmetry. Measurements were performed across all energies with a water-equivalent range interval of 1 g/cm², spanning the lowest range of 4.1 g/cm² to the highest range of 32.0

g/cm², and for 12 gantry angles at 30° intervals. A 5-spot pattern was created for measurement, placing one spot at the centre and one in each quadrant of the Cartesian coordinate system, with coordinates at (0, 0), (127.8 mm, 127.8 mm), (-124.8 mm, 130.9 mm), (127.7 mm, -124.8 mm), and (-127.8 mm, -127.8 mm), as shown in Figure 3.1. Six month measurements resulted in 1800 5-spot patterns, encompassing a total of 9000 individual spots. All the measurements are done using a dedicated scintillator detector called Lynx2D. The baseline spot size values specified by IBA for all energies are presented in Table 3.1. These baseline spot size values are the same for a particular energy or range across all gantry angles and are identical in the X and Y directions. The measured spot size values were compared against these baseline values to evaluate accuracy. The MU per spot of each energy is selected in such a way that the Lynx2D detector should measure 70 % - 90 % signal. So that the scintillator will not reach the saturation level during measurement. The values of MU per spot for each energy are also tabulated in Table 3.1. In addition to spot size, the position of each spot was measured and tabulated to evaluate the accuracy of spot position.

Measurement setup errors heavily influence the accuracy of measured spot position values. Each spot's relative positional error values were calculated to overcome these dependencies. This approach aimed to minimise the impact of setup errors on spot position values by assessing the deviation of each spot's position from the intended irradiation position. The relative positional error values were calculated for each spot by subtracting the measured spot position from the measured central spot position and further subtracting this result from the actual set value of each spot.

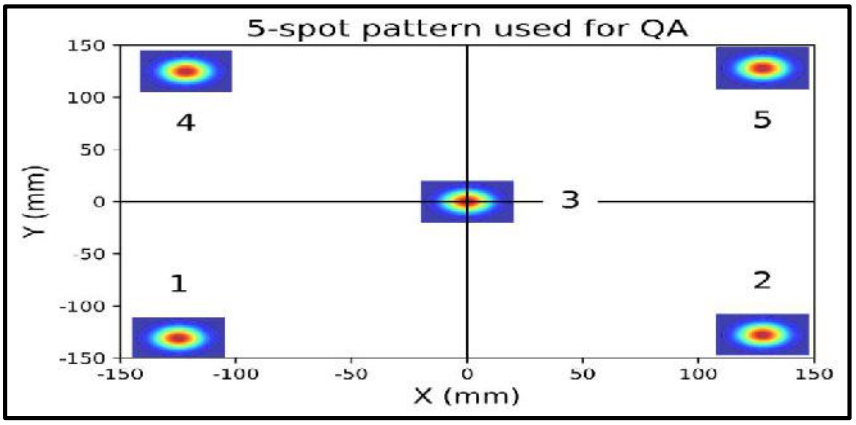

Figure 3.1: The Schematic diagram of the 5-spot pattern. Representing spot in each Cartesian coordinate.

Table 3.1: Tabulated the baseline spot size values used for this study. Tabulated the baseline spot size value of each range and the MU per spot of each spot.

Range (g/cm²)	Energy (MeV)	Baseline spot size (mm)	MU per spot used for the measurement (MU)
4.10	70.18	6.5	1.3
4.50	73.92	6.32	1.3
5.50	82.69	5.9	1.3
6.50	90.80	5.5	1.3
7.50	98.40	5.28	0.75
8.50	105.58	4.89	0.75
9.50	112.42	4.69	0.75
10.50	118.97	4.52	0.75
11.50	125.26	4.36	0.75
12.50	131.34	4.21	0.75
13.50	137.23	4.08	0.6
14.50	142.94	3.96	0.6
15.50	148.50	3.84	0.6
16.50	153.91	3.74	0.5
17.50	159.20	3.64	0.5
18.50	164.37	3.55	0.4
19.50	169.44	3.47	0.4
20.50	174.40	3.39	0.4
21.50	179.27	3.32	0.4
22.50	184.05	3.26	0.4
23.50	188.76	3.2	0.4
24.50	193.39	3.14	0.35
25.50	197.94	3.09	0.35
26.50	202.43	3.04	0.35
27.50	206.86	2.99	0.35
28.50	211.23	2.95	0.35
29.50	215.54	2.9	0.35
30.50	219.79	2.86	0.35
31.50	224.00	2.82	0.3
32.00	226.08	2.8	0.3

3.2.2 Lynx 2D detector

The Lynx 2D detector, optimized for PBS spot measurements in proton therapy, uses a gadolinium-based scintillator to convert radiation into visible light. This scintillator, known for its high sensitivity and efficiency, enables the detection of fine details within

each proton spot. Combined with a high-resolution Charge Coupled Device (CCD) camera, the system captures precise two-dimensional dose distributions with a 0.5 mm pixel resolution over a 30 cm x 30 cm active area. This design allows the Lynx 2D to measure critical PBS parameters such as spot size, position, and intensity across high-energy proton beams, including up to 250 MeV [9]. Integrated software processes the data in real-time, supporting adaptive and automated QA workflows to maintain the accuracy and stability of proton beam delivery. Figure 3.2 shows the Lynx2D detector and schematic diagram of the CCD camera and scintillator assembly.

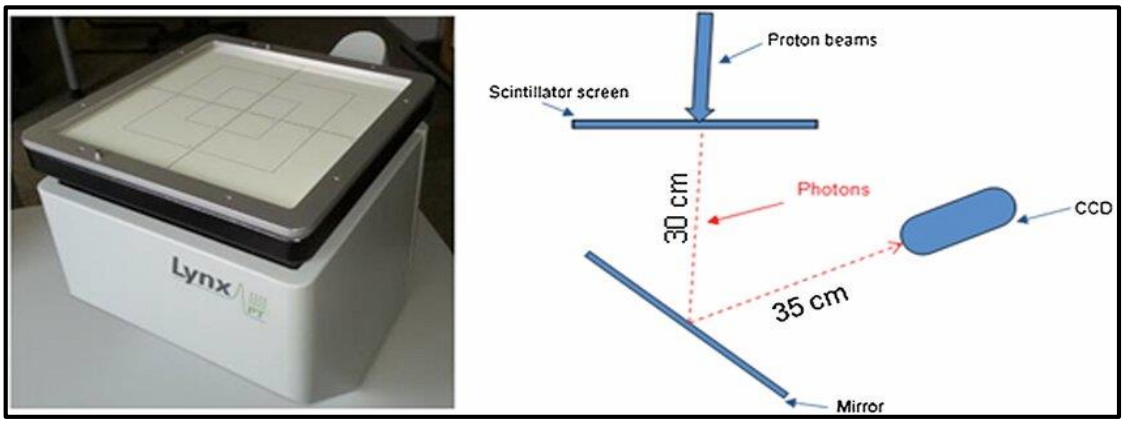

Figure 3.2: Lynx 2D Detector and graphical representation of the spot measurement process. [5].

3.2.3 Spot Measurement

The Lynx 2D scintillator detector was securely mounted onto a dedicated holder designed to attach to the machine gantry head, referred to as the nozzle. This holder ensures proper alignment of the Lynx 2D detector with the gantry head, facilitating the measurement of spot parameters at various gantry angles. Accurate detector alignment is crucial for reliable measurements; therefore, the alignment was verified and corrected before data acquisition. To verify alignment, a plumb attached to a string was used to detect and correct any tilt in the detector. The string, when properly aligned with the plumb, hangs perpendicularly. Kilo-voltage (kV) imaging of the string was employed to quantify and rectify any tilt. Adjustments were made until the tilt was reduced to less than 0.3 mm per metre. Figure 3.3 illustrates the gantry-mounted Lynx 2D detector with the plumb attached.

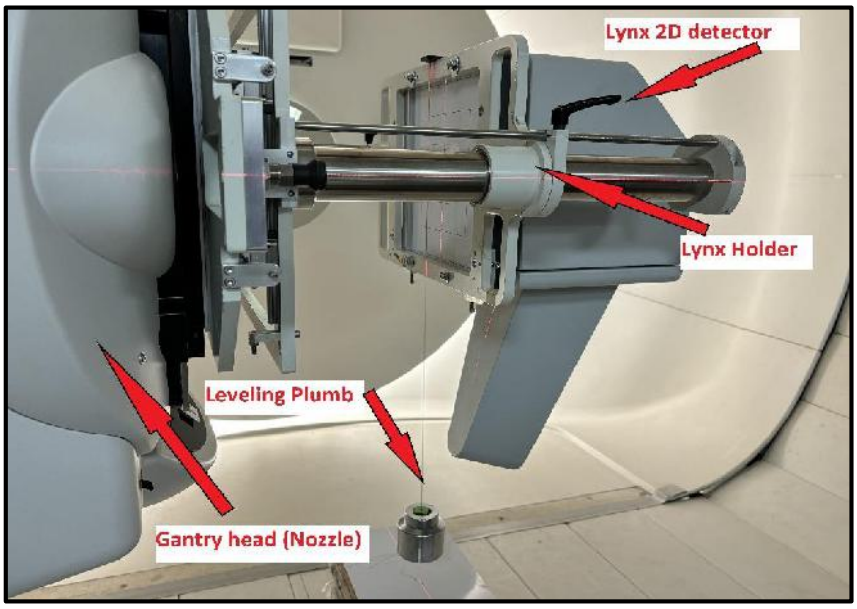

Figure 3.3: The Lynx2D attached to the gantry head using the Lynx holder. The levelling plumb is attached to level the detector.

Once the alignment was confirmed, the 5-spot pattern (Figure 3.1) was irradiated for each energy and the spot parameters were analysed using MyQA Fast Track software (IBA Dosimetry GmbH, Germany). The PBS spots exhibited an elliptical shape (Figure 3.4), necessitating the measurement and analysis of spot size along both major and minor axes, in addition to the X and Y directions. Spot size accuracy was assessed by evaluating spot dimensions in these directions. Spot symmetry was also calculated along the X-Y axes as well as the major-minor axes using Equations 3.1 and 3.2. Furthermore, the relative positional errors were compared against the reference value. All values are compared against the tolerance values.

$$Spot\ 2D\ symmetry(\%) = \frac{(major\ axis\ spot\ size - minor\ axis\ spot\ size)}{(major\ axis\ spot\ size + minor\ axis\ spot\ size)}\ X100 \quad (3.1)$$

$$XY\ symmetry\ (\%) = \frac{(X-axis\ spot\ size - Y-axis\ spot\ size)}{(X-axis\ spot\ size + Y-axis\ spot\ size)} X100 \quad (3.2)$$

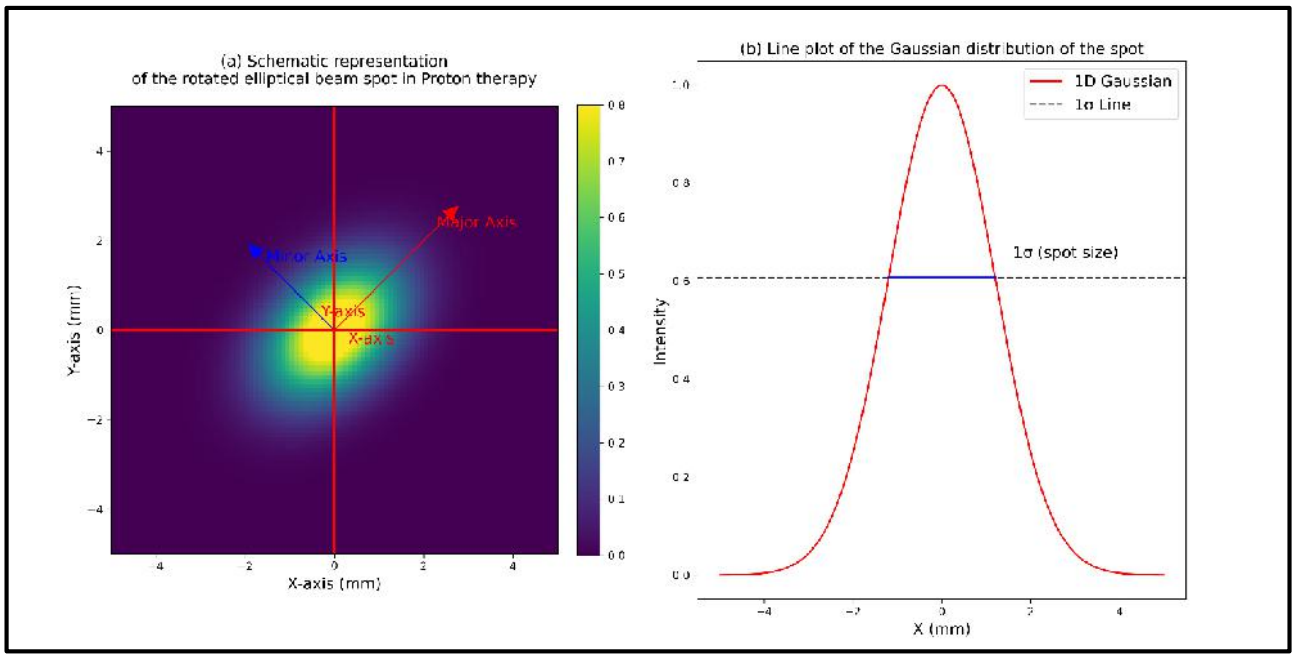

Figure 3.4: PBS spot shows an elliptical shape. (a) represents the elliptical shape of the spot, (b) Line plot of the Gaussian distribution of the spot.

3.2.4 Nozzle and Beam Monitoring

The irradiation log file in the PBS proton therapy system comprehensively records all parameters associated with beam delivery, including spot parameters, machine settings, and beam tuning details. The IBA Proteus Plus PBS system employs a specialised nozzle head for precise beam control and monitoring. The schematic representation (Figure 3.5) of the IBA Proteus Plus PBS nozzle head illustrates the beam path and associated components. Initially, the proton beam passes through IC1, which comprises 12 copper strips aligned along the X and Y directions, with a spacing of 3.5 mm between adjacent strips. IC1 primarily verifies the positional accuracy of each spot. The beam then passes through a quadrupole magnet, which maintains alignment along the central axis, ensuring stability before reaching the scanning magnets.

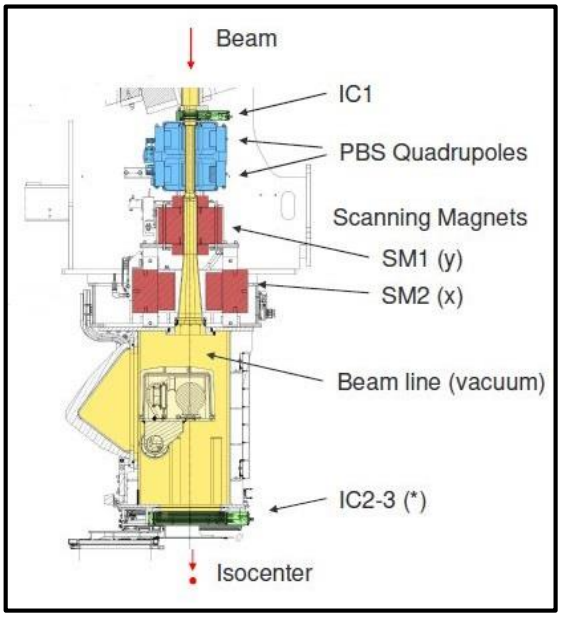

Figure 3.5: The IBA Proteus plus dedicated PBS nozzle schematic representation.

*IC2-3- Ionisation chamber.

The nozzle has two scanning magnets called X and Y scanning magnets, which deflect the pencil beam along the X and Y axes. The deflection currents of these magnets vary based on the desired spot positions and the beam energy. After deflection, the beam exits the nozzle and encounters another ionisation chamber called IC23 (Figure 3.6 (a) and 3.6 (b)). This chamber comprises two ionisation layers, with a total of 64 copper strips spaced 5 mm apart. The IC23 system records the position and size of each spot by measuring the charge collected across its strips. Additionally, IC23 is equipped with a dose pad, which accumulates charge during spot delivery. The MU for each spot is directly proportional to the charge collected in IC23, where a charge of three Nano coulombs corresponds to 1 MU in standard pressure and temperature. The IC23 is a vented chamber. The log file generated by the system encapsulates critical beam irradiation data, including spot positions and sizes measured by IC1 and IC23, scanning magnet currents and voltages, beam current, spot-specific charge collected by IC23, gantry angles, and set ranges.

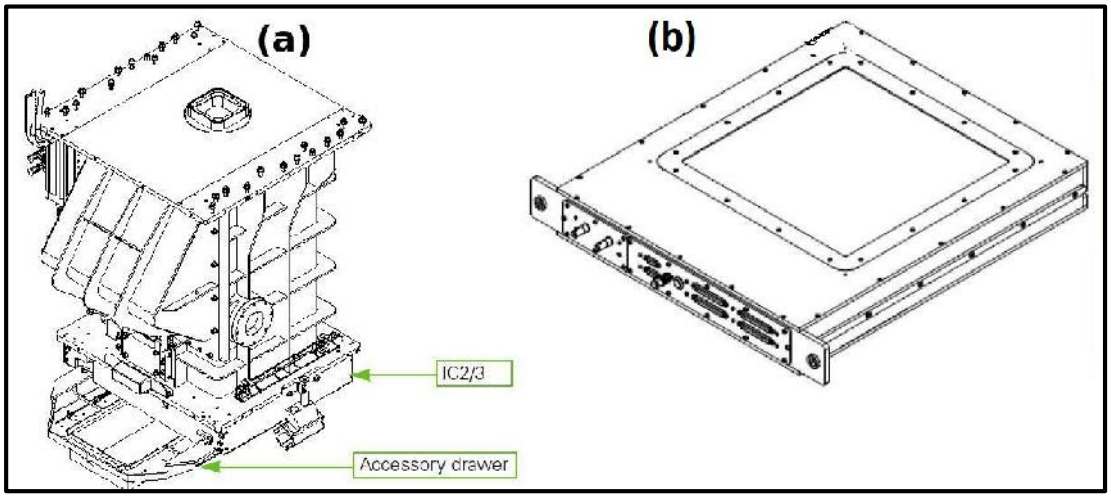

Figure 3.6: (a) IC23 assembly in the nozzle. (b) IC23 chamber schematic representation.

3.2.5 Log file generation

The beam log file plays a critical role in proton therapy delivery, ensuring accurate monitoring and control of beam parameters. A typical treatment plan consists of multiple energy layers, each containing numerous spots. The TPS defines the spot positions at the isocentre and assigns MU to each spot. These parameters, including the energy of each layer, spot positions, and MU per spot, are organised into a tabulated format and exported to the Oncology Information System (OIS), Mosaiq (Elekta Pvt Ltd), as control points.

For each energy layer, the log file generates three primary Comma-Separated Value (CSV) files: a specification file containing planned parameters, a tuning pulse data file, and an irradiation data file. Additionally, a file detailing the beam configuration is created. The input to the specification file is the data from the Mosaiq, using this data, the IBA beam delivery system generates the beam specification file. The system calculates the range for each energy layer based on Equation 3.3 and translates the TPS-defined spot positions at the isocentre into corresponding positions at the IC23 level for verification during delivery. The specification file records these IC23-level spot positions, along with other critical parameters such as the unique identification number for each spot, the intended charge for the specified MU, energy-specific scanning magnet currents and voltages, range of each spot and beam currents for each spot.

$$Range\left(\frac{g}{cm^2}\right) = \exp[(a * \ln(Energy)^3 + b * \ln(Energy)^2 + c * \ln(Energy)\, d] \quad (3.3)$$

Energy in MeV. The coefficients a=-0.0133, b=0.15248, c=1.2193, and d=-5.5064

The specification file serves as the reference for real-time monitoring, while the log file provides a detailed record of beam irradiation data during delivery. Any deviation from the predefined tolerances specified in the beam specification file triggers an immediate beam interruption, ensuring precise and safe proton therapy. The tolerance for spot size, position and MU are given in Table 3.2. In Table 3.2, the comparison of AAPM TG224 recommended tolerance values with the log file tolerance provided.

Table 3.2: Comparison of AAPM-TG224 Recommended Tolerances for Spot Parameters and IBA-Proteus Plus Log File Tolerances for Triggering Beam Interruption

	Spot Size	Spot Position		Monitor Unit (MU)	Spot symmetry
		X-Axis	Y-Axis		
AAPM-TG224 recommended Tolerances.	10 % of baseline spot size	1 mm	1 mm	2 %	10 %
Log file tolerances.	1 mm	2.03 mm*	2.25 mm*	2.5 %	Not specified in the log file.

* The values are given for the IC23 level.

3.2.6 Tuning Pulse

The IC23 continuously monitors the spot position and MU for each spot during proton beam delivery. To ensure positional accuracy within each energy layer, the system employs a mechanism known as the tuning pulse. In this process, a spot near the beam's central axis is selected, and a minimal dose of 0.02 MU is delivered to that spot. The IC23 records the spot’s position and compares it with the intended position, calculating the deviation or error in the spot position within the layer. This positional error is corrected by assigning an offset value to the scanning magnets for the specific energy layer. Consequently, the corrected offset ensures accurate positioning of all subsequent spots in that layer. This tuning pulse process is performed for every layer of beam delivery to maintain precision across all spots. The log file captures the offset values recorded during each tuning pulse, and during log file analysis, these offset values are extracted to determine the actual delivered positions of the spots accurately.

3.2.7 Data extraction from log file

Log file data extraction is conducted using an in-house Python script designed for the systematic processing of beam irradiation data. The script reads and processes all the log files including beam configuration files, specification files, tuning pulse files and irradiation files to facilitate comprehensive analysis and quality assurance.

The script begins by reading the beam.csv file, which records general beam irradiation data, including the gantry name, temperature, and pressure during delivery. Using this information, the script calculates the temperature and pressure correction factor (K) to adjust the temperature and pressure change inside the IC23 chamber for each spot. The correction factor is calculated using Equation 3.4. One MU corresponds to 3nC of charge under standard temperature and pressure (STP) conditions. The IC23 measured charge is multiplied by the factor K and calculates the MU of each spot.

$$K = \frac{(T+273.2)}{(To+273.2)} * \frac{P0}{P} \tag{3.4}$$

K is the temperature and pressure correction factor. T is the temperature of the IC23 in degree (standard temperature 22^0c) and P is the pressure of the air in the IC23 in mbar. The Po is the standard pressure of 1013.2 mbar.

Next, the script processes the irradiation.csv file, which contains detailed information for all delivered spots, including spot positions at IC23 and IC1, spot sizes at IC1 and IC23, charge collected at IC23, scanning magnet currents and voltages, beam current, set range, degrader feedback, and tuning pulse offset values. The tuning pulse offset is subtracted from all spots to determine the actual delivered positions at IC23. Additionally, the script identifies the tuning pulse spot number and adds its charge to the corresponding spot.

The script also reads the specification file for each layer, which contains the planned parameters such as the number of spots, intended positions, sizes, energy of each spot and charges. It tabulates these values and also calculates the minimum and maximum allowable values based on predefined tolerances specified in Table 3.2.

Finally, the script consolidates data from all sources to create a detailed tabulation of spot information for each energy layer. Additionally, measured data from the Lynx 2D scintillation detector, including spot sizes along the X and Y axes, major and minor axis spot sizes, and spot symmetry, is tabulated and compared with the corresponding values recorded in the log file.

3.3 Results

3.3.1 Five-Spot measurement

The smallest spot size measured in the scintillator was 2.69 mm in the x direction and 2.66 mm in the y direction for the energy 226.2 MeV, while the largest spot size measured 6.59 mm in the x direction and 6.71 mm in the y direction for the 70.18 MeV. Similarly, the minimum major axis spot size was 2.765 mm for 226.2 MeV, whereas the maximum major axis spot size was 6.663 mm for 70.18 MeV. The minimum for the minor axis spot size was 2.548 mm for 226.2 MeV, and the maximum was 6.48 mm for 70.18 MeV. The maximum relative positional error along the X-axis was -0.85 mm and 0.86 mm for relative positional error on the Y-axis. The statistics of measured data are given in Table 3.3**.** The maximum 2D symmetry was 9.5% and XY symmetry was 3.9%.

Table 3.3: The statistics of all Lynx2D scintillator measured spot parameters.

	Minimum	Maximum	Mean	Standard Deviation	25th Percentile (1st Quartile)	50th Percentile (Median)	75th Percentile(3rd Quartile)
Range (gm/cm^2)	4.1	32.0	18.0	8.6	10.5	18.0	25.5
Gantry angle (Degree)	0.0	330.0	165.0	103.6	82.5	165.0	247.5
Measured X position(mm)	-127.3	129.6	1.1	112.2	-123.4	-0.7	126.5
Measured Y position(mm)	-132.4	128.3	-1.7	114.3	-128.0	-0.7	124.2
Measured X spot size(mm)	2.7	6.6	3.9	1.0	3.1	3.5	4.5
Measured Y spot size(mm)	2.7	6.7	3.9	1.0	3.1	3.5	4.5
Measured Major axis spot size (mm)	2.8	7.0	4.0	1.1	3.2	3.6	4.7
Measured Minor axis spot size (mm)	2.5	6.5	3.8	1.0	3.0	3.4	4.4
2D symmetry (%)	2.0%	9.5%	3.5%	2.0%	1.8%	3.2%	4.8%
XY Symmetry(%)	1.0%	3.9%	0.9%	0.7%	0.3%	0.8%	1.3%
Relative positional error along X-axis(mm)	-0.85	0.71	0.05	0.36	0.00	0.10	0.30
Relative positional error along y-axis (mm)	-0.41	0.86	0.22	0.31	0.00	0.04	0.52

The measured spot sizes across all ranges and gantry angles were compared with the baseline spot size values, and the results are summarised in Table 3.4. The comparison demonstrated excellent agreement between the measured and baseline values. For the X-axis spot size, the maximum variation was observed to be 6.5% at a range of 25.5 g/cm² for a gantry angle of 270°. Similarly, the maximum difference in the Y-axis spot size was 7.31 % at a range of 30.5 g/cm² for a gantry angle of 30°.

The Standard Deviation (SD) of the differences in the X-axis spot size was less than 2.6 %, while for the Y-axis spot size, it was under 3 %. The maximum Root Mean Square Error (RMSE) for the X-axis spot size difference was 2.5 %, and for the Y-axis spot size difference, it was 2.9 %. Importantly, all the observed variations were well within the

AAPM TG-224 specified tolerance of 10 % highlighting the consistency and accuracy of the spot size measurements.

Table 3.4: Comparison of Lynx2D-measured X and Y spot sizes with the manufacturer-specified baseline values, including the differences in X and Y spot sizes, along with the mean, standard deviation, and root mean square error (RMSE).

Gantry Angle (Degrees)	Maximum difference in X spot size (%)	Mean (SD) X-spot size difference (%)	RMSE of X-spot size difference (%)	Maximum difference in Y spot size (%)	Mean (SD) Y-spot size difference (%)	RMSE of Y spot size difference (%)
0	6.1	0.00 (2.42)	2.42	5.76	-0.56 (2.27)	2.26
30	5.29	0.27 (1.87)	1.86	7.31	-0.06 (1.57)	1.57
60	3.03	-0.54 (1.78)	1.78	7.30	-0.41 (2.32)	2.31
90	0.29	-2.50 (1.31)	1.31	4.27	-0.73 (1.74)	1.74
120	0.13	-2.83 (1.34)	1.33	1.91	-2.29 (2.04)	2.03
150	2.17	-1.32 (1.42)	1.42	2.72	-1.49 (1.69)	1.69
180	5.60	0.61 (2.10)	2.10	6.69	2.67 (2.93)	2.92
210	6.04	0.75 (2.56)	2.55	4.89	-0.47 (2.08)	2.07
240	1.74	-0.73 (1.33)	1.33	5.56	-1.11 (2.18)	2.17
270	6.50	-0.52 (1.82)	1.82	3.78	0.14 (1.64)	1.63
300	0.14	-2.65 (1.34)	1.34	0.82	-2.05 (1.38)	1.37
330	3.41	-0.74 (2.20)	2.19	2.04	-0.99 (1.30)	1.30

Figure 3.7 illustrates the relationship between the measured X and Y spot sizes and the range. The plot reveals a clear trend where the spot size decreases as the range increases, indicating a dependence of spot size on the beam energy, with higher energy beams producing smaller spots. This behaviour aligns with expectations, as higher energy beams exhibit less scattering resulting in reduced spot size in air.

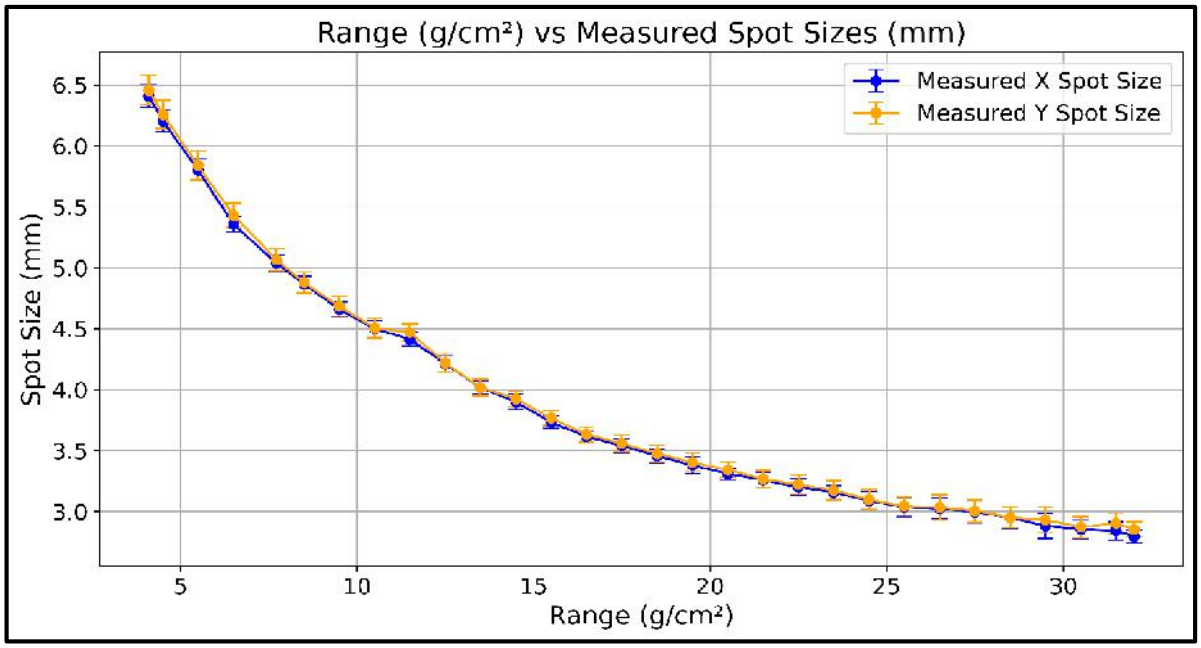

Figure 3.7: The measures of spot size (X and Y direction) plotted against the range.

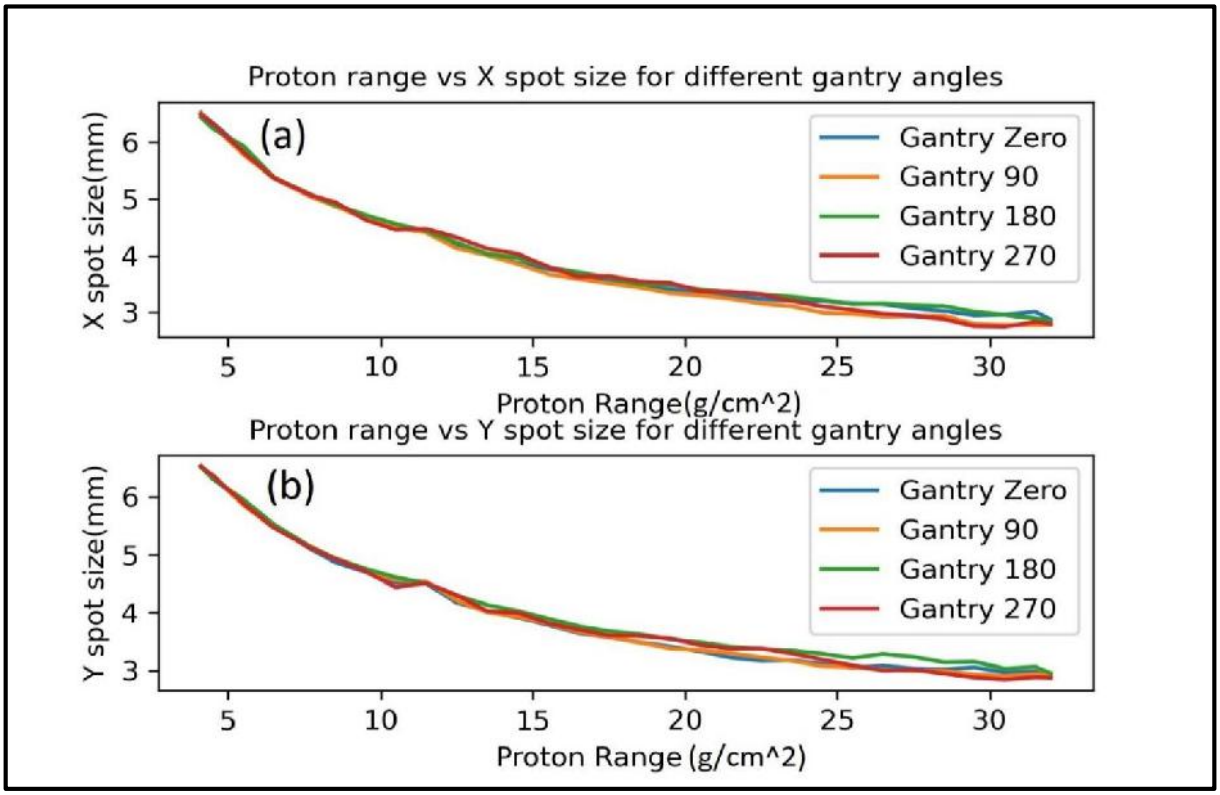

Figure 3.8: The measured spot size along X and Y direction versus range plotted for different gantry angles. (a) X spot size versus range for different gantry angles. (b) Y spot size versus range for different gantry angles.

Figure 3.8 presents the measured spot sizes for different gantry angles plotted against the range. The data show slight variations in the measured spot sizes for different gantry angles, highlighting the influence of the beam's orientation on spot size characteristics. The variations are more pronounced for spots at higher ranges, where the differences between gantry angles become more evident.

3.3.2 Log file data analysis

The study collected all irradiation log files of the corresponding 5-spot pattern measured using the Lynx2D detector. The log file data analysis was done using an in-house tool developed using Python script. The log file recorded spot size, and relative positional error values were compared against the lynx2D measured data to evaluate the correlation between the data.

The log file also captures the scanning magnet currents corresponding to each spot. Scanning magnet currents are inherently a function of the beam's range or energy, as they control the deflection and positioning of the proton beam for accurate spot delivery. Figures 3.9 and 3.10 depict the variations in X and Y scanning magnet currents as a function of the range. These plots highlight the dependency of the scanning magnet currents on the energy levels, with distinct trends observed across the range spectrum. Such data are invaluable for verifying the consistency and accuracy of the scanning magnet performance, ensuring the correct positioning of spots during treatment delivery.

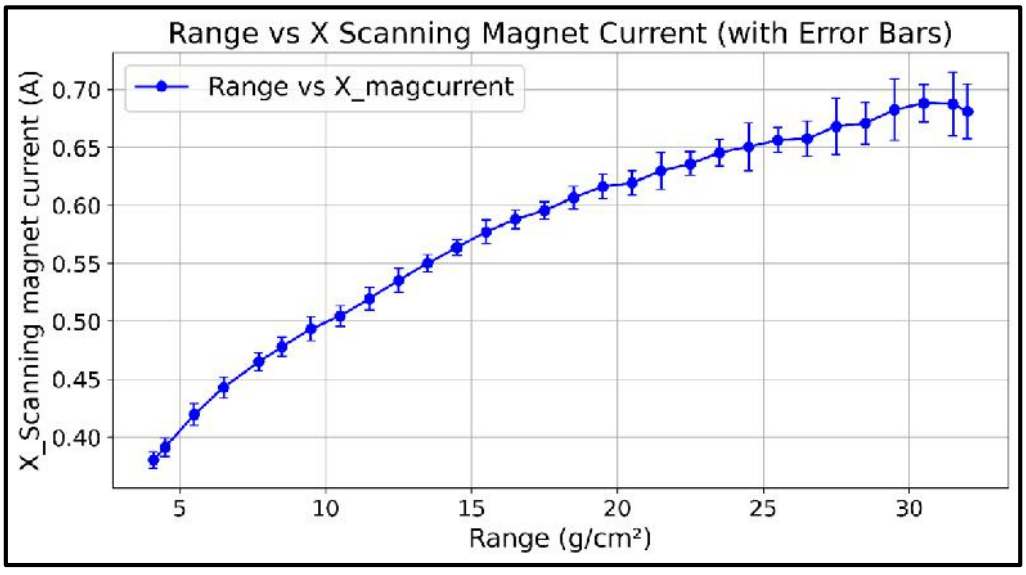

Figure: 3.9: Range versus X scanning magnet current recorded in the log file data.

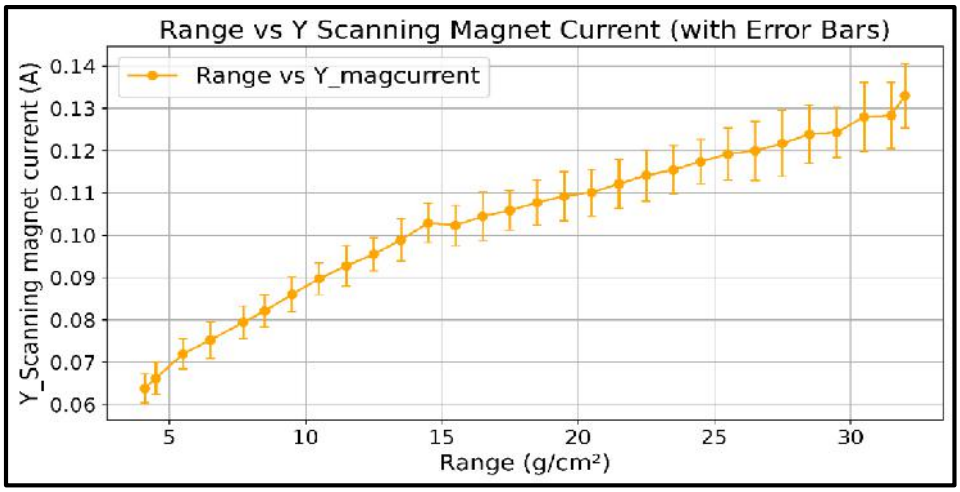

Figure 3.10: Range versus X scanning magnet current recorded in the log file data.

The log file records spot size data measured by the IC23 ionisation chamber, which is equipped with copper strips spaced 5 mm apart. The spot size is determined by fitting a Gaussian function to the charge collected across these strips. However, due to the limited resolution of the IC23, the recorded spot size values are less precise when compared to those obtained using a high-resolution scintillator detector, such as the Lynx2D.

Figures 3.11 and 3.12 display the relationship between the range and the spot sizes recorded along the X and Y axes in the IC23, respectively. These graphs include error bars to illustrate the variation in recorded spot sizes for each energy or range. The log file recorded spot size shows a longer error bar with respect to range.

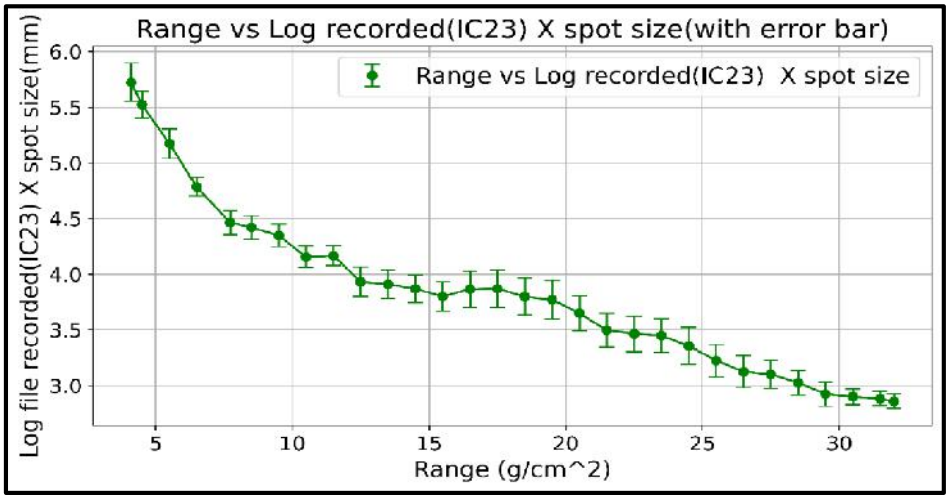

Figure 3.11: Range versus log file recorded X spot size with error bar.

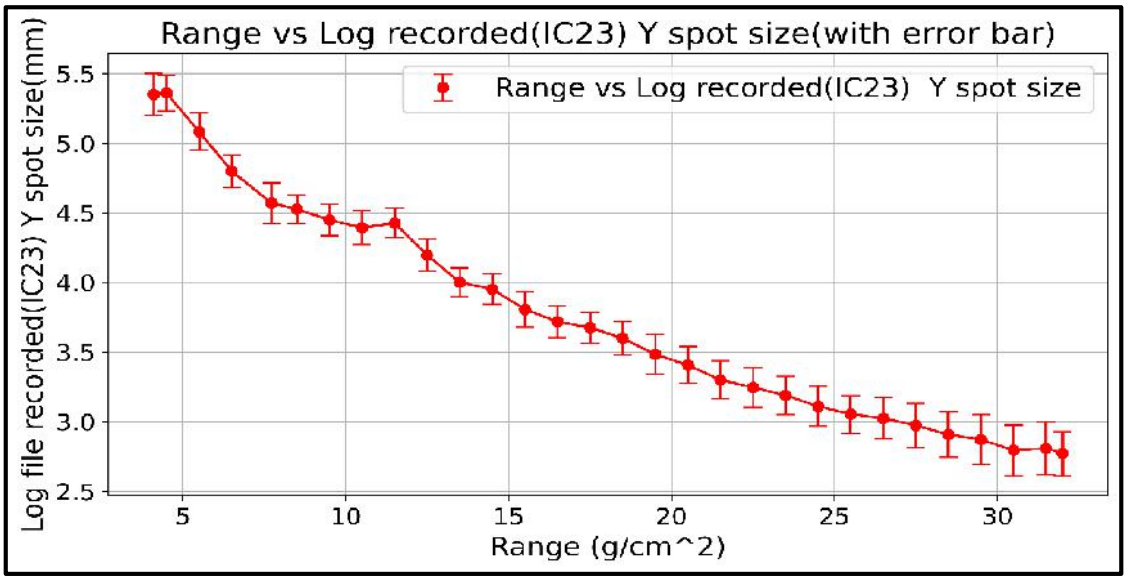

Figure 3.12: Range versus log file recorded X spot size with error bar.

Table 3.5: The difference in spot size along X and Y directions between the Lynx2D measured and log file recorded data. The maximum difference, RMSE, mean and standard deviation of the difference are given for different gantry angles.

Gantry Angle (Degrees)	Maximum difference in X spot size (%)	Mean(SD) X-spot size difference (%)	RMSE of X-spot size difference (%)	Maximum difference in Y spot size (%)	Mean(SD) Y-spot size difference (%)	RMSE of Y-spot size difference (%)
0	21.88	6.91(4.95)	8.50	16.04	4.05(4.19)	5.82
30	14.90	6.75(3.67)	7.68	17.42	4.87(4.47)	6.61
60	16.58	6.78(3.55)	7.65	18.51	5.20(4.68)	7.00
90	23.88	6.41(4.86)	8.04	18.93	5.85(4.11)	7.15
120	13.72	6.68(3.31)	7.45	17.69	5.99(3.81)	7.10
150	15.27	7.14(3.51)	7.96	16.27	5.08(3.79)	6.33
180	26.32	7.64(5.62)	9.48	16.44	4.51(3.95)	5.99
210	14.51	6.66(3.83)	7.68	19.38	6.70(4.75)	8.21
240	14.16	6.83(3.85)	7.84	21.04	6.35(5.15)	8.17
270	18.82	6.88(4.85)	8.42	19.43	5.76(4.35)	7.22
300	15.41	7.19(3.58)	8.03	19.32	5.67(4.35)	7.15
330	14.48	7.29(3.72)	8.19	16.31	4.54(3.76)	5.89

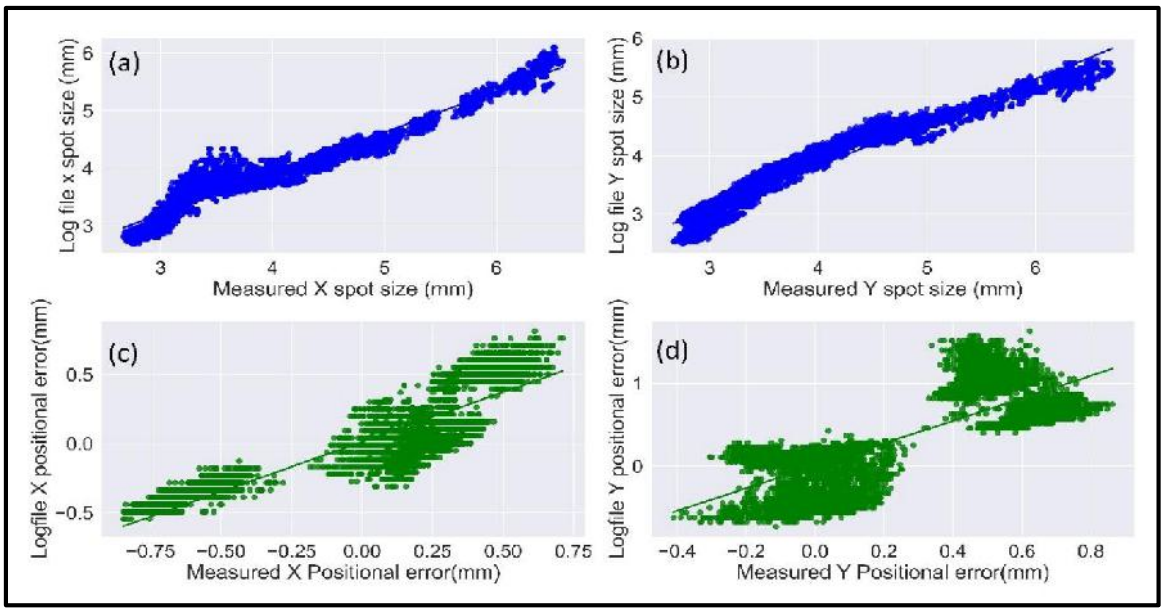

Figure 3.13: Plots of measured spot parameters versus log file recorded spot parameters. (a) Measured X-spot size versus log file recorded X-spot size. (b) Measured Y spot size versus log file recorded Y spot size. (c) Measured relative X positional error versus log file recorded relative X-positional error. (d) Measured relative Y positional error versus log file recorded relative Y positional error.

The comparison of Lynx2D-measured spot parameters with the spot size values recorded in the log file is summarised in Table 3.5. Additionally, the relationships between Lynx2D-measured and log file-recorded spot sizes in the X and Y directions, as well as the correlation between their relative positional errors, are illustrated in Figure 3.13.

From Table 3.5, the maximum observed difference in X-spot size was 23.9 %, corresponding to a range of 19.5 g/cm² and a gantry angle of 90^0. For the Y-spot size, the maximum difference was 21.04 %, observed at a range of 4.1 g/cm² and a gantry angle of 240^0. The highest mean X-spot size difference was 7.64 %, with a SD of 5.62 %, while the highest mean Y-spot size difference was 6.7 %, with an SD of 4.75 %. The maximum RMSE was 9.5 % for the X-spot size and 8.21 % for the Y-spot size. These values indicate that the spot size differences recorded in the log file exceed the AAPM TG224 recommended tolerance of 10 %. Furthermore, the maximum differences between the log file-recorded relative positional errors and the Lynx2D-measured relative positional errors were found to be 0.910 mm and 1.610 mm for the X and Y directions, respectively. These deviations surpass the TG224-recommended tolerance of 1 mm for relative positional error.

The findings suggest that the log file-recorded spot sizes and positional data exhibit variations and uncertainties that exceed the established tolerance limits when compared to scintillator-measured values. Consequently, the direct use of log file data for evaluating spot size and position in quality assurance processes may introduce significant errors, highlighting the necessity for independent verification using reliable measurement tools such as the Lynx2D detector.

3.4 Discussion

Spot dosimetric accuracy is a critical determinant of precise dose delivery in proton therapy, directly influencing patient treatment outcomes. This chapter comprehensively describes the methodologies employed for spot parameter measurement and evaluates the accuracy of key dosimetric parameters. It also details the analysis of irradiation log file data compared with detector-measured values. The study systematically investigates the accuracy of spot size, position, and symmetry for individual spots in the proton PBS system, highlighting their significance in ensuring optimal treatment precision.

A study conducted by Kraan AC et al. [10] investigated the impact of spot size variations on dose delivery by altering the nominal spot size by 5 % to 50 % and calculating the dose in seven patient datasets. The findings demonstrated that variations in spot size significantly influence treatment plan quality. Similarly, Liu C et al. [11] evaluated the relationship between spot size and spot spacing in treatment plan quality. Their study concluded that beams with smaller spot sizes are more robust in managing interplay effects and anatomical variations compared to larger spot sizes. Rana S et al. [3] focused on the effect of spot size variations in Stereotactic Body Radiation Therapy (SBRT) lung cases, revealing that a 20 % variation in spot size led to a 3 % change in target dose coverage, while a 15 % variation resulted in less than a 2 % dose difference. These results align with the AAPM TG224-recommended spot size tolerance of 10 %.

In this study, the Lynx2D measured spot size across all energy ranges and gantry angles demonstrated high accuracy, with maximum deviations of less than 8 % compared to baseline values well within the 10 % tolerance specified by AAPM TG224. This underscores the importance of routine verification of spot size in PBS systems. Ensuring spot size accuracy is essential for maintaining treatment plan quality and delivering precise

doses to patients, reinforcing the need for regular quality assurance checks as part of standard PBS practice.

Numerous studies have utilised irradiation log files for PSQA. Winterhalter C et al. [12] demonstrated the potential of log file data combined with MC dose calculation algorithms, reporting that over 90 % of voxels exhibited dose errors of less than 3 % when comparing planned and recalculated doses. This finding suggests that log file and MC-based methods could serve as viable alternatives to conventional measurement-based PSQA. Similarly, Jeon C et al. [13] employed the TOPAS-MC dose engine to recalculate doses for a line-scanning PBS system using spot position and MU information from log files. Their results showed a gamma analysis passing rate exceeding 90 % for 2 mm/2 % criteria, although their study did not account for potential variations in machine output. Ates O et al. [6] conducted a comprehensive analysis of six years of log file data from a PBS proton therapy machine, focusing on the accuracy of spot MU, position, and size compared to TPS-specified values. Their findings revealed that MU accuracy and spot position errors were both within acceptable limits, with deviations of less than 1 %. However, significant discrepancies in spot size were observed, with many exceeding the 10 % tolerance specified by AAPM TG224.

In this study, the variation between measured spot sizes and log file-recorded values frequently exceeded the AAPM TG224 recommended tolerance of 10 % across most ranges and gantry angles. The mean error was greater than 7 %, with an SD exceeding 5 % for numerous ranges and angles. While earlier studies have primarily focused on log file derived MU and spot position data for MC-based dose recalculations in PSQA, this approach often overlooks the critical contributions of spot size and symmetry. These parameters are essential for ensuring accurate dose comparisons between the TPS and delivered doses.

The findings of Toscano S et al. [8] underscore the inherent uncertainties in log file data, particularly for spot position and spot size, emphasising the limitations of directly utilising log file data for PSQA or machine QA without thorough evaluation. In this study, the substantial SD and variations in spot size exceeding 10 % between Lynx2D-measured and log file-recorded data further highlight the degree of error and uncertainty in log file-reported spot size values. A comprehensive assessment of log file inaccuracies is

imperative to account for these discrepancies and to ensure robust quality assurance in proton therapy. Rigorous validation of log file data, particularly spot size and symmetry, is essential to enhance the reliability of PSQA and machine QA processes.

Measurement-based PSQA has traditionally been the gold standard for verifying treatment accuracy. However, this approach is time-consuming, requiring significant machine time and manpower. Automation in QA processes for PBS is increasingly critical to ensure fast and reliable evaluations of beam delivery accuracy. Current PSQA methods using MC dose recalculations with log file data primarily focus on spot position and MU values, often neglecting variations in parameters such as spot size and symmetry. These parameters are crucial for accurate dose evaluation, as their variations can significantly affect treatment quality.

In this study, log file-recorded data were compared with measurements obtained using the Lynx2D scintillation detector to evaluate their correlation. While the spot size data from the log files showed some correlation with measured values, the associated errors exceeded the tolerance limits set by international guidelines, raising concerns about their direct use for QA without correction.

The introduction of ML models offers a promising solution to address these uncertainties. ML models can effectively handle non-linearity in the data and improve the accuracy of parameter predictions, including spot size and symmetry. By mitigating uncertainties in log file data, ML based approaches can provide a more robust framework for utilising log file data in both machine QA and PSQA. This advancement represents a significant step toward improving automation, enhancing reliability, and ensuring precision in PBS proton therapy.

3.5 Conclusions

This chapter analysed and compared Lynx2D scintillation detector measurement data with log file-recorded data for spot parameters in a proton PBS system. The findings demonstrate a correlation between the log file and measured data; however, significant errors were identified, particularly in spot size and, to a lesser extent, in spot position. These discrepancies highlight the limitations of using log file data directly for quality assurance processes without correction.

The insights gained in this chapter set the stage for the next phase of the study, which explores the development of ML models. These models aim to use log file data as input and measured data as output to address existing inaccuracies and establish a robust framework for improving log file data reliability. This approach represents a critical step toward enhancing the precision and efficiency of quality assurance in PBS proton therapy.

3.6 References

1. Van der Merwe D, Van Dyk J, Healy B, Zubizarreta E, Izewska J, Mijnheer B, Meghzifene A. Accuracy requirements and uncertainties in radiotherapy: a report of the International Atomic Energy Agency. Acta oncologica. 2017 Jan 2;56(1):1-6.
2. Arjomandy B, Taylor P, Ainsley C, Safai S, Sahoo N, Pankuch M, Farr JB, Yong Park S, Klein E, Flanz J, Yorke ED. AAPM task group 224: comprehensive proton therapy machine quality assurance. Medical physics. 2019 Aug;46(8):e678-705.
3. Rana S, Rosenfeld AB. Impact of errors in spot size and spot position in robustly optimized pencil beam scanning proton-based stereotactic body radiation therapy (SBRT) lung plans. Journal of Applied Clinical Medical Physics. 2021 Jul;22(7):147-54.
4. Noufal MP, Sharma SD, Patro K, Arjunan M, Krishnan G, Tyagarajan R, Rana S, Chillukuri S, Jalali R. Impact of spot positional errors in robustly optimized intensity-modulated proton therapy plan of craniospinal irradiation. Radiological Physics and Technology. 2021 Sep;14(3):271-8.
5. Marmitt GG, Pin A, Siang KN, Janssens G, Souris K, Cohilis M, Langendijk JA, Both S, Knopf A, Meijers A. Platform for automatic patient quality assurance via Monte Carlo simulations in proton therapy. Physica Medica. 2020 Feb 1;70:49-57.
6. Ates O, Pirlepesov F, Zhao L, Hua CH, Merchant TE. Development of a log file analysis tool for proton patient QA, system performance tracking, and delivered dose reconstruction. Journal of Applied Clinical Medical Physics. 2023 Jul;24(7):e13972.
7. Siochi RA, Pennington EC, Waldron TJ, Bayouth JE. Radiation therapy plan checks in a paperless clinic. Journal of Applied Clinical Medical Physics. 2009 Dec;10(1):43-62.
8. Toscano S, Souris K, Goma C, Barragán-Montero A, Puydupin S, Vander Stappen F, Janssens G, Matic A, Geets X, Sterpin E. Impact of machine log-files uncertainties on the quality assurance of proton pencil beam scanning treatment delivery. Physics in Medicine & Biology. 2019 Apr 29;64(9):095021
9. Lin L, Ainsley CG, Mertens T, De Wilde O, Talla PT, McDonough JE. A novel technique for measuring the low-dose envelope of pencil-beam scanning spot profiles. Physics in Medicine & Biology. 2013 Jun 5;58(12):N171.
10. Kraan AC, Depauw N, Clasie B, Madden T, Kooy HM. Impact of spot size variations on dose in scanned proton beam therapy. Physica Medica. 2019 Jan 1;57:58-64.
11. Liu C, Schild SE, Chang JY, Liao Z, Korte S, Shen J, Ding X, Hu Y, Kang Y, Keole SR, Sio TT. Impact of spot size and spacing on the quality of robustly optimized

intensity modulated proton therapy plans for lung cancer. International Journal of Radiation Oncology* Biology* Physics. 2018 Jun 1;101(2):479-89.
12. Winterhalter C, Meier G, Oxley D, Weber DC, Lomax AJ, Safai S. Log file based Monte Carlo calculations for proton pencil beam scanning therapy. Physics in Medicine & Biology. 2019 Jan 29;64(3):035014.
13. Jeon C, Lee J, Shin J, Cheon W, Ahn S, Jo K, Han Y. Monte Carlo simulation-based patient-specific QA using machine log files for line-scanning proton radiation therapy. Medical Physics. 2023 Nov;50(11):7139-53.

Chapter 4

Development and Validation of Machine Learning Models for Predicting Spot Dosimetric Parameters

Chapter 4

Title: Development and Validation of Machine Learning Models for Predicting Spot Dosimetric Parameters.

4.1 Introduction

The ML is revolutionising radiation therapy by introducing advanced computational techniques that enhance clinical workflow precision, efficiency, and automation. In recent years, ML has emerged as a powerful tool for addressing the challenges associated with QA, auto contouring, and treatment planning in proton therapy. By leveraging complex algorithms and large datasets, ML models can identify patterns, predict outcomes, and optimise processes, leading to more accurate and efficient treatment delivery [1,2].

The proton radiotherapy system is very complex in nature and requires more accuracy in treatment and quality assurance to ensure proper dose delivery to the patient. ML models can automate many of the QA workflows to provide a fast and accurate troubleshooting mechanism. ML has shown promise in automating QA tasks in proton therapy. For example, Grewal et al. [3] utilised GPR and an SNN to predict output and MU in a double scattering proton therapy system, using parameters such as range, field size, and modulation as inputs to the models. Similarly, Li Z et al. [4] applied feed-forward and recurrent neural network models to predict proton therapy range and dose by analysing data from proton-induced positron emitters.

The irradiation log files are the records of the treatment. The log files provide a rich data source for ML applications, especially in PBS systems, where they can be used to predict spot positions and MU per spot [5]. Dominic Maes et al. [6] demonstrated that ML models trained on log files and treatment planning data from 20 PBS patient plans could accurately predict delivered spot positions and MU values. The deep learning models have been explored for dose calculation improvements. Chao Wu et al. [7] introduced a deep learning framework to convert pencil beam dose distributions into MC-equivalent distributions, significantly enhancing dose calculation accuracy and integration into treatment planning. Additionally, advanced architectures, such as recurrent U-nets and 3D convolutional neural networks, have been developed for dose prediction, showing promising results [8,9].

Neishabouri A et al. [10] applied a long short-term memory (LSTM) neural network to model dose deposition characteristics, successfully capturing variations across the entrance region, Bragg peak, and distal fall-off, even in complex and heterogeneous geometries. Similarly, Pastor-Serrano et al. [11] used a CNN to predict dose deposition by mono-energetic proton beams for different energies and patient geometries, further advancing the field. Meijers A et al. [12] explored the use of log file data in conjunction with patient breathing patterns to reconstruct 4D dose distributions. Their work enabled comparisons between planned and delivered doses by integrating weekly 4D CT scans, highlighting the potential of ML and log file data in adaptive proton therapy workflows.

However, the direct use of log file-recorded data for QA processes, such as spot position, size and MU poses challenges. Log file spot position and size are determined through a Gaussian fit approximation, introducing inherent uncertainties. These uncertainties can exceed the precision of the scanning system, even after magnet commissioning [13]. This limitation becomes particularly significant when using log file data for pencil beam scanning PSQA or machine QA. Uncertainties in spot parameters can result in inaccurate interpretations, potentially affecting treatment accuracy.

The ML models offer a powerful and comprehensive solution to mitigate uncertainties in proton therapy by leveraging advanced data processing techniques. By training on extensive, diverse, and high-quality datasets, ML algorithms can identify intricate patterns, account for variability in recorded data, and significantly reduce the impact of systematic and random errors. This capability firmly establishes ML as an indispensable tool for enhancing the reliability and accuracy of log file data, enabling precise predictions and ensuring robust quality assurance processes in proton therapy.

In Chapter 3, a detailed analysis comparing spot parameters measured with the Lynx2D scintillation detector to those recorded in log files for a PBS system revealed a correlation between the datasets. However, significant discrepancies were identified, particularly in spot size and, to a lesser extent, in spot position. These findings highlight that the direct use of log file data for analysing the dosimetric parameters of PBS is not accurate without applying appropriate corrections. ML models, with their capability to handle the non-linearity and inherent complexity of the data, can develop predictive

frameworks that utilise log file data to accurately determine spot parameters, ensuring they remain within the acceptable tolerance limits and improving overall treatment precision.

This chapter details the development and validation of ANN-based ML models designed to predict spot size along the X, Y major, and minor axis direction of a spot and relative spot positional errors along the X and Y axis using irradiation log file data as input. The process of model creation, hyper parameter tuning, and validation through various statistical tools is systematically summarised in this chapter.

4.2 Materials and Methods

4.2.1 Artificial Neural Network (ANN)

An ANN is a computational model inspired by the structure and function of biological neural networks [14]. It consists of layers of interconnected nodes, or neurons, that process information. An ANN typically includes an input layer to receive data, one or more hidden layers to learn patterns and relationships, and an output layer to produce predictions or classifications. Each neuron applies a mathematical operation using weights, biases, and an activation function to introduce non-linearity. The network learns by adjusting these parameters during training to minimise the error between predicted and actual outputs, making it a powerful tool for solving complex, non-linear problems.

4.2.2 ANN model architecture

This study developed six distinct ANN models, including X spot size prediction, Y spot size prediction, major axis spot size prediction, minor axis spot size prediction, relative positional error along the X-axis prediction, and relative positional error along the Y-axis prediction. These ANN models are based on the Multi-Layer Perceptron (MLP) architecture, which consists of one input layer, three hidden layers, and one output layer [15]. The same architecture was applied consistently across all models. The detailed architecture specifications are provided below.

4.2.2.1 Multi-Layer Perceptron (MLP) model

The MLP model is a class of ANN that consists of multiple layers of interconnected nodes, also known as neurons. A schematic diagram of an MLP neural-based model is shown in Figure 4.1. The MLP model is a feedforward neural network, meaning data flows

from the input layer through the hidden layers to the output layer without looping back. The training process involves adjusting the weights and biases of the neurons using algorithms like backpropagation and optimisation techniques. These adjustments minimise the error between the predicted and actual outputs by iteratively updating parameters based on the error gradient.

The inclusion of one or more hidden layers allows the MLP to model complex, non-linear relationships between input features and target variables, making it well-suited for a wide range of tasks, including regression, classification, and pattern recognition. The number of neurons in each layer, the choice of activation functions, and the optimisation algorithm significantly influence the model's performance and its ability to generalise to unseen data.

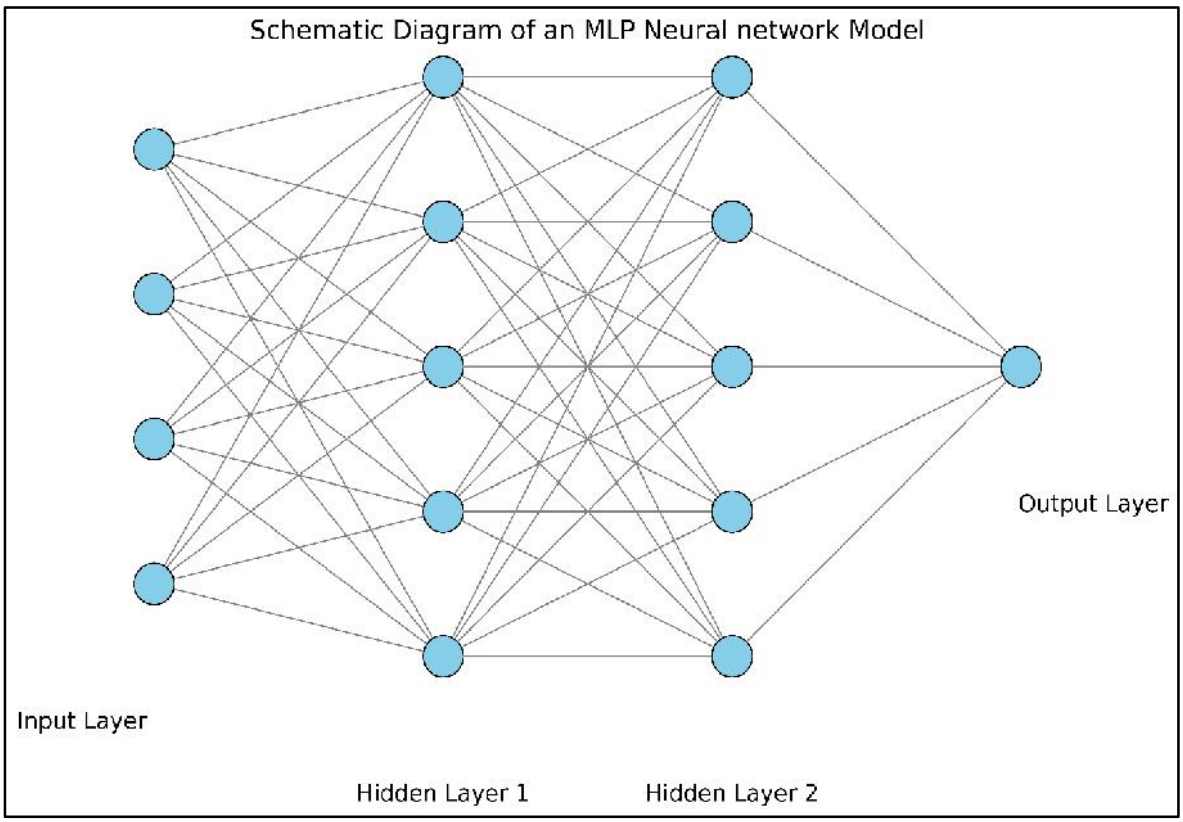

Figure 4.1: Schematic diagram of an MLP neural network model with one input layer, two hidden layers, and one output layer.

In this study, the MLP model creation was carried out in Python, a high-level, general-purpose programming language renowned for its readability and extensive support for scientific computing. The development environment utilized was Spyder, an open-

source Integrated Development Environment (IDE) designed specifically for scientific programming in Python. Spyder offers features such as advanced editing, analysis, debugging, and profiling, making it suitable for data-intensive applications.

For building and training the ANN, the Keras library was employed**.** Keras is a high-level neural network API that facilitates the creation of deep ML models with minimal code [16]. It operates as an interface for the Tensor Flow library, which serves as the backend. TensorFlow is an open-source platform developed by Google for ML and AI tasks, providing a comprehensive ecosystem of tools and libraries for model development and deployment [17].

This combination of Python, Spyder, Keras, and TensorFlow provided a robust framework for developing the ANN model, enabling efficient experimentation and implementation of the MLP architecture for the study.

Here is the script snippet of how the necessary libraries were imported and the Sequential model was instantiated:

Python script for importing the sequential model from tensorflow.

$import\ tensorflow\ as\ tf$

$from\ tensorflow.keras.models\ import\ Sequential$

$from\ tensorflow.keras.layers\ import\ Dense$

$\#Initialize\ the\ Sequential\ model$

$model\ =\ Sequential()$

4.2.2.2 Input layer parameters

The input layer is the initial stage where data enters the network. Each neuron in this layer represents a specific feature or attribute of the input data, effectively capturing the independent variables or predictor variables. The primary function of the input layer is to receive these features and transmit them to the subsequent hidden layers for further processing.

In this study, the input variables for all six ML models are taken from the log file data. The prediction models for the X and Y spot sizes, as well as the major and minor axis

spot sizes, utilized a common set of eight input variables. These variables encompassed the X and Y spot sizes recorded in IC23 and IC1, the primary current of the scanning magnets, beam current, and gantry angle. In contrast, the models predicting the X-axis and Y-axis relative positional errors incorporated nine input variables: The X and Y spot sizes recorded in IC23, the X and Y position values recorded in IC23, the X and Y positional errors in IC23, the primary current of the X and Y scanning magnets, and the beam current.

4.2.2.3 Output layer

The output layer represents the dependent variables, also called the label values. The ML model optimises the network to minimize the difference between the predicted values and the label values. In this study, the Lynx2D measured spot parameters were used as label variables, such as X spot size, Y spot size, Major axis spot size, minor axis spot size, X spot relative positional error, and Y spot relative positional error. The Pearson correlation coefficient is calculated using the input and output variables.

4.2.2.4 Hidden Layers

The hidden layer in a neural network serves as an intermediate stage between the input and output layers. It contains neurons that transform the input data by applying weighted connections and activation functions, allowing the network to identify and learn complex patterns. The structure of the hidden layers, including the number of layers and neurons in each layer, influences the model's ability to capture and represent intricate patterns within the data. In this study, three hidden layers are used with 30 neurons each for all models.

The following equation demonstrates the calculation of the weighted sum in a neuron within a neural network.

$$z = i\sum wixi + b \tag{4.1}$$

Where:

z: The weighted sum, or the input to the activation function, which is the result of applying weights and bias to the input features.

$i\sum wixi$: The summation of each input feature Xi multiplied by its corresponding weight Wi.

This operation captures the importance of each input feature based on the learned weights.

b: The bias term, which allows the neuron to adjust the output independently of the input features. It enables the model to shift the activation function, helping the network learn better.

4.2.2.5 Rectified Linear Unit – Activation function

The activation function is a mathematical operation applied to each neuron's output. It introduces non-linearity into the model, enabling the network to learn and represent complex patterns in data. Without activation functions, the network would behave as a linear model, regardless of its depth, limiting its ability to solve non-linear problems. Activation functions also help regulate the flow of information through the network, ensuring effective learning during training.

One of the most widely used activation functions in ANN models is the Rectified Linear Unit (ReLU) [18]. It is preferred due to its simplicity, efficiency, and ability to introduce non-linearity. In this study, the ReLU activation function is used for all models. The ReLU function is mathematically defined as:

$$f(x) = \max(0, x) \tag{4.2}$$

$$f'(x) = \begin{cases} 1 \; if \; x > 0 \\ 0 \; if \; x \leq 0 \end{cases} \tag{4.3}$$

When a neuron's output consistently falls in the non-positive range $(x \leq 0)$ its gradient becomes zero, effectively rendering the neuron inactive. This means that for values of $(x \leq 0)$, the ReLU function will output zero, and the gradient during backpropagation will not update the weights associated with those neurons. The simplicity of this operation ensures computational efficiency, making ReLU a natural choice for large-scale models. Figure 4.2 represents the schematic diagram of the ReLU activation function.

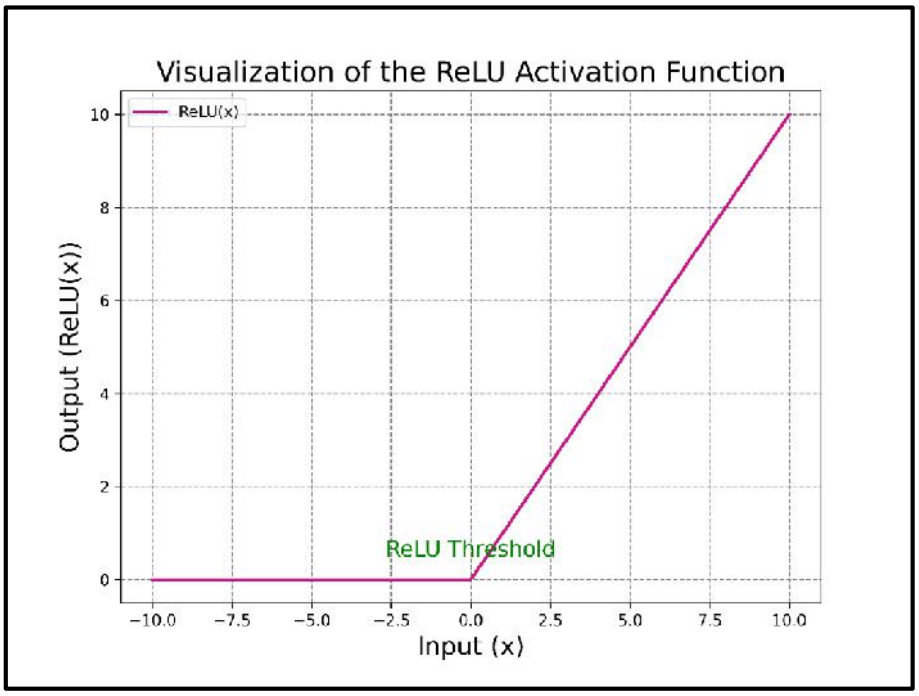

Figure 4.2: The visualisation of ReLU activation function.

The ReLU activation function is used in this study because it introduces non-linearity, enabling the model to capture complex patterns in the log file data, which is essential for accurate spot parameter prediction. Additionally, ReLU helps prevent the vanishing gradient problem, ensuring effective learning in deeper neural networks. Its computational simplicity speeds up the training process, making it well-suited for handling large datasets. Furthermore, the sparse activations generated by ReLU direct the model's focus to the most relevant features, reducing overfitting and enhancing generalisation.

4.2.2.6 Optimiser

An optimizer in an ANN model is an algorithm that adjusts the model's weights and biases to minimize the loss function and improve performance. It updates the parameters by calculating the gradients of the loss function and modifying the weights accordingly. Model training is done by optimising the weights and bias of each neuron in the hidden layers to reduce the error in the prediction. In this study, an optimiser called Adaptive Moment Estimation (Adam) is a widely used gradient-based optimization algorithm for training ML models [19]. It combines the strengths of two other optimizers: Momentum and RMSprop, to provide efficient and effective updates to the model's parameters.

The Adam optimizer is a highly regarded algorithm in ML due to its ability to adjust learning rates for individual parameters dynamically. It achieves this by leveraging the first and second moments of the gradients, which helps maintain stability and ensures efficient convergence. The algorithm also employs momentum by averaging past gradients, which smooths updates and effectively handles noisy or sparse gradients. Additionally, Adam corrects biases in these moving averages, particularly early in training, when the estimates are skewed towards zero. Typically, the default learning rate for Adam is set to 0.001, which serves as a reliable starting point, though it can be fine-tuned to meet specific requirements.

The Adam optimizer is used in this study due to its key features adaptive learning rates, momentum integration, and bias correction. These attributes allow Adam to efficiently adjust the learning rate during training, improving convergence speed and model performance. By incorporating momentum, Adam helps accelerate learning in relevant directions, while bias correction ensures more accurate parameter updates, especially during the initial stages of training.

The Adam maintains two moving averages during training

First moment (m_t): The mean of the gradients (similar to momentum)

Second moment (v_t): The mean of the squared gradients (used for scaling).

The algorithm's update rules are:

1. Compute Gradient:

$$g_t = \nabla_{\theta_t} J(\theta_t) \tag{4.4}$$

where g_t is the gradient of the loss function; $J(\theta_t)$ with respect to the model parameters; θ_t at time step t.

2. Update Moving Averages:

$$m_t = \beta_1 m_{t-1} + (1 - \beta_1) g_t \tag{4.5}$$

$$v_t = \beta_2 v_{t-1} + (1 - \beta_2) g_t^2 \tag{4.6}$$

Here β_1 (default 0.9) and β_2 (default 0.999) are decay rates for the moving averages.

3. Bias Correction:

Since m_t and v_t are initially biased toward zero, the corrected values are:

$$\hat{m}_t = \frac{m_t}{1-\beta_1^t} \tag{4.7}$$

$$\hat{v}_t = \frac{v_t}{1-\beta_2^t} \tag{4.8}$$

4. Parameter Update:

Parameters are updated using:

$$\theta_{t+1} = \theta_t - \eta \frac{\hat{m}_t}{\sqrt{\hat{v}_t}+\epsilon} \tag{4.9}$$

Where η is the learning rate and ϵ is a small constant to avoid division by zero.

4.2.2.7 Loss function

A loss function is a mathematical function used to measure the difference between the predicted output of an ML model and the actual target values. It quantifies how well or poorly the model is performing. The goal during training is to minimize this loss function, which helps to optimize the model's parameters (e.g., weights in a neural network) so that predictions are as close as possible to the actual outcomes.

In this study, used MSE as the loss function [20]. MSE is commonly used in regression tasks, where the objective is to predict continuous values.

4.2.3 Model training

The training process for the six ML models X spot size prediction, Y spot size prediction, major axis spot size prediction, minor axis spot size prediction, X spot relative positional error prediction, and Y spot relative positional error prediction was carefully structured to ensure accuracy and reliability. The input and target values for these models and also the architecture of the models are presented in Figures 4.3 and 4.4. The log file recorded data used as input variables and the scintillator measured data used as output or label values. While the four spot size prediction models shared 8 input variables as shown in Figure 4.3, the two positional error prediction models used 9 input variables, as

illustrated in Figure 4.4. These specific configurations ensured that each model was tailored to its respective predictive task.

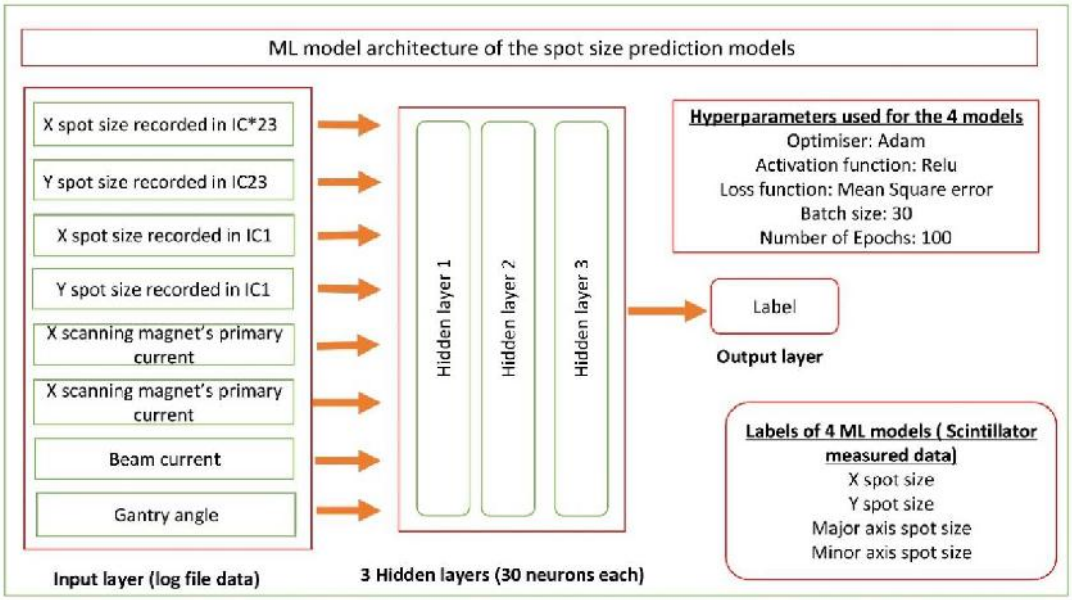

Figure 4.3: The ANN model architecture of the spot size prediction models. The x-spot size, y-spot size, major axis spot size and minor axis spot size prediction models are shown in the figure. All four models share the same input variables, hidden layers and hyper parameters. *IC- Ionisation chamber.

The data used for this study was divided into three parts: 70 % for model training, 15 % for evaluation, and 15 % for testing. All models followed a uniform architecture, employing the ReLU activation function in the hidden layers. ReLU introduced essential non-linearity, enabling the models to learn intricate patterns by selectively activating neurons based on their input. The training spanned 100 epochs with a batch size of 30, which provided a balance between computational efficiency and stable updates.

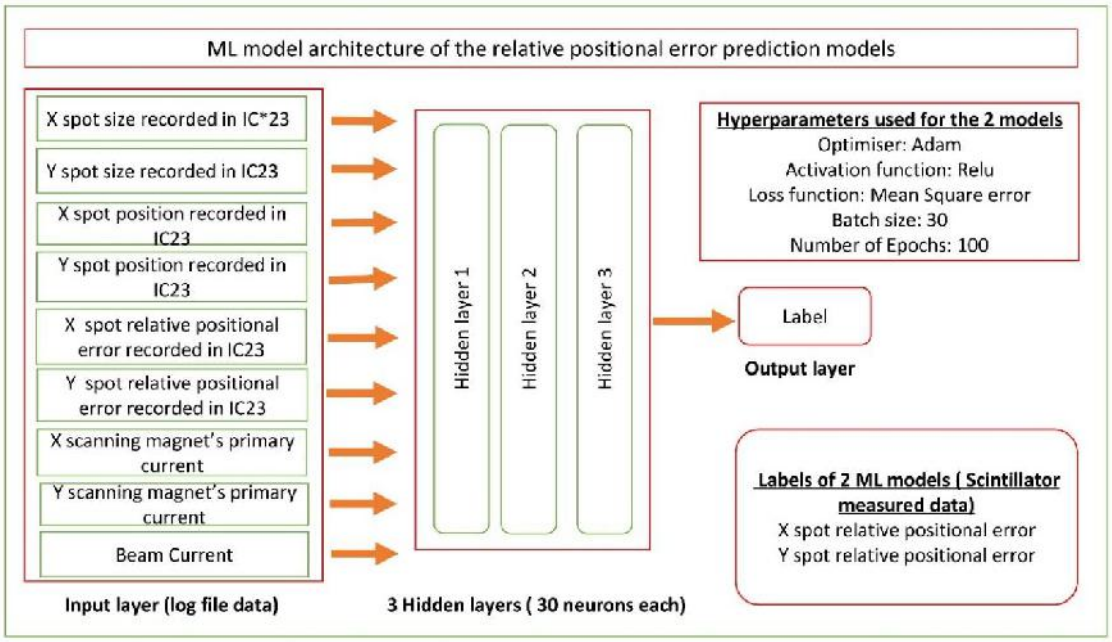

Figure 4.4: The ANN model architecture of the relative positional error prediction models. The x-spot relative positional error and y-spot relative positional error prediction models are shown in the figure. All the two models share the same input variables, hidden layers and hyper parameters. * IC- Ionisation chamber.

During each training epoch, the models adjusted weights and biases for neurons to produce predictions based on the input data. The MSE loss function was used to calculate the error by measuring the squared difference between predicted and true values. This error was then used by the Adam optimizer, which adjusted the model parameters by applying adaptive learning rates and momentum to progressively minimize the error. This iterative process continued across all epochs, fine-tuning the models to enhance their predictive accuracy. The combined use of ReLU, MSE, and Adam ensured an effective training process, resulting in models capable of generating highly reliable predictions.

4.2.4 Model validation

Model validation plays a crucial role in evaluating the effectiveness and generalizability of ML models. It helps to ensure that the models are not overly tuned to the training data and can make accurate predictions on new, unseen data. In this study, model validation was essential to verify the reliability and precision of the developed models in predicting spot sizes and positional errors. By applying various validation

techniques, assessed how well the models generalized to different datasets, ensuring their predictive capabilities in practical, clinical settings. This process also allows for identifying any biases or weaknesses, leading to necessary refinements.

In this study, the model validation tools employed include quantitative analysis through the calculation of metrics such as RMSE, MSE, R-squared, and Mean Absolute Percentage Error (MAPE), as well as qualitative analysis using tools such as histogram of residuals, scatter plot of errors, and Q-Q plot, and cross-validation using K fold cross validation method as outlined below.

4.2.4.1 Quantitative analysis

Each quantitative metric provides a unique perspective: RMSE and MSE offer insights into the magnitude of errors, with RMSE being more interpretable in the original units of the data. R^2 helps assess the proportion of variance explained by the model, indicating its overall fit. MAPE provides a percentage-based measure of error, making it scale-independent. Together, these metrics offer a comprehensive analysis, ensuring a thorough evaluation of model accuracy and robustness from different angles.

4.2.4.1.1 Mean Squared Error (MSE)

The MSE is a fundamental metric used to evaluate the performance of predictive models by measuring the average squared difference between predicted values and actual values It indicates how well a model captures the underlying patterns in the data, with smaller MSE values signifying higher accuracy. Unlike RMSE, MSE does not involve taking the square root, making it more sensitive to large errors. The formula for MSE is

$$\text{MSE} = \frac{1}{n}\sum_{i=1}^{n}(y_i^{pred} - y_i^{true})^2 \tag{4.10}$$

Here,

n is the number of observations.

y_i^{pred} represents the predicted values.

y_i^{true} represents the true values.

In this study, the MSE of the model residuals was calculated for all six ML models and plotted to analyse the data's normality and assess the accuracy of each model's

predictions. By comparing the MSE values across models, insights were gained into their relative performance.

4.2.4.1.2 Root Mean Squared Error (RMSE)

The RMSE is a commonly used measure to assess the performance of predictive models by quantifying the average deviation between predicted values and observed values It is computed as the square root of the mean of the squared differences between these values, providing a single value that represents the model's accuracy. Smaller RMSE values indicate that the model's predictions are closer to the actual values. The RMSE formula is:

$$\text{RMSE} = \sqrt{\frac{1}{n}\sum_{i=1}^{n}(y_i^{pred} - y_i^{true})^2} \tag{4.11}$$

Here,

n is the number of observations.

y_i^{pred} represents the predicted values.

y_i^{true} represents the true values.

In this study, the RMSE of the model residuals was computed and visualized for all six ML models to assess data normality and verify the accuracy of their predictions

4.2.4.1.3 Mean Absolute Percentage Error (MAPE)

The MAPE is a widely used metric to evaluate the accuracy of a predictive model, particularly in regression problems. Unlike MSE and RMSE, MAPE measures the error as a percentage of the actual values, making it easier to interpret, especially when comparing models across different datasets. MAPE calculates the average of the absolute percentage differences between the predicted values and the actual values.

The formula for MAPE is:

$$MAPE = \frac{1}{n}\sum_{i=1}^{n}\left|\frac{y_i^{pred} - y_i^{true}}{y_i^{true}}\right| X\ 100 \tag{4.12}$$

In this study, in addition to MSE and RMSE, also calculated MAPE also for the spot size prediction models. However, The MAPE metric was not computed for the positional error prediction models due to the potential for the MAPE to produce undefined or infinite values when actual values are zero or close to zero.

4.2.4.1.4 R-squared (R^2) –Coefficient of determination

R-squared (R^2) also referred to as the coefficient of determination, is a statistical metric that assesses the proportion of the variance in the dependent variable that can be explained by the independent variables in a regression model. It indicates how well the model fits the data. A higher R^2 value suggests that the model explains a larger portion of the variance, whereas a lower value indicates a poorer fit.

The formula for calculating R^2 is :

$$R^2 = 1 - \frac{\sum_{i=1}^{n}(y_i^{true} - y_i^{pred})^2}{\sum_{i=1}^{n}(y_i^{true} - \bar{y}_i)^2} \quad (4.13)$$

here,

$\bar{y}_i$ is the mean of the observed values.

The interpretation of R^2 is as follows: when R^2=1, the model fully captures the variance in the data, indicating perfect prediction accuracy. If R^2 =0, the model does not account for any variance and performs no better than predicting the mean value. A value of R^2 between 0 and 1 suggests that the model explains some variance in the data, but there is still scope for enhancing the model's performance.

In this study, calculated R^2 for all six ML models to assess the proportion of variance explained by each model. This evaluation helps to understand how well each model fits the data and captures the underlying patterns.

4.2.4.2 K-fold cross-validation

To ensure the reliability and robustness of the ML models, K-fold cross-validation was employed. This technique is widely used in ML to evaluate the performance of predictive models on datasets [21]. The concept of k-fold cross-validation involves splitting a dataset into equal parts or folds. Then, the model was trained and evaluated k times using a different fold as the test set and the rest of the folds as the training set. K-fold cross-

validation aids in assessing the generalisation performance of a model and mitigates the risk of overfitting. The performance metrics, such as RMSE, are then averaged across all folds to provide a more accurate estimate of the model's generalizability and overall performance. The resulting performance metrics can better estimate the model's performance on new, unseen data by training the model on different training sets. Figure 4.5 illustrates the application of K-fold cross-validation within a machine-learning model.

In this study, K was set to 5 for cross-validation. The six models were validated by dividing the dataset into 5 folds, and the prediction accuracy of each model was assessed by calculating the RMSE for the predictions made with each fold.

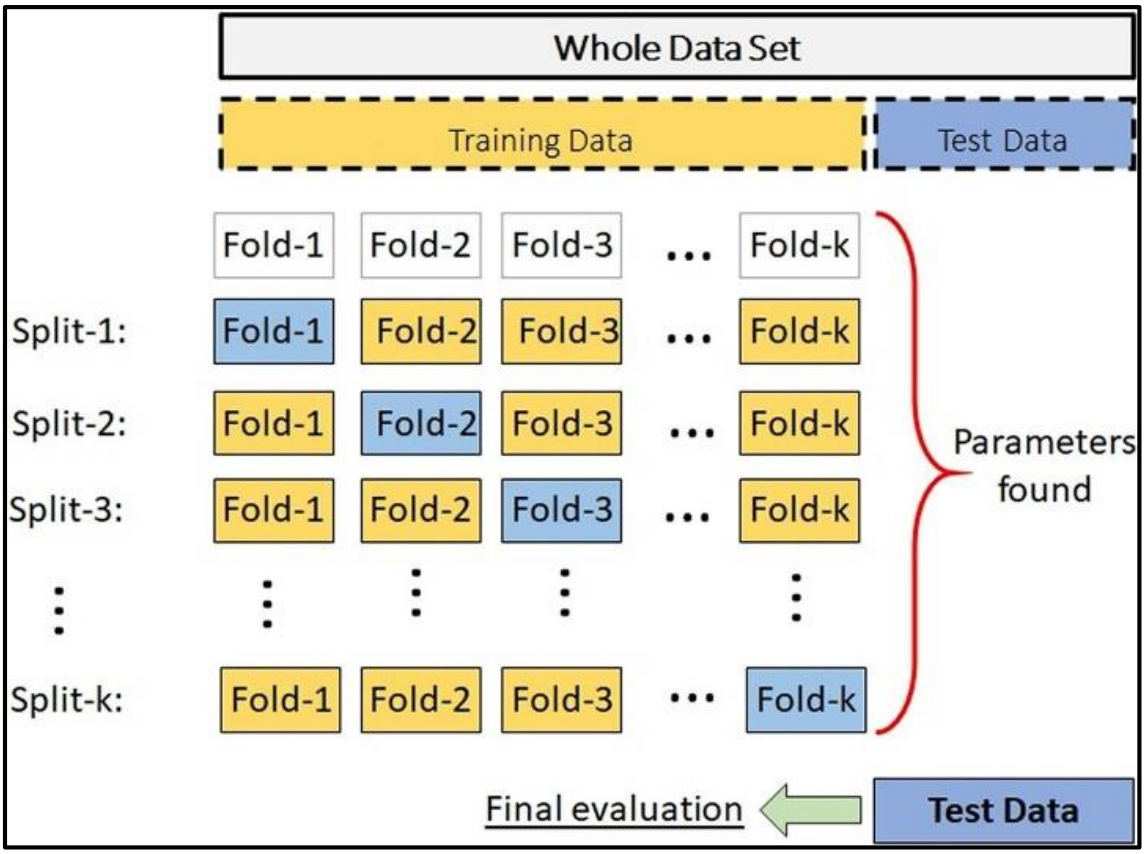

Figure 4.5: Graphical representation of how the K fold cross-validation works in a model validation (Picture courtesy Sevinç E et al [21])

4.2.4.3 Quartile- Quartile plot (Q-Q) plot

The ML model prediction accuracy can be evaluated by plotting the residual (difference between the predicted and true value) values. If the ML model is well-calibrated or prediction accuracy is good, these residuals should ideally follow a normal distribution. The Q-Q plot is a method to evaluate the normality of the residual plot [22].

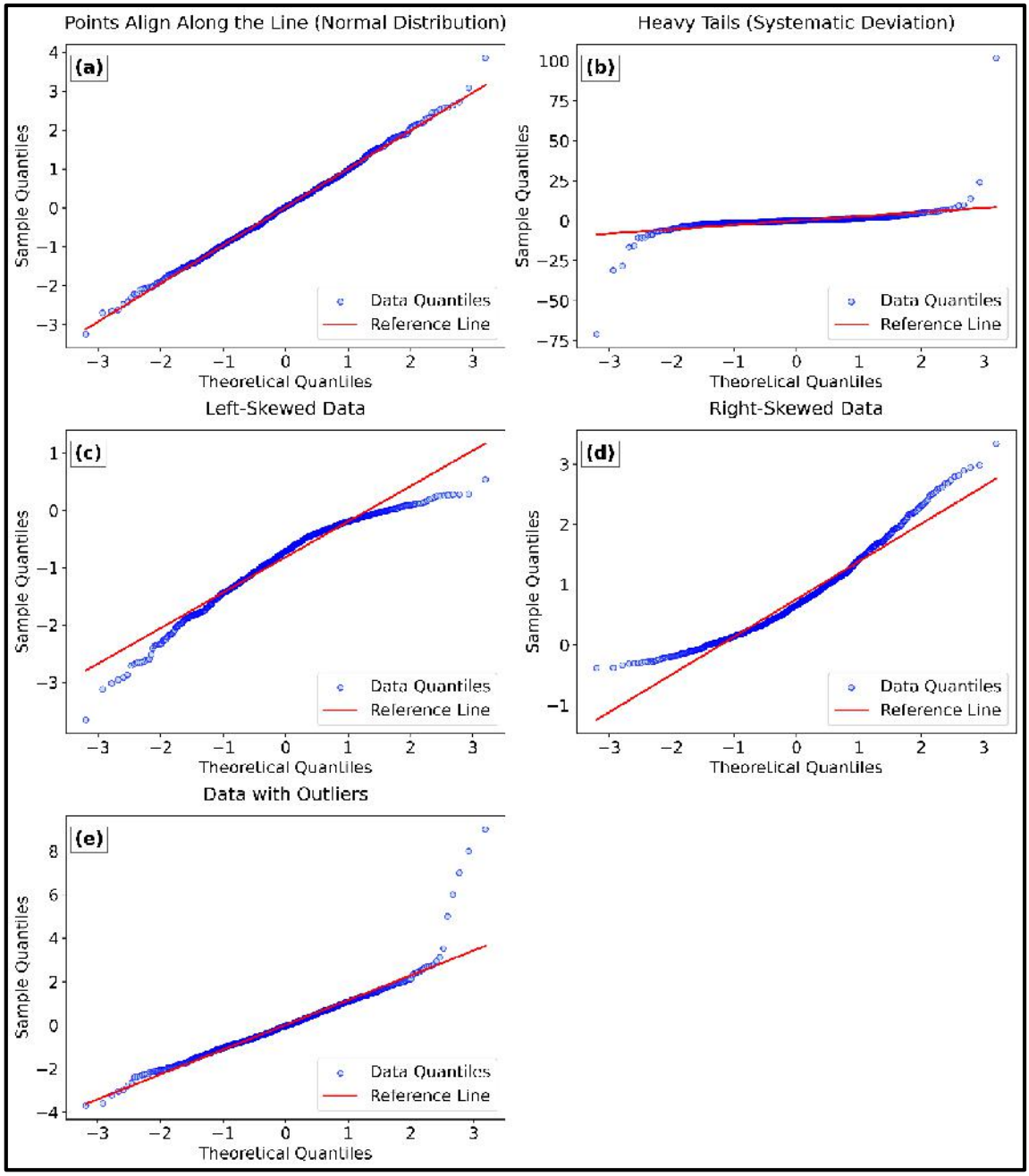

Figure 4.6: Q-Q Plots Demonstrating Distribution Characteristics: (a) Normal Distribution, (b) Heavy Tails, (c) Left-Skewed Data, (d) Right-Skewed Data, and (e) Data with Outliers. (Pleil JD et al [22]).

The Q-Q plot is based on the concept of quantiles. Quantiles divide a dataset into equal intervals, and the Q-Q plot compares the quantiles of the observed data against the quantiles of a reference theoretical distribution. If the two distributions are similar, the points will lie approximately on a straight line.

Different Q- Q plot types are depicted in Figure 4.6 and the details are given below.

(a) Normal distribution – points align along the line:

This plot displays data sampled from a normal distribution. The data points align well with the reference line, showing that the sample quantiles closely follow the theoretical quantiles, confirming the dataset's normality.

(b) Systematic deviation (heavy tails):

The plot shows systematic deviations of data points from the reference line, especially at the extremes. This pattern is characteristic of heavy-tailed distributions, such as the t-distribution with a low degree of freedom.

(c) Left skewed data:

This plot depicts a dataset with left skewness. The points dip below the reference line at smaller quantiles and rise above it at larger quantiles, indicating an extended tail on the left side of the distribution.

(d) Right skewed data:

The dataset in this plot exhibits right skewness. Points rise above the line at smaller quantiles and fall below it at larger quantiles, reflecting an extended tail on the right side of the distribution.

(e) Data with outliers:

This plot highlights the presence of outliers in the dataset. While most data points are close to the reference line, a few extreme points deviate significantly, indicating anomalies or rare observations in the data.

In this study, the Q-Q plot is used to analyse the normality of the residuals of all six ML models.

4.2.4.4 Histogram of Residuals

A histogram of residuals is a visual tool used to examine the distribution of residuals, which are the differences between the actual and predicted values in a model. This plot allows you to check if the residuals follow a normal distribution, an assumption often required in regression analysis. Ideally, a symmetrical, bell-shaped histogram indicates that the errors are normally distributed, suggesting a good fit for the model. However, if the histogram shows significant skewness or irregular patterns, it could point to problems such as outliers, incorrect model assumptions, or non-linearity.

4.3 Results

4.3.1 Correlation Analysis Between Input and Output Variables

The Pearson correlation coefficients were calculated to assess the relationships between the label values (scintillator-measured parameters) and the input variables (log file-recorded data) for six ML models. These correlation values are presented in Table 4.1 and Table 4.2. While many input variables exhibit strong correlations with the label values, some variables show weaker relationships. For instance, the correlation between the x positional error and the x-spot size recorded in IC23 is only 0.19, indicating a weak linear association. This suggests that some input variables may not contribute significantly to predictive performance if only linear relationships are considered.

However, ANNs are designed to capture complex, non-linear dependencies between variables. Unlike traditional linear models, ANNs can identify intricate patterns and relationships that may not be evident through simple linear correlation analysis. Therefore, even variables with poor Pearson correlation values, such as the x positional error, may still contain valuable information for the ANN model.

To ensure comprehensive training and to leverage the ability of ANNs to identify non-linear interactions, all input variables tabulated were included in the ANN model training process. This approach allows the model to explore and utilise hidden dependencies that linear correlation measures, such as the Pearson coefficient, might overlook.

Table 4.1: The person correlation coefficients between the input variables and label values of the x spot size, y spot size, major axis spot size and minor axis spot size prediction ANN models.

Pearson correlation coefficients				
	label values (Scintillator measured data)			
input variables (log file data)	X spot size	Y spot size	Spot size along the major axis	Spot size along the minor axis
X spot size recorded in IC23	0.971	0.974	0.972	0.971
Y spot size recorded in IC23	0.978	0.974	0.975	0.977
X spot size recorded in IC1	0.832	0.832	0.832	0.829
Y spot size recorded in IC1	0.751	0.749	0.748	0.750
X-scanning magnet's primary current	-0.946	-0.943	-0.942	-0.945
Y-scanning magnet's primary current	-0.977	-0.978	-0.977	-0.976
Beam current	0.596	0.597	0.596	0.597

Table 4.2: The Pearson correlation coefficients between the input variables and label values of the x and y relative positional error prediction ANN models.

Pearson correlation coefficients		
	label values (Scintillator measured data)	
input variables (log file data)	Relative X positional error	Relative Y positional error
X spot size recorded in IC23	0.191	0.182
Y spot size recorded in IC23	0.186	0.184
X position recorded in IC23	0.884	-0.301
Y position recorded in IC23	-0.233	-0.748
X positional error recorded in the IC23	0.874	0.295
X positional error recorded in the IC23	-0.485	0.817
X-scanning magnet's primary current	0.870	-0.327
Y-scanning magnet's primary current	-0.321	-0.730
Beam current	-0.330	-0.420

4.3.2 Model Hyper parameter tuning

Hyper parameter tuning plays a pivotal role in optimising the performance of ML models by identifying configurations that achieve the best balance between accuracy and computational efficiency. In this study, various configurations of neural networks were systematically explored to minimise the loss function across six models. Key hyper parameters were adjusted, including the number of hidden layers (2 and 3), the number of neurons per layer (30 and 50), epochs (200,100 and 50), the batch size (30 and 100), and the learning rate (0.01 and 0.001) for the Adam optimiser. These adjustments created three different configurations for each model, allowing for a thorough evaluation of the impact of architectural and training dynamics on model performance.

Three scenarios were tested for each model to determine the optimal combination of hyper parameters. The results consistently indicated that the configuration of 3 hidden layers with 30 neurons per layer, a batch size of 30, and a learning rate of 0.001 yielded the lowest RMSE values. As summarised in Table 4.3, this combination demonstrated superior performance across all models, ensuring robust generalisation to unseen data while maintaining computational efficiency. This systematic approach provided valuable insights into the influence of hyper parameter choices, leading to the selection of a configuration that effectively optimises the learning process and enhances model precision. Figure 4.7 plots the model accuracy metrics for the X spot size prediction model, showing a reduction in MAPE (%) as epochs increase.

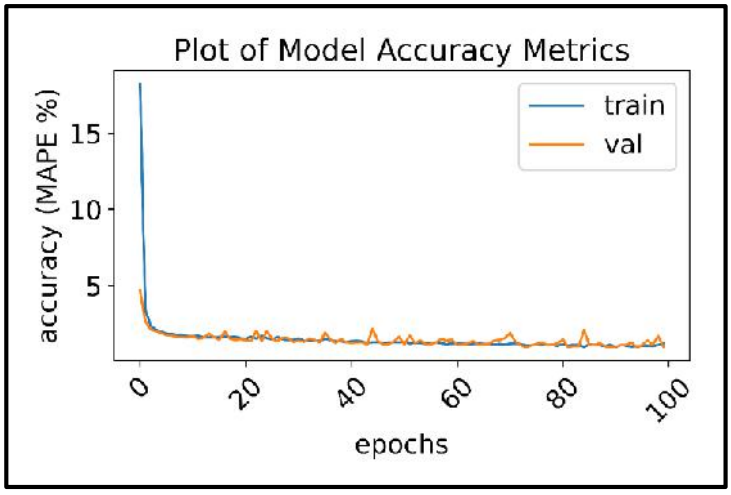

Figure 4.7: Model accuracy metrics plot for the X spot size prediction model, showing a reduction in MAPE (%) as epochs increase. Train- training data, Val- validation set.

Table 4.3: The summary of different hyper parameter combinations used for the six ML model tuning and the obtained RMSE and R-square are tabulated.

Model	Training	Hidden layers	Epochs	Neurons in each layer	Batch size	Learning rate	RMSE (mm)	R-Square
X spot size	Training 1	2	200	50	100	0.01	0.075	0.989
	Training 2	3	100	30	30	0.001	0.051	0.993
	Training 3	3	50	30	30	0.001	0.065	0.990
Y spot size	Training 1	2	200	50	100	0.01	0.065	0.985
	Training 2	3	100	30	30	0.001	0.050	0.992
	Training 3	3	50	30	30	0.001	0.072	0.980
Major axis spot size	Training 1	2	200	50	100	0.01	0.073	0.975
	Training 2	3	100	30	30	0.001	0.049	0.998
	Training 3	3	50	30	30	0.001	0.067	0.981
Minor axis spot size	Training 1	2	200	50	100	0.01	0.073	0.975
	Training 2	3	100	30	30	0.001	0.049	0.998
	Training 3	3	50	30	30	0.001	0.067	0.981
Relative X positional error	Training 1	2	200	50	100	0.01	0.052	0.981
	Training 2	3	100	30	30	0.001	0.030	0.991
	Training 3	3	50	30	30	0.001	0.045	0.989
Relative Y positional error	Training 1	2	200	50	100	0.01	0.054	0.982
	Training 2	3	100	30	30	0.001	0.030	0.996
	Training 3	3	50	30	30	0.001	0.047	0.987

4.3.3 Model Performance Evaluation

The trained models were evaluated using a testing dataset comprising 15 % of the overall data, a subset not employed in the initial model generation process. Each model's prediction accuracy was evaluated using a few statistical evaluation metrics. Table 4.4 presents a concise overview of the evaluation metrics for the six ML models. It offers a consolidated and comprehensive view of the performance assessments for each ML model. The metrics include MSE, MAPE, RMSE, R-square, and maximum prediction error. The

spot size measurement models demonstrated excellent prediction accuracy, with MSE values below 0.0028 mm and MAPE below 1 %. The highest observed RMSE value is 0.050 mm (R-square 0.991). In the relative positional error prediction models, the y relative positional error prediction model exhibited the highest MSE value of 0.001 mm, with an RMSE of 0.035 mm (R-square of 0.996).

Table 4.4: The evaluation matrices of all the Six ML Models. The values of MSE, MAPE, RMSE, R- square and maximum error of each ML model.

ML Models	MSE(mm)	MAPE(%)	RMSE(mm)	R-Square	max error (mm)
X spot size prediction	0.003	0.991	0.050	0.993	0.251
Y spot size prediction	0.002	0.892	0.050	0.992	0.255
Spot size along major axis prediction	0.003	0.942	0.050	0.998	0.300
Spot size along minor axis prediction	0.002	0.950	0.050	0.994	0.311
Relative X positional error prediction	0.001	NA*	0.030	0.991	0.160
Relative Y positional error prediction	0.001	NA*	0.030	0.996	0.170

NA – Not applicable, MSE- Mean squared error, MAPE – Mean absolute percentage error, RMSE- Root mean squared error, R-square- Coefficient of determination

*The MAPE (%) is not calculated for the relative positional error prediction model.

Figure 4.8 illustrates the results of the six ML models, showcasing the comparison between the measured and predicted parameters. The linear relationship depicted in the figure provides a visual representation of the prediction accuracy for each model.

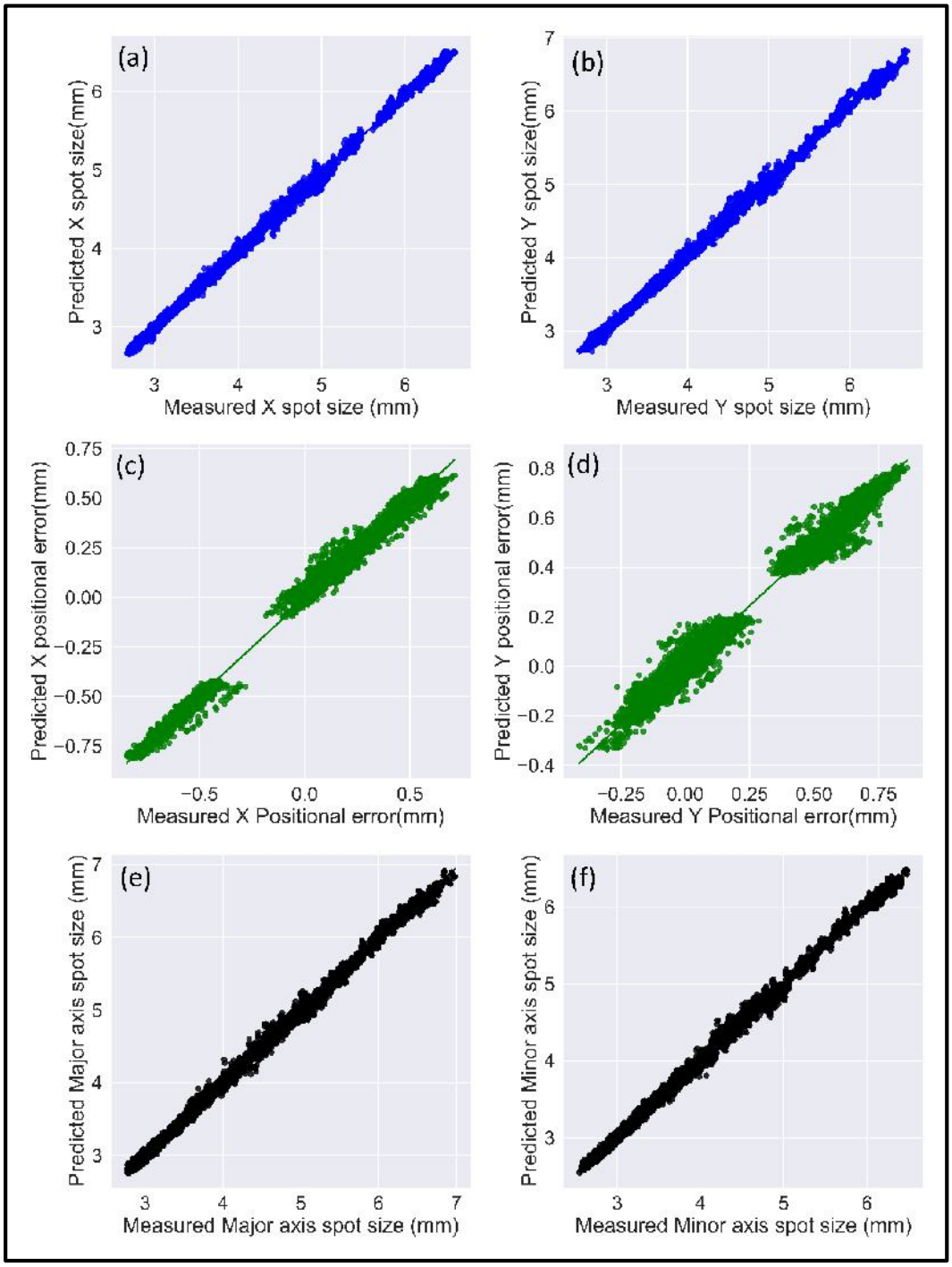

Figure 4.8**:** Plots of measured and ML model predicted spot parameters. (a) The measured and predicted X spot size. (b) The measured and predicted Y spot size. (c) The measured versus predicted relative positional error in the X direction. (d) The measured versus predicted relative positional error in the Y direction. (e)The measured versus predicted Major axis spot sizes. (f) The measured versus predicted Minor axis spot sizes

Table 4.5 presents the results of K-fold (k=5) cross-validation, showing the excellent performance of the models. Remarkably, all the RMSE values are below 0.150

mm, indicating minimal average differences between the predicted and actual values. Additionally, all the R-square values exceeding 0.960 signify an exceptional degree of variance explained by the models, highlighting a strong relationship between the predictors and the target variable. A good result in k-fold cross-validation indicates that the model is robust and consistent across different partitions of the data, reducing the risk of overfitting to a specific subset. It suggests the model will likely generalize well to new, unseen data.

Table 4.5: Root Mean Square Error (RMSE) and R-Square Values of the K-Fold Cross-Validation (k=5) of Six ML Models.

	RMSE(R-square) values of K fold (k=5) cross-validation in mm				
ML Models	Fold 1 (R-square)	Fold 2 (R-square)	Fold 3 (R-square)	Fold 4 (R-square)	Fold 5 (R-square)
X spot size prediction	0.068 (0.996)	0.074 (0.995)	0.108 (0.989)	0.056 (0.997)	0.053 (0.998)
Y spot size prediction	0.085 (0.994)	0.083 (0.993)	0.112 (0.988)	0.083 (0.994)	0.080 (0.994)
Spot size along major axis prediction	0.120 (0.987)	0.113 (0.988)	0.123 (0.986)	0.109 (0.989)	0.097 (0.992)
Spot size along minor axis prediction	0.090 (0.992)	0.127 (0.984)	0.147 (0.979)	0.098 (0.991)	0.110 (0.988)
Relative X positional error prediction	0.032 (0.993)	0.029 (0.994)	0.052 (0.977)	0.034 (0.990)	0.032 (0.993)
Relative Y positional error prediction	0.031 (0.991)	0.045 (0.981)	0.055 (0.963)	0.038 (0.983)	0.033 (0.987)

RMSE- Root Mean Squared Error, R-Square- Coefficient of determination.

Figure 4.9 shows the histogram of the residuals (difference between true and predicted values) for the six models. All the plots exhibit a normal distribution of data with a mean near zero; a normally distributed residual plot in an ML prediction model suggests unbiased and accurate predictions, validates the model's assumptions, and enhances the reliability of inference. It provides confidence in the model's performance and supports its applicability in making reliable predictions on new, unseen data.

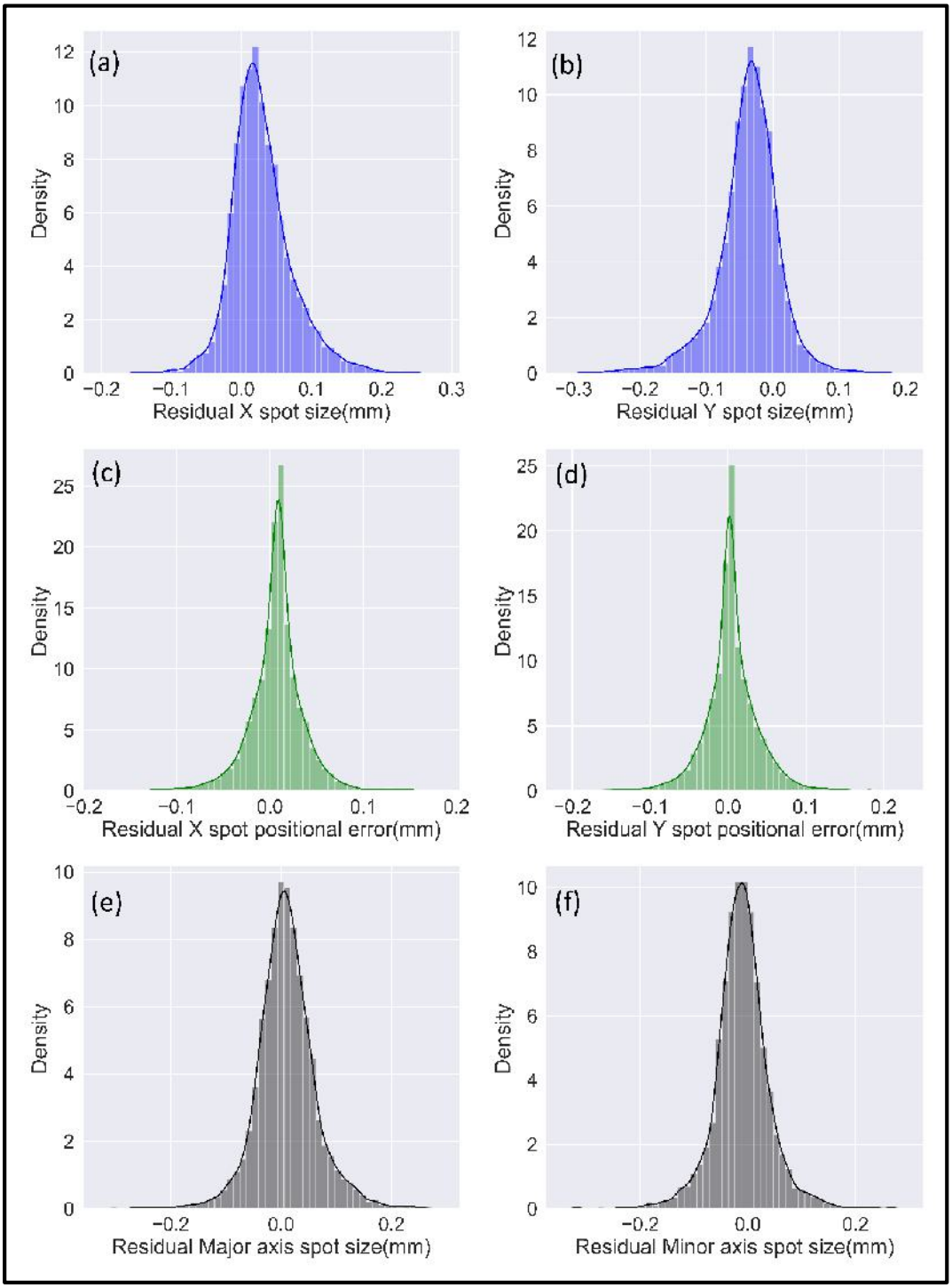

Figure 4.9: Histogram of residuals (Difference between measured and predicted) of the ML models. (a) Histogram of residuals of the X spot size prediction model. (d) Histogram of residuals of the Y spot size prediction model. (c) Histogram of residuals of the X relative positional error prediction model. (d) Histogram of the Y relative positional error prediction model. (e) Histogram of residuals of the Major axis spot size prediction model. (f) Histogram of Minor axis spot size prediction model.

The normality was again tested using the Q-Q plot (Figure 4.10). The Q-Q plot is an additional diagnostic tool to confirm the normality assumption. All the points in the Q-Q plot follow the reference line. The histogram and Q-Q plot indicate that the model's predictions are mainly close to the true values.

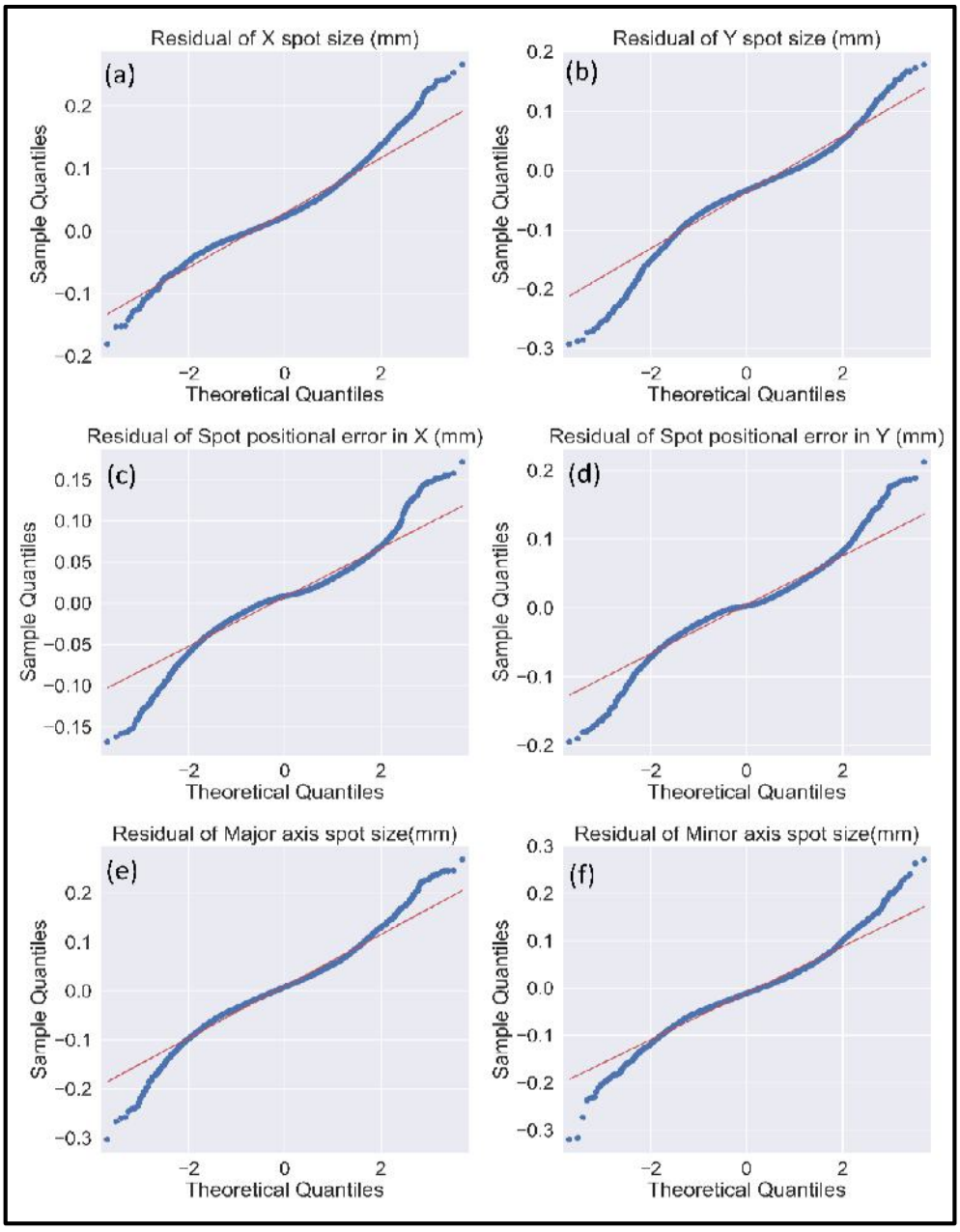

Figure 4.10: Quartile- Quartile (Q-Q) plot of the model residuals. (a) Q-Q plot of residuals of the X spot size prediction model. (b) Q-Q plot of residuals of the Y spot size prediction model. (c) Q-Q plot of residuals of the X relative positional error prediction model. (d) Q-Q plot of residuals of the Y relative positional error prediction model. (e) Q-Q plot of the

residual of the Major axis spot size prediction model. (f) Q-Q plot of residuals of the Minor axis spot size prediction model.

4.4 Discussion

The PBS proton therapy beam delivery system is complex and needs rigorous QA protocols to ensure accurate dose delivery to the patient. Our institute's standard protocol for the daily dosimetric QA includes measurement of machine output using a parallel plate chamber, proton range verification using a Multilayer ionisation chamber, and spot size and positional accuracy verification using the Lynx 2D detector. The average time for the daily dosimetric QA is 1.30 hours. Different compact daily QA phantoms are available for daily QA within 30 minutes [23,24]. In a proton therapy centre with multiple treatment rooms, it's challenging to use quality assurance equipment across all the rooms efficiently and make the most of clinical hours. The spot measurement for different energies in different gantry angles requires attaching the detector to the machine head and proper tilt correction, which is time-consuming. Therefore, there was a need to investigate more straightforward methods to address this challenge.

Current study aimed to develop accessible and cost-effective solutions for daily verification of proton spot characteristics by leveraging ML models and irradiation log file data. This chapter outlines the development and validation of ML models designed to predict spot dosimetric parameters using log files as input. Newpower MA et al. [5] developed a neural network model for predicting the spot position using measured and log file recorded spot position data. The MSE of the prediction model was 0.300 mm. A similar study was done by Maes D et al. [6], and the maximum MSE value of the position prediction model was 0.150 mm. In this study, the models demonstrated high precision, with RMSE values below 0.05 mm for predicting X, Y, major, and minor axis spot sizes. The maximum prediction error was under 0.3 mm, and the MPAE remained below 1 %. These results align well with the AAPM TG-224 [25] recommended tolerance of 10 % for spot size accuracy and 1 mm for positional error, highlighting the reliability of the ML models compared to established benchmarks.

Similarly, the ML models for relative positional error prediction achieved an RMSE of less than 0.03 mm, with a maximum error of just 0.17 mm, demonstrating exceptional precision. These findings highlight the utility of ML models in routine machine QA,

offering a reliable, efficient, and manpower-saving alternative to traditional methods that often rely on physical dosimeters. The application of these models ensures robust QA processes, enhancing the effectiveness and efficiency of modern proton therapy systems.

By analysing Figure 4.8 it becomes apparent that the ML models exhibit accurate and precise predictions of the spot parameters using the log file data. Notably, all the curves in Figure 4.8 demonstrate a linear relationship, indicating a high level of prediction accuracy.

Hyper parameter tuning plays a critical role in optimizing the performance of ML models used in this study. Hyperparameters, unlike model parameters, are not learned during training but must be predefined and carefully selected to ensure the model's reliability and accuracy. Key hyper parameters tuned in this study included the learning rate, batch size, number of hidden layers and number of neurons per layer. The multiple combinations of hyper parameters help to find optimum solutions for the six ML models. The combination of 3 hidden layers with 30 neurons each and 100 epochs with a batch size of 30 and learning rate for Adam optimizer 0.001 yielded the best results for all the six models with RMSE less than 0.05 mm (R^2- 0.99) for all four spot size prediction models and similarly for spot relative positional error models the RMSE was less than 0.03 mm (R^2 0.99).

The model performance was evaluated using the K-fold cross-validation technique with k=5. Table 4.5 summarises the results, showing that the maximum RMSE among the four spot size prediction models was less than 0.14 mm (R^2 >0.97), while the maximum RMSE for spot relative positional error prediction models was under 0.06 mm (R^2 >0.96). These results demonstrate the high accuracy and reliability of the models, with minimal prediction errors. The consistently low RMSE values across folds confirm the models' robustness and strong generalisation capabilities. This ensures their suitability for practical applications, such as routine quality assurance in proton therapy, where precision and consistency are critical.

The residuals for all six models were examined using histograms (Figure 4.9) and Q-Q plots (Figure 4.10). The histogram showed a normal distribution with a mean near zero, indicating unbiased and accurate predictions. This supports the model's reliability and validates the assumptions made during model development. The normality assumption was

further confirmed by the Q-Q plot, where all points closely followed the reference line. These findings provide confidence in the models' performance and demonstrate their suitability for making reliable predictions on unseen data.

Extensive literature has discussed using spot positions from the log file for patient-specific quality assurance (PSQA). In a study by Belosi MF et al. [34], more than 95 % of the plans passed their gamma criteria compared to the log file-based reconstruction and calculated dose planes. The log file can be a potential tool for machine QA and PSQA. However, many studies focused on spot position and MU prediction using log file data, and there are no studies on spot size prediction using log files. The spot size prediction model validation results show the accuracy of the models. These results highlight the reliability of the ML models for predicting proton spot size and relative positional error. The spot size prediction models will facilitate the analysis of daily variations in spot size without requiring measurements using dosimeters such as scintillators.

4.5 Conclusions

In conclusion, this study successfully demonstrates the application of ML models for accurate and efficient daily verification of proton spot characteristics, offering a significant advancement in routine quality assurance processes in proton therapy. By leveraging irradiation log file data, the developed models for predicting spot size and relative positional error achieved high precision, with RMSE values consistently below 0.05 mm for spot size and below 0.03 mm for positional error. These results align with the AAPM TG-224 recommended tolerances, underscoring the reliability and robustness of the ML models. The models' performance was further validated through K-fold cross-validation, histograms, and Q-Q plots, ensuring their generalisation capabilities and confirming their suitability for deployment in clinical environments.

The successful implementation of ML models for proton spot size and positional error prediction addresses the challenges of time-consuming, resource-intensive traditional QA methods. By providing an accessible, cost-effective alternative that reduces the need for physical dosimeters, the models contribute to enhanced operational efficiency and streamlined workflows in proton therapy centres. This work also lays the foundation for future applications of log file data in proton therapy, particularly in patient-specific quality

assurance, and demonstrates the growing potential of ML in optimising and automating clinical QA procedures.

4.6 References

1. Wall PD, Fontenot JD. Application and comparison of machine learning models for predicting quality assurance outcomes in radiation therapy treatment planning. Informatics in Medicine Unlocked. 2020 Jan 1;18:100292.
2. Ranjith CP, Arunkrishnan MP, Vysakh R, Irfad MP, Vijayagopal KS, Jayashanker S. Mean parotid dose prediction model using machine learning regression method for intensity-modulated radiotherapy in head and neck cancer. Medical Dosimetry. 2021 Sep 1;46(3):283-8.
3. Grewal HS, Chacko MS, Ahmad S, Jin H. Prediction of the output factor using machine and deep learning approach in uniform scanning proton therapy. J Appl Clin Med Phys. 2020;21(7):128-134.
4. Li Z, Wang Y, Yu Y, Fan K, Xing L, Peng H. Machine learning approaches for range and dose verification in proton therapy using proton-induced positron emitters. Medical physics. 2019 Dec;46(12):5748-57.
5. Newpower MA, Chiang BH, Ahmad S, Chen Y. Spot delivery error predictions for intensity modulated proton therapy using robustness analysis with machine learning. Journal of Applied Clinical Medical Physics. 2023 Feb 7:e13911.
6. Maes D, Bowen SR, Regmi R, Bloch C, Wong T, Rosenfeld A, Saini J. A machine learning-based framework for delivery error prediction in proton pencil beam scanning using irradiation log-files. Physica Medica. 2020 Oct 1;78:179-86.
7. Wu C, Nguyen D, Xing Y, Montero AB, Schuemann J, Shang H, Pu Y, Jiang S. Improving proton dose calculation accuracy by using deep learning. Machine learning: science and technology. 2021 Apr 6;2(1):015017.
8. Wang W, Chang Y, Liu Y, Liang Z, Liao Y, Qin B, Liu X, Yang Z. Feasibility study of fast intensity-modulated proton therapy dose prediction method using deep neural networks for prostate cancer. Medical Physics. 2022 Aug;49(8):5451-63.
9. Nomura Y, Wang J, Shirato H, Shimizu S, Xing L. Fast spot-scanning proton dose calculation method with uncertainty quantification using a three-dimensional convolutional neural network. Physics in Medicine & Biology. 2020 Oct 19;65(21):215007.
10. Neishabouri A, Wahl N, Mairani A, Köthe U, Bangert M. Long short-term memory networks for proton dose calculation in highly heterogeneous tissues. Medical physics. 2021 Apr;48(4):1893-908.
11. Pastor-Serrano O, Perkó Z. Learning the physics of particle transport via transformers. InProceedings of the AAAI Conference on Artificial Intelligence 2022 Jun 28 (Vol. 36, No. 11, pp. 12071-12079).
12. Meijers A, Jakobi A, Stützer K, Guterres Marmitt G, Both S, Langendijk JA, Richter C, Knopf A. Log file-based dose reconstruction and accumulation for 4D adaptive pencil beam scanned proton therapy in a clinical treatment planning system: Implementation and proof-of-concept. Medical Physics. 2019 Mar;46(3):1140-9.
13. Toscano S, Souris K, Goma C, Barragán-Montero A, Puydupin S, Vander Stappen F, Janssens G, Matic A, Geets X, Sterpin E. Impact of machine log-files uncertainties on the quality assurance of proton pencil beam scanning treatment delivery. Physics in Medicine & Biology. 2019 Apr 29;64(9):095021.

14. Shanmuganathan S. Artificial neural network modelling: An introduction. Springer International Publishing; 2016.
15. Ali Z, Hussain I, Faisal M, Nazir HM, Hussain T, Shad MY, Mohamd Shoukry A, Hussain Gani S. Forecasting drought using multilayer perceptron artificial neural network model. Advances in meteorology. 2017;2017(1):5681308.
16. Ketkar N. Introduction to keras. Deep learning with python: a hands-on introduction. 2017:97-111.
17. Pang B, Nijkamp E, Wu YN. Deep learning with tensorflow: A review. Journal of Educational and Behavioral Statistics. 2020 Apr;45(2):227-48.
18. Agarap AF. Deep learning using rectified linear units (relu). arXiv preprint arXiv:1803.08375. 2018.
19. Zhang Z. Improved adam optimizer for deep neural networks. In2018 IEEE/ACM 26th international symposium on quality of service (IWQoS) 2018 Jun 4 (pp. 1-2). Ieee.
20. Cherkassky V, Ma Y. Comparison of loss functions for linear regression. In2004 IEEE International Joint Conference on Neural Networks (IEEE Cat. No. 04CH37541) 2004 Jul 25 (Vol. 1, pp. 395-400). IEEE.
21. Sevinç E. An empowered AdaBoost algorithm implementation: A COVID-19 dataset study. Computers & Industrial Engineering. 2022 Mar 1;165:107912.
22. Pleil JD. QQ-plots for assessing distributions of biomarker measurements and generating defensible summary statistics. Journal of breath research. 2016 Aug 5;10(3):035001.
23. Actis O, Meer D, König S, Weber DC, Mayor A. A comprehensive and efficient daily quality assurance for PBS proton therapy. Physics in Medicine & Biology. 2017 Feb 6;62(5):1661.
24. Rana S, Bennouna J, Samuel EJ, Gutierrez AN. Development and long-term stability of a comprehensive daily QA program for a modern pencil beam scanning (PBS) proton therapy delivery system. Journal of Applied Clinical Medical Physics. 2019 Apr;20(4):29-44.
25. Arjomandy B, Taylor P, Ainsley C, Safai S, Sahoo N, Pankuch M, Farr JB, Yong Park S, Klein E, Flanz J, Yorke ED. AAPM task group 224: Comprehensive proton therapy machine quality assurance. Medical physics. 2019 Aug;46(8): e678-705.

Chapter 5

Development of an In-House Tool for PSQA Analysis Using Machine Learning Models and Log File Data.

Chapter 5

Title: Development of an In-House Tool for PSQA Analysis Using Machine Learning Models and Log File Data.

5.1 Introduction

Proton therapy is a highly precise and effective form of radiation therapy used to treat cancer, leveraging the unique physical properties of protons to deliver targeted doses to tumours while minimizing damage to surrounding healthy tissues. This ability to deliver precision has made proton therapy a vital tool in modern radiation oncology. However, the clinical effectiveness of proton therapy depends on the accurate delivery of the proton beams as specified by the treatment plan, necessitating thorough QA procedures to ensure consistent and reliable performance across multiple treatment sessions.

There are many studies to simplify the QA of proton therapy systems using advanced tools such as the MC dose algorithm and automation. A study by Liu C et al. [1] introduced a fast MC-squared dose calculation algorithm to cross-check doses from the Raystation TPS, showcasing the integration of MC-based methods to improve dose verification in proton therapy. Similarly, Albertini F et al. [2] developed the first clinical online adaptive re-planning system, relying solely on machine log files and in-room CT images. Several studies have utilized MC and log files, which record spot position and MU values for secondary dose evaluation [3,4,5]. These studies exclusively relied on log file data and employed gamma analysis for verification. However, a limitation of MC-based dose evaluation is its reliance on GPU-based systems for rapid calculations. Despite this, MC-based methods remain valuable as they eliminate the need for dedicated dosimeter measurements, which consume significant beam time and manpower [6].

A study by Toscano S et al. [7] evaluated the uncertainties in data recorded in log files, particularly in spot position and MU. This research underscores that log-file data carries inherent uncertainties, which must be carefully considered when using log files directly in Monte Carlo-based dose calculations. Addressing these uncertainties in dose evaluation ensures a more accurate assessment of treatment delivery quality, emphasizing the importance of accounting for limitations of log files in PSQA workflows. The detailed analysis of log file data and its correlation with dosimetric parameters measured using a dedicated dosimeter is very important to avoid any wrong interpretation of data if solely

depends on data in the log file for PSQA and machine QA. Ates O, et al [8] did a detailed study of the log file data of the PROBEAT-V proton therapy system (Hitachi Ltd., Tokyo, Japan) of 6-year data. The results suggest that the log file data analysis is a very good tool for tracking the performance of the machine over time.

The irradiation log file of a PBS proton therapy system contains vast amounts of data, making manual analysis and interpretation both labour-intensive and time-consuming. Automating log file analysis through scripting provides a practical and efficient solution, improving time management and simplifying the workflow. Chapter 3 discussed the uncertainties associated with log file data, emphasizing that addressing these uncertainties is critical to enhancing the reliability of log files for machine QA and PSQA workflows.

Chapter 4 introduced and validated ML models for predicting dosimetric parameters, including spot size and relative positional errors, using log file data as input. While the ML models demonstrated high prediction accuracy, effectively utilising these models requires automated methods, such as scripting, to streamline the workflow. Automating data segregation from log files and applying ML models saves time and enhances the process's overall efficiency, enabling their meaningful application in PSQA and machine QA.

This chapter focuses on developing and implementing an in-house script-based tool to automate log file data extraction and integrate previously developed ML models for predicting spot parameters. By automating the analysis of patient-specific beam irradiation data, this tool combines data extraction with ML-based predictions to streamline the QA process. Integrating ML into the QA process optimises the workflow, improving the precision of proton therapy. The chapter details the tool’s framework, data processing, and the comparison of predicted parameters with specifications, demonstrating its potential to streamline PSQA in PBS proton therapy.

5.2 Materials and Methods

This session provides an overview of the materials and methods used to develop an in-house automated tool for data extraction, spot parameter prediction, comprehensive data analysis, and reporting results for each treatment beam in the PBS proton therapy system

5.2.1 IBA Proteus plus multi-room system

The IBA Proteus Plus proton therapy system installed at ACTREC, Tata Memorial Centre, Mumbai, utilized in this study is a multi-room setup equipped with multiple treatment gantries. Specifically, the system includes three treatment gantries, as illustrated in Figure 5.1. The cyclotron produced proton beam transfer to each gantry through the beam transport system. While these gantries are identical in operation, their beam characteristics are not beam-matched. Consequently, slight variations can occur between the gantries in parameters such as spot size, range, nozzle water-equivalent thickness (WET), and source-to-detector distance. To address these differences, the development of the in-house tool accounted for these small variations, enabling the analysis of all irradiated beams from any gantry.

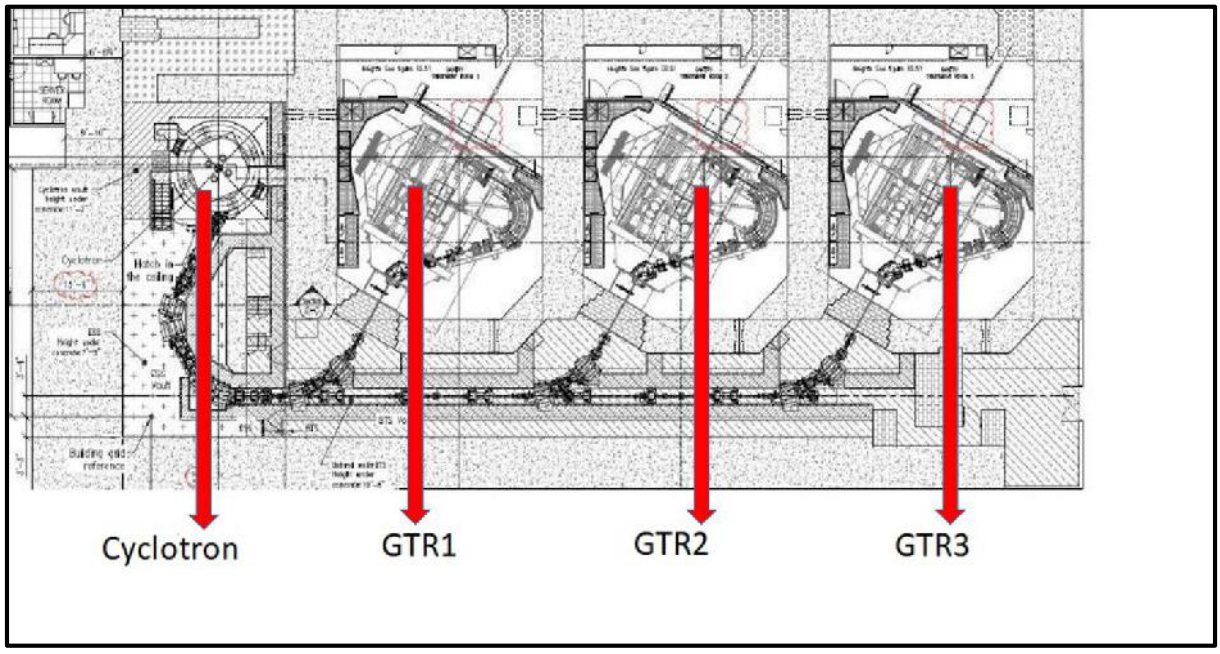

Figure 5.1: The Schematic representation of the layout of the Proton therapy system installed at ACTREC Proton Therapy Centre, Navi Mumbai, India. GTR- Gantry.

5.2.2 Log file data extraction

The log files are generated and saved in a dedicated directory named "Data Recorder" within the IBA beam delivery system after each beam delivery. These log files are stored in .zip format, with a separate .zip file created for each beam. Each .zip file contains seven .csv files that record detailed beam delivery data.

The information from these log files is extracted using an in-house Python-based script designed to automate the data extraction process efficiently. After each beam delivery, the data from these log files is analysed by the script and tabulated alongside the planned data received from the Mosaiq OIS. The analysis involves comparing the planned data with the delivered data, focusing particularly on the range of each layer and key spot dosimetric parameters such as spot size, position, MU etc.

A detailed description of each file is provided below:

5.2.2.1. beam.csv:

The file contains general information about the irradiation session (room, gantry angle, cyclo current, temperature, humidity, and ionization chamber configuration)

5.2.2.2. beam_config.csv:

This file is a copy of the scanalgo database (configuration file of the scanning controller). It contains all the scanning calibration parameters as well as the safety tolerances.

5.2.2.3. beam_settings.csv:

The file contains treatment settings and parameters (including BMS, PMS, and Scanalgo database).

5.2.2.4. event.csv:

This file has the timeline of the full irradiation, this file lists the timestamps of all the important steps of one field irradiation (each tuning pulse, each layer, and each set range)

5.2.2.5.map_record_tuning.csv

The Irradiation log of the initial tuning pulse. There is at least one tuning pulse at the beginning of every range. During the tuning pulse, the alignment of the beam is verified and adjusted, if necessary. This tuning pulse is done on the spot of the field that is closest

to the un-scanned location of the beam. The tuning pulse is taken into account in the total dose.

5.2.2.6. map_specif.csv file:

This file represents the TPS data, including the planned spot position, range, and MU for each spot within a beam. The TPS transfers treatment planning data to the Mosaiq OIS. The Mosaiq OIS transfers all spot-related data required by the IBA beam delivery system, such as the spot position in the isocentre plane, the MU per spot, and the range or energy of each spot.

The IBA beam delivery system converts the data into the format required for delivery. Specifically, the IBA system verifies and records the size, position, and MU of each spot using the IC23 ionisation chamber. The system transforms the spot positions from the isocentre plane to the IC23 plane and calculates the beam range from the energy value. Based on the range, the system assigns baseline spot size values to each spot. Additionally, the MU values are converted into charge values to ensure the IC23 chamber halts beam irradiation once the prescribed MU is delivered.

Furthermore, the IBA beam delivery system calculates the minimum and maximum positional values in the X and Y directions and the spot size in the IC23 plane along both axes. These calculations are based on tolerance values provided in Chapter 3, Table 3.2. All the aforementioned data is recorded in the beam specification file for each range. The specification file is generated for each layer. The in-house tool read this specification file to extract the above-mentioned data.

5.2.2.7. map_record.csv

This .csv file records all major dosimetric parameters for each spot. It contains detailed irradiation data for every spot, with a separate file generated for each range. The file logs data at intervals of 200 µs, creating a new row for each spot at these intervals. If a single spot lasts longer than 200 µs, its data will appear across multiple rows.

The recorded data includes measurements from the nozzle head ionisation chambers and scanning magnets. Key parameters captured in the file include:

- Spot ID
- Spot widths (X and Y) recorded in both the IC23 and IC1 ionisation chambers
- Spot positions (X and Y) recorded in the IC23 and IC1 chambers
- Charge collected in the primary and secondary dosimeters within the IC23 for each spot
- Primary and secondary currents of the X and Y scanning magnets
- Beam current
- Degrader feedback
- Gantry name
- Layer ID

The beam specification file serves as a reference for beam irradiation. The beam delivery system continuously monitors parameters such as spot position, charge, and size, as recorded in the IC23 chamber. These are compared with the corresponding values in the beam specification file. If any parameter deviates beyond the specified tolerance values, the system triggers a beam interruption. The irradiation file is used to extract all irradiated spot parameters for the analysis.

5.2.3 Conversion of spot position in IC23 to the isocentre plane

The spot positions recorded in IC23 must be converted back to the isocentre plane for direct comparison with the spot positions defined by the TPS system. This conversion is performed using the equivalent triangle method, as described in Figure 5.2. The calculation for the equivalent triangle method requires parameters such as the distance from the isocentre to the centre of each scanning magnet, referred to as the source-to-axis distance (SAD), and the distance from the IC23 plane to the centre of each scanning magnet.

While the SAD values are identical for all gantries, slight variations exist in the distance from the IC23 plane to the scanning magnet centres. These values are summarised in Table 5.1. The script incorporates these differences to accurately convert the spot positions recorded in IC23 to the isocentre plane.

Table 5.1: The tabulation of different distance values for the calculation of spot position conversion from the IC23 plane to the isocentre. GTR- represents each gantry.

	Distance from the isocentre to the centre of each scanning magnet			Distance from IC23 plane to scanning magnet centre (same for all gantries)
	GTR1 (mm)	GTR2 (mm)	GTR3 (mm)	
X scanning magnet	1239.9	1236.6	1241.3	1835.5
Y scanning magnet	1657.5	1653.7	1657.9	2214.2

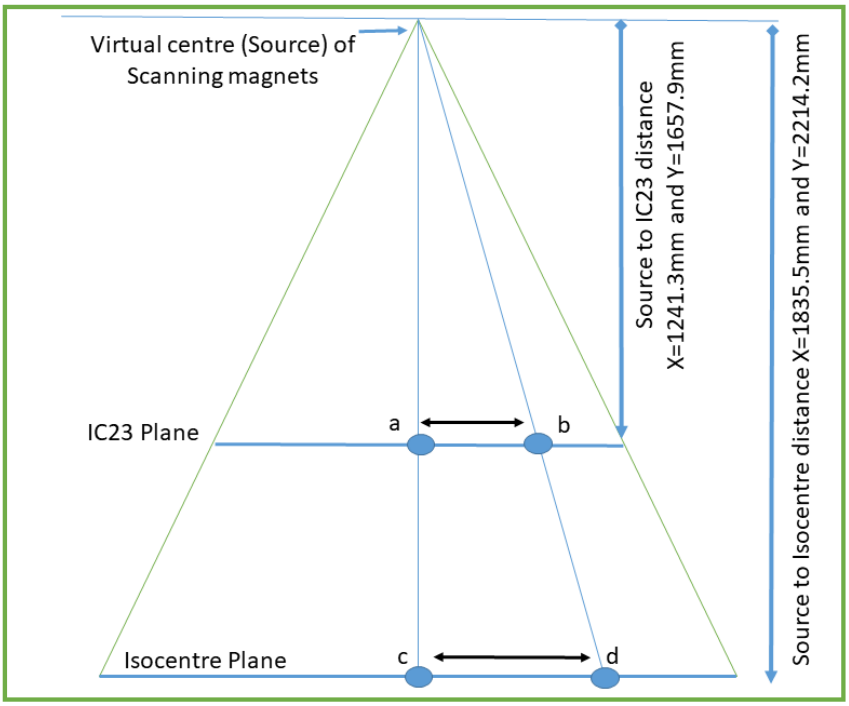

Figure 5.2: Equivalent triangle method. This method converts the spot positions from the isocentre plane to the IC23 plane.

5.2.4 Range calculation

The energy value of each spot is transferred from the TPS to the Mosaiq OIS and subsequently to the IBA beam delivery system. The IBA delivery system converts this energy into a range value using Equation 3.3 provided in Chapter 3, Section 3.2.5. The calculated range represents the penetration depth of the proton beam in water.

The nozzle head includes a thin copper window to protect equipment from physical damage. However, this protective layer causes minor attenuation of the proton beam. The WET of this protective sheet must be considered when calculating the range of each spot provided by the TPS. The IBA specification file records the range of each spot by subtracting the WET of the nozzle entrance window.

To determine the actual range or energy recorded in the specification file, the WET of the entrance window must be added back to the range recorded in the file. The WET of the nozzle entrance window is energy-dependent and is calculated using a third-order polynomial equation. Since the thickness of the entrance window varies slightly between the three gantries, the coefficients of the polynomial equation differ for each gantry. The specific coefficients are provided below.

$$WET\ (Nozzle\ entrance\ ) in\ mm = aR^3 + bR^2 + cR + d \qquad (5.1)$$

Where R is the range of the spot at the nozzle entrance.

The Coefficients for different gantries are tabulated in table 5.2.

Table 5.2: The coefficients of equation 5.1 for different gantries. GTR- Gantry.

Coefficients	a	b	c	d
GTR1	-1.7E-05	7.5E-04	-4.7E-03	1.8E-01
GTR2	-8.0E-06	3.5E-04	-7.2E-04	1.9E-01
GTR3	-8.0E-06	3.5E-04	-7.2E-04	1.5E-01

The in-house script uses this information to calculate the range of each spot delivered and recorded in the log file, which is then compared with the range specified by the TPS.

5.2.5 Spot size calculation

The spot size for each range or energy has a baseline value that remains consistent across all gantry angles for a specific energy. This baseline spot size is inherently linked to the range, with the spot size typically decreasing as the range increases. In the log file analysis, ML models are employed to predict the spot size in both the X and Y axes for all spots irradiated in the beam. These predictions are based on the irradiation data captured in the log files. However, to make meaningful comparisons between the predicted spot sizes and the actual measurements, a baseline spot size value is required. This baseline value, representing the expected spot size for a given energy or range, is calculated using an analytical equation 5.2. The equation accounts for the relationship between the energy or range and the corresponding spot size, providing a reference for comparison with the ML model's predicted values. The equation for calculating the baseline spot size is given below

$$Spot\ size(mm) = aE^4 + b\,E^3 + cE^2 + dE + e \qquad (5.2)$$

E-Energy in MeV and the coefficients are, a = 5.47E-09, b = -4.03E-06, c = 0.001172, d= -0.1715, and e= 14.03009.

The in-house script calculates the baseline spot size for each spot specified in the specification file using the provided equation and the corresponding spot's range information. It then compares these baseline spot size values with the spot sizes predicted by the ML model.

5.3 Results

5.3.1 Nozzle WET calculation

The script utilises Equation 5.1 to calculate the nozzle WET and determine the range of each spot during log file analysis. As shown in Table 5.3, the calculated nozzle WET values for five selected energies are presented for all three gantries. The log file records the machine name, which is used to identify the machine and apply the corresponding coefficients tabulated in Table 5.2 for nozzle WET calculation in the script.

As presented in Table 5.3, the maximum calculated WET value of the nozzle entrance window is 0.27 mm for an energy of 200 MeV. This finding highlights the

importance of correcting the range values recorded in the log file using the nozzle WET value. Such corrections are critical for accurately determining the actual range of each spot, especially when comparing these values with TPS data. The TPS computes the beam range in water as it passes through the nozzle head. To ensure consistency in this comparison, the beam range derived from TPS energy data is matched against the nozzle WET-corrected range recorded in the log file. This correction involves subtracting the nozzle WET value from the range recorded in the log file, ensuring an accurate depiction of the actual range for each spot.

Table 5.3: Provided the calculated nozzle WET values for different energies for all three gantries.

Energy (MeV)	Range (g/cm^2)	Calculated Nozzle WET values		
		GTR1(mm)	GTR2 (mm)	GTR3 (mm)
70.18	4.1	0.17	0.19	0.15
100	7.72	0.18	0.20	0.16
150	15.78	0.23	0.23	0.19
200	25.4	0.27	0.27	0.22
226.2	32.02	0.24	0.26	0.22

5.3.2 The Automated script workflow

The in-house script automates the analysis of spot dosimetric parameters for an irradiated beam using log file data and ML models. The irradiation log files, along with the specification files, are processed by the script, which converts the data into meaningful spot dosimetric parameters, as described in the methods section. The script tabulates the converted spot position and MU values for each spot from the irradiation file. Additionally, it creates a table of input data for the ML models to predict spot size information.

Each ML model is executed, and the predicted spot size values are tabulated alongside the baseline spot size values. The script compares the predicted values with the TPS-specified data and the irradiation data to assess the accuracy of the spot dosimetric parameters. The predicted spot size values along the Major and Minor axis are used to calculate the spot symmetry using the equation provided below.

$$spot\ symmetry = \frac{(Spot\ size\ Major\ axis - spot\ size\ along\ Minor\ axis)}{(Spot\ size\ \ Major\ axis + Spot\ size\ along\ Minor\ axis)}\ \text{x}100 \qquad (5.3)$$

This approach can be used to automates the analysis of spot dosimetric parameters for thousands of spots in each irradiated beam of a patient-specific treatment plan. The workflow of the in-house tool is shown in Figure 5.3.

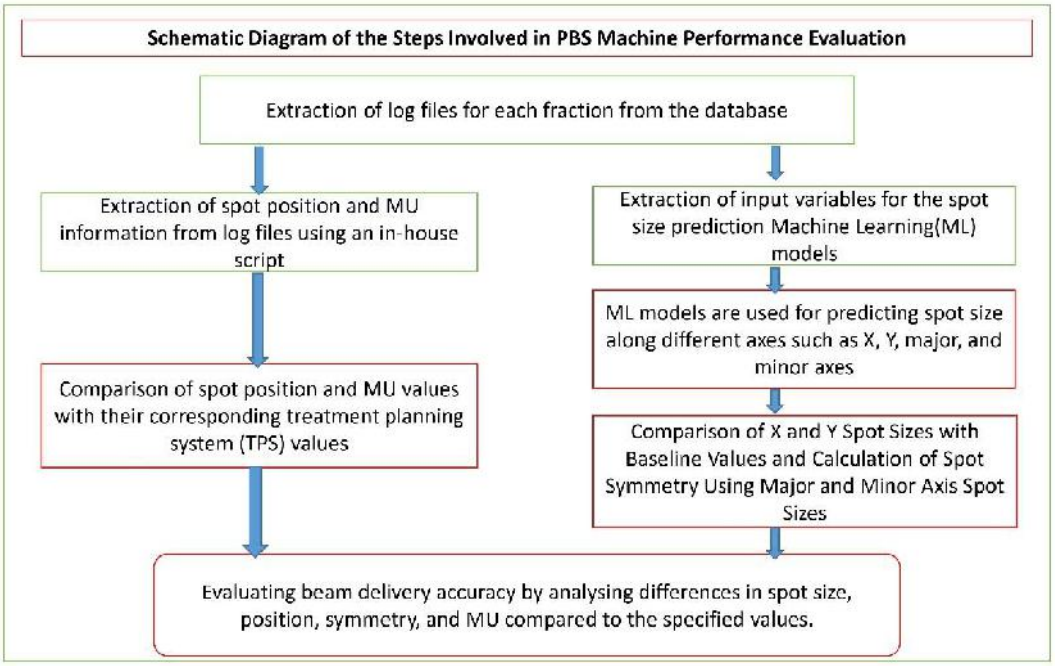

Figure 5.3: The Illustration of the steps involved in the log file analysis using the In-house automated tool.

5.3.3 Report generation

The in-house script generates a comprehensive final report based on the data analysis. This report includes key details such as the total number of layers, the spots in each layer, the MU of each layer, the total MU of the beam, and the percentage of spots with variations in spot size, position, symmetry, and MU. Specifically, the report highlights the percentage of spots with a variation of less than 10 %, spot position variation within 1 mm, spot symmetry below 10 %, and MU variation of less than 2 %.

A sample report is illustrated in Tables 5.4, 5.5, and 5.6. These tables represent the output format produced by the in-house script after analysing the irradiated beam's log file data. All the values shown in these tables are based on the sample data extracted and processed by the script.

Table 5.4**:** Sample data table illustrating the total number of spots, layers, and MU. This table represents the format generated by the in-house script when processing the irradiated log file data of a beam. * All values are sample values only.

Parameters	**Value ***
QA plan name	XXXXXX
Beam Name	XXXXX
Total number of layers in Plan	22
Total number of layers irradiated	22
Total number of spots in Plan	1107
Total number of spots irradiated	1104
Difference in number of layers	0
The difference in the total number of spots	3
Total MU (TPS)	263.98
Total MU (Irradiated)	263.49
Difference in delivered MU	-0.49

Table 5.5**:** Sample format of the table displaying spot information for each layer. This table represents the structure generated by the in-house script when processing the log file data for a patient's treatment beam. * All values are sample values only.

Range (cm) *	Energy (MeV) *	No. of Spots. *	MU/Layer *	Number of spots Irradiated per layer *	Irradiated MU/Layer *
11.36	124.41	12	5.93	12	5.92
10.98	122.01	18	6.63	18	6.61
…..	…..	…..	…..	…..	…..
…..	…..	…..	…..	…..	…..
…..	…..	…..	…..	…..	…..
4.93	77.81	13	2.5	12	2.49

Table 5.6**:** Sample table displaying the results of spot parameter analysis, including the percentage of spots in the beam with spot size differences of less than 10 %, spot symmetry of less than 10 %, spot position errors within 1 mm, and MU per spot variation of less than 2 %. * All values are sample values only.

Parameters	**Sample Value (%)***
Spots with X spot size variation within 10 %	90.3
Spots with Y spot size variation within 10 %	93.1
Spots with 2D symmetry less than 10 %	93.5

Spots with X position variation within 1 mm	92.0
Spots with Y position variation within 1 mm	95.0
Spots with MU variation within 2 %	98

All the above tables represent sample data produced as an output of the in-house script after analyzing the irradiation log file data.

5.4 Discussion

The PBS proton therapy treatment involves thousands of spots per beam, making it impractical and cumbersome to measure and analyse the dosimetric parameters for each spot individually. Ideally, if all the spots in a treatment beam meet the tolerance criteria and all dosimetric parameters are within specified limits, the beam irradiation would be considered accurate and complete. However, measuring these parameters for every spot using a dedicated dosimeter is practically impossible, requiring significant beam-on time and manpower. Consequently, the conventional approach for PSQA involves measuring dose planes at various depths and performing gamma analysis [9]. While this method provides a convenient tool for PSQA, it often struggles with the complexity of highly modulated dose distributions in intensity-modulated proton therapy, frequently failing to detect clinically significant discrepancies. Moreover, this process requires substantial setup time and consumes valuable clinical treatment time [10].

The need for a fast and reliable tool for PSQA in proton therapy has driven the development of MC-based PSQA systems that utilize log files as input parameters [3, 4, 5]. This approach reduces the reliance on dedicated dosimeter measurements and minimizes beam-on time, though it necessitates a GPU-based system for rapid dose calculation. Additionally, gamma analysis is employed for dose evaluation. A study by Ates et al. [8], which analyzed six years of patient data, demonstrated that log file analysis can serve as a valuable tool for machine performance evaluation. However, the uncertainties associated with log file data must be carefully considered before it can be adopted as a comprehensive analysis tool in proton therapy.

This chapter discusses the development of an in-house tool designed to analyse the dosimetric accuracy of all spots within a treatment beam using log files and ML models. The implementation of this automated, script-based tool represents a substantial

advancement in QA processes for PBS proton therapy systems. By addressing challenges related to non-beam-matched gantries in the IBA Proteus Plus system—such as variations in spot size, range, and source-to-detector distances—this tool integrates system-specific configurations to enhance its applicability.

The automated extraction of key parameters, including spot size, position, and MU, facilitates efficient and precise analysis, significantly reducing the time required compared to manual methods. This streamlined approach supports proactive identification and correction of discrepancies, ensuring compliance with QA standards, such as AAPM-TG224 [11]. The integration of ML models further enhances the tool's capability to optimise dosimetric accuracy, thereby strengthening its role in modern QA frameworks for proton therapy.

5.5 Conclusions

In conclusion, this chapter summarises the development of the in-house automated tool that integrates log file data and ML models, marking a significant advancement in ensuring the accuracy and efficiency of proton therapy beam delivery. This tool enables quick and comprehensive analysis of PSQA beams, allowing for the prompt identification of discrepancies and ensuring adherence to QA standards. By improving the precision of beam delivery evaluation, the methodology has the potential to streamline PSQA and machine QA processes, ultimately contributing to enhanced patient outcomes.

Chapter 6 will provide a detailed exploration of the application of this in-house tool for PSQA and machine QA, focusing on its role in validating the beam delivery accuracy of the IBA Proteus Plus system.

5.6 References

1. Liu C, Ho MW, Park J, Hsi WC, Liang X, Li Z, Song Y, Feng H, Zhang Y. Fast MCsquare-based independent dose verification platform for pencil beam scanning proton therapy. Technology in cancer research & treatment. 2021 Jul 31;20:15330338211033076.
2. Albertini F, Czerska K, Vazquez M, Andaca I, Bachtiary B, Besson R, Bolsi A, Bogaert A, Choulilitsa E, Hrbacek J, Jakobsen S. First clinical implementation of a highly efficient daily online adapted proton therapy (DAPT) workflow. Physics in Medicine & Biology. 2024 Nov 11;69(21):215030.
3. Jeon C, Lee J, Shin J, Cheon W, Ahn S, Jo K, Han Y. Monte Carlo simulation-based patient-specific QA using machine log files for line-scanning proton radiation therapy. Medical Physics. 2023 Nov;50(11):7139-53.

4. Feng H, Patel SH, Wong WW, Younkin JE, Penoncello GP, Morales DH, Stoker JB, Robertson DG, Fatyga M, Bues M, Schild SE. GPU-accelerated Monte Carlo-based online adaptive proton therapy: a feasibility study. Medical physics. 2022 Jun;49(6):3550-63.
5. Lysakovski P, Ferrari A, Tessonnier T, Besuglow J, Kopp B, Mein S, Haberer T, Debus J, Mairani A. Development and benchmarking of a Monte Carlo dose engine for proton radiation therapy. Frontiers in Physics. 2021 Nov 3;9:741453.
6. Nelson NP, Culberson WS, Hyer DE, Geoghegan TJ, Patwardhan KA, Smith BR, Flynn RT, Yu J, Gutiérrez AN, Hill PM. Dosimetric delivery validation of dynamically collimated pencil beam scanning proton therapy. Physics in medicine & biology. 2023 Feb 20;68(5):055003.
7. Toscano S, Souris K, Goma C, Barragán-Montero A, Puydupin S, Vander Stappen F, Janssens G, Matic A, Geets X, Sterpin E. Impact of machine log-files uncertainties on the quality assurance of proton pencil beam scanning treatment delivery. Physics in Medicine & Biology. 2019 Apr 29;64(9):095021.
8. Ates O, Pirlepesov F, Zhao L, Hua CH, Merchant TE. Development of a log file analysis tool for proton patient QA, system performance tracking, and delivered dose reconstruction. Journal of Applied Clinical Medical Physics. 2023 Jul;24(7):e13972.
9. Arjunan M, Sharma DS, Kaushik S, Krishnan G, Patro KC, Padanthaiyil NM, Rajesh T, Jalali R. A novel hybrid 3D dose reconstruction approach for pre-treatment verification of intensity modulated proton therapy plans. Physics in Medicine & Biology. 2021 Feb 19;66(5):055015.
10. Zhu XR, Li Y, Mackin D, Li H, Poenisch F, Lee AK, Mahajan A, Frank SJ, Gillin MT, Sahoo N, Zhang X. Towards effective and efficient patient-specific quality assurance for spot scanning proton therapy. Cancers. 2015 Apr 13;7(2):631-47.
11. Arjomandy B, Taylor P, Ainsley C, Safai S, Sahoo N, Pankuch M, Farr JB, Yong Park S, Klein E, Flanz J, Yorke ED. AAPM task group 224: comprehensive proton therapy machine quality assurance. Medical physics. 2019 Aug;46(8):e678-705.

Chapter 6

Application of the In-House Automated Tool for Patient-Specific and Machine Quality Assurance in Proton Beam Therapy Using Log Files and Machine Learning Models

Chapter 6

Title: Application of the In-House Automated Tool for Patient-Specific and Machine Quality Assurance in Proton Beam Therapy Using Log Files and Machine Learning Models.

6.1 Introduction

Achieving precise treatment delivery, as outlined by the TPS, is essential for optimal clinical outcomes in radiotherapy [1]. In PBS proton therapy, proton spots are delivered dynamically with varying energies and positions to construct the planned dose distribution layer by layer. Robust QA protocols are crucial to ensure that the machine delivers treatments as intended, verifying parameters against the treatment plan and addressing errors before they affect patient outcomes. The precision required in PBS, involving thousands of spots, makes meticulous QA a cornerstone of effective and safe proton therapy. [2]. The AAPM-TG-224 report [3] highlights the necessity of routine verification of beam parameters and PSQA. Spot profiles, which play a pivotal role in determining dose distribution accuracy, depend on the beam optics, which are meticulously optimised during machine installation and commissioning [4]. Although the baseline spot size for each energy is designed to remain consistent across all gantry angles, minor variations can arise due to adjustments in beam optics for specific energy and angle combinations. Consequently, routine QA protocols are designed to evaluate spot size, position, and symmetry for selected energies and angles.

In clinical scenarios, treatment fields comprise thousands of proton spots with varying energies, closely arranged to ensure uniform dose coverage and adequate distribution to the target. Conventional QA equipment lacks the capability to directly verify the dosimetric accuracy of every individual spot within a treatment field. As a result, standard PSQA procedures rely on array detectors to measure dose fluence at fixed gantry angles, with the evaluation commonly performed through gamma analysis [5]. However, this method is labour-intensive, limited to specific gantry angles, consumes significant beam-on time, and may not reliably represent the dosimetric accuracy at the actual treatment angle during patient delivery [6,7].

Given these challenges, many centres have transitioned to MC methods to enhance PSQA by leveraging data from irradiation log files [8–10]. MC algorithms extract essential spot data, including positions and MU values, from these log files to calculate the delivered

dose. Numerous studies have investigated the accuracy of the spot position and MU data recorded in log files [11–13]. For instance, Noufal et al. [14] demonstrated that random errors in spot positions could significantly impact dose delivery, potentially affecting both target coverage and sparing of normal tissues. Furthermore, variations in spot size can introduce in homogeneities in dose distribution, leading to suboptimal treatment outcomes [15]. In PBS proton therapy, inconsistencies in beam transport and extraction systems can result in delivered spot sizes deviating from their planned values, risking underdoing of the target or overdosing of nearby critical structures [16–19].

While MC and log file-based PSQA methods are effective for verifying specific beam parameters, they do not address variations in the delivered spot sizes. Typically, spot size data recorded in log files are derived using Gaussian fitting of signals from strip ionisation chambers. However, these recorded values frequently show poor correlation with the actual spot sizes measured using high-resolution scintillators. These inconsistencies complicate the direct analysis of spot size data from log files, underscoring the necessity for more advanced methodologies to ensure accurate dosimetric evaluation and improve treatment precision.

The ML has emerged as a transformative technology in radiation therapy, with an increasing number of studies exploring its potential for predicting dosimetric parameters and automating QA processes [20–23]. Several investigations have successfully employed ML models to predict spot positions and MU values using irradiation log files as input data [24,25]. However, ensuring accurate PBS treatments requires a more comprehensive evaluation of all spot parameters, including spot size, symmetry, position, and MU for each spot in a treatment field. Despite progress in ML applications, a fully integrated ML-based approach that systematically assesses all these parameters for every individual spot within a treatment field is still lacking.

In Chapter 3, a comprehensive analysis was conducted to compare the spot parameters recorded in log files with those measured using a high-resolution scintillator detector. The findings revealed a linear correlation between the log file data and scintillator measurements. However, the accuracy of the log file data remains questionable for direct use in machine performance evaluation or machine QA, as inherent data limitations affect its reliability. Chapter 4 focused on developing ML models to predict spot dosimetric

parameters using log file data as input. These ML models demonstrated high predictive accuracy, effectively addressing discrepancies in log file data and serving as a robust tool for machine QA.

Chapter 5 combined the capabilities of the ML models and log file data analysis into an in-house automated tool. This tool was designed using scripts to facilitate comprehensive log file evaluation. It enabled the extraction of significant data from log files, segregation of input parameters for the ML models, automated prediction of spot parameters, generation of beam-specific reports, and analysis of all spot dosimetric parameters.

This chapter summarises the application of the in-house tool for evaluating beam delivery accuracy using routine QA beams and PSQA beams. Log file data from multiple beams, recorded during the PSQA procedures were collected and analysed using an in-house automated tool. The results demonstrated that this method could serve as a potential solution for machine QA, PSQA and the performance evaluation of the IBA Proteus Plus proton therapy system. The tool offers a time-efficient and resource-effective alternative to conventional PSQA methods by enabling the analysis of all spot parameters in treatment beams without requiring dedicated dosimeters. This approach not only reduces beam-on time and manpower but also eliminates the complexities associated with traditional PSQA procedures.

6.2 Materials and Methods

6.2.1 Data collection

The performance of the in-house tool was evaluated using routine machine QA data. It was also employed to analyse the accuracy of PSQA beams by processing irradiated log file data collected post-irradiation.

The routine QA analysis of the IBA Proteus Plus PBS machine focused on spot dosimetric parameter accuracy using a 5-spot pattern across 30 different energy levels, with a range interval of 1 gm/cm². The energy range varied from 70.18 MeV (corresponding to a range of 4.1 gm/cm²) to 226.2 MeV (corresponding to 32.0 gm/cm²). These QA measurements were conducted using a Lynx2D scintillator detector. For each energy level,

the same 5-spot pattern was measured at 12 different gantry angles with gantry angle intervals of 30^0. The IBA Proteus Plus machine is equipped with three gantries, and QA was performed on all three to ensure spot accuracy. Data from all three gantries were collected over three months from August 2023 to October 2023, resulting in a total of 1080 spot patterns and a total of 5400 spots and their corresponding log file data for subsequent analysis using the in-house tool.

For the PSQA beams, log file data were collected from PSQA procedures conducted before actual patient treatments. During PSQA, each treatment plan typically consisting of 2 to 5 beams are recalculated in a virtual water phantom within the TPS and delivered to an actual water phantom. Dose measurements at various depths are acquired using a dedicated matrix ionisation chamber array detector. Log files corresponding to these beams were recorded during the PSQA water phantom measurements, capturing detailed irradiation parameters. Over a period of 10 months, from August 2023 to May 2024, a total of 935 beam log files were gathered and subsequently analysed using an in-house automated tool. Each beam contains thousands of spots, and in total, approximately 3 million spots were analysed using the in-house tool, providing a comprehensive dataset for evaluating beam delivery accuracy and ensuring the reliability of the treatment process. The ethical clearance (DYPMCK/11/2022/IEC) obtained before taking data. Table 6.1 summarizes the statistical data from the 935 PSQA beams analysed in this study. Key parameters include the number of layers per beam, the energy span, the MU per spot, and the spot position range. This statistical overview provides insights into the characteristics of the treatment beams, offering a comprehensive understanding of the data.

Table 6.1: Summary statistics of beam parameters analyzed in this study. The number of layers, Energy range, spot size range, spot position in X and Y directions and MU per spot.

Beam parameters	mean	Standard Deviation	Minimum	1st Quartile (25%)	2nd Quartile (50%)	3rd Quartile (75%)	Maximum
Number of layers	14.10	7.66	1.00	8.00	13.00	19.00	50.00
Energy (MeV)	140.81	28.70	75.41	119.01	140.82	163.72	203.24
Spot size (mm)	4.13	0.65	3.08	3.60	4.02	4.53	6.20

Spot position at Isocentre - X direction(mm)	-1.17	38.81	-132.46	-27.36	-0.34	25.77	111.67
Spot position at Isocentre - Y direction (mm)	2.19	35.93	-121.06	-21.46	2.64	27.34	86.14
MU per spot	0.11	0.12	0.01	0.04	0.06	0.13	2.71

6.2.2 Data Processing

All the machine QA log file data and PSQA beam log file data were retrieved from the data recorder folder of the IBA beam delivery system after beam irradiation. The recorded log files were unzipped and processed using the in-house tool described in Section 5.3.2 of Chapter 5. This tool enabled the reading and extraction of relevant data, applied ML models to predict spot dosimetric parameters, and generated comprehensive reports summarising the analysis results.

For machine QA, the predicted spot size values in the X and Y directions and the spot position accuracy of each spot were assessed by comparing log file recorded data with both measured data and ML model predictions. For patient treatment beam data analysis, the in-house tool generated a report for each beam, which was segregated and evaluated to determine the percentage of spots within each gantry angle interval meeting accuracy criteria for spot position, size, symmetry, and MU. The extracted data was compared with the TPS-specified values. A box and whiskers plot was used to visualise the results. Spots with spot size variation less than 10 %, position differences within 1 mm, symmetry within 10 %, and MU differences within 2 % were evaluated based on the tolerances specified by AAPM TG224.

6.3 Results

6.3.1 Machine QA data

The log files of monthly QA data of all three gantries were analyzed using the in-house tool and compared the predicted spot size values and extracted spot position values with the Lynx 2D measured data. The results are tabulated in Table 6.2.

The log file extracted spot positions are closely matching with the measured spot positions and the spot size values predicted by the ML models are closely matching with the measured spot size values.

Table 6.2: Comparison of spot parameters using the 5-spot pattern for machine QA: measured, predicted, and log file-recorded spot sizes (X and Y axes) along with measured versus log file-recorded spot positions. Mean and standard deviation values across 12 gantry angles are presented.

	Spot Size Comparison (Measured vs Log File Recorded vs ML Model Predicted)				The difference in Spot position(mm)	
	Percentage Difference in X spot size (%)		Percentage Difference in Y spot size (%)			
Gantry angle (Degre)	(Measured vs. Log File) - Mean (SD) %	(Measured vs. Predicted) – Mean (SD)%	(Measured vs. Log File) - Mean (SD) %	(Measured vs. Predicted) - Mean (SD) %	Spot Position in the X axis (Measured vs. Log file) – Mean (±SD)	Spot Position in the Y axis (Measured vs. Log file) – Mean (±SD)
0	1.16 (7.84)	0.08 (1.17)	2.00 (6.24)	0.81 (1.05)	0.37(0.33)	0.37(0.38)
30	1.09 (7.21)	0.27 (1.15)	0.74 (7.08)	1.24 (1.01)	0.38(0.33)	0.38(0.39)
60	0.81 (7.82)	0.32 (1.02)	0.83 (6.23)	0.97 (1.03)	0.37(0.32)	0.38(0.39)
90	1.76 (7.44)	0.11 (1.04)	3.02 (6.58)	0.58 (1.13)	0.38(0.32)	0.38(0.39)
120	2.07 (7.45)	0.12 (0.97)	2.66 (6.57)	0.82 (0.91)	0.37(0.32)	0.37(0.37)
150	0.98 (8.26)	0.57 (1.61)	1.11 (7.27)	1.05 (1.12)	0.40(0.31)	0.40(0.37)
180	1.09 (8.61)	0.41 (1.37)	2.26 (6.25)	1.19 (1.19)	0.39(0.31)	0.39(0.37)
210	2.21 (7.59)	0.25 (1.33)	4.01 (6.47)	0.57 (1.58)	0.47(0.28)	0.43(0.33)
240	2.16 (7.63)	0.45 (1.07)	3.67 (7.32)	0.77 (1.39)	0.37(0.31)	0.38(0.36)
270	3.63 (7.66)	0.17 (1.57)	1.08 (7.47)	1.11 (1.36)	0.44(0.28)	0.44(0.35)
300	1.12 (7.71)	0.59 (1.07)	0.97 (7.26)	1.21 (1.19)	0.38(0.33)	0.38(0.39)
330	3.67 (8.06)	0.72 (1.18)	0.69 (6.98)	1.00 (0.96)	0.37(0.32)	0.37(0.37)

The analysis demonstrated a high level of agreement between the measured and recorded spot positions. On average, the difference between the measured and log file-recorded positions across all gantry angles was under 0.5 mm, with a standard deviation below 0.4 mm for both the X and Y axes. This indicates that the spot positions documented in the log file align closely with the measured values, confirming an accuracy of within 0.5 mm for the log file spot positions.

The spot size values comparison is also tabulated in Table 6.2. This analysis highlights the percentage differences between the measured and log file-recorded spot sizes and those between the measured and ML model-predicted spot sizes for both X and Y directions. The measured and log file-recorded spot sizes exhibited notable discrepancies, with mean differences ranging from 0.7 % to 4.0 % and standard deviations between 6.3 % and 8.6 % across all gantry angles. In contrast, the comparison between measured and predicted spot sizes showed much closer alignment, with mean differences between 0.5 % and 1.25 % and standard deviations from 0.9 % to 1.6 %. These findings demonstrate a stronger agreement between measured and predicted spot sizes, whereas the measured and log file-recorded spot sizes displayed greater variability. Additionally, the calculated spot symmetry for all spots, based on the predicted major and minor axis spot sizes, was below 10 %. When compared to the measured spot symmetry, the difference was less than 1 %, confirming the high accuracy of the predicted symmetry values. Also, the MU per spot for each 5-spot pattern was compared to the values recorded in the log file, revealing that all differences were within 1 % of the specified MU per spot values.

Figure 6.1 presents a plot of Lynx2D-measured spot sizes versus ML model-predicted and log file-recorded spot sizes for the X-direction. The comparison reveals a strong correlation between the measured and predicted spot sizes, while the log file-recorded values show more noticeable deviations from the measured data. Figure 6.2, on the other hand, illustrates the same comparison for the Y-direction spot sizes. Like in Figure 6.1, the plot shows that the ML model-predicted values align closely with the measured spot sizes, whereas the log file-recorded values exhibit greater discrepancies. These figures provide a clear visual representation of the accuracy of the ML models and highlight the variation observed in the log file-recorded spot sizes, underscoring the effectiveness of the ML models in accurately predicting spot size values.

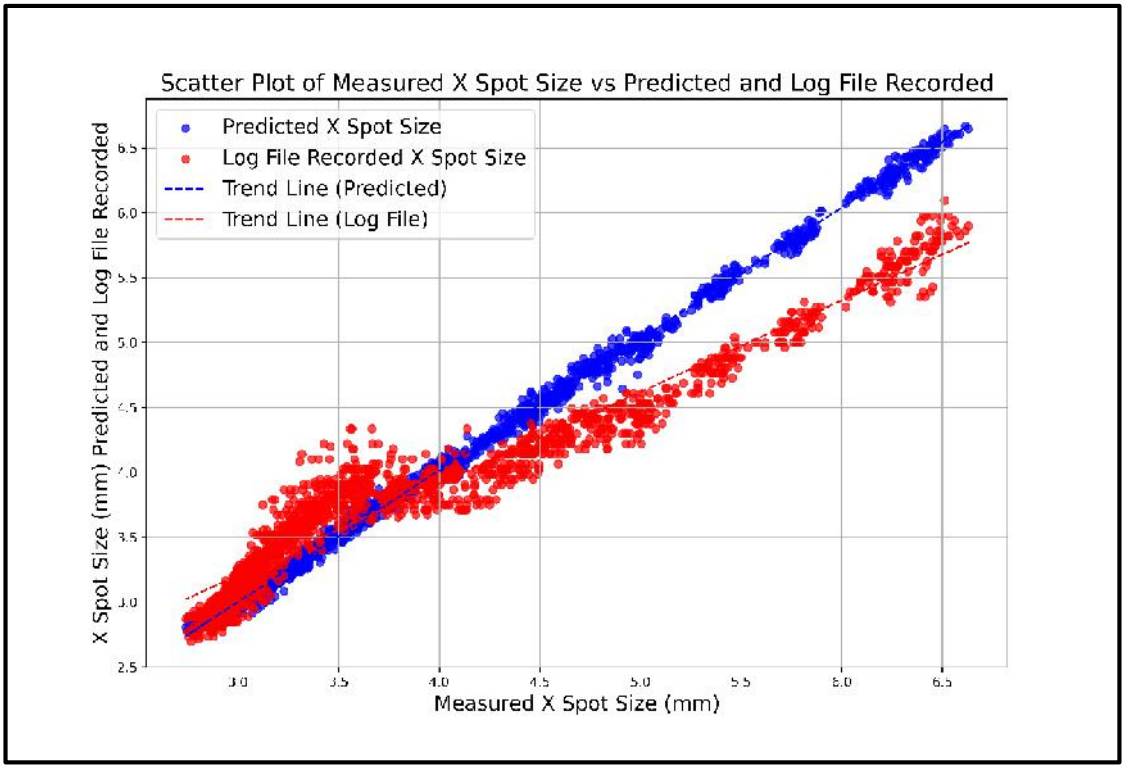

Figure 6.1: The plot of measured spot sizes versus ML model predicted (Blue) and Log file (Red) recorded X spot size.

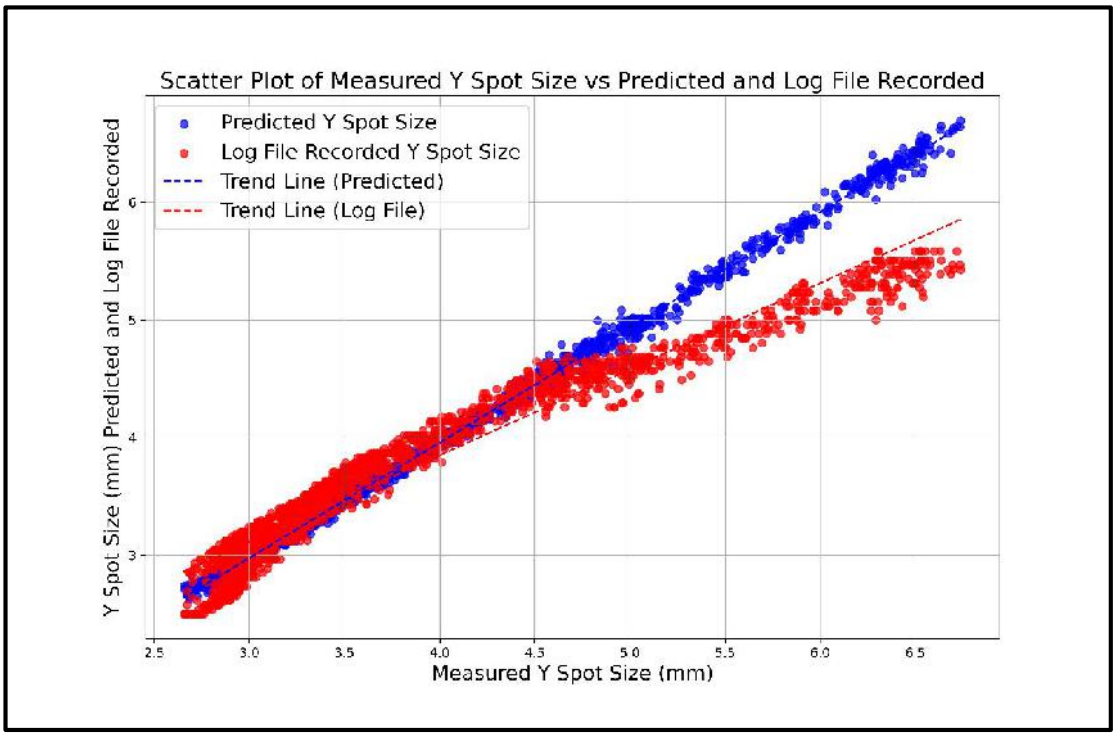

Figure 6.2: The plot of measured spot sizes versus ML model predicted (Blue) and Log file recorded (Red) Y spot size.

6.3.2 PSQA Beam Data Analysis

6.3.2.1 Spot position

The study compared 935 PSQA beam data using the automated script. The X and Y spot positional differences versus different gantry angle intervals are plotted in Figures 6.3 and 6.4, respectively, using box-and-whisker plots.

The comparison indicates that 99.5 % of spot positions are within a 1 mm margin in the X and Y directions. For the 60^0-90^0 gantry angle interval, a few spots showed a Y positional error of more than 1 mm. Over 95 % of spots demonstrate position accuracy within 0.5 mm. The mean and standard deviation of X positional error were -0.021 mm and 0.181 mm, respectively, and for Y positional error, the mean and standard deviations were -0.002 mm and 0.132 mm, respectively. These findings highlight the machine's excellent and consistent performance in spot position accuracy across varying gantry angles. It aligns well with the AAM-TG 224 recommended tolerance of 1mm for spot position accuracy.

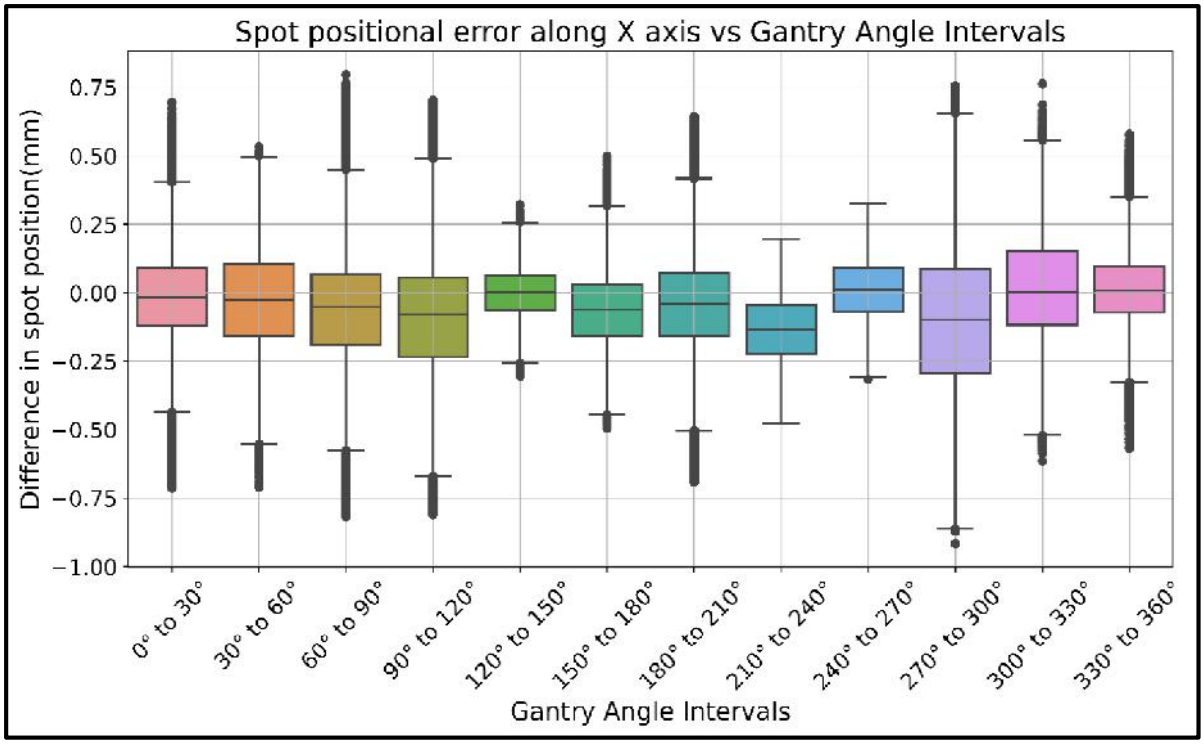

Figure 6.3: Box plots show the X positional error in different gantry angle intervals.

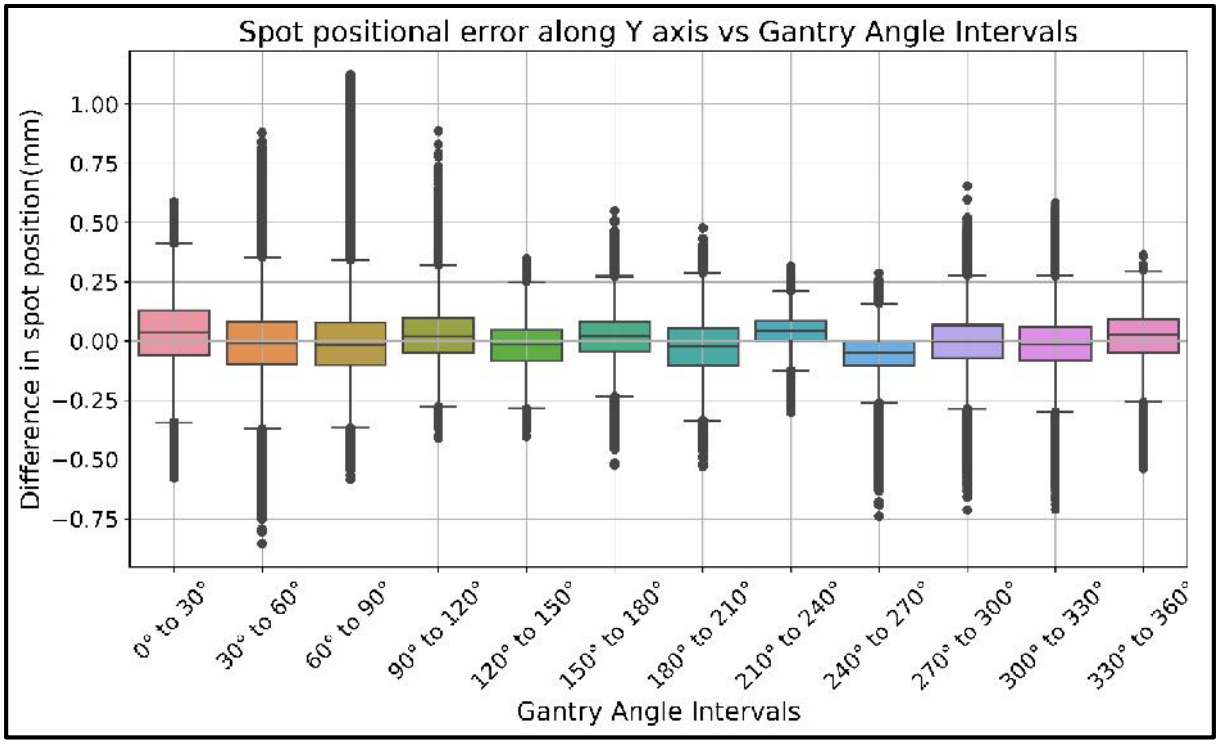

Figure 6.4: Box plots showing Y positional error in different gantry angle intervals.

6.3.2.2 Spot size and symmetry

The spot size for each spot in the 935 PSQA beam dataset was predicted using log file data as input to the ML models. The prediction covered spot sizes along different directions, including the X, Y, major, and minor axis directions for each spot in the irradiated beam. These predicted spot sizes were then compared to the baseline spot size for each energy.

To assess the accuracy of the predictions, the percentage of spots with spot size variations less than 10 % from the baseline was calculated for each beam. Figures 6.5 and 6.6 present box plots illustrating the percentage of spots in which the spot size differences in the X and Y directions were within 10 % across different gantry intervals, respectively. In the X-direction (Figure 6.5), spot size variation remained within 10 % for over 92 % of spots in all gantry intervals, except in the 150^0-180^0 range. Similarly, Figure 6.6 demonstrates that more than 95 % of spots in each gantry angle interval showed a Y-direction spot size variation of less than 10 %, except the 270^0-300^0 gantry interval.

The RMSE values for the X and Y spot sizes were 0.15 mm and 0.16 mm, respectively. These results indicate that the predicted spot sizes for each pencil beam at all

gantry angles remain within acceptable limits, confirming the accuracy and reliability of the ML models in predicting spot size variations across different beam angles.

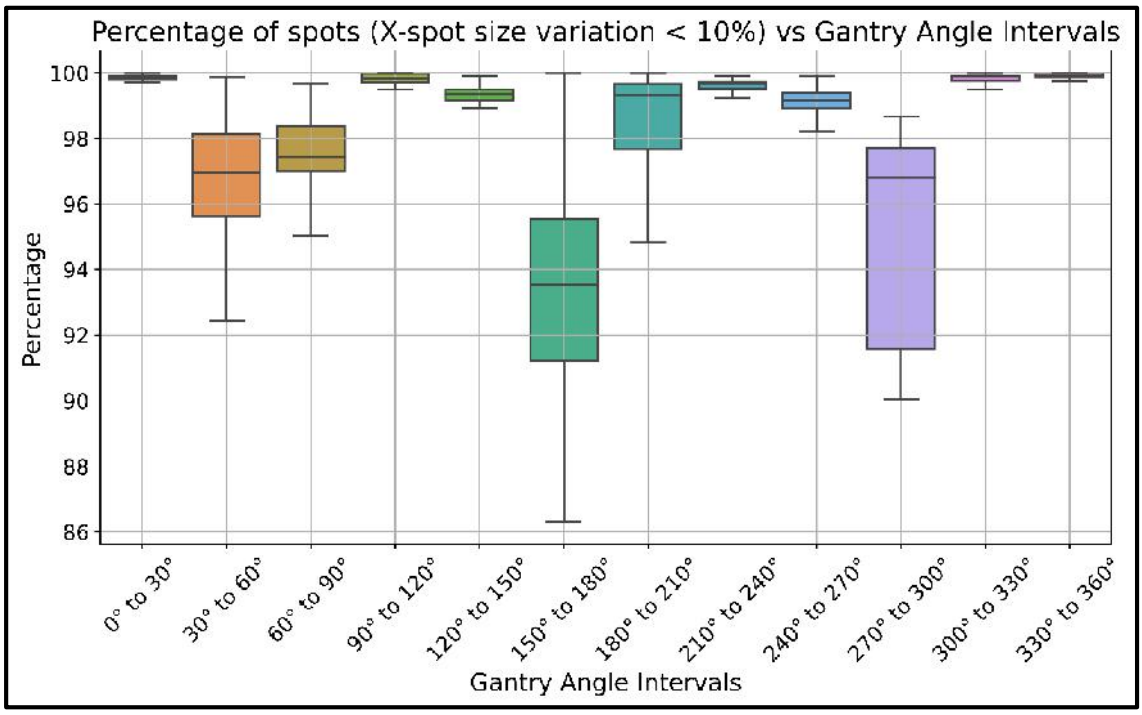

Figure 6.5: The box plot of the percentage of spots in each gantry angle interval has an X spot size variation of less than 10 % from the baseline values.

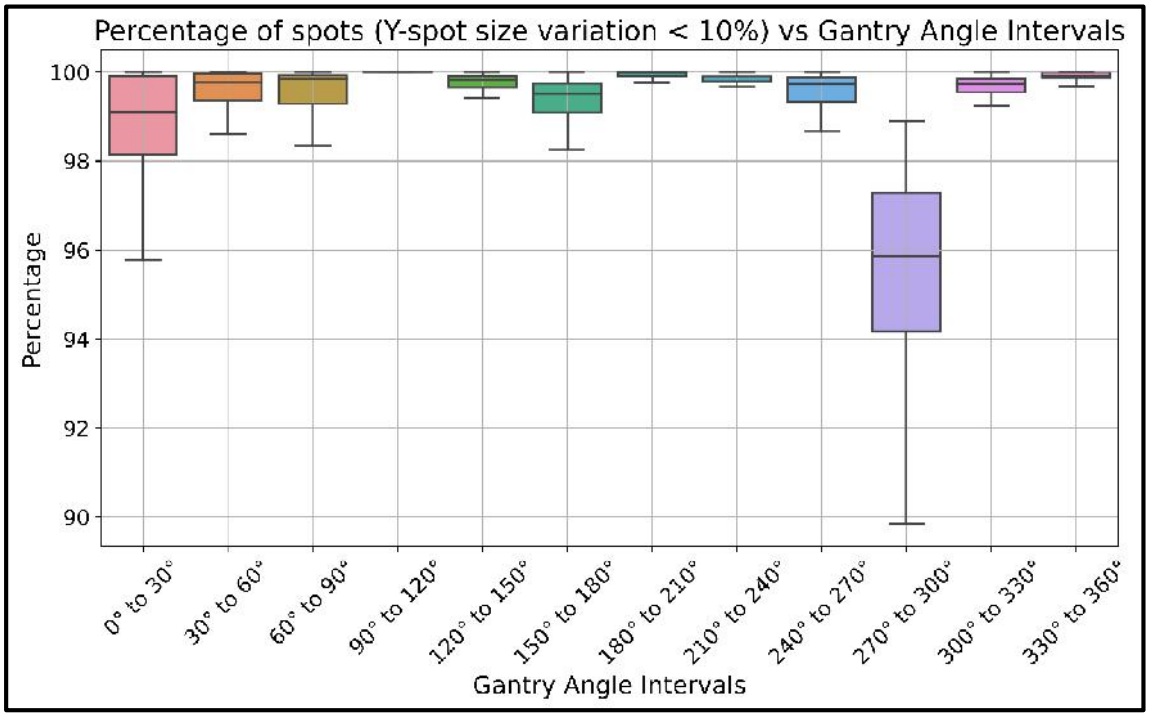

Figure 6.6: The box plot shows the percentage of spots in each gantry angle interval with a Y spot size variation of less than 10 % from the baseline values.

The number of spots in different energy intervals was also assessed. Figure 6.7 displays a histogram of spots across various energy intervals. The majority of spots are belonging to the 130-160 MeV energy range. For each energy interval, the percentage of spots with a spot size variation of less than 10 % and greater than 10 % is plotted. The middle energy intervals, particularly between 130 and 160 MeV, exhibit a higher proportion of spots with spot size variations exceeding 10 %. In contrast, for all other energy intervals, less than 10 % of spots show spot size variations greater than 10 % for both the X and Y directions.

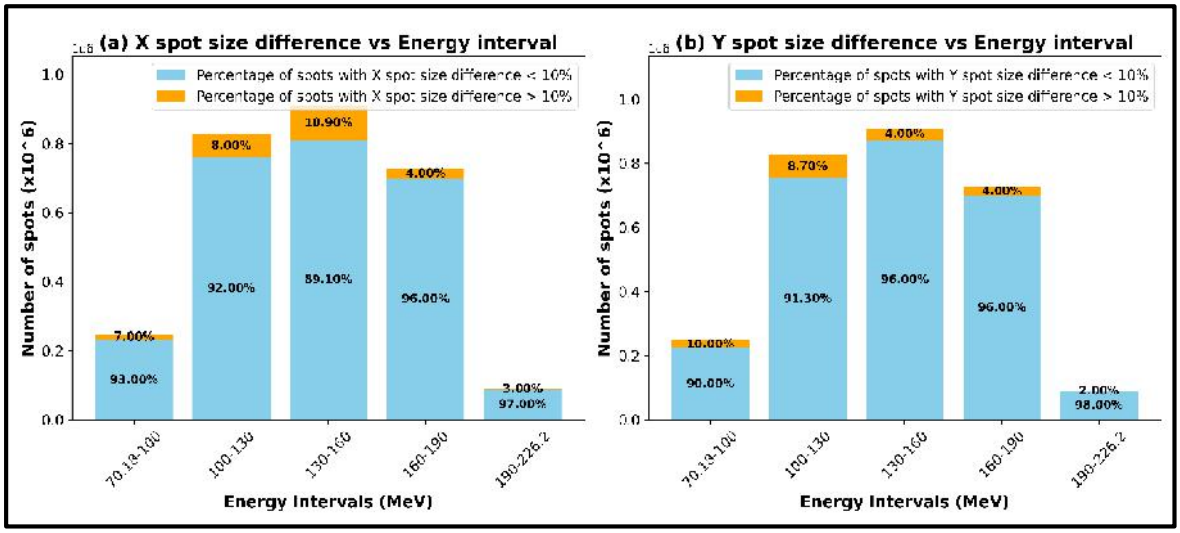

Figure 6.7: Histogram of the number of spots in each energy interval, with each bar divided into the percentage of spots with spot size variation less than 10 % and those with spot size variation greater than 10 % of baseline spot size.

Focusing solely on spot size in the X and Y directions may provide limited insight into the elliptical nature of the spot. Therefore, assessing spot symmetry along the major and minor axes is an essential part of routine quality checks. In this study, the symmetry of all spots irradiated in the beam was calculated using the predicted spot sizes along the major and minor axes. The tolerance for spot symmetry is 10 %, as specified by TG 224.

The results showed that all spots across the beams exhibited spot symmetry within the 10 % tolerance. The highest observed spot symmetry deviation was 9.8 % for the 100 MeV beam at a gantry angle of 30^0, indicating that the spots met the required quality standards for symmetry in proton therapy.

6.3.2.3 Monitor unit accuracy

In the Proteus plus PBS system's clinical settings, the minimum and maximum deliverable MU are 0.02 MU and 12 MU, respectively. The study analysed data from 3 million spots across 935 PSQA beams. The MU per spot ranged from a minimum of 0.02 MU to a maximum of 2.71 MU.

The in-house script was employed to extract the charge collected by the nozzle ionization chamber, correcting it for temperature and pressure, to calculate the MU for each spot. These calculated MU values were compared with the TPS-specified MU values. Figure 6.8 presents a box plot showing the percentage of spots in each gantry angle interval with an MU variation of less than 2 % between the delivered and TPS-specified MU values. In all gantry intervals, over 95 % of the spots had an MU variation of less than 2 %, except for the 120-150° gantry interval.

The mean MU difference was found to be zero, with a standard deviation of 0.009 MU. Additionally, the MU variation for all evaluated spots was less than 0.1 MU. Figure 6.9 illustrates a scatter plot of the total MU difference for each beam, with the total MU per beam ranging from 35.31 MU to 768.3 MU. The maximum difference between the delivered and prescribed beam MU was under 3.5 MU, representing less than 0.5 % of the total MU for each beam. These results indicate a high level of precision in the MU delivery process within the PBS system.

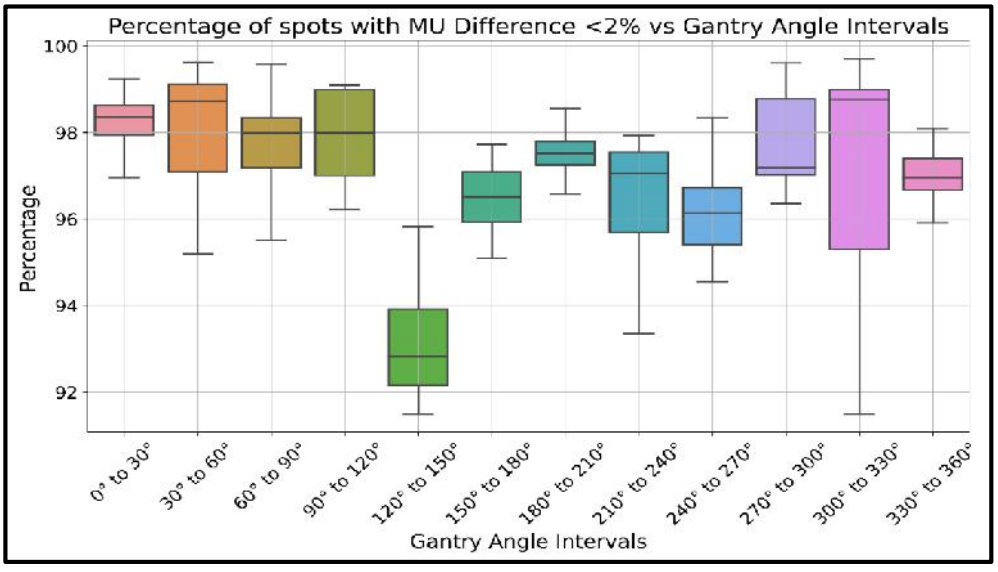

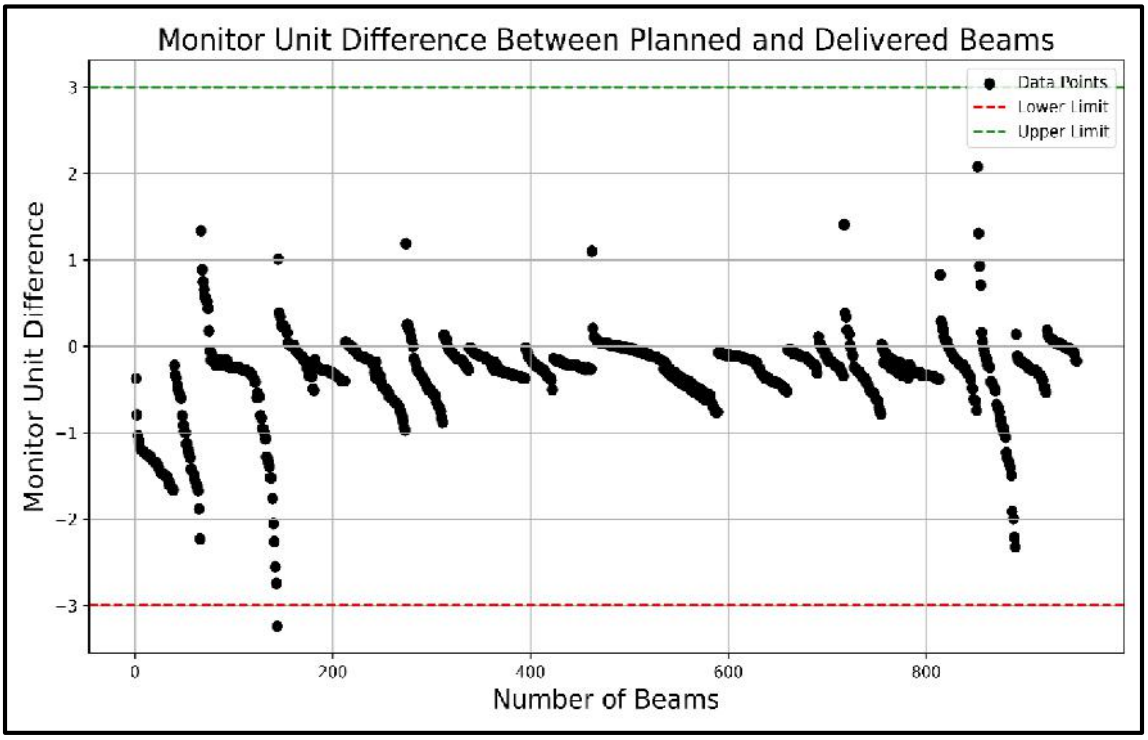

Figure 6.8: The box plot shows the percentage of spots in each gantry angle interval with a Monitor Unit (MU) difference of less than 2 %.

Figure 6.9: Scatter plot Showing the difference of Monitor Unit (MU) between planned and delivered beams.

6.4 Discussion

At our institute, the standard approach for evaluating beam delivery accuracy involves conducting PSQA prior to the first fraction of treatment. This process includes measuring dose fluence and performing gamma analysis using a 2D array detector. Additionally, for spot dosimetric parameter evaluation, conducted 5-spot pattern measurements at different energy levels and gantry angles using the Lynx2D scintillator detector. These methods ensure accurate assessment of the beam's dosimetric parameters; however, they are time-consuming and require dedicated equipment, specialised dosimeters, and software for data measurement and analysis.

The current study, however, proposes a more time-efficient and streamlined alternative for analysing beam delivery parameters, utilizing in-house developed scripts and ML models. By leveraging irradiation log files, can accurately predict key dosimetric parameters such as MU, spot size, symmetry, and position, without the need for direct

measurements or specialized dosimeters. This approach simplifies the analysis process while maintaining high accuracy, offering a more practical solution for routine QA in proton therapy.

In PBS, key parameters like MU, spot size, symmetry, and position play a crucial role in determining the accuracy of dose delivery. The study analysis focused on comparing the TPS-calculated MU per spot with the corresponding values recorded in the irradiation log files. The comparison revealed a mean difference of zero and a standard deviation of 0.009 MU, which indicates excellent agreement between the delivered and specified MUs. Furthermore, more than 95 % of the spots exhibited an MU variation of less than 2 %, reflecting the high precision of the PBS system.

The study also evaluated the positional accuracy of spots in both the X and Y directions by comparing the log file-recorded positions with those specified by the TPS. Over 95 % of spots showed positional differences of less than 0.5 mm, with the standard deviations of the X and Y spot position errors being 0.181 mm and 0.132 mm, respectively. These results confirm that the spot positional errors are well within the 1 mm tolerance limit set by TG224, ensuring accurate delivery of radiation to the targeted area.

The findings are consistent with those reported by Maes D et al. [24], who observed similar spot position accuracy, with standard deviations of 0.39 mm and 0.44 mm for the X and Y directions, respectively. This agreement further validates the robustness of in-house analysis method and its potential for routine use in proton therapy quality assurance. The adoption of this log file-based approach, powered by ML models, not only enhances the efficiency of spot parameter evaluation but also maintains the high standards required for clinical practice.

Toscano et al. [11] assessed the spot positional accuracy on the IBA Proteus Plus machine using standardized spot patterns, and their findings indicated a spot positional error of less than 0.6 mm in both the X and Y directions. This aligns with the results from Li et al. [13] and Ates O et al. [12], who evaluated spot position errors in proton therapy systems using log file data from the Hitachi PROBEAT machine (Hitachi, Ltd, Tokyo, Japan). Li et al. [13] analysed the log file data from 14 patients and reported standard deviations of 0.26 mm for the X positional error and 0.42 mm for the Y positional error.

Their study also demonstrated that the total MU accuracy remained within 0.1 % of the TPS-specified MU values.

Ates O et al. [12] conducted an evaluation with data from 992 patients, finding standard deviations of 0.125 mm and 0.175 mm for the X and Y spot positions, respectively. Furthermore, the standard deviation in the MU difference was found to be less than 0.001 MU, indicating excellent agreement between the log file and TPS values for MU. In another study, Arjunan M et al. [26] highlighted that random spot positional errors in treatment plans can lead to significant dose variation, especially in small-sized tumours, compared to plans involving larger target volumes. This emphasizes the importance of precise spot positioning in achieving accurate dose delivery, particularly for smaller and more sensitive targets.

Many studies, including those mentioned above, have utilized log file-recorded spot positions and MUs for MC-based PSQA calculations. These studies provide valuable insights into the effectiveness of log file data for evaluating and ensuring the accuracy of proton therapy treatments, reinforcing the role of log files in modern QA practices.

The results of the current study, when compared to existing literature, confirm that the spot positions and MU values recorded in the irradiation log files of the IBA Proteus Plus machine show strong agreement with the TPS-specified values. The analysis revealed that most spot positions were within a 1 mm tolerance; however, the log file's beam interruption threshold is set to 3 mm, which is higher than the 1 mm tolerance recommended by TG224. This means that the system will not interrupt the beam unless spot position deviations exceed 3 mm. Consequently, the proposed method, which employs in-house scripts to verify each spot position individually against the 1 mm tolerance, plays a crucial role in ensuring the accuracy and performance of PBS systems. The findings underscore that log file data is a highly effective tool for assessing the accuracy of both spot positions and MU values in treatment fields.

In addition to assessing spot position and MU, it is essential to evaluate the accuracy of spot size and symmetry to ensure proper beam delivery. In Chapter 3, it was noted a weak correlation between the spot size recorded in the log file and the spot size measured with a scintillator detector. The comparison between measured and log file recorded spot sizes showed notable variation, with standard deviations ranging from 6.3 % to 8.6 %.

Possible reasons for this discrepancy include differences in measurement conditions and resolution. Routine QA measurements for spot size are taken at the isocentre plane using a 2D scintillator detector with a resolution of 0.5 mm. In contrast, the log file records the spot size at the IC23 level using a strip chamber with a resolution of 5 mm and employs a Gaussian fit to estimate the spot size. Furthermore, the log file does not capture the spot size along the major and minor axes. The lower resolution of the IC23 strip chamber introduces errors in the spot size measurements. Therefore, the spot size recorded in the log file may not accurately reflect the true spot size for each spot, and it cannot be relied upon for evaluating spot size accuracy.

An alternative approach for predicting spot size using ML models with log file data as input parameters was investigated in chapter 4. The accuracy of these models was evaluated, resulting in RMSE values of 0.053 mm, 0.049 mm, 0.053 mm, and 0.052 mm for the X, Y, major, and minor axis spot sizes, respectively. In this chapter, these ML models were applied to predict the spot sizes for all spots in 935 treatment beams. The analysis revealed that over 95 % of X and Y spot size values were within 10 % of the baseline values across all gantry angle intervals. The RMSE for X and Y spot sizes was determined to be 0.15 mm and 0.16 mm, respectively. Additionally, when evaluating the 5-spot pattern, the difference between measured and predicted spot size values showed a standard deviation ranging from 0.9 % to 1.6 %. These results highlight the reliability and accuracy of ML models in predicting spot size within the PBS system, leveraging log file data as input parameters. Moreover, spot symmetry was assessed along the major and minor axis directions using the predicted spot sizes, with all spots demonstrating symmetry values below 10%, which aligns with the TG224 recommended tolerance.

Performing PSQA using dosimeters for each fraction is a challenging and time-consuming task. Although MC-based PSQA [8,9,10] can be applied across all fractions, it has several limitations. These include the reliance on spot position and MU data from the log file, the need for dedicated computing resources to perform rapid dose calculations, and the inability to account for variations in spot size and symmetry during beam delivery. While PSQA for a single fraction ensures dose delivery accuracy, subsequent fractions may experience delivery errors due to variations in spot parameters. The beam delivery accuracy evaluation method proposed in this study offers a more efficient and practical solution. This method provides a quick and straightforward approach for evaluating the accuracy of all

spot parameters such as position, size, symmetry, and MU at the actual beam angle for each fraction. It can serve as an effective tool for validating the vendor's beam delivery safety interlock system and as an alternative to routine spot parameter evaluations or MC-based PSQA, especially in the context of adaptive treatments where time is a critical factor.

6.5 Conclusions

The proposed log file-based approach offers a time-efficient and accurate alternative to traditional PSQA methods for evaluating proton beam delivery parameters. By leveraging in-house scripts and ML models, this method ensures compliance with TG224 recommendations, enhances QA efficiency, and supports adaptive treatments, particularly in workflows where time is critical. The findings highlight its potential for routine QA, enabling precise and reliable assessments of MU, spot size, position, and symmetry without the need for specialised dosimeters. By streamlining beam delivery evaluations, this approach not only enhances patient safety and clinical efficiency but also validates the use of log file data as a robust tool for ensuring dosimetric accuracy in modern proton therapy practices.

6.6 References

1. Hernandez V, Hansen CR, Widesott L, Bäck A, Canters R, Fusella M, Götstedt J, Jurado-Bruggeman D, Mukumoto N, Kaplan LP, Koniarová I. What is plan quality in radiotherapy? The importance of evaluating dose metrics, complexity, and robustness of treatment plans. Radiotherapy and Oncology. 2020 Dec 1;153:26-33.
2. Rana S, Bennouna J, Samuel EJ, Gutierrez AN. Development and long-term stability of a comprehensive daily QA program for a modern pencil beam scanning (PBS) proton therapy delivery system. Journal of Applied Clinical Medical Physics. 2019 Apr;20(4):29-44.
3. Arjomandy B, Taylor P, Ainsley C, Safai S, Sahoo N, Pankuch M, Farr JB, Yong Park S, Klein E, Flanz J, Yorke ED. AAPM task group 224: Comprehensive proton therapy machine quality assurance. Medical physics. 2019 Aug;46(8): e678-705.
4. Pedroni E, Meer D, Bula C, Safai S, Zenklusen S. Pencil beam characteristics of the next-generation proton scanning gantry of PSI: design issues and initial commissioning results. The European Physical Journal Plus. 2011 Jul;126:1-27.
5. Low DA, Dempsey JF. Evaluation of the gamma dose distribution comparison method. Medical physics. 2003 Sep;30(9):2455-64.
6. Lin L, Kang M, Solberg TD, Mertens T, Baumer C, Ainsley CG, McDonough JE. Use of a novel two-dimensional ionisation chamber array for pencil beam scanning proton therapy beam quality assurance. Journal of applied clinical medical physics. 2015 May;16(3):270-6.
7. Matter M, Nenoff L, Meier G, Weber DC, Lomax AJ, Albertini F. Alternatives to patient-specific verification measurements in proton therapy: a comparative

experimental study with intentional errors. Physics in Medicine & Biology. 2018 Oct 17;63(20):205014.
8. Jeon C, Lee J, Shin J, Cheon W, Ahn S, Jo K, Han Y. Monte Carlo simulation-based patient-specific QA using machine log files for line-scanning proton radiation therapy. Medical Physics. 2023 Nov;50(11):7139-53.
9. Matter M, Nenoff L, Marc L, Weber DC, Lomax AJ, Albertini F. Update on yesterday's dose—use of delivery log-files for daily adaptive proton therapy (DAPT). Physics in Medicine & Biology. 2020 Sep 23;65(19):195011.
10. Marmitt GG, Pin A, Siang KN, Janssens G, Souris K, Cohilis M, Langendijk JA, Both S, Knopf A, Meijers A. Platform for automatic patient quality assurance via Monte Carlo simulations in proton therapy. Physica Medica. 2020 Feb 1;70:49-57.
11. Toscano S, Souris K, Goma C, Barragán-Montero A, Puydupin S, Vander Stappen F, Janssens G, Matic A, Geets X, Sterpin E. Impact of machine log-files uncertainties on the quality assurance of proton pencil beam scanning treatment delivery. Physics in Medicine & Biology. 2019 Apr 29;64(9):095021.
12. Ates O, Pirlepesov F, Zhao L, Hua CH, Merchant TE. Development of a log file analysis tool for proton patient QA, system performance tracking, and delivered dose reconstruction. Journal of Applied Clinical Medical Physics. 2023 Jul;24(7): e13972.
13. Li H, Sahoo N, Poenisch F, Suzuki K, Li Y, Li X, Zhang X, Lee AK, Gillin MT, Zhu XR. Use treatment log files in spot scanning proton therapy as part of patient-specific quality assurance. Medical physics. 2013 Feb;40(2):021703.
14. Noufal MP, Sharma SD, Patro K, Arjunan M, Krishnan G, Tyagarajan R, Rana S, Chillukuri S, Jalali R. Impact of spot positional errors in robustly optimised intensity-modulated proton therapy plan of craniospinal irradiation. Radiological Physics and Technology. 2021 Sep;14(3):271-8.
15. Rana S, Rosenfeld AB. Impact of errors in spot size and spot position in robustly optimised pencil beam scanning proton-based stereotactic body radiation therapy (SBRT) lung plans. Journal of Applied Clinical Medical Physics. 2021 Jul;22(7):147-54.
16. Parodi K, Mairani A, Brons S, Naumann J, Krämer M, Sommerer F, Haberer T. The influence of lateral beam profile modifications in scanned proton and carbon ion therapy: a Monte Carlo study. Physics in Medicine & Biology. 2010 Aug 16;55(17):5169.
17. Chanrion MA, Ammazzalorso F, Wittig A, Engenhart-Cabillic R, Jelen U. Dosimetric consequences of pencil beam width variations in scanned beam particle therapy. Physics in Medicine & Biology. 2013 May 17;58(12):3979.
18. Parodi K, Mairani A, Brons S, Naumann J, Krämer M, Sommerer F, Haberer T. The influence of lateral beam profile modifications in scanned proton and carbon ion therapy: a Monte Carlo study. Physics in Medicine & Biology. 2010 Aug 16;55(17):5169.
19. Kraan AC, Depauw N, Clasie B, Madden T, Kooy HM. Impact of spot size variations on dose in scanned proton beam therapy. Physica Medica. 2019 Jan 1;57:58-64.
20. Wall PD, Fontenot JD. Application and comparison of machine learning models for predicting quality assurance outcomes in radiation therapy treatment planning. Informatics in Medicine Unlocked. 2020 Jan 1;18:100292.
21. Ranjith CP, Arunkrishnan MP, Vysakh R, Irfad MP, Vijayagopal KS, Jayashanker S. Mean parotid dose prediction model using machine learning regression method

for intensity-modulated radiotherapy in head and neck cancer. Medical Dosimetry. 2021 Sep 1;46(3):283-8.
22. Wu C, Nguyen D, Xing Y, Montero AB, Schuemann J, Shang H, Pu Y, Jiang S. Improving proton dose calculation accuracy by using deep learning. Machine learning: science and technology. 2021 Apr 6;2(1):015017.
23. Padannayil NM, Sharma DS, Nangia S, Patro KC, Gaikwad U, Burela N. IMPT of head and neck cancer: unsupervised machine learning treatment planning strategy for reducing radiation dermatitis. Radiation Oncology. 2023 Jan 14;18(1):11.
24. Maes D, Bowen SR, Regmi R, Bloch C, Wong T, Rosenfeld A, Saini J. A machine learning-based framework for delivery error prediction in proton pencil beam scanning using irradiation log-files. Physica Medica. 2020 Oct 1;78:179-86.
25. Newpower MA, Chiang BH, Ahmad S, Chen Y. Spot delivery error predictions for intensity modulated proton therapy using robustness analysis with machine learning. Journal of Applied Clinical Medical Physics. 2023 May;24(5):e13911.
26. Arjunan M, Krishnan G, Sharma DS, MP N, Patro KC, Thiyagarajan R, Srinivas C, Jalali R. Dosimetric impact of random spot positioning errors in intensity modulated proton therapy plans of small and large volume tumors. The British Journal of Radiology. 2021 Mar 1;94(1119):20201031.

Chapter 7

Summary and conclusions

Chapter 7

Summary and conclusions

The QA process is crucial for ensuring the precision, safety, and effectiveness of radiotherapy, directly impacting patient outcomes. The adoption of automated, reliable tools is essential to replace traditional, labour-intensive methods, thus streamlining workflows without compromising patient care. These tools save time, optimise beam-on time, and enhance overall efficiency, ensuring timely and accurate treatments for cancer patients. Medical physicists play a pivotal role in implementing these advanced protocols, maintaining equipment performance, and upholding the highest standards of radiotherapy delivery, ultimately improving the effectiveness of the treatment workflow.

Proton beam therapy employs PBS to deliver precisely controlled proton beam spots, generated by a cyclotron and guided through quadrupole magnets for focusing, bending magnets for steering, and tuning components for optimal performance. Due to its complexity, rigorous QA is required to assess dosimetric parameters and the accuracy of dose distributions. However, both machine QA and PSQA are labour-intensive and time-consuming. This study focuses on implementing ML-based predictive models for PBS proton therapy QA.

Chapter 1 provides a comprehensive overview of proton therapy, focusing on its principles and clinical applications. It delves into the technical specifications of the IBA Proteus Plus machine with PBS, which was utilised in this study. Additionally, the chapter introduces the significance of log file data in proton therapy and highlights the role of ML models in automating machine QA and PSQA processes.

Chapter 2 provides a comprehensive literature review on the development of particle therapy and the clinical implementation of proton therapy in cancer management. The review highlights the distinct advantages of PBS proton therapy, particularly its ability to deliver highly conformal doses with exceptional precision, targeting tumours while sparing surrounding healthy tissues and critical structures. The layer-by-layer dose delivery enabled by PBS is especially effective for treating complex tumour geometries and tumours located near sensitive organs. This approach is particularly advantageous in paediatric oncology, as it significantly reduces the risk of long-term toxicities and secondary malignancies. Additionally, PBS delivers lower integral and skin doses, minimising overall

treatment-related side effects. Its compatibility with advanced techniques, such as IMPT and adaptive therapy, further ensures superior clinical outcomes in challenging cases.

Chapter 2 also explores the role of log file data in radiotherapy, emphasising its utility in monitoring and evaluating treatment delivery. Furthermore, it reviews the application of ML models in automating the QA workflow in radiotherapy, highlighting their potential to enhance efficiency and accuracy in both machine QA and patient-specific QA processes.

The irradiation log file data of the PBS system records all beam irradiation-related information in the machine nozzle head ionisation chambers, along with the parameters of all the beam-related components. Numerous data points are recorded in the log file during each beam irradiation, including spot dosimetric data.

Chapter 3 presents a detailed analysis of PBS irradiation log file data and its correlation with spot parameters measured using the dedicated Lynx2D scintillator detector. The study involved measuring spot dosimetric parameters using a 5-spot pattern across various gantry angles and energy levels. Spot sizes along different axes were measured and compared with the corresponding log file-recorded spot size values. Additionally, the relative positional errors of the spots in the X and Y directions were evaluated by comparing Lynx2D measurements with log file data. Various statistical tools were employed for this correlation study, and the steps involved in log file data extraction were comprehensively summarised.

The analysis revealed that Lynx2D-measured spot sizes demonstrated deviations of less than 8% across all energy ranges and gantry angles when compared with the baseline values and all the values were well within the 10% tolerance specified by AAPM TG224. Similarly, the spot positional error was less than 0.6 mm, meeting the recommended standard tolerance limits. However, when comparing log file-recorded spot sizes with Lynx2D measurements, the maximum difference observed was 23.9%. These findings indicate that log file-recorded spot sizes and positional data exhibit variations and uncertainties that exceed established tolerance limits when compared to scintillator-measured values. This underscores the limitations of relying solely on log file data for QA processes and highlights the necessity of independent verification using reliable

measurement tools, such as the Lynx2D detector, to ensure accurate evaluation of spot dosimetric parameters.

Chapter 4 examines the use of ML models to develop methods for QA in PBS proton therapy using log file data as input. The chapter details the development and validation of ANN-based ML models to predict spot sizes along the X, Y, major, and minor axes, as well as relative positional errors in the X and Y directions. Input parameters for the ML models were derived from log file data recorded by the nozzle head ICs (IC23 and IC1), which included spot size and position values, scanning magnet currents for both X and Y directions, beam current, and gantry angle. The ML model architecture, hyper parameter optimisation, and validation were thoroughly described, using statistical and cross-validation techniques to ensure robust performance.

The MLP architecture was used for all six models, with three hidden layers containing 30 neurons each. The training was conducted over 100 epochs with a batch size of 30, employing the ReLU activation function and the Adam optimiser. The MSE loss function guided backpropagation to improve model accuracy. Individual models were developed to predict spot sizes along each axis and relative positional errors. The ML models achieved high precision, with RMSE values below 0.05 mm for the spot size prediction models and RMSE values below 0.03 mm for the positional error prediction models. The maximum prediction error was under 0.3 mm, and the MPAE remained below 1%. These results align with the AAPM TG-224 tolerance limits of 10% for spot size and 1 mm for positional error.

This study demonstrates the reliability and efficiency of ML models as an alternative to traditional dosimeter-based QA methods, offering a precise, time-saving approach that enhances the accuracy and efficiency of PBS proton therapy systems.

Chapters 3 and 4 provided a detailed analysis of log file data, including its comparison with Lynx2D-measured spot parameters, and described the development and validation of ML models. Chapter 5 focuses on developing an in-house tool to automate log file analysis and integrate these ML models. This tool facilitates the prediction of spot parameters and evaluates the accuracy of all dosimetric parameters for individual spots within a patient treatment beam using PSQA beam log file data.

Chapter 7

An in-house tool was developed to streamline the process of log file analysis and enhance the integration of ML models for proton therapy QA. This tool uses custom scripts to efficiently read and analyse log file data, extract the input variables required for ML models, and predict spot parameters. The predicted parameters are systematically compared with the TPS-specified values, ensuring a detailed and accurate evaluation of all dosimetric parameters. Additionally, the tool generates comprehensive reports and conducts in-depth analyses, enabling an efficient and automated workflow for QA.

The in-house tool is specifically designed to handle the intricacies of irradiation log file data. It separates data from the log file and converts spot positions recorded at the IC23 level to the isocentre plane. It also converts the range specified in the specification file into corresponding energy values, ensuring compatibility with treatment planning and delivery parameters. Furthermore, the tool calculates baseline spot size values for each spot recorded in the log file, providing essential reference data for QA checks.

To account for variations in nozzle head specifications across different gantry systems, the tool incorporates machine-specific details using the machine ID. This allows precise calculation of spot positions and ranges for each spot, tailored to the unique characteristics of the gantry. By automating these complex and time-intensive processes, the in-house tool significantly simplifies data analysis, improves accuracy, and enhances the overall efficiency of QA workflows in proton therapy.

Chapter 6 discusses the application of the in-house tool described in Chapter 5 to evaluate the accuracy of dosimetric parameters for machine QA and PSQA beams. The study used 935 PSQA beam datasets for analysis. Routine QA data was also analysed using a comparison of Lynx2D-measured data with ML model-predicted data. The data comparison was conducted for different energies and gantry angles, and the mean difference between the Lynx2D-measured and ML model-predicted spot size values was less than 2%, with a standard deviation of less than 1.6%. The results showed excellent agreement between the predicted and Lynx2D-measured data, indicating that the use of dedicated dosimeters for routine QA can be replaced with the in-house tool for a quick check of parameters, without requiring excessive beam time, dosimeter usage, or manpower.

Chapter 7

The in-house tool was used to analyse 935 PSQA beams, leading to an in-depth evaluation of all spot parameters for over 3 million spots in total. TPS-specified spot position, range, MU per spot, and baseline spot size values were compared with the data extracted from the log files and ML model predictions using the in-house tool. The study showed excellent results in the analysis. The proposed approach demonstrated strong agreement between TPS-specified and log file-recorded parameters, with MU variations for over 95% of the spots remaining below 2% and a standard deviation of 0.009 MU. Spot positional accuracy was also confirmed, with more than 95% of spots exhibiting deviations of less than 0.5 mm, with standard deviations of 0.181 mm and 0.132 mm for the X and Y directions, respectively, well within the 1 mm tolerance.

While the log file data was less reliable for spot size evaluation due to its lower resolution, ML models provided a robust solution, achieving RMSE values of 0.15 mm and 0.16 mm for X and Y spot sizes, respectively. Additionally, over 95% of spot sizes were within 10% of baseline values across all gantry angles. This integrated method simplifies the QA workflow, reduces reliance on direct measurements, and maintains precision, making it a time-efficient and reliable solution for routine QA and PSQA, particularly in adaptive proton therapy workflows, where time constraints are critical.

This thesis, titled “Implementation of ML in the Proton Therapy QA”, presents an in-depth exploration of the application of ML models and log file data to enhance QA in PBS proton therapy. The study demonstrates that the integration of ML-based predictive models and a custom-designed in-house tool provides a reliable, efficient, and accurate alternative to traditional, labour-intensive QA methods. The in-house tool facilitates the automated analysis of log file data, precise prediction of spot parameters, and comprehensive evaluation of dosimetric parameters for both routine QA and PSQA beams. The results validate the robustness of this approach, showing excellent agreement between ML-predicted spot parameters and dedicated dosimeter measurements, with deviations consistently within established tolerance limits. This work establishes a novel framework for leveraging ML in proton therapy QA, significantly streamlining workflows while ensuring dosimetric precision. The findings underline the transformative potential of this approach in advancing adaptive proton therapy workflows, optimizing resource utilisation, and improving patient safety and treatment outcomes.

Chapter 8

Recommendations

Chapter 8

Recommendations

Implementation of ML Models for Automation in Proton Therapy QA

This research has detailed and summarised the implementation of ML models to automate QA in PBS proton therapy. A significant contribution of this work is the effective utilisation of log file data as input for ML models to analyse all spot dosimetric parameters of the PBS system, thereby simplifying the QA process. The research highlights the development and validation of an in-house method that employs ML models and log file data for PBS machine QA. This method eliminates the need for dedicated dosimeters, reduces time-consuming measurements, and minimises manpower requirements while also reducing beam-on time.

The proposed approach significantly enhances the efficiency of QA workflows by reducing dependency on traditional methods, which often involve extensive manual measurements and the use of specialised equipment. By leveraging log file data and ML algorithms, this research ensures that proton therapy machines can be optimally utilised for cancer treatments without dedicating excessive time to QA and analysis. The automation of QA and PSQA workflows not only streamlines operations but also minimises treatment interruptions, ensuring that patients receive timely and uninterrupted care.

Furthermore, the automated system facilitates real-time feedback, enabling early detection and correction of potential errors. This advancement represents a critical step forward in improving the precision, reliability, and time efficiency of QA processes in proton therapy centres.

Recommendations for Integration into Clinical Practice

1. **Integration of Developed Tools:** To ensure seamless clinical adoption, the developed tools should be integrated into the existing software environment of proton therapy systems, such as the IBA Proteus Plus machine. Adding these tools to the current IBA software will enable real-time data extraction and analysis. This integration ensures that immediately after each beam irradiation, the QA system can automatically perform the required analyses using ML models.

2. **Staff Training:** Training clinical staff is crucial to ensure a smooth transition from traditional QA methods to ML-based automated systems. Dedicated training programmes should be developed to help medical physicists and radiation therapists understand the principles of ML tools and how to use them effectively in routine QA.

Future Research Recommendations

1. **Multi-Institutional Validation:** To enhance the robustness and reliability of the developed ML models, future studies should focus on validating the tools across multiple proton therapy centres. Such multi-institutional studies will ensure that the models are adaptable to diverse configurations and systems, broadening their utility and practical application.
2. **Development of User-Friendly Interfaces:** Intuitive software interfaces should be designed to make ML-based tools accessible to clinicians and physicists without requiring extensive technical expertise. User-friendly interfaces will promote wider adoption and ensure that these tools can be effectively utilised in clinical settings.
3. **Extension to Dose Prediction Models:** The scope of the study can be extended to include dose distribution prediction in patient CT scans using predicted spot parameters. Such an approach will provide detailed information about the actual delivered dose distribution in the patient CT scan, offering greater clarity in analysing tumour response and normal tissue toxicity in patients undergoing proton therapy. Dose prediction models can be developed using advanced deep learning techniques such as Convolutional Neural Networks (CNNs) and Generative Adversarial Networks (GANs). These models would allow for a comprehensive assessment of treatment efficacy and potential side effects, thus contributing to improved patient outcomes.

By addressing these recommendations, this study can serve as a foundation for advancing proton therapy QA processes and expanding the clinical application of ML models. These steps will ensure that proton therapy continues to evolve as a precise and efficient treatment modality for cancer patients.

Annexure

List of Publications and Conference Proceedings

1. List of Publications.

Sr No	Title of the Publication	Year of Publication	Journal	Indexing	Impact Factor	Cite Score
1	A narrative review of particle therapy in cancer	2023	Cancer Research, Statistics, and Treatment	Scopus Indexed	NA	4.8
2	An artificial neural network-based approach for predicting the proton beam spot dosimetric characteristics of a pencil beam scanning technique	2024	Biomedical Physics & Engineering Express	Scopus and ESCI Indexed	1.3	2.8
3	Assessment of pencil beam scanning proton therapy beam delivery accuracy through machine learning and log file analysis	2024	Physica Medica	Scopus and SCIE Indexed	3.3	6.8

2. List of Conferences attended

No.	Conference Name	Year	Title of Topic	Place	Presentation Type
1	International Conference of Medical Physicists (AMPICON), Association of Medical Physicists in India	2022	Comparison of two approaches for generating Mass density to HU unit table for Proton therapy dose calculation in Raystation TPS	Delhi, India	Oral
2	ARIRT – National Seminar by Andhra University	2023	Automation of Proton Beam Therapy Quality Assurance using Machine Learning Models	Vishakhapatnam, Andhra Pradesh, India	Poster
3	International Conference on Medical Physics (ICMP) – AMPI & IOMP	2023	Development and Validation of Machine Learning Approach for Predicting Proton Therapy Beam Spot Characteristics	Mumbai, India	Oral
4	Flash Radiotherapy and Particle Therapy (FRPT)	2024	The Machine Learning Based Approach for Measuring Spot Parameters in Pencil Beam Scanning Proton Therapy	Rome, Italy	E-Poster
5	International Conference of Medical Physicists (AMPICON), Association of Medical Physicists in India	2024	Evaluation of Beam Delivery Accuracy in a PBS System Using an In-house Automated Tool Using Log File Data	Hyderabad, India	Poster
6	International Conference on Nanotechnology (IC-NACMBM-2024), D Y Patil Education Society	2024	Precision and Reliability Assessment of IBA Proteus Plus Proton Therapy: A Comprehensive Study	Kolhapur, India	Oral

43rd Annual Conference of Association of Medical Physicists of India

AMPICON 2022

Theme: Medical Physics Research and Practice in the Era of Precision Medicine

5th-7th November 2022 | JLN Auditorium, AIIMS New Delhi

Organized by Department of Radiation Oncology, AIIMS, New Delhi

Certificate of Participation

THIS IS TO CERTIFY THAT

Mr. RANJITH CP

has actively participated as Delegate in the
43rd Annual Conference of Association of Medical Physicists of India - AMPICON 2022
from 5th - 7th November, 2022 at JLN Auditorium, AIIMS, New Delhi, India

Dr. D. N. Sharma	Dr. S. D. Sharma	Dr. V. Subramani	Dr. Arun Chougule
Organizing Chairman	President, AMPI	Organizing Secretary	Scientific Chairman

D. Y. PATIL EDUCATION SOCIETY,

(Deemed to be University) Kolhapur

Accredited NAAC with 'A' Grade

DNYANSHODH -2023

(Search For Knowledge)

Certificate

This is to certify that

Mr/Ms. Ranjith C. P.

has presented a Poster on 9th March 2023, in Dnyanshodh -2023,

organized by Centre for Interdisciplinary Research (CIR), D. Y. Patil Education Society

(Deemed to be University), Kolhapur - 416006.

Chairman
Prof. (Dr.) C. D. Lokhande
Dean,
Centre for Interdisciplinary Research

Convener
Dr. Arpita Pandey -Tiwari
Associate Professor,
Department of Medical Biotechnology.


International Conference on Medical Physics - 2023
ICMP 2023
The 25th International Conference of the IOMP
Theme: Innovations in Radiation Technology & Medical Physics for Better Healthcare
6th - 9th December 2023 | Venue: DAE Convention Centre, Anushaktinagar, Mumbai, India
AMPICON 2023 AOCMP 2023 ISEACOMP 2023
CERTIFICATE OF PRESENTATI
This is to certify that
MR. RANJITH C P
has presented a Oral Paper in the International Conference on Medical Physics - 2
held from 06 - 09 December, 2023 at DAE Convention Centre, Anushaktinagar, M
John Damilakis
Dr. John Damilakis
President, IOMP
Dr. Sunil Dutt Sharma
President, AMPI
Eva Bezak
Dr. Eva Bezak
President, AFOMP
Dr. Chai
Presiden

BASAVATARAKAM INDO-AMERICAN CANCER HOSPITAL & RESEARCH INSTITUTE

AMPICON 2024

45th Annual Conference of Association of Medical Physicists of India

ASSOCIATION OF MEDICAL PHYSICISTS OF INDIA AMPI ESTD - 1976

CERTIFICATE OF PARTICIPATION

This certificate is proudly awarded to

Mr. Ranjith C P

*for their participation in the **45th Annual Conference of Association of Medical Physicists of India, AMPICON 2024**, held from 8th to 10th of November 2024, at Sevalal Banjara Bhavan, Banjara Hills, Hyderabad.*

Dr. Manoj K Semwal
President, AMPI

Dr. Anuj Kumar Tyagi
Secretary, AMPI

Dr. A Krishnam Raju
Chairman, AMPICON-24

Dr. G Dileep Kumar
Vice Chairman, AMPICON-24

Dr. NVN Madhusudhan Sresty
Organizing Secretary
AMPICON-24

Dr. C Ramakrishna Rao
Chairman, Scientific Committee
AMPICON-24

CME/CPD Certificate

This is to certify that

Ranjith Cholakkara Poyil Msc

participated in the

4th Flash Radiotherapy and Particle Therapy Conference

Rome, Italy & Online

4-6 December 2024

and received 17 credits

Prof. Vassilios Papalois
President of UEMS

Dr João Grenho
Secretary General of UEMS

European Accreditation Council for Continuing Medical Education (UEMS/EACCME)

The **4th Flash Radiotherapy and Particle Therapy Conference (FRPT 2024)** is accredited by the European Accreditation Council for Continuing Medical Education (EACCME) to provide the following CME activity for medical specialists. The EACCME is an institution of the European Union of Medical Specialists (UEMS): www.uems.eu

The **4th Flash Radiotherapy and Particle Therapy Conference (FRPT 2024)** is designated for a maximum of, or up to, 17 European external CME credits. Each medical specialist should claim only those hours of credit that he/she actually spent in the educational activity.

American Medical Association (AMA)

Through an agreement between the European Union of Medical Specialists and the American Medical Association, physicians may convert EACCME credits to an equivalent number of *AMA PRA Category 1 Credits*™. Information on the process to convert EACCME credit to AMA credit can be found at https://www.ama-assn.org/education/ama-pra-credit-system/agreement-european-union-medical-specialties-uems

Royal College of Physicians and Surgeons of Canada

Live educational activities, occurring outside of Canada, recognized by the UEMS-EACCME for ECMEC credits are deemed to be Accredited Group Learning Activities (Section 1) as defined by the Maintenance of Certification Program of The Royal College of Physicians and Surgeons of Canada. For more information, visit: www.royalcollege.ca/rcsite/cpd/providers/international-accreditation-agreements-e

Presentation ID: O-072 **Abstract ID: G4999**

DEVELOPMENT AND VALIDATION OF MACHINE LEARNING APPROACH FOR PREDICTING PROTON THERAPY BEAM SPOT CHARACTERISTICS

Ranjith C P[1,2], Mayakannan Krishnan[1], Vysakh R[2], Lalit Chaudhari[2], Siddhartha Laskar[3]

1. D. Y. Patil Education Society Deemed to be University, Kolhapur, Maharashtra, India
2. Department of Radiation Oncology, Advanced Centre for Treatment Research and Education in Cancer, Homi Bhabha National Institute, Mumbai, Maharashtra
3. Department of Radiation Oncology, Tata Memorial Centre, Homi Bhabha National Institute, Mumbai, Maharashtra, India

Email: ranjithcp007@gmail.com

PURPOSE/BACKGROUND: Machine learning (ML) approaches have evolved as a promising method for enhancing and automating quality control and machine performance evaluation in advanced radiotherapy techniques such as Proton beam therapy. Verifying the proton spot characteristics is a crucial quality assurance (QA) test in Pencil Beam Scanning (PBS) proton therapy. These tests can be performed virtually using the irradiation log file information rather than physical measurements. By employing ML techniques on log file information, more robust and efficient QA procedures can be developed, reducing the time and human resources required. This work focuses on developing and validating an Artificial Neural Network (ANN) model for predicting spot dosimetric characteristics.

MATERIALS/METHODS: Dosimetric measurements of proton spots were conducted in the energy range of 70.2 MeV to 226 MeV using a scintillation-based detector in the IBA (Ion Beam Applications, Louvain-la-Neuve, Belgium) proteus plus proton therapy machine. The corresponding irradiation log files were obtained and compared with the measurement data, revealing certain inconsistencies. An ANN model was developed using both measured and log file information to address this issue and to improve the accuracy of spot dosimetric characteristic prediction. The ANN model was fine-tuned by determining the optimal number of neurons and hidden layers, and the activation function and optimiser were selected through trial and error. Separate ANN models were created to predict spot size and position. The accuracy of the model's predictions was evaluated using various statistical tools.

RESULTS : The model's prediction accuracy was evaluated using different statistical metrics such as root mean squared error, mean squared error, R-Square etc. All the spot size prediction model's RMSE was less than 0.05 mm with R square values greater than 99%. The different normality tests and residual plots show that the model prediction is unbiased to the input data. The k-fold cross-validation R-square values are greater than 98% for all the models.

CONCLUSION :A novel ANN-ML model was developed and validated for predicting the spot characteristics based on log file data. This tool can be used in the clinical setting as a potential solution for automating the PBS QA.

KEYWORDS: Proton therapy, Machine learning, Quality assurance, Log file analysis.

Automation of Proton Beam Radiation Therapy Quality Assurance using Machine Learning Models.

Ranjith C P[1,2], Mayakannan[2], Vysakh R[1]

1. Department of Radiation Oncology, Advanced Centre for Treatment Research and Education in Cancer (ACTREC), Tata Memorial Centre, Department of Atomic Energy, Mumbai

2. Centre for Interdisciplinary Research, D.Y. Patil Education Society (Deemed to be University), Kolhapur-416006

Mail id: ranjithcp007@gmail.com

The proton radiation therapy is the latest technology in the field of radiation therapy which is used for cancer treatment [1]. The proton therapy using pencil beam scanning technique [2] require more precise and accurate quality checks. In this study, we have developed and validated Machine Learning (ML) algorithms [3] used for predicting the pencil beam proton beam spot size.

In our study, we have developed a multilayer perception [4] [Artificial Neural Network (ANN) model using the Machine Learning (ML) platform of python programming language to predict the proton therapy beam spot size using 1800 irradiation log files. The proton beam spot was measured using Lynx2D (Scintillator detector) for energies ranging from 70.18MeV to 226.2MeV. The model was trained using 70% of the data and validated using 30% data. The Model validated using various statistical tools.

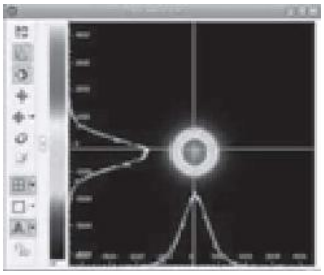

Figure 1: Proton beam spot

The model prediction means the square error is 0.0027mm with an R-Square value of 0.99. The model was validated using the K fold cross-validation method (R-square 0.99). The ML model can be effectively used for reducing QA time and efficiency.

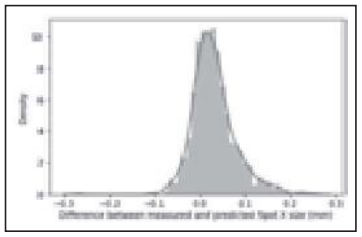

Fig2: Residuals Histogram

The developed ML models can be used for effective quality assurance of the proton beam therapy. Thus ensure the safety and accuracy of the therapy delivered to the cancer patients.

References

1. Smith AR. Proton therapy. Physics in Medicine & Biology. 2006 Jun 20;51(13):R491.
2. Kooy HM et al. A case study in proton pencil-beam scanning delivery. International Journal of Radiation Oncology* Biology* Physics. 2010 Feb 1;76(2):624-30.
3. Pillai M,et. al. Using artificial intelligence to improve the quality and safety of radiation therapy. Journal of the American College of Radiology. 2019 Sep 1;16(9):1267-72.
4. Yagli GM,et al. Automatic hourly solar forecasting using machine learning models. Renewable and Sustainable Energy Reviews. 2019 May 1;105:487-98.

Souvenir of AMPICON 2024, November 8 - 10, 2024 at Hyderabad, India

P-1 **AMC-0185**

Evaluation of Beam Delivery Accuracy in a Pencil Beam Scanning Proton Therapy System Using an In-House Automated Tool using log file data.

Ranjith C P [1,2], Mayakannan Krishnan [2] , Vysakh R [1] , Lalit Chaudhari [1] , Siddhartha Laskar [1] .

[1] *Department of Radiation Oncology, Advanced Centre for Treatment Research and Education in Cancer, Homi Bhabha National Institute, Mumbai, Maharashtra, India.*

[2] *Department of Medical Physics, Centre for Interdisciplinary Research, D. Y. Patil Education Society (Deemed to be University), Kolhapur, Maharashtra, India.*

email id of presenting Author: ranjithcp007@gmail.com.

Objective: The analysis of beam delivery accuracy is important in the Proton therapy system. This study evaluates the accuracy of an in-house tool developed to analyse spot delivery accuracy evaluation using irradiation log files.

Materials and Methods: This study, conducted on an IBA Proteus Plus machine, developed an automated Machine Learning (ML) based script to assess the beam delivery accuracy of PBS beam irradiation. The tool extracts log file data, analyzes spot parameters, predicts spot sizes for all spots using ML models, and evaluates the accuracy of spot size, symmetry, position, and MU per spot. A dataset of 500 irradiation beams and routine QA data was utilized for the evaluation.

Results The ML model predicted spot size values for both X and Y directions, with RMSE values under 0.12 mm. For patient beam data, 96% of spot position values were within 1 mm, while all spot positions were within 0.5 mm for machine QA beams. However, the difference between measured and log file recorded spot size showed a more than 6% standard deviation. The MU values demonstrated a mean difference of 0.01 MU. Additionally, over 94% of spots exhibited less than 10% symmetry deviations.

Conclusion: The automated script effectively analyzed the log file data and utilized ML models to evaluate spot parameters in PBS. This approach is a viable alternative for rapidly assessing all spot parameters in a patient's treatment beam. Additionally, it can be applied to evaluate machine interlocks and performance.

Keywords: Pencil beam scanning, Log file, machine learning, QA automation.

Harnessing the Power of Artificial Intelligence to Revolutionise Proton Therapy: Enhancing Precision, Efficiency, and Patient Outcomes

Ranjith C P [1,2] , Mayakannan Krishnan[1]

1. Department of Medical Physics, Centre for Interdisciplinary Research, D. Y. Patil Education Society (Deemed to be University), Kolhapur, Maharashtra, India
2. Department of Radiation Oncology, Advanced Centre for Treatment Research and Education in Cancer, Homi Bhabha National Institute, Mumbai, Maharashtra, India.

Corresponding author: Mayakannan Krishnan (kmayakannan.phy@gmail.com)

Krishnan and Ranjith

Introduction

Proton therapy is a sophisticated form of radiotherapy that utilises protons to deliver highly precise radiation to tumours, offering a superior dose distribution profile compared to traditional photon-based therapies. This precision allows for the sparing of surrounding healthy tissues, making it particularly advantageous for tumours located near critical structures. Despite these benefits, proton therapy is still susceptible to patient-specific variations, anatomical changes, and daily setup inconsistencies, which present significant challenges to consistently delivering accurate doses.

Artificial Intelligence (AI) integration into proton therapy workflows offers promising potential to address these complexities. AI-powered technologies enable the creation of adaptive treatment protocols that leverage data-driven decision-making to improve treatment precision and efficiency [1]. This article explores how AI advancements help manage uncertainties in proton therapy, focusing on real-time adaptations to anatomical variations. Conventional workflows often struggle to accommodate these variations effectively, which can lead to suboptimal outcomes. In contrast, AI-based techniques offer automated solutions for online adaptive proton therapy, integrating synthetic CT (sCT) generation, automated planning, and advanced quality assurance (QA) protocols.

Review Article

A narrative review of particle therapy in cancer

ABSTRACT

The use of high-energy charged particles in radiotherapy has evolved into an advanced cancer treatment. Even though proton beams and carbon ions are currently the popular particles used for radiotherapy in cancer, ions such as pions, helium, argon, and neon were previously used. To prepare this article, reviewed the literature relevant to the history, current status, and clinical outcomes of particle therapy for specific types of tumors by searching in PubMed and Google Scholar using specific search terms. This article reviews the history, current status, physics, and radiobiological advantages of particle therapy. Outcomes of particle therapy for sites such as the head-and-neck, central nervous system, lung, and prostate have been discussed. The physical and biological properties of particle therapy have been shown to be effective in reducing radiation-induced acute toxicities to a large extent as well as reducing the integral dose, i.e., the sum of dose delivered at every point in a patient's body, multiplied by the volume of tissue at each point and then added up over the entire treated volume. It is used to assess the potential risks associated with radiation therapy. The advantages of particle therapy over conventional photon therapy in terms of overall survival and local control rates have been described. Advances in image guidance and newer particle acceleration technologies have improved the efficiency of particle therapy treatment.

Keywords: Carbon ion therapy, heavy ion therapy, proton pion, helium, argon, neon

INTRODUCTION

Radiation therapy plays a significant role in treating more than 50% of patients with cancer.[1] Photon and electron therapy are conventional radiation therapy techniques that have been used for many years. They are effective in treating many types of cancers, but can also damage healthy tissue surrounding the tumor. Charged-particle therapy can reduce the dose to the normal tissues and has been practiced for the past five decades, with proton and carbon ion therapy being currently popular. In addition to carbon ion and proton therapy, other particles such as helium, pion, and neon are also used for particle therapy.[2] This type of therapy uses heavy charged particles that have unique physical and biological properties such as high linear energy transfer and low oxygen enhancement ratio. Linear energy transfer is a measure of the amount of energy that charged particles transfer to tissues as they travel through them. Heavier charged particles have a higher energy deposition rate, which can cause more damage to tumor cells and result in a more effective cancer treatment. The oxygen enhancement ratio is determined by comparing the amount of radiation needed to produce a specific biological effect in the absence of oxygen to the amount of radiation needed to produce the same effect under normal oxygen conditions. Tumor cells usually have a lower oxygen concentration than normal tissue, so particles with a low oxygen enhancement ratio may be more effective in treating tumors. Particle therapy has unique depth dose characteristics such as Bragg peak and sharp dose fall off,

Mayakannan Krishnan[1], Ranjith C. P.[1,2,3]

[1]Department of Medical Physics, Center for Interdisciplinary Research, D. Y. Patil Education Society (Deemed to be University), Kolhapur, [2]Department of Radiation Oncology, Advanced Center for Treatment Research and Education in Cancer, Tata Memorial Center, Kharghar, Navi Mumbai, Maharashtra, [3]Homi Bhabha National Institute, Anushakti Nagar, Mumbai, India

Address for correspondence: Dr. Mayakannan Krishnan, Department of Medical Physics, Center for Interdisciplinary Research, D. Y. Patil Education Society (Deemed to be University), Kolhapur, Maharashtra - 416006, India.
E-mail: kmayakannan.phy@gmail.com

Access this article online	
Website: https://journals.lww.com/crst	Quick Response Code
DOI: 10.4103/crst.crst_272_22	

How to cite this article: Krishnan M, Ranjith CP. A narrative review of particle therapy in cancer. Cancer Res Stat Treat 2023;6:248-60.

Submitted: 17-Sep-2022 **Revised:** 27-May-2023
Accepted: 27-May-2023 **Published:** 02-Aug-2023

IOP Publishing Biomed. Phys. Eng. Express 10 (2024) 035033 https://doi.org/10.1088/2057-1976/ad3ce0

Biomedical Physics & Engineering Express

RECEIVED
29 November 2023

REVISED
28 March 2024

ACCEPTED FOR PUBLICATION
10 April 2024

PUBLISHED
22 April 2024

PAPER

An artificial neural network based approach for predicting the proton beam spot dosimetric characteristics of a pencil beam scanning technique

C P Ranjith[1,2], **Mayakannan Krishnan**[1,*], **Vysakh Raveendran**[2], **Lalit Chaudhari**[2] and **Siddhartha Laskar**[2]

[1] Department of Medical Physics, Centre for Interdisciplinary Research, D. Y. Patil Education Society (Deemed to be University), Kolhapur, Maharashtra, India
[2] Department of Radiation Oncology, Advanced Centre for Treatment Research and Education in Cancer, Homi Bhabha National Institute, Mumbai, Maharashtra, India
[*] Author to whom any correspondence should be addressed.

E-mail: ranjithcp007@gmail.com, kmayakannan.phy@gmail.com, vysakhraveendran92@gmail.com, lalitnc2006@gmail.com and laskarss@tmc.gov.in

Keywords: machine learning, pencil beam scanning, quality assurance, log file, proton therapy

Abstract

Utilising Machine Learning (ML) models to predict dosimetric parameters in pencil beam scanning proton therapy presents a promising and practical approach. The study developed Artificial Neural Network (ANN) models to predict proton beam spot size and relative positional errors using 9000 proton spot data. The irradiation log files as input variables and corresponding scintillation detector measurements as the label values. The ANN models were developed to predict six variables: spot size in the *x*-axis, *y*-axis, major axis, minor axis, and relative positional errors in the *x*-axis and *y*-axis. All ANN models used a Multi-layer perception (MLP) network using one input layer, three hidden layers, and one output layer. Model performance was validated using various statistical tools. The log file recorded spot size and relative positional errors, which were compared with scintillator-measured data. The Root Mean Squared Error (RMSE) values for the x-spot and y-spot sizes were 0.356 mm and 0.362 mm, respectively. Additionally, the maximum variation for the x-spot relative positional error was 0.910 mm, while for the y-spot, it was 1.610 mm. The ANN models exhibit lower prediction errors. Specifically, the RMSE values for spot size prediction in the x, y, major, and minor axes are 0.053 mm, 0.049 mm, 0.053 mm, and 0.052 mm, respectively. Additionally, the relative spot positional error prediction model for the x and y axes yielded maximum errors of 0.160 mm and 0.170 mm, respectively. The normality of models was validated using the residual histogram and Q-Q plot. The data over fit, and bias were tested using K ($k = 5$) fold cross-validation, and the maximum RMSE value of the K fold cross-validation among all the six ML models was less than 0.150 mm (R-Square 0.960). All the models showed excellent prediction accuracy. Accurately predicting beam spot size and positional errors enhances efficiency in routine dosimetric checks.

1. Introduction

Integrating the pencil beam scanning (PBS) technique into proton therapy systems (PTS) has significantly improved dose conformity and accelerated beam delivery, enhancing treatment precision compared to the passive scattering technique. PBS does not rely on physical apertures or range-modulating devices, allowing for greater flexibility and efficiency in beam delivery, including rapid switching between beam energies and scan patterns. This versatility and precision enable PBS to dynamically adjust beam delivery in real time, improving treatment efficiency. The inverse planning technique of PBS, involving multiple sets of energies and spot positions, has further advanced the complexity of beam delivery techniques [1]. Despite the presence of beamline components such as electromagnets for steering and focusing the beam and

Physica Medica 127 (2024) 104854

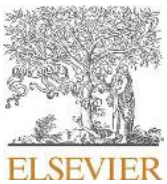

Contents lists available at ScienceDirect

Physica Medica

journal homepage: www.elsevier.com/locate/ejmp

Assessment of pencil beam scanning proton therapy beam delivery accuracy through machine learning and log file analysis

Ranjith C.P. [a,b,1], Mayakannan Krishnan [a,2,*], Vysakh Raveendran [b,3], Lalit Chaudhari [b], Siddhartha Laskar [c]

[a] Department of Medical Physics, Centre for Interdisciplinary Research, D. Y. Patil Education Society (Deemed to be University), Kolhapur, Maharashtra, India
[b] Department of Radiation Oncology, Advanced Centre for Treatment Research and Education in Cancer, Homi Bhabha National Institute, Mumbai, Maharashtra, India
[c] Department of Radiation Oncology, Tata Memorial Hospital, Homi Bhabha National Institute, Mumbai, Maharashtra, India

ARTICLE INFO

Keywords:
Pencil beam scanning
Log file
machine learning
QA automation
Proton therapy

ABSTRACT

Purpose: Comprehensive Quality Assurance (QA) protocols are necessary for complex beam delivery systems like Pencil Beam Scanning (PBS) proton therapy. This study focuses on automating the evaluation of beam delivery accuracy using irradiation log files and machine learning (ML) models.

Methods: Irradiation log files of 935 clinical treatment fields and routine QA beams were analysed to evaluate spot parameters and Monitor Unit (MU) accuracy. ML models predicted spot size along the X, Y, major, and minor axes. In-house scripts automated log file analysis and spot size predictions. Predicted spot sizes were compared with expected baselines, and the accuracy of spot position, symmetry, and MU for each spot in the beam was evaluated.

Results: More than 99.5 % of spot positions were accurate within a 1 mm. The mean and Standard Deviation (SD) of X positional error were −0.021 mm (SD: 0.181 mm), and for Y positional error, they were −0.002 mm (SD: 0.132 mm). ML models accurately predicted spot sizes, with over 95 % of spots demonstrating size variations within 10 % of the baseline. The Root Mean Squared Error (RMSE) of X and Y spot size differences were 0.15 mm and 0.16 mm, respectively. Spot symmetry was within 10 %, and MU accuracy showed 95 % of spots with MU per spot variation less than 2 %.

Conclusion: This method can validate the vendor's beam delivery safety interlock system and serve as a quick alternative to patient-specific QA in adaptive treatment, where time is limited, as well as for routine QA spot parameter evaluations.

1. Introduction

Achieving optimal clinical outcomes in radiotherapy depends on precisely delivering the treatment as planned by the Treatment Planning System (TPS) [1]. In Pencil Beam Scanning (PBS) proton therapy, where proton spots are dynamically delivered with varying energies and positions, rigorous quality assurance (QA) protocols are essential [2]. The American Association of Physicists in Medicine (AAPM) Task Group (TG)-224 report [3] recommends regular verification of beam parameters and Patient-Specific QA (PSQA). The spot profiles crucial for dose distribution are influenced by beam optics, optimised during machine installation and beam commissioning [4]. The baseline spot size for each energy is the same across all gantry angles. However, since beam optics are adjusted for each energy and gantry angle, slight variations in spot size can occur. Therefore, routine QA checks spot size, position, and symmetry at selected energies and angles. However, a treatment field contains thousands of closely spaced spots with varying energies to ensure adequate dose coverage and uniformity. Standard QA equipment cannot assess the dosimetric accuracy of each spot in a treatment field. So, the conventional PSQA procedure uses array detectors to measure dose fluence at a fixed gantry angle and performs gamma analysis [5]. However, the measurement-based PSQA is resource-intensive, often

* Corresponding author.
E-mail address: kmayakannan.phy@gmail.com (M. Krishnan).
[1] Orcid id: 0000-0002-4668-9099.
[2] Orcid id: 0000-0003-2345-2029.
[3] Orcid id: 0000-0001-9549-4231.

https://doi.org/10.1016/j.ejmp.2024.104854
Received 13 June 2024; Received in revised form 10 September 2024; Accepted 28 October 2024

43rd Annual Conference of Association of Medical Physicists of India

AMPICON 2022

Theme: Medical Physics Research and Practice in the Era of Precision Medicine

5th-7th November 2022 | JLN Auditorium, AIIMS New Delhi

Organized by Department of Radiation Oncology, AIIMS, New Delhi

Certificate of Participation

THIS IS TO CERTIFY THAT

Mr. RANJITH CP

has actively participated as Delegate in the
43rd Annual Conference of Association of Medical Physicists of India - AMPICON 2022
from 5th - 7th November, 2022 at JLN Auditorium, AIIMS, New Delhi, India

Dr. D. N. Sharma	Dr. S. D. Sharma	Dr. V. Subramani	Dr. Arun Chougule
Organizing Chairman	President, AMPI	Organizing Secretary	Scientific Chairman

D. Y. PATIL EDUCATION SOCIETY,

(Deemed to be University) Kolhapur

Accredited NAAC with 'A' Grade

DNYANSHODH -2023

(Search For Knowledge)

Certificate

This is to certify that

Mr/Ms. Ranjith C. P.

has presented a Poster on 9th March 2023, in Dnyanshodh -2023,

organized by Centre for Interdisciplinary Research (CIR), D. Y. Patil Education Society

(Deemed to be University), Kolhapur - 416006.

Chairman
Prof. (Dr.) C. D. Lokhande
Dean,
Centre for Interdisciplinary Research

Convener
Dr. Arpita Pandey -Tiwari
Associate Professor,
Department of Medical Biotechnology.


International Conference on Medical Physics - 2023
ICMP 2023
The 25th International Conference of the IOMP
Theme: Innovations in Radiation Technology & Medical Physics for Better Healthcare
6th - 9th December 2023 | Venue: DAE Convention Centre, Anushaktinagar, Mumbai, India
AMPICON 2023 AOCMP 2023 ISEACOMP 2023
CERTIFICATE OF PRESENTATI
This is to certify that
MR. RANJITH C P
has presented a Oral Paper in the International Conference on Medical Physics - 2
held from 06 - 09 December, 2023 at DAE Convention Centre, Anushaktinagar, M
John Damilakis
Dr. John Damilakis
President, IOMP
Dr. Sunil Dutt Sharma
President, AMPI
Eva Bezak
Dr. Eva Bezak
President, AFOMP
Dr. Chai
Presiden

BASAVATARAKAM INDO-AMERICAN CANCER HOSPITAL & RESEARCH INSTITUTE

AMPICON 2024

45th Annual Conference of Association of Medical Physicists of India

ASSOCIATION OF MEDICAL PHYSICISTS OF INDIA AMPI ESTD - 1976

CERTIFICATE OF PARTICIPATION

This certificate is proudly awarded to

Mr. Ranjith C P

*for their participation in the **45th Annual Conference of Association of Medical Physicists of India, AMPICON 2024**, held from 8th to 10th of November 2024, at Sevalal Banjara Bhavan, Banjara Hills, Hyderabad.*

Dr. Manoj K Semwal
President, AMPI

Dr. Anuj Kumar Tyagi
Secretary, AMPI

Dr. A Krishnam Raju
Chairman, AMPICON-24

Dr. G Dileep Kumar
Vice Chairman, AMPICON-24

Dr. NVN Madhusudhan Sresty
Organizing Secretary
AMPICON-24

Dr. C Ramakrishna Rao
Chairman, Scientific Committee
AMPICON-24

CME/CPD Certificate

This is to certify that

Ranjith Cholakkara Poyil Msc

participated in the

4th Flash Radiotherapy and Particle Therapy Conference

Rome, Italy & Online

4-6 December 2024

and received 17 credits

Prof. Vassilios Papalois
President of UEMS

Dr João Grenho
Secretary General of UEMS

European Accreditation Council for Continuing Medical Education (UEMS/EACCME)

The **4th Flash Radiotherapy and Particle Therapy Conference (FRPT 2024)** is accredited by the European Accreditation Council for Continuing Medical Education (EACCME) to provide the following CME activity for medical specialists. The EACCME is an institution of the European Union of Medical Specialists (UEMS): www.uems.eu

The **4th Flash Radiotherapy and Particle Therapy Conference (FRPT 2024)** is designated for a maximum of, or up to, 17 European external CME credits. Each medical specialist should claim only those hours of credit that he/she actually spent in the educational activity.

American Medical Association (AMA)

Through an agreement between the European Union of Medical Specialists and the American Medical Association, physicians may convert EACCME credits to an equivalent number of *AMA PRA Category 1 Credits*™. Information on the process to convert EACCME credit to AMA credit can be found at https://www.ama-assn.org/education/ama-pra-credit-system/agreement-european-union-medical-specialties-uems

Royal College of Physicians and Surgeons of Canada

Live educational activities, occurring outside of Canada, recognized by the UEMS-EACCME for ECMEC credits are deemed to be Accredited Group Learning Activities (Section 1) as defined by the Maintenance of Certification Program of The Royal College of Physicians and Surgeons of Canada. For more information, visit: www.royalcollege.ca/rcsite/cpd/providers/international-accreditation-agreements-e

Presentation ID: O-072 **Abstract ID: G4999**

DEVELOPMENT AND VALIDATION OF MACHINE LEARNING APPROACH FOR PREDICTING PROTON THERAPY BEAM SPOT CHARACTERISTICS

Ranjith C P[1,2], Mayakannan Krishnan[1], Vysakh R[2], Lalit Chaudhari[2], Siddhartha Laskar[3]

1. D. Y. Patil Education Society Deemed to be University, Kolhapur, Maharashtra, India
2. Department of Radiation Oncology, Advanced Centre for Treatment Research and Education in Cancer, Homi Bhabha National Institute, Mumbai, Maharashtra
3. Department of Radiation Oncology, Tata Memorial Centre, Homi Bhabha National Institute, Mumbai, Maharashtra, India

Email: ranjithcp007@gmail.com

PURPOSE/BACKGROUND: Machine learning (ML) approaches have evolved as a promising method for enhancing and automating quality control and machine performance evaluation in advanced radiotherapy techniques such as Proton beam therapy. Verifying the proton spot characteristics is a crucial quality assurance (QA) test in Pencil Beam Scanning (PBS) proton therapy. These tests can be performed virtually using the irradiation log file information rather than physical measurements. By employing ML techniques on log file information, more robust and efficient QA procedures can be developed, reducing the time and human resources required. This work focuses on developing and validating an Artificial Neural Network (ANN) model for predicting spot dosimetric characteristics.

MATERIALS/METHODS: Dosimetric measurements of proton spots were conducted in the energy range of 70.2 MeV to 226 MeV using a scintillation-based detector in the IBA (Ion Beam Applications, Louvain-la-Neuve, Belgium) proteus plus proton therapy machine. The corresponding irradiation log files were obtained and compared with the measurement data, revealing certain inconsistencies. An ANN model was developed using both measured and log file information to address this issue and to improve the accuracy of spot dosimetric characteristic prediction. The ANN model was fine-tuned by determining the optimal number of neurons and hidden layers, and the activation function and optimiser were selected through trial and error. Separate ANN models were created to predict spot size and position. The accuracy of the model's predictions was evaluated using various statistical tools.

RESULTS : The model's prediction accuracy was evaluated using different statistical metrics such as root mean squared error, mean squared error, R-Square etc. All the spot size prediction model's RMSE was less than 0.05 mm with R square values greater than 99%. The different normality tests and residual plots show that the model prediction is unbiased to the input data. The k-fold cross-validation R-square values are greater than 98% for all the models.

CONCLUSION :A novel ANN-ML model was developed and validated for predicting the spot characteristics based on log file data. This tool can be used in the clinical setting as a potential solution for automating the PBS QA.

KEYWORDS: Proton therapy, Machine learning, Quality assurance, Log file analysis.

Automation of Proton Beam Radiation Therapy Quality Assurance using Machine Learning Models.

Ranjith C P[1,2], Mayakannan[2], Vysakh R[1]

1. Department of Radiation Oncology, Advanced Centre for Treatment Research and Education in Cancer (ACTREC), Tata Memorial Centre, Department of Atomic Energy, Mumbai

2. Centre for Interdisciplinary Research, D.Y. Patil Education Society (Deemed to be University), Kolhapur-416006

Mail id: ranjithcp007@gmail.com

The proton radiation therapy is the latest technology in the field of radiation therapy which is used for cancer treatment [1]. The proton therapy using pencil beam scanning technique [2] require more precise and accurate quality checks. In this study, we have developed and validated Machine Learning (ML) algorithms [3] used for predicting the pencil beam proton beam spot size.

In our study, we have developed a multilayer perception [4] [Artificial Neural Network (ANN) model using the Machine Learning (ML) platform of python programming language to predict the proton therapy beam spot size using 1800 irradiation log files. The proton beam spot was measured using Lynx2D (Scintillator detector) for energies ranging from 70.18MeV to 226.2MeV. The model was trained using 70% of the data and validated using 30% data. The Model validated using various statistical tools.

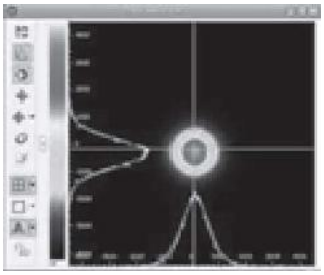

Figure 1: Proton beam spot

The model prediction means the square error is 0.0027mm with an R-Square value of 0.99. The model was validated using the K fold cross-validation method (R-square 0.99). The ML model can be effectively used for reducing QA time and efficiency.

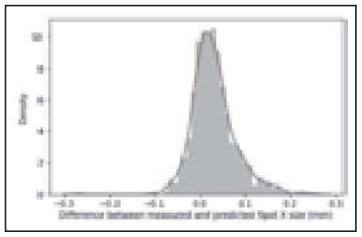

Fig2: Residuals Histogram

The developed ML models can be used for effective quality assurance of the proton beam therapy. Thus ensure the safety and accuracy of the therapy delivered to the cancer patients.

References

1. Smith AR. Proton therapy. Physics in Medicine & Biology. 2006 Jun 20;51(13):R491.
2. Kooy HM et al. A case study in proton pencil-beam scanning delivery. International Journal of Radiation Oncology* Biology* Physics. 2010 Feb 1;76(2):624-30.
3. Pillai M,et. al. Using artificial intelligence to improve the quality and safety of radiation therapy. Journal of the American College of Radiology. 2019 Sep 1;16(9):1267-72.
4. Yagli GM,et al. Automatic hourly solar forecasting using machine learning models. Renewable and Sustainable Energy Reviews. 2019 May 1;105:487-98.

Souvenir of AMPICON 2024, November 8 - 10, 2024 at Hyderabad, India

P-1 **AMC-0185**

Evaluation of Beam Delivery Accuracy in a Pencil Beam Scanning Proton Therapy System Using an In-House Automated Tool using log file data.

Ranjith C P [1,2], Mayakannan Krishnan [2] , Vysakh R [1] , Lalit Chaudhari [1] , Siddhartha Laskar [1] .

[1] *Department of Radiation Oncology, Advanced Centre for Treatment Research and Education in Cancer, Homi Bhabha National Institute, Mumbai, Maharashtra, India.*

[2] *Department of Medical Physics, Centre for Interdisciplinary Research, D. Y. Patil Education Society (Deemed to be University), Kolhapur, Maharashtra, India.*

email id of presenting Author: ranjithcp007@gmail.com.

Objective: The analysis of beam delivery accuracy is important in the Proton therapy system. This study evaluates the accuracy of an in-house tool developed to analyse spot delivery accuracy evaluation using irradiation log files.

Materials and Methods: This study, conducted on an IBA Proteus Plus machine, developed an automated Machine Learning (ML) based script to assess the beam delivery accuracy of PBS beam irradiation. The tool extracts log file data, analyzes spot parameters, predicts spot sizes for all spots using ML models, and evaluates the accuracy of spot size, symmetry, position, and MU per spot. A dataset of 500 irradiation beams and routine QA data was utilized for the evaluation.

Results The ML model predicted spot size values for both X and Y directions, with RMSE values under 0.12 mm. For patient beam data, 96% of spot position values were within 1 mm, while all spot positions were within 0.5 mm for machine QA beams. However, the difference between measured and log file recorded spot size showed a more than 6% standard deviation. The MU values demonstrated a mean difference of 0.01 MU. Additionally, over 94% of spots exhibited less than 10% symmetry deviations.

Conclusion: The automated script effectively analyzed the log file data and utilized ML models to evaluate spot parameters in PBS. This approach is a viable alternative for rapidly assessing all spot parameters in a patient's treatment beam. Additionally, it can be applied to evaluate machine interlocks and performance.

Keywords: Pencil beam scanning, Log file, machine learning, QA automation.

Harnessing the Power of Artificial Intelligence to Revolutionise Proton Therapy: Enhancing Precision, Efficiency, and Patient Outcomes

Ranjith C P [1,2] , Mayakannan Krishnan[1]

1. Department of Medical Physics, Centre for Interdisciplinary Research, D. Y. Patil Education Society (Deemed to be University), Kolhapur, Maharashtra, India
2. Department of Radiation Oncology, Advanced Centre for Treatment Research and Education in Cancer, Homi Bhabha National Institute, Mumbai, Maharashtra, India.

Corresponding author: Mayakannan Krishnan (kmayakannan.phy@gmail.com)

Krishnan and Ranjith

Introduction

Proton therapy is a sophisticated form of radiotherapy that utilises protons to deliver highly precise radiation to tumours, offering a superior dose distribution profile compared to traditional photon-based therapies. This precision allows for the sparing of surrounding healthy tissues, making it particularly advantageous for tumours located near critical structures. Despite these benefits, proton therapy is still susceptible to patient-specific variations, anatomical changes, and daily setup inconsistencies, which present significant challenges to consistently delivering accurate doses.

Artificial Intelligence (AI) integration into proton therapy workflows offers promising potential to address these complexities. AI-powered technologies enable the creation of adaptive treatment protocols that leverage data-driven decision-making to improve treatment precision and efficiency [1]. This article explores how AI advancements help manage uncertainties in proton therapy, focusing on real-time adaptations to anatomical variations. Conventional workflows often struggle to accommodate these variations effectively, which can lead to suboptimal outcomes. In contrast, AI-based techniques offer automated solutions for online adaptive proton therapy, integrating synthetic CT (sCT) generation, automated planning, and advanced quality assurance (QA) protocols.

Review Article

A narrative review of particle therapy in cancer

ABSTRACT

The use of high-energy charged particles in radiotherapy has evolved into an advanced cancer treatment. Even though proton beams and carbon ions are currently the popular particles used for radiotherapy in cancer, ions such as pions, helium, argon, and neon were previously used. To prepare this article, reviewed the literature relevant to the history, current status, and clinical outcomes of particle therapy for specific types of tumors by searching in PubMed and Google Scholar using specific search terms. This article reviews the history, current status, physics, and radiobiological advantages of particle therapy. Outcomes of particle therapy for sites such as the head-and-neck, central nervous system, lung, and prostate have been discussed. The physical and biological properties of particle therapy have been shown to be effective in reducing radiation-induced acute toxicities to a large extent as well as reducing the integral dose, i.e., the sum of dose delivered at every point in a patient's body, multiplied by the volume of tissue at each point and then added up over the entire treated volume. It is used to assess the potential risks associated with radiation therapy. The advantages of particle therapy over conventional photon therapy in terms of overall survival and local control rates have been described. Advances in image guidance and newer particle acceleration technologies have improved the efficiency of particle therapy treatment.

Keywords: Carbon ion therapy, heavy ion therapy, proton pion, helium, argon, neon

INTRODUCTION

Radiation therapy plays a significant role in treating more than 50% of patients with cancer.[1] Photon and electron therapy are conventional radiation therapy techniques that have been used for many years. They are effective in treating many types of cancers, but can also damage healthy tissue surrounding the tumor. Charged-particle therapy can reduce the dose to the normal tissues and has been practiced for the past five decades, with proton and carbon ion therapy being currently popular. In addition to carbon ion and proton therapy, other particles such as helium, pion, and neon are also used for particle therapy.[2] This type of therapy uses heavy charged particles that have unique physical and biological properties such as high linear energy transfer and low oxygen enhancement ratio. Linear energy transfer is a measure of the amount of energy that charged particles transfer to tissues as they travel through them. Heavier charged particles have a higher energy deposition rate, which can cause more damage to tumor cells and result in a more effective cancer treatment. The oxygen enhancement ratio is determined by comparing the amount of radiation needed to produce a specific biological effect in the absence of oxygen to the amount of radiation needed to produce the same effect under normal oxygen conditions. Tumor cells usually have a lower oxygen concentration than normal tissue, so particles with a low oxygen enhancement ratio may be more effective in treating tumors. Particle therapy has unique depth dose characteristics such as Bragg peak and sharp dose fall off,

Mayakannan Krishnan[1], Ranjith C. P.[1,2,3]

[1]Department of Medical Physics, Center for Interdisciplinary Research, D. Y. Patil Education Society (Deemed to be University), Kolhapur, [2]Department of Radiation Oncology, Advanced Center for Treatment Research and Education in Cancer, Tata Memorial Center, Kharghar, Navi Mumbai, Maharashtra, [3]Homi Bhabha National Institute, Anushakti Nagar, Mumbai, India

Address for correspondence: Dr. Mayakannan Krishnan, Department of Medical Physics, Center for Interdisciplinary Research, D. Y. Patil Education Society (Deemed to be University), Kolhapur, Maharashtra - 416006, India.
E-mail: kmayakannan.phy@gmail.com

Access this article online	
Website: https://journals.lww.com/crst	Quick Response Code
DOI: 10.4103/crst.crst_272_22	

How to cite this article: Krishnan M, Ranjith CP. A narrative review of particle therapy in cancer. Cancer Res Stat Treat 2023;6:248-60.

Submitted: 17-Sep-2022 **Revised:** 27-May-2023
Accepted: 27-May-2023 **Published:** 02-Aug-2023

IOP Publishing Biomed. Phys. Eng. Express 10 (2024) 035033 https://doi.org/10.1088/2057-1976/ad3ce0

Biomedical Physics & Engineering Express

RECEIVED
29 November 2023

REVISED
28 March 2024

ACCEPTED FOR PUBLICATION
10 April 2024

PUBLISHED
22 April 2024

PAPER

An artificial neural network based approach for predicting the proton beam spot dosimetric characteristics of a pencil beam scanning technique

C P Ranjith[1,2], **Mayakannan Krishnan**[1,*], **Vysakh Raveendran**[2], **Lalit Chaudhari**[2] and **Siddhartha Laskar**[2]

[1] Department of Medical Physics, Centre for Interdisciplinary Research, D. Y. Patil Education Society (Deemed to be University), Kolhapur, Maharashtra, India
[2] Department of Radiation Oncology, Advanced Centre for Treatment Research and Education in Cancer, Homi Bhabha National Institute, Mumbai, Maharashtra, India
[*] Author to whom any correspondence should be addressed.

E-mail: ranjithcp007@gmail.com, kmayakannan.phy@gmail.com, vysakhraveendran92@gmail.com, lalitnc2006@gmail.com and laskarss@tmc.gov.in

Keywords: machine learning, pencil beam scanning, quality assurance, log file, proton therapy

Abstract

Utilising Machine Learning (ML) models to predict dosimetric parameters in pencil beam scanning proton therapy presents a promising and practical approach. The study developed Artificial Neural Network (ANN) models to predict proton beam spot size and relative positional errors using 9000 proton spot data. The irradiation log files as input variables and corresponding scintillation detector measurements as the label values. The ANN models were developed to predict six variables: spot size in the *x*-axis, *y*-axis, major axis, minor axis, and relative positional errors in the *x*-axis and *y*-axis. All ANN models used a Multi-layer perception (MLP) network using one input layer, three hidden layers, and one output layer. Model performance was validated using various statistical tools. The log file recorded spot size and relative positional errors, which were compared with scintillator-measured data. The Root Mean Squared Error (RMSE) values for the x-spot and y-spot sizes were 0.356 mm and 0.362 mm, respectively. Additionally, the maximum variation for the x-spot relative positional error was 0.910 mm, while for the y-spot, it was 1.610 mm. The ANN models exhibit lower prediction errors. Specifically, the RMSE values for spot size prediction in the x, y, major, and minor axes are 0.053 mm, 0.049 mm, 0.053 mm, and 0.052 mm, respectively. Additionally, the relative spot positional error prediction model for the x and y axes yielded maximum errors of 0.160 mm and 0.170 mm, respectively. The normality of models was validated using the residual histogram and Q-Q plot. The data over fit, and bias were tested using K ($k = 5$) fold cross-validation, and the maximum RMSE value of the K fold cross-validation among all the six ML models was less than 0.150 mm (R-Square 0.960). All the models showed excellent prediction accuracy. Accurately predicting beam spot size and positional errors enhances efficiency in routine dosimetric checks.

1. Introduction

Integrating the pencil beam scanning (PBS) technique into proton therapy systems (PTS) has significantly improved dose conformity and accelerated beam delivery, enhancing treatment precision compared to the passive scattering technique. PBS does not rely on physical apertures or range-modulating devices, allowing for greater flexibility and efficiency in beam delivery, including rapid switching between beam energies and scan patterns. This versatility and precision enable PBS to dynamically adjust beam delivery in real time, improving treatment efficiency. The inverse planning technique of PBS, involving multiple sets of energies and spot positions, has further advanced the complexity of beam delivery techniques [1]. Despite the presence of beamline components such as electromagnets for steering and focusing the beam and

Physica Medica 127 (2024) 104854

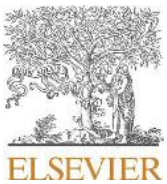

Contents lists available at ScienceDirect

Physica Medica

journal homepage: www.elsevier.com/locate/ejmp

Assessment of pencil beam scanning proton therapy beam delivery accuracy through machine learning and log file analysis

Ranjith C.P. [a,b,1], Mayakannan Krishnan [a,2,*], Vysakh Raveendran [b,3], Lalit Chaudhari [b], Siddhartha Laskar [c]

[a] Department of Medical Physics, Centre for Interdisciplinary Research, D. Y. Patil Education Society (Deemed to be University), Kolhapur, Maharashtra, India
[b] Department of Radiation Oncology, Advanced Centre for Treatment Research and Education in Cancer, Homi Bhabha National Institute, Mumbai, Maharashtra, India
[c] Department of Radiation Oncology, Tata Memorial Hospital, Homi Bhabha National Institute, Mumbai, Maharashtra, India

ARTICLE INFO

Keywords:
Pencil beam scanning
Log file
machine learning
QA automation
Proton therapy

ABSTRACT

Purpose: Comprehensive Quality Assurance (QA) protocols are necessary for complex beam delivery systems like Pencil Beam Scanning (PBS) proton therapy. This study focuses on automating the evaluation of beam delivery accuracy using irradiation log files and machine learning (ML) models.

Methods: Irradiation log files of 935 clinical treatment fields and routine QA beams were analysed to evaluate spot parameters and Monitor Unit (MU) accuracy. ML models predicted spot size along the X, Y, major, and minor axes. In-house scripts automated log file analysis and spot size predictions. Predicted spot sizes were compared with expected baselines, and the accuracy of spot position, symmetry, and MU for each spot in the beam was evaluated.

Results: More than 99.5 % of spot positions were accurate within a 1 mm. The mean and Standard Deviation (SD) of X positional error were −0.021 mm (SD: 0.181 mm), and for Y positional error, they were −0.002 mm (SD: 0.132 mm). ML models accurately predicted spot sizes, with over 95 % of spots demonstrating size variations within 10 % of the baseline. The Root Mean Squared Error (RMSE) of X and Y spot size differences were 0.15 mm and 0.16 mm, respectively. Spot symmetry was within 10 %, and MU accuracy showed 95 % of spots with MU per spot variation less than 2 %.

Conclusion: This method can validate the vendor's beam delivery safety interlock system and serve as a quick alternative to patient-specific QA in adaptive treatment, where time is limited, as well as for routine QA spot parameter evaluations.

1. Introduction

Achieving optimal clinical outcomes in radiotherapy depends on precisely delivering the treatment as planned by the Treatment Planning System (TPS) [1]. In Pencil Beam Scanning (PBS) proton therapy, where proton spots are dynamically delivered with varying energies and positions, rigorous quality assurance (QA) protocols are essential [2]. The American Association of Physicists in Medicine (AAPM) Task Group (TG)-224 report [3] recommends regular verification of beam parameters and Patient-Specific QA (PSQA). The spot profiles crucial for dose distribution are influenced by beam optics, optimised during machine installation and beam commissioning [4]. The baseline spot size for each energy is the same across all gantry angles. However, since beam optics are adjusted for each energy and gantry angle, slight variations in spot size can occur. Therefore, routine QA checks spot size, position, and symmetry at selected energies and angles. However, a treatment field contains thousands of closely spaced spots with varying energies to ensure adequate dose coverage and uniformity. Standard QA equipment cannot assess the dosimetric accuracy of each spot in a treatment field. So, the conventional PSQA procedure uses array detectors to measure dose fluence at a fixed gantry angle and performs gamma analysis [5]. However, the measurement-based PSQA is resource-intensive, often

* Corresponding author.
E-mail address: kmayakannan.phy@gmail.com (M. Krishnan).
[1] Orcid id: 0000-0002-4668-9099.
[2] Orcid id: 0000-0003-2345-2029.
[3] Orcid id: 0000-0001-9549-4231.

https://doi.org/10.1016/j.ejmp.2024.104854
Received 13 June 2024; Received in revised form 10 September 2024; Accepted 28 October 2024

D. Y. PATIL EDUCATION SOCIETY, KOLHAPUR
(Deemed to be University)

(Declared u/s 3 of the UGC Act 1956 vide Notification No. F.9-26/2004-U.3 dt. 01-09-2005 of the GOI)

Reaccredited by NAAC with 'A' Grade

869, 'E', D. Y. Patil Vidyanagar, Kolhapur-416 006

Phone No. : (0231) 2601335-36, Fax: (0231) 2601595

Dr. V.V. Bhosale
Registrar

Web: www.dypatilunikop.org, E-mail: info@dypatilkolhapur.org

No. DYPES/DU/Ph.D./2513

Date: 13.10.2021

To,
Ranjith CP
kunnathirikunnu house Elankur,
manhappatta

Sub: Ph.D. Admission 2021- Physics

With reference to your application for the Ph.D. Programme and subsequent CET, Personal Interview before the Ph.D. Admission Committee in **"Centre for Interdisciplinary Research"**, I am directed to inform you that you have been given provisional admission for Ph.D. Programme under the faculty of interdisciplinary studies.

Considering your research interest, title and requirement of the topic you will be allotted guide/supervisor.

You are required to give the Joining Report with original documents within seven days. The fees to be paid are as follows:

1.	Registration Fee	Rs.2,000/- (One time)
2.	Tuition Fee	Rs.50,000/- (Per annum)
3.	Development Fee	Rs. 5,000/-(Per annum)

Total- Rs. 57, 000/-

The tenure of the programme will be as per UGC norms i.e. minimum 3 years to maximum 6 years.

REGISTRAR

Copy to:
1. Research Director
2. Accounts Section

टाटा स्मारक केन्द्र
TATA MEMORIAL CENTRE

कैंसर उपचार, अनुसंधान एवं शिक्षा का प्रगत केन्द्र
ADVANCED CENTRE FOR TREATMENT RESEARCH & EDUCATION IN CANCER

- CANCER RESEARCH INSTITUTE
- CLINICAL RESEARCH CENTRE
- CENTRE FOR CANCER EPIDEMIOLOGY

प.ऊ.वि. भारत सरकार का एक सहायता अनुदान प्राप्त संस्थान
A GRANT-IN-AID INSTITUTION OF THE DEPARTMENT OF ATOMIC ENERGY, GOVT. OF INDIA

11341

No. EST/RCP/271704/6019/2021

8th November, 2021

No Objection Certificate

This is to certify that Mr. Ranjith C P is working in the employment of TMC-ACTREC since 31st May, 2021 and at present holding the post of Medical Physicist 'D' in the pay matrix Level 11 at ACTREC of TMC.

This centre has no objection for him to apply for Ph.D. program in Physics/Medical Physics/Radiation Physics subject at D. Y. Patil Education Society, Kolhapur.

(S. V. Deshmukh)
Asst Administrative Officer

खारघर, नवी मुंबई - ४१० २१०. भारत.
दूरभाष : +९१-२२-२७४० ५०००
+९१-२२-६८७३ ५०००
फैक्स : +९१-२२-२७४० ५०८५

Kharghar,
Navi Mumbai - 410 210. INDIA.
Phone: +91 - 22 - 2740 5000
+91 - 22 - 6873 5000
Fax: +91 - 22 - 2740 5085

E-mail : mail@actrec.gov.in
Website : www.actrec.gov.in

D. Y. PATIL
EDUCATION SOCIETY
KOLHAPUR

(INSTITUTION DEEMED TO BE UNIVERSITY)
(Deemed to be University Declared u/s 3 of the UGC Act 1956 vide Notification No. F.9-26/2004- U.3 dt. 01-09- 2005 of the GOI)
NAAC 'A' Grade

No. DYPEU/DU/Ph.D./2022/1136 Date: 27.04.2022

To,
Ranjith CP
kunnathirikunnu house,
Elankur manhappatta,
Keral.

Sub: Confirmation of registration to Ph.D. degree program.
Ref.: DYPES/DU/Ph.D./2513 date: 13.10.2021, PRN – 2021013020.

Dear Student,

I am directed to inform you that you have been registered to Ph.D. degree program in **Physics** in the Faculty of **Interdisciplinary Studies**, w.e.f. 13.10.2021 [Registration No. DYPES/DU/Ph.D/2513 dated: 13.10.2021] under the guidance of Dr. K. Mayakannan.

The Research and Recognition Committee has approved your title of proposed research work as **"Implementation of Machine Learning in the Proton Therapy Quality Assurance."**

The Research and Recognition Committee has resolved to implement the following rule:

"The researcher is expected to review six monthly progress presentations with his/her research advisory committee. Any deviation from the approved protocol i.e. reflected in the title must have approval of concerned research advisory committee and must be recommended by the chairperson of the research committee".

Please note that you will have to work fulltime; otherwise your admission will be discontinued. Please also note that your admission is subject to various conditions as laid down in UGC (Minimum Standard and Procedure for the award of Ph.D. Degree) Regulation 2016.

Registrar

Copy to: *Concerned Ph.D. Supervisor*

address: 869, 'E', D. Y. Patil Vidyanagar, Kolhapur-416 006 | **phone:** (0231) 2601235-36
fax: (0231) 2601595 | **email**: info@dypatilkolhapur.org | **website**: www.dypatilunikop.org

D. Y. PATIL MEDICAL COLLEGE KOLHAPUR

Constiuent Unit of D. Y. Patil Education Society (Deemed to be University),Kolhapur.
Re-accredited by NAAC with 'A' Grade

Dr. Rakesh Kumar Sharma
Dean & Professor (Obst. & Gyn)

Padmashree Dr. D. Y. Patil
Founder president

Dr. Sanjay D. Patil
President

No. DYPMCK/.....11...../2022/IEC

Date: 24 JUN 2022

INSTITUTIONAL ETHICS COMMITTEE, D. Y. PATIL MEDICAL COLLEGE, KOLHAPUR.

This is to certify that the research project titled,

"Implementation of Machine Learning in the Proton Therapy Quality Assurance."

Submitted by : **Mr. Ranjith C. P.**

Under the supervision of appointed Guide (if any): **Dr. K. Mayakannan**

Has been studied by the Institutional Ethics Committee (IEC) at its meeting held on **07/04/2022** and after corrected has granted approval for the study with due effect with the following caveats:

1. If you desire any change in the protocol or standard recording document at any time, please submit the same to the IEC for information and approval before the change is implemented.
2. As per recommendations of ICMR, you must register your study with the Central Trials Registry-India (CTRI), hosted at the ICMR's National Institute of Medical Statistics (http://icmr-nims.nic.in). The registration details as provided by the website are to be submitted to the Institutional Ethics Committee within a period of 3 months from issue of this letter.
3. All serious and/or unexpected adverse events due to the drug/procedures tested in the study must be informed to the IEC within 24 hours and steps for appropriate treatment must be immediately instituted.
4. In case of injury/disability/death of any participant attributable to the drug/procedure under study, all compensation is to be made by the sponsor of the study.
5. The Chief investigator/Researcher must inform the IEC immediately if the study is terminated earlier than planned with the reasons for the same.
6. The final results of the study must be communicated to the IEC within 3 months of the completion of data collection.
7. The researcher must take all precautions to safeguard the rights, safety, dignity and wellbeing of the participants in the study.
8. The researcher must be up to date about all information regarding the risk/benefit ratio of any drug/procedure being used and any new information must be conveyed to the IEC immediately. The IEC reserves the right to change a decision on the project in the light of any new knowledge.
9. Before publishing the results of the study, the researcher must take permission from the Dean of the Institution.
10. Annual progress report should be submitted for all sponsored projects to the committee.
11. Unethical conduct of research in non-sponsored projects will result in withdrawal of the ethics approval and negation of all data collected till that date.

Dr. Mrs. Shimpa R. Sharma
(Member Secretary, IEC)

Dr. (Mrs.) Shimpa Sharma
Member Secretary,
Institutional Ethics Committee
D. Y. Patil Medical College,
Kolhapur - 416 006

टाटा स्मारक केन्द्र
TATA MEMORIAL CENTRE

कैंसर उपचार, अनुसंधान एवं शिक्षा का प्रगत केन्द्र
ADVANCED CENTRE FOR TREATMENT RESEARCH & EDUCATION IN CANCER

- CANCER RESEARCH INSTITUTE
- CLINICAL RESEARCH CENTRE
- CENTRE FOR CANCER EPIDEMIOLOGY

12283

प.ऊ.वि. भारत सरकार का एक सहायता अनुदान प्राप्त संस्थान
A GRANT-IN-AID INSTITUTION OF THE DEPARTMENT OF ATOMIC ENERGY, GOVT. OF INDIA

Permission Letter

date: 18/04/2022

Ranjith C P is a Medical physicist working under my supervision in the department of Radiation Oncology, ACTREC, Tata memorial center, Mumbai. Here, I am giving permission to him for collecting the required data from the Proton therapy treatment log files and from the Treatment Planning System which will be required for his Ph.D. work. He is also allowed to conduct Proton Beam-measurements related to his course of Ph.D. which is registered in the Centre for Interdisciplinary Studies, D.Y. Patil Education Society (Deemed to be University), Kolhapur, Maharashtra.

Reena Devi Ph

Sr. Medical physicist and Radiation Safety Officer (RSO)-III

ACTREC

Tata memorial center

DAE, Mumbai

खारघर, नवी मुंबई - ४१० २१०. भारत.
दूरभाष : +९१-२२-२७४० ५०००
+९१-२२-६८७३ ५०००
फैक्स : +९१-२२-२७४० ५०८५

E-mail : mail@actrec.gov.in
Website : www.actrec.gov.in

Kharghar,
Navi Mumbai - 410 210. INDIA.
Phone: +91 - 22 - 2740 5000
+91 - 22 - 6873 5000
Fax: +91 - 22 - 2740 5085